The role of Math5 (Atoh7) in retinal and optic nerve development and human disease

by

Lev Prasov

A dissertation submitted in partial fulfillment
of the requirements for the degree of
Doctor of Philosophy
(Human Genetics)
in the University of Michigan
2012

Doctoral Committee:

Associate Professor Thomas M. Glaser, Chair
Professor Sally A. Camper
Professor Pamela A. Raymond
Associate Professor Donna M. Martin
Associate Professor David L. Turner

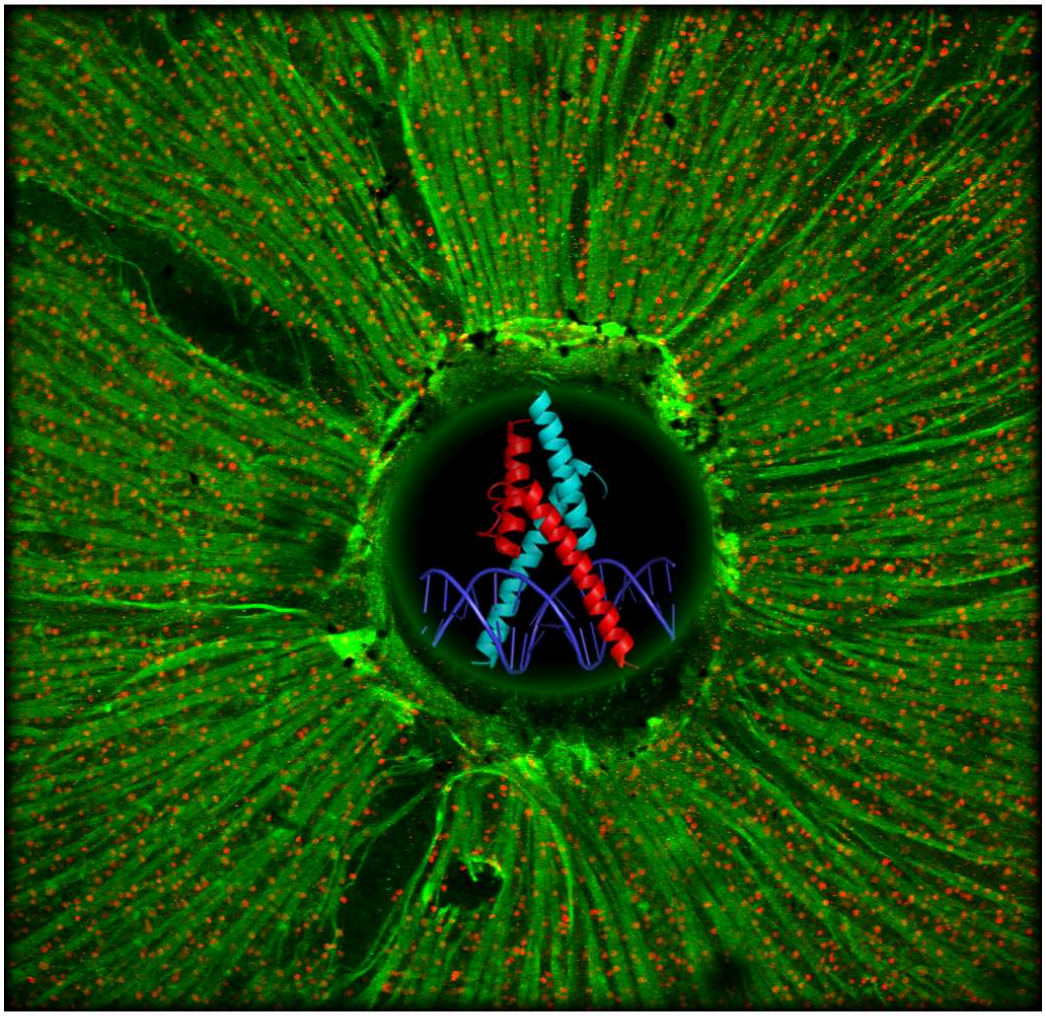

"The great tragedy of Science —
the slaying of a beautiful hypothesis
by an ugly fact."

— Thomas Henry Huxley (1825 - 1895)

2012

To my parents and grandparents,

for the genes and environment

ACKNOWLEDGEMENTS

Many people have contributed to the work presented in this thesis. First and foremost, I would like to thank my advisor, Tom Glaser, for his guidance and support throughout this process. He deserves much of the credit for my success as a graduate student, and has truly taught me to be a good and rigorous scientist. I would like to thank my thesis committee (David Turner, Donna Martin, Sally Camper, and Pamela Raymond) for fruitful discussions and constructive feedback. I would like to thank all of the Glaser lab members past and present (Chris Chou, Dellaney Rudolph, Mindy Nagy, Nate Vale, and Sherry Taylor) for creating a vibrant and productive work environment, including the entertaining discussions both about science and about "nothing." I would also like to acknowledge the efforts and support of all the people that have provided me with reagents, shared ideas, assisted with experiments, and helped with manuscripts. Foremost, I would like to thank Chris Chou, Joe Brzezinski, Dave Turner, and Nadean Brown, whose advice and support have been truly invaluable. I'd like to thank the staff at the MSTP and HG department, especially Ron Koenig, Ellen Elkin, and Karen Grahl, for their administrative support and advice. I'd like to thank my friends, who have helped me stay sane throughout the PhD process. Finally, I'd like to thank my parents and grandparents for their love and support, and my brother, Zahar, for being my first and best teacher.

PREFACE

The work presented in this thesis comprises most of my efforts in Glaser laboratory since August of 2007. Many of the chapters have been accepted or submitted for publication, and were done as a collaborative effort with other scientists. Outside contributions and publication status are noted below. Additionally, acknowledgements are appended to each chapter to recognize other contributors.

Chapter II describes a critical analysis of *Math5 (Atoh7)* splicing in the developing retina and brain. For this project, Nadean Brown conducted the original Northern blot analysis and tested *Math5* antibodies on retinal tissues. This work was published as: Prasov L, Brown NL, Glaser T. "A critical analysis of Atoh7 (Math5) mRNA splicing in the developing mouse retina." *PLoS One*. 2010, 5(8), pii:e12315.

Chapter III describes an analysis of the lineage and cell cycle properties of *Math5* expression. Joe Brzezinski generated and characterized the Math5>Cre BAC transgenic mice. He also collected the data for quantitative lineage analysis in Math5 wild-type and knockout backgrounds, conducted the reporter concordance, rod vs. cone birthdating experiments, and did some preliminary cell cycle analysis. A modified version of this chapter has been accepted for

publication as: Brzezinski JA IV, Prasov L, Glaser T. “Math5 establishes an early RGC competence state in a subpopulation of exiting retinal progenitor cells.” *Dev. Biol*. 2012.

Chapter IV describes cell cycle and clonal analysis that pinpoints the timing of the RGC fate decision. Chapter V describes *Math5* over-expression experiments. These experiments were carried out by me, with technical support in cloning and mouse colony management from Dellaney Rudolph and Sue Tarlé. Transgenic mice were generated by the UM Transgenic Animal Model Core, and Mitchell Gillett assisted with histology of plastic sections. Modified versions are being submitted for publication as Prasov L., Glaser T. “Dynamic expression of ganglion cell markers in retinal progenitors during the terminal cell cycle” and Prasov L**,** Glaser T. “Pushing the envelope of retinal ganglion cell genesis: context dependent function of *Math5* (*Atoh7*).”

Chapter VI describes the screening and identification of *ATOH7* (*MATH5*) mutations in congenital neural and vascular diseases of the retina. I designed and carried out all of the functional analysis. Tehmina Masud and Edward Oliver assisted with the identification of ATOH7 mutations, and screening of cases. Aiysa Abid, Shagufta Khaliq, Qasim Mehdi, Eduardo Silva, Amy Lewanda, Mark Borchert, Mehul Dattani provided DNA samples and clinical information for cases screened in this study. Dan Kelberman and Jane Snowden screened ONH cases for coding *ATOH7* variants. Genome-wide Illumina-OmniQuad genotype was done with Susan Dagenais and Bob Lyons at the UM DNA sequencing core. A modified version of this chapter has been submitted for publication as Prasov L,

Masud T, Khaliq S, Mehdi SQ, Abid, AY, Oliver ER, Silva E, Brodsky MC, Borchert M, Kelberman D, Snowden JC, Dattani M, Glaser T. “Mutations in Atoh7 cause recessive persistent hyperplasia of the primary vitreous.”

TABLE OF CONTENTS

LIST OF FIGURES

CHAPTER I:

CHAPTER II:

CHAPTER III:

CHAPTER IV:

CHAPTER V:

CHAPTER VI:

CHAPTER VII:

LIST OF TABLES

ABSTRACT

Vertebrate retinal histogenesis is controlled by both intrinsic transcriptional programs and the microenvironment. The basic helix-loop-helix (bHLH) factor Math5 (Atoh7) is required for differentiation of retinal ganglion cells (RGC), which form the optic nerve. *Math5* knockout mice lack RGCs, but only 10% of Math5-expressing progenitors adopt the RGC fate, and only 55% of RGCs are lineal descendents of Math5+ cells.

To define the role of *Math5* in RGC development, I characterized the transcriptional anatomy of mouse *Math5*, and showed that it is an unspliced, single-exon gene, contrary to a recent high-profile report. I then tested the contribution of Math5-expressing cells to the earliest born cohort of mouse retinal neurons, which consist primarily of RGCs (~80%). Unexpectedly, I found that only 20-30% of this cohort expresses Math5, yet most early RGCs depend on Math5 function, suggesting a non-autonomous role for Math5-expressing cells in RGC specification.

Next, I evaluated the onset of Math5 expression, and that of RGC markers Brn3b and Isl1, with respect to the terminal cell cycle. Surprisingly, these markers were expressed by neurogenic cells prior to terminal mitosis during early development (<E14), but restricted to post-mitotic cells during later stages. By retroviral clone analysis, I confirmed that early neurogenic cells often divide

symmetrically, leading to paired RGC daughters. Retinal fate determination is thus not strictly synchronized to cell cycle exit.

I then evaluated whether Math5 can bias terminally mitotic progenitors toward the RGC fate. I broadly over-expressed Math5 using BAC and conventional transgenes controlled by Crx regulatory DNA. Unexpectedly, I found that ectopic Math5 did not alter cell fate in a wild-type environment, but partially rescued RGC development in *Math5* mutant retinas. Early (pioneering) RGCs are deficient in these mice, and rescue was incomplete. Transgene-derived late-born RGCs exhibited pathfinding defects and were prone to apoptosis.

Finally, I evaluated the role of *ATOH7* (*MATH5*) in human optic nerve aplasia and hypoplasia, and familial persistent hyperplastic primary vitreous (PHPV) disease. I identified a basic domain mutation (p.N46>H) in PHPV, and established causation, using biochemical and functional assays. Together, these studies provide important insights into the function of *Math5* and RGC development.

CHAPTER I

VERTEBRATE RETINAL DEVELOPMENT

Structure and composition of the retina

The vertebrate eye is a complex tissue that transmits visual information from the environment to the central nervous system. Light enters the eye through the cornea, is focused by the lens, and strikes the neural retina (Fig. I-1A). The retina converts an electromagnetic signal (light) into an electrical and neurochemical signal that can be processed by the central nervous system (CNS) (Rodieck, 1998). The neural retina comprises six major classes of neurons and one type of glia (Fig. I-1B). The neurons include rod and cone photoreceptors; horizontal, bipolar, and amacrine interneurons; and retinal ganglion cells. These form an organized structure with three layers of cell bodies, including the outer nuclear layer (ONL), the inner nuclear layer (INL), and the ganglion cell layer (GCL). The cellular layers are separated by two fiber layers called the outer plexiform layer (OPL) and inner plexiform layer (IPL), respectively, which contain precisely stratified synaptic connections between photoreceptor endfeet or interneuron terminals and dendrites.

The ONL contains the cell bodies of ciliary photoreceptors, the major class of cells that perceive light. They are subdivided into rods and cones, based on

cellular morphology, physiology, and role in the visual system. In most mammals, particularly nocturnal species, rods are the most abundant cell class in the retina and have relatively uniform properties (Jeon et al., 1998). These photoreceptors sense low-levels of light. In contrast, cones are responsible for color vision, and have heterogeneous spectral properties. Cones sense characteristic wavelengths of light, depending on the opsin isotype that they express. In primates, cones form a high-density cluster in the central retina called the fovea or macula, an avascular region that provides the highest acuity color vision (Yamada, 1969; Yuodelis and Hendrickson, 1986). In response to light, a cyclic GMP cascade is triggered by photoisomerization of a retinoid chromophore and conformational change in the photopigment protein (rhodopsin in rods, and L-, M-, or S-opsin in cones of trichromatic animals), leading to graded membrane hyperpolarization and stimulation of downstream bipolar neurons (Yau and Baylor, 1989).

Bipolar cell interneurons reside in the outer aspect of the INL. Their primary function is to transmit electrical signals from photoreceptors to ganglion cells, which reside in the GCL (Rodieck, 1998). Amacrine and horizontal interneurons also occupy characteristic positions in the inner and outer INL, respectively, and have distinct roles in the processing of visual information. These cells modulate the electrical signals of other neurons through excitatory or inhibitory inputs, enhancing spatial integration and contrast detection (Rodieck, 1998). Müller glia cells also have somata that are located in the INL, but their processes extend radially across the entire retinal thickness, from the outer

limiting membrane (OLM) to the inner limiting membrane (ILM) (Fig. I-1B). These glial cells are important for maintaining the physiology and laminar structure of the retina (Bringmann et al., 2006; Willbold et al., 2000).

Bipolar cells synapse on retinal ganglion cells (RGCs), whose cell bodies reside in the GCL. RGC axons coalesce to form the optic nerves, which project to areas in the central nervous system (CNS) that are responsible for visual processing, and autonomic tasks, including eye positioning and object tracking, modulating sensitivity to different levels of light, and controlling circadian rhythm (Rodieck, 1998). These areas include the superior colliculi (SC), the lateral geniculate nuclei (LGN), intergeniculate leaflets, the pretectum, the accessory optic system (AOS), and the suprachiasmatic nuclei (SCN) (Schiller and Malpeli, 1977; Simpson, 1984). A small number of RGCs have intrinsic photosensitivity (ipRGCs), express the photopigment melanopsin, project to the SCN, and are important for photoentrainment of circadian rhythms (Gooley et al., 2001; Hattar et al., 2002; Provencio et al., 1998). In addition to RGCs, the mammalian GCL contains displaced amacrine cells (Masland, 1988), which have similar functions as their INL counterparts.

There is significant diversity in the retina beyond the seven major cell types (Masland, 2001), with particularly many subclasses of amacrine (MacNeil and Masland, 1998), bipolar (Ghosh et al., 2004; Kim et al., 2008) and ganglion cell (Rockhill et al., 2002) neurons. The relative abundance of each retinal cell type is also quite different (Jeon et al., 1998). In particular, the ratio between photoreceptors (input) and RGCs (output) highlights the importance of signal

integration, and varies widely across the retina, giving different levels of spatial resolution. The overall number of photoreceptors vastly exceeds the number of bipolar cells (~11:1), which in turn exceeds the number of ganglion cells (~12:1). This integration greatly increases the sensitivity of the retina.

Control of retinal development

The vertebrate retina develops in two major phases. During the morphogenetic phase, the optic vesicles evaginate from the ventral diencephalon and invaginate to form bilayered optic cups (Chow and Lang, 2001; Spemann, 1901). Initially, there is an open cleft in the ventral retina, termed the optic or choroid fissure. Gradually, this closes during early development through a combination of cell signaling and adhesion (Barishak, 1992; Gregory-Evans et al., 2004). In the histogenic phase, beginning at embryonic day E11 in the mouse or 5th week in human gestation, some retinal progenitors (RPCs) begin to exit the cell cycle and differentiate, while most continue to proliferate to expand the progenitor pool.

Pioneering birthdating studies, in which [^{3}H]-thymidine was used to identify terminal progenitors by labeling the last phase of DNA replication, have established an invariant, but overlapping, histogenic birth order across all vertebrate species (Carter-Dawson and LaVail, 1979; Rapaport et al., 2004; Sidman, 1961; Young, 1985a) (Fig. I-2A). At the onset of neurogenesis, ganglion cells are the first cell type to exit the cell cycle and differentiate. In the mouse, RGC birthdates initiate at E11, peak at E14, and terminate by P0 (Drager, 1985;

Young, 1985a). This temporal profile overlaps significantly with that of cone, horizontal, amacrine cells. Rods, Müller glia and bipolar cells have characteristically later birthdates, which peak in the perinatal or neonatal periods in rodents.

Clonal analyses of retinal progenitors in frog and rodents, using retroviral or plasmid vectors with histochemical markers, have revealed that the seven major retinal cell types are generated from a common progenitor pool (Holt et al., 1988; Turner and Cepko, 1987; Turner et al., 1990; Wetts and Fraser, 1988). In these studies, composition and size among various clones was largely heterogeneous, suggesting that no strictly determined lineages exist in the retina, unlike those observed in the *C. elegans* nervous system (Ruvkun, 1997). Indeed, large clones could contain both "early" and "late" cell types. Additionally, the existence of two-cell clones with discordant fates suggests that commitment to a particular cell fate must occur during or after the terminal division.

Heterochronic co-culture and transplantation experiments in rodents likewise provided clues towards the mechanism of retinal fate determination. When "late" (post-natal) progenitors were mixed at low density with a large number of "early" cells (early embryonic), these "late" progenitors were incapable of adopting early fates, suggesting an intrinsic restriction in competence, i.e. the ability to respond to environmental signals (Belliveau and Cepko, 1999; Reh, 1992; Watanabe and Raff, 1990). In reciprocal experiments, "early" progenitors were capable of adopting "late" fates, such as rod photoreceptor fate (Reh, 1992; Watanabe and Raff, 1990). However, these RPCs were still heavily biased

towards “early” fates. In co-culture and transplantation experiments in frogs, early progenitors were incapable of adopting late fates, suggesting that competence in this species is temporally restricted (Rapaport et al., 2001).

The observations from heterochronic co-culture, clonal analysis, and birthdating experiments have led to the development of a temporal competence model for retinal development (Cepko et al., 1996; Livesey and Cepko, 2001; Reh and Cagan, 1994; Wong and Rapaport, 2009) (Fig. I-2B). In this model, progenitors progress through distinct intrinsic competence states in which RPCs can adopt one or a small number of cell fates. During development, RPCs either exit the cell cycle or continue to divide and progress to a new competence state. The decision to stop dividing, and the ultimate histotypic fate, for cells in a particular competence state is largely determined by environmental (extrinsic) signals.

Alternatively, this set of observations is also consistent with a progressive restriction model, similar to that proposed for the nervous system (Desai and McConnell, 2000). In this model, early progenitors are multipotent, but heavily biased toward the selection of early fates. As development proceeds, this bias is altered by the changing environment, and RPCs are gradually restricted in their selection of fates as the diversity of histotypic options narrows.

Cell divisions and the retinal cell cycle

In parallel with large changes in cell fate trajectory, there are alterations in temporal parameters of the progenitor cell cycle, and the mode of cell division. During early development, neural progenitors rapidly expand by employing a

symmetric self-renewing mode of division (P-P), in which both daughters continue to proliferate (Gotz and Huttner, 2005; Huttner and Kosodo, 2005; Lu et al., 2000). At the onset of neurogenesis, some progenitors give rise to daughter cells that permanently exit the cell cycle and differentiate into neurons. The vast majority of these divisions are asymmetric or stem-like (P-N), such that one daughter continues to proliferate, while the other differentiates. In contrast, very few symmetric terminal divisions occur (N-N), as these counteract the expansion of the progenitor pool. As development proceeds, the balance of divisions progressively shifts towards symmetric neurogenic divisions, which give rise to two post-mitotic daughter cells (N-N). It is unclear what role, if any, the mode of division (N-N vs. P-N) has on the final fate choice.

The kinetic parameters of the progenitor cell cycle also change significantly over developmental time. The eukaryotic cell cycle is anchored by two major events: S phase, in which DNA is replicated, and M phase, in which mitosis and cytokinesis occur (Nurse, 2000). These are separated by two gap phases, G2 and G1, respectively. Generally, G1 and S phases are the longest in the progenitor cell cycle, while cells rapidly progress through G2 and M phases (Young, 1985b). In the developing vertebrate retina, elongated progenitors span the pseudostratified neuroepithlium. Their nuclei migrate along radial spindles in a stereotypic oscillation, as cells progress through the cell cycle, in a process known as interkinetic nuclear migration (Baye and Link, 2008) (Fig. I-2C). Nuclei typically reside at the base of the retina (vitread surface) during DNA replication, quickly migrate towards the apical surface during G2, undergo mitosis at the

apical (sclerad) surface of the retina, and return to the base in G1. After terminal M phase, differentiating neurons migrate to their final laminar positions in the neuroepithelium.

The dynamics of the RPC cell cycle have been extensively characterized in rodents and other vertebrate species by window and cumulative nucleoside labeling, cell counting, and percent labeled mitosis (PLM) methods (Alexiades and Cepko, 1996; Fujita, 1962; Li et al., 2000; Sinitsina, 1971; Young, 1985b). The common conclusion from these studies is that the overall cell cycle progressively lengthens during development. This increase is largely attributed to prolonged G1 and S phases of the cell cycle (Alexiades and Cepko, 1996; Young, 1985b). Though much is known about the kinetics of the RPC cell cycle, it remains unclear what role cycle dynamics play in the ultimate cell fate choice.

It is clear, however, that the cell cycle exit and fate determination are correlated. Genetic overexpression or loss of cell cycle regulators, such as p27, p57, Rb, cyclinD1, can have wide-spread effects on the retina, including the distribution of retinal cell types (Das et al., 2009; Dyer and Cepko, 2000; Fantl et al., 1995; Ohnuma et al., 1999; Zhang et al., 2004). Mitogenic factors, such as Notch or Shh signaling molecules, tend to promote generation of “late” fates (Jadhav et al., 2006; Levine et al., 1997); while loss of these and the presence of neurogenic factors promote the generation of “early” fates (Dyer et al., 2003; Riesenberg et al., 2009; Yaron et al., 2006). Despite these large influences, cell cycle progression is not required for the generation of a wide array of neuronal cell types in frog retina (Harris and Hartenstein, 1991). Thus, it remains to be

determined whether many of these effects are secondary to differences in the retinal microenvironment or to the reduced number of RPCs during late stages of development.

Despite many studies on fate determination and the cell cycle, the precise timing of the fate decision relative to cycle exit is unknown. Some cells, such as VC1.1+ amacrine precursors, may lose responsiveness to environmental signals prior to terminal M phase (Belliveau and Cepko, 1999), similar to progenitors in the ferret cortex (McConnell and Kaznowski, 1991). However, post-mitotic precursors can also be biased toward other fates by intrinsic or environmental signals (Adler and Hatlee, 1989; Brzezinski et al., 2010; Oh et al., 2007). Given this heterogeneity in environmental response, it remains unclear whether the fate decisions are made before or after terminal mitosis, and whether this property varies among different cell types and different developmental stages.

Cell death in the retina

Programmed cell death is an additional regulatory mechanism that ensures proper ratios of each cell type in the retina. During development, some cell types are produced in vast excess. Half of the neurons in the GCL and INL are culled during development (Voyvodic et al., 1995; Young, 1984). Inhibition of programmed cell death pathways, by overexpression of *Bcl-1* or deletion of *Bax*, can significantly reduce this culling, indicating that canonical apoptosis is the major regulatory mechanism (Martinou et al., 1994; Pequignot et al., 2003). The death of the ganglion cells has been most extensively examined. It is estimated

that 50-70% of RGCs undergo cell death, with peak apoptosis in the neonatal period (Crespo et al., 1985; Erkman et al., 2000; Farah and Easter, 2005; Galli-Resta and Ensini, 1996; Strom and Williams, 1998; Young, 1984). Activity-dependent axon competition and defects in pathfinding are thought to be the major mechanism underlying this neonatal cell death (Fawcett et al., 1984; O'Leary et al., 1986; Scheetz et al., 1995).

Intrinsic and extrinsic signals in retinal development

The relative contribution of an intrinsic transcription program ("clock") and extrinsic signals in fate specification is heavily debated. Dissociated rat retinal progenitors can produce a similar composition of progeny as those in the intact retina, suggesting that progenitors retain at least a rudimentary intrinsic program (Cayouette et al., 2003). This program is largely stochastic, but can generate the appropriate numbers of various cell types (Gomes et al., 2011). Similarly, progenitors in the frog retina appear to follow a rigidly fixed order of cell genesis within clones, such that a single progenitor is only competent to produce only one cell type at a given time (Wong and Rapaport, 2009). These results suggest that a "hard-wired" intrinsic program is the dominant mechanism for retinal development.

Despite the prominent role of intrinsic factors in specification, signals from the retinal environment have a tremendous impact on the ultimate fate choice, and can effectively override the intrinsic program. The retina has adapted many negative feedback signals to ensure proper ratios of cell types. For example,

Delta ligands and secreted Shh, which are produced by nascent RGCs, are known to negatively RGC genesis (Austin et al., 1995; Belliveau and Cepko, 1999; Waid and McLoon, 1998; Wang et al., 2005; Zhang and Yang, 2001). These same signaling pathways (Notch and Hedgehog) also promote the generation of other cell types (Furukawa et al., 2000; Jadhav et al., 2006; Levine et al., 1997; Shkumatava et al., 2004). It is unclear, however, whether these effects on cell fate are secondary to altering general progenitor dynamics (Austin et al., 1995; Jensen and Wallace, 1997; Levine et al., 1997). For example, the mitogenic and fate effects of Notch signaling are intertwined. Inhibition of the Notch pathway may promote early fates simply by causing premature cell cycle exit, increasing the fraction of cells that are specified in an early environment (Austin et al., 1995; Nelson et al., 2007). Additionally, extrinsic factors can have dual roles. They can support the differentiation of a particular cell type, while inhibiting specification of new cells. For example, Shh produced in RGCs can also promote axon pathfinding among nascent ganglion cells (Kolpak et al., 2005; Sanchez-Camacho and Bovolenta, 2008). A vast array of other signaling molecules, including ciliary neurotrophic factor (CNTF), fibroblast growth factor (FGF), and transforming growth factor (TGF), also actively fine tune the production of different cell types in the retina (Cepko, 1999; Ezzeddine et al., 1997; Kim et al., 2005; Yang, 2004).

In an integrated view of retinal histogenesis, cell fate is fundamentally controlled by intrinsic transcriptional cascades, which are influenced by the environment (Fig. I-2D). A critical point in a progenitor's life history is the

decision to exit the cell cycle. Thus, several core homeodomain (HD) and basic-helix-loop-helix (bHLH) transcription factors, such as Chx10, Pax6, and Hes1, are thought to control the progenitor proliferation and maintain RPCs in an undifferentiated state (Ashery-Padan and Gruss, 2001; Marquardt, 2003; Takatsuka et al., 2004).

Histotypic differentiation, the acquisition of unique cellular morphology and functional features, is controlled by downstream transcriptional hierarchies, which are similarly complex (Fig. I-2D). Although precise control of specification remains largely unclear, many insights have emerged in recent years regarding the hierarchy of differentiation from analysis of gene expression in loss- and gain-of-function animal models. For example, in the development of inhibitory amacrine and horizontal cells, it clear that both the HD factor FoxN4 and bHLH factor Ptf1a (P48) are necessary for the development of these cell types, and also bias progenitors toward this fate (Fujitani et al., 2006; Li et al., 2004). The pattern of molecular epistasis (Lehner, 2011) in reciprocal mutants suggests that *FoxN4* precedes *Ptf1a* in the pathway. Loss of *Ptf1a* does not affect *FoxN4* expression, but loss of *FoxN4* impairs *Ptf1a* expression. Thus, a clear hierarchy emerges, in which *FoxN4* functions upstream of *Ptf1a* (Fujitani et al., 2006). Similar transcriptional hierarchies have been established for the differentiation of photoreceptors and other cell types (Ohsawa and Kageyama, 2008; Swaroop et al., 2010). However, basic mechanisms controlling the fate choice, i.e. the events that trigger these cascades, remain largely unknown.

Math5 (*Atoh7*) and control of RGC fate

The identification of the fly *atonal* homolog *Math5* (mammalian atonal homolog 5), also known as *Atoh7* (atonal homolog 7) in vertebrate species provided a critical insight into the mechanism of RGC development. In *Drosophila*, *atonal* is vital for the specification of the first retinal neuron in the fly ommatidium, the R8 photoreceptor (Jarman et al., 1994), which allows formation of photoreceptors R1-R7 through a series of cell-cell inductive interactions. In the vertebrate eye, this function of *atonal* is conserved, in that RGCs are the first-born cell type. Homologs of *atonal* have been identified in the frog (Kanekar et al., 1997), mouse (Brown et al., 1998), chicken (Liu et al., 2001; Matter-Sadzinski et al., 2001), and human genomes (Brown et al., 2002). In mice, *Math5* is transiently expressed in a small population of retinal precursors in a pattern that closely follows the RGC birthdating curve, with onset at E11 and cessation by birth (Brown et al., 1998; Brown et al., 2001).

Atoh7 (*Math5*) is necessary for the development of more than 95% of ganglion cells (Brown et al., 2001; Wang et al., 2001) (Fig. I-3). Although RGCs represent on 0.5% of adult retinal cells (Jeon et al., 1998), *Atoh7* mutant mice have significantly thinner retinas (Brzezinski et al., 2005), ostensibly due to loss of mitogenic effects from RGC-derived Shh (Dakubo and Wallace, 2004; Jensen and Wallace, 1997; Levine et al., 1997). In the absence of RGC axons, there are essentially no optic nerves. Because the optic nerves convey all photic stimuli to the brain, mutant mice have no pupillary light reflex and their endogenous circadian rhythms do not entrain to light (Brzezinski et al., 2005; Van Gelder et

al., 2003; Wee et al., 2002). Because the inner retina is thin, and bipolar neurons are deficient, the mutants have abnormal retinal electrophysiology, with reduced *b*-wave amplitudes in electroretinogram (ERG) recordings (Brzezinski et al., 2005). *Math5* -/- mice retain each of the other 7 major cell types, indicating that *Math5* is only required for ganglion cell development. Similarly, in zebrafish, the ortholog *ath5* is required for RGC development, as a point mutation in this gene (*lakritz*) causes agenesis of RGCs and optic nerves (Kay et al., 2001).

Although *Math5* is required for RGC development, it acts as a permissive factor for RGC genesis. Lineage-tracing studies using a *Math5-Cre* knock-in allele and BAC transgene have shown that Math5 descendents comprise most major cell types in addition to RGCs (Brzezinski and Glaser, 2004; Feng et al., 2010; Yang et al., 2003). Likewise, *Math5* over-expression studies in chick and frog suggest that this factor is not instructive for RGC fate. In both species, overexpression of orthologs *Xath5* and *Cath5* in proliferating RPCs during early development mildly biases progenitors toward the RGC fate (Brown et al., 1998; Kanekar et al., 1997; Liu et al., 2001). However, when *Xath5* is misexpressed during late developmental stages in frogs, it promotes other neuronal fates (Moore et al., 2002). In general, high-level expression of proneural bHLH factors may drive cell cycle exit and neuronal differentiation (Farah et al., 2000). Thus, the observed shifts in fate distribution may largely be due to this property of bHLH factors, rather than a specific role of ath5.

The hierarchy of RGC differentiation remains incompletely understood despite many genetic and genomic studies (Mu and Klein, 2004). It is clear that

POU-domain Brn3b (Pou4f2) and LIM-domain Isl1 (Islet-1) transcription factors form two important regulatory nodes in ganglion cell specification and differentiation (Mu et al., 2008; Pan et al., 2008). These factors, which are thought to function downstream of *Math5*, are necessary for RGC development and have distinct, but overlapping, transcriptional targets (Erkman et al., 1996; Gan et al., 1996; Mu et al., 2008; Pan et al., 2008; Xiang, 1998). Brn3b is likely to act as an instructive factor for RGC specification. It is expressed exclusively in most developing RGCs and biases progenitors toward the RGC fate when ectopically expressed (Badea et al., 2009; Feng et al., 2011; Liu et al., 2000; Qiu et al., 2008). Two closely related paralogs, Brn3a and Brn3c, are functionally interchangeable with Brn3b at the protein level (Liu et al., 2000; Pan et al., 2005). However, their distinct spatiotemporal expression patterns confer unique roles in RGC differentiation (Badea et al., 2009; Wang et al., 2002a; Xiang et al., 1995; Xiang et al., 1993). Transcriptional profiling of *Brn3b* and *Math5* knockout retinas has led to the identification of other factors that function downstream in RGC differentiation, such as HD protein eomesodermin (*Eomes/Tbr2*) (Mao et al., 2008a; Mu et al., 2004). Despite these advances, much remains to be learned about the factors that control the RGC fate decision and downstream differentiation events.

Retinal vascular development and the role of RGCs

The retina is supplied by two major vascular systems (Fruttiger, 2007; Gariano and Gardner, 2005; Provis, 2001). The outer retina is supplied by diffusion from high-flow, fenestrated vessels in the choroid layer. The inner

retina is supplied by the hyaloid artery, which enters the eye through the optic stalk and the embryonic fissure during early development (Zhu et al., 1999). The choroidal and hyaloid vessels branch from the dorsal ophthalmic artery. The hyaloid artery extends into the vitreous and forms the hyaloid vascular network, which nourishes the lens and the inner retina (Fig. I-4). In order to accommodate vision through an optically clear media, this vasculature remodels during the early post-natal period in mice or late gestation in humans (Fruttiger, 2007; Gariano and Gardner, 2005). The hyaloid vasculature regresses by apoptosis of vascular endothelial cells, which is triggered by macrophage phagocytosis (Lang et al., 1994). In turn, the blood vessels sprout by angiogenesis, following a migrating astrocyte network that initiates at the optic stalk and spreads radially along the inner surface of the retina (Fruttiger, 2007). These surface vessels then dive into the retina to form two deep vascular plexi that surround the INL and supply the inner retina. Astrocytes, marked by platelet-derived growth factor receptor alpha (PDGFRα) expression, form a scaffold for angiogenesis and are important for proper development of the vasculature (Dorrell et al., 2002; Laterra et al., 1990; Watanabe and Raff, 1988). RGCs elaborate platelet-derived growth factor A ligand (PDGFRA), sonic hedgehog (Shh), and other trophic molecules that are critical for astrocyte proliferation and migration (Dakubo et al., 2003; Fruttiger et al., 1996; Fruttiger et al., 2000).

The retinal vasculature develops abnormally in *Atoh7* mutant mice lacking RGCs (Brzezinski et al., 2003; Edwards et al., 2011) (Fig. I-4). In these mice, the mature retinal vasculature fails to form and the hyaloid vasculature persists,

continuing to supply the mature retina. These abnormal vessels typically invade and neovascularize the neural retina, and they are prone to hemorrhage, which can occur in the subretinal space, vitreous, or spread into the anterior chamber (Brown et al., 2001; Brzezinski et al., 2003).

Diseases of the optic nerve and retinal vasculature

Congenital optic nerve diseases are important causes of hereditary blindness (Taylor, 2007). Optic nerve hypoplasia (ONH), in which nerves are reduced in size, and optic nerve aplasia (ONA), in which nerves are completely absent, are thought to be caused by primary defects in the specification, differentiation, or survival of RGCs (Lambert et al., 1987). The less severe clinical entity, ONH, is much more common than ONA (Borchert and Garcia-Filion, 2008). Each can occur as an isolated malformation, or as part of a syndrome, together with central nervous system (CNS) and pituitary defects (Borchert and Garcia-Filion, 2008; McCabe et al., 2011). In ONA, the mature retinal vasculature typically fails to develop, and fetal vessels may persist in the vitreous (Blanco et al., 1992; Brodsky et al., 2004; Lee et al., 1996; Little et al., 1976; Scott et al., 1997). Most cases of ONA and ONH are sporadic. Few genetic causes have been identified and these explain only a very small fraction of cases. Mutations in *HESX1, OTX2*, *SOX2* or *PAX6* can lead to severe ONH or ONA (Azuma et al., 2003; Dattani et al., 1998; Kelberman and Dattani, 2007; McCabe et al., 2011; Ragge et al., 2005). These Mendelian cases usually present with hypothalamic-pituitary dysfunction, and global eye and CNS malformations. The diagnostic terms Syndrome of Optic Nerve Hypoplasia

(SONH), Septo-Optic Dysplasia (SOD) or de Morsier syndrome (MIM 182230) are applied when ONH coexists with hypoplasia of the midline structures such as the pituitary, hypothalamus or septum pellucidum (Borchert and Garcia-Filion, 2008; Brodsky and Glasier, 1993; De Morsier, 1962; Haddad and Eugster, 2005).

Other hereditary diseases may affect the physiology of ganglion cells. These include Leber's hereditary optic neuropathy and autosomal dominant optic atrophy. These diseases involve mtDNA genes or autosomal loci that encode mitrochondrial proteins. The pathology is predominantly caused by mitochrondrial dysfunction, which ultimately leads to RGC cell death (Abu-Amero, 2011; Olichon et al., 2006). It remains to be determined why RGCs are particularly prone to these metabolic defects, but it is hypothesized that accumulation of reactive oxygen species in mitochrondria at the optic disc leads to degeneration (Ghelli et al., 2003; Howell, 1998; Olichon et al., 2006) and may be correlated with the degree of myelination (Carelli et al., 2002; Sadun and Carelli, 2003).

Glaucoma is a leading cause of bilateral blindness worldwide (Lee and Higginbotham, 2005; Quigley, 1996). Genetic analysis has provided many insights into the pathogenesis of this disease (Allingham et al., 2009; Challa, 2004). Glaucoma is caused by optic nerve head injury or dysfunction, which ultimately leads to RGC cell death. Often this insult is triggered by increased intraocular pressure (IOP) due to inadequate drainage of front of the eye (the anterior segment). However, many cases of glaucoma can present with normal IOP (normal tension glaucoma), and thus may be caused by primary defects in RGC function (Buono et al., 2002), and longstanding ocular hypertension has

been noted in some patients with normal vision (Copt et al., 1999). Despite numerous advances in recent years, many cases of glaucoma remain unexplained, and the pathogenesis is incompletely understood.

Retinal vascular diseases are also major causes of blindness (Gariano and Gardner, 2005). Retinopathy of prematurity (ROP) is vascular disorder that primarily affects premature infants and can be triggered by excessive oxygen exposure in newborns. It is characterized by vascular loss and incomplete vascularization followed by a compensatory hyperproliferation of the remaining retinal vessels (Chen and Smith, 2007). ROP can be accompanied by persistent hyperplasia of the primary vitreous (PHPV). In this disorder, the primary fetal vasculature fail to regress, likely due to impaired apoptosis, abnormalities in the mature vascular development, or hypoxic conditions (Goldberg, 1997; Reese, 1955; Shastry, 2009). Most cases are sporadic, but rare familial cases have been characterized (Haddad et al., 1978; Khaliq et al., 2001). PHPV predisposes retinas towards detachment, hemorrhage, and anterior chamber defects (Pruett, 1975). A small number of cases may be explained by genetic defects in the Wnt signaling pathway (Robitaille et al., 2009). Mutations in these genes can also cause Norrie's disease or familial exudative vitreoretinopathy (FEVR), which share similar clinical features (Berger et al., 1992a; Berger et al., 1992b; Gariano and Gardner, 2005; Robitaille et al., 2009). Few other genetic causes for these diseases have been identified.

Novel insights into RGC development and the role of Math5 (*ATOH7)*

Ganglion cells play an essential role in the visual system. They transmit all visual information to the CNS and are required for the development of retinal vasculature. Thus, the development of RGCs remains an important area of study for understanding the causes of blindness and the mechanisms of visual system development. In this dissertation, I have focused my analysis on the *ATOH7* (*Math5*) gene, which plays a particularly important role in the initial development of this retinal cell type.

In Chapter II, I thoroughly and systematically analyze the transcriptional architecture of the mouse *Math5* gene. I found that this single-exon gene makes one predominant mRNA isoform, which is unspliced. This study starkly contrasts a prior report that suggested a *major* role of alternative splicing in the regulation of the gene (Kanadia and Cepko, 2010).

In Chapter III, Joseph Brzezinski and I quantitatively characterized the lineage and cell cycle properties of the *Math5*-expressing cells. We show that *Math5* is variably expressed in progenitors during or after their terminal cell cycle, with a gradual restriction to post-mitotic cells as development proceeds. Using Math5>Cre BAC transgenic mice, we show that only 11% of lineage-derived cells adopt the RGC fate, and that only 55% of ganglion cells are marked by *Math5* expression. Surprisingly, the *Math5*-independent fraction is substantial even during early development, suggesting a non-autonomous role of *Math5* in ganglion cell fate specification.

In Chapter IV, I extend the analysis of *Math5* cell cycle dynamics by examining the properties of key transcription factors in RGC, amacrine, and horizontal cell development. Surprisingly, I found that Brn3b, a marker of committed RGCs, and co-regulator Isl1 can be expressed in some cells prior to the last progenitor mitosis. Consistent with fate specification prior to cycle exit, I observed pairs of Brn3b+ cells during cytokinesis and clonal pairs of RGCs resulting from terminal symmetric divisions in retinal explants. These results suggest that the cell fate decision is not synchronized to cycle exit.

In Chapter V, I thoroughly test the sufficiency of *Math5* (*Atoh7*) in promoting ganglion cell fate, or biasing retinal progenitors. By broadly overexpressing *Math5* in mouse neurogenic cells using a transgene with Crx (cone-rod homeodomain) regulatory DNA, I found that *Math5* does not extensively promote RGC fate in the wild-type retinal environment. In contrast, ectopic *Math5* can partially rescue RGC fate in *Math5* -/- mice. However, given the late temporal profile of transgene expression, the rescue is heterochronic, such that early-born RGCs are absent. The transgene-derived, late-born RGCs exhibit pathfinding defects and undergo apoptosis, suggesting that early RGCs provide vital trophic support for late-born RGCs.

In Chapter VI, we explore the role of human *ATOH7* in optic nerve and vascular diseases of the retina. We identified point mutations in a family with autosomal recessive PHPV and a sporadic case of bilateral optic nerve hypoplasia. Subsequently, I characterized these point mutations through biochemical and functional studies. I found a p.N46>H mutation in the arPHPV

family to be the likely cause of disease, as the mutant protein is incapable of binding to DNA, activating transcription, or rescuing ganglion cell development in *Atoh7* -/- mouse retinal explants. Taken together, this dissertation highlights the importance of *ATOH7* in eye development and disease, and provides novel insights into the structure and function of ATOH7 and the development of RGCs.

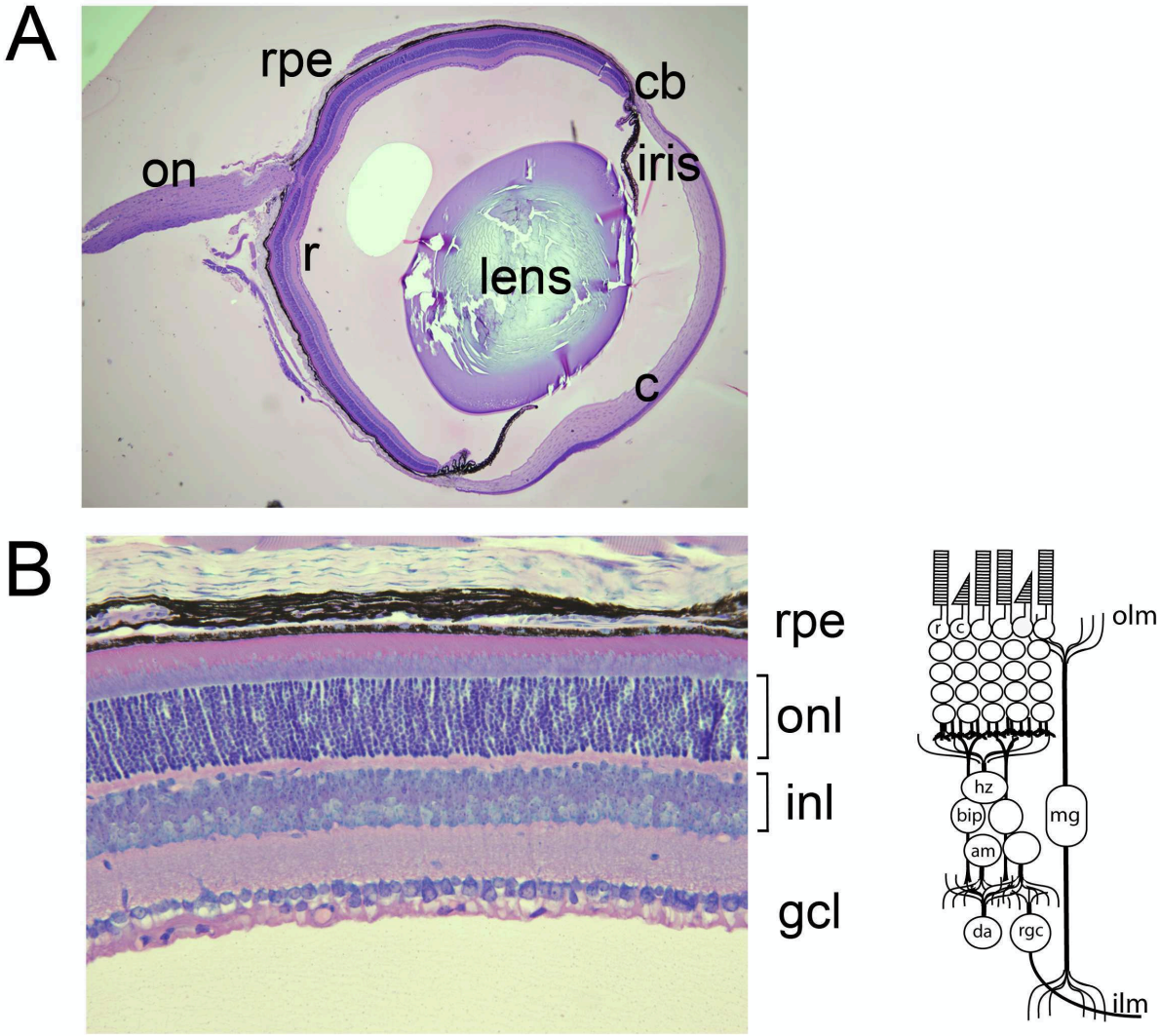

Figure I-1. Structure of the eye and retina. (A) Basic fuschin and methylene blue staining of a central section of a mouse eye. Major structures of the eye are highlighted. (B) H+E staining showing the trilaminated mouse retina. A schematic diagram of the 7 major retinal cell types is shown on the right. rpe, retinal pigmented epithelium; on, optic nerve; ret, retina; cb, ciliary body; corn, cornea; onl, outer nuclear layer, inl, inner nuclear layer; gcl, ganglion cell layer; ilm, inner limiting membrane; olm, outer limiting membrane; r, rod; c, cone; hz, horizontal neuron; bip, bipolar cell; am, amacrine; da, displaced amacrine; rgc, retinal ganglion cell; mg, Müller glia.

Figure I-2. Molecular mechanisms of retinal development. (A) Schematic birthdating curves for the 7 major cell types. Ganglion cells are the first born cell-type, but there is extensive overlap among birthdates across the 7 cell types. Adapted from (Marquardt and Gruss, 2002). (B) The serial competence model posits that retinal progenitors pass through discrete competence states in which they can adopt a small number of cell fates. Cell fate within these states is determined largely by environmental influences. Adapted from (Livesey and Cepko, 2001). (C) Adapted from (D) Transcription factors in retinal development. The diagram shows the major steps in retinal histogenesis, and several key intrinsic transcription factors that are involved in the specification and differentiation of each cell type.

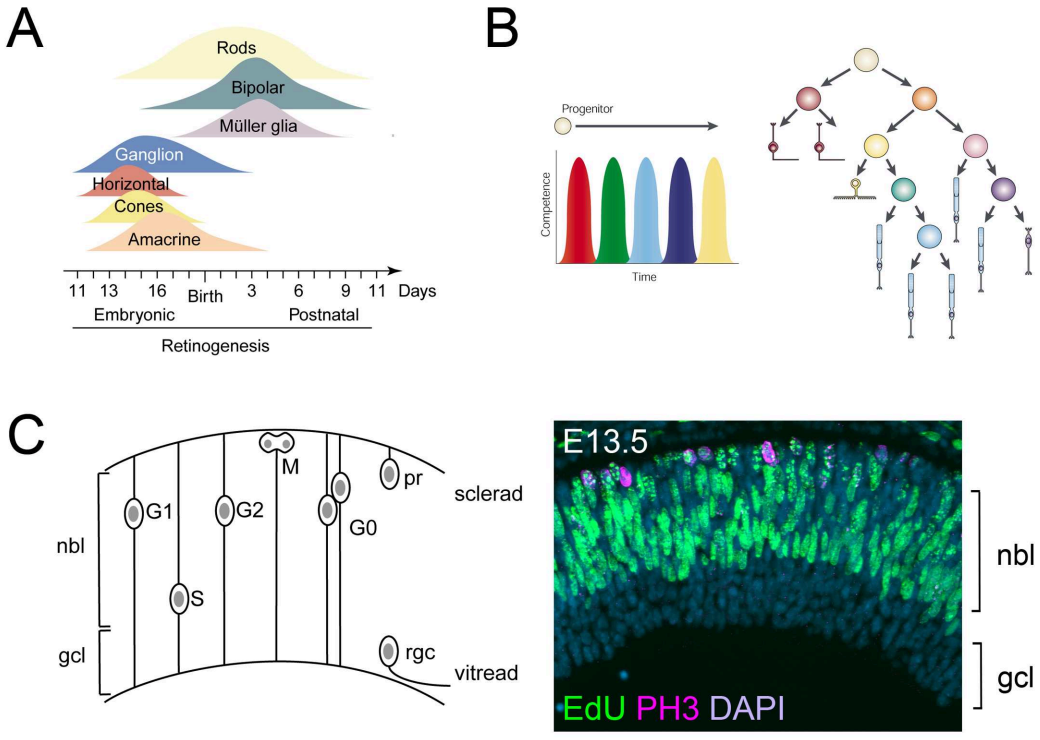
A
Rods
Bipolar
Müller glia
Ganglion
Horizontal
Cones
Amacrine
11 13 16 Birth 3 6 9 11 Days
Embryonic
Postnatal
Retinogenesis
B
Progenitor
Competence
Time
C
M
pr
sclerad
G1
G2
G0
nbl
S
gcl
rgc
vitread
E13.5
nbl
gcl
EdU PH3 DAPI
D
Pax6
Rx1 Six3
Lhx2 Six6
Chx10
Hes1
RPCs
1. maintaining the progenitor pool
Pax6
Math5
Math3
Mash1
Chx10
Pax6/Six3
Math3
NeuroD
Prox1
FoxN2
Otx2
Ngn2
NeuroD
Otx2
Ngn2
Crx
Rx1
Notch
Hes1
2. establishing competence
Brn3b
Brn3a
Isl1
Chx10
Crx
Pax6/Six3
Math3
NeuroD
Prox1
FoxN2
Ptf1a
NRL
Nr2e3
Blimp1
Trβ2
Blimp1
NeuroD
Rx1
Notch
Hes1
3. cell fate committment and differentiation
RGC
BiP
Am
Hz
rod
cone
MG
4. mature cell types

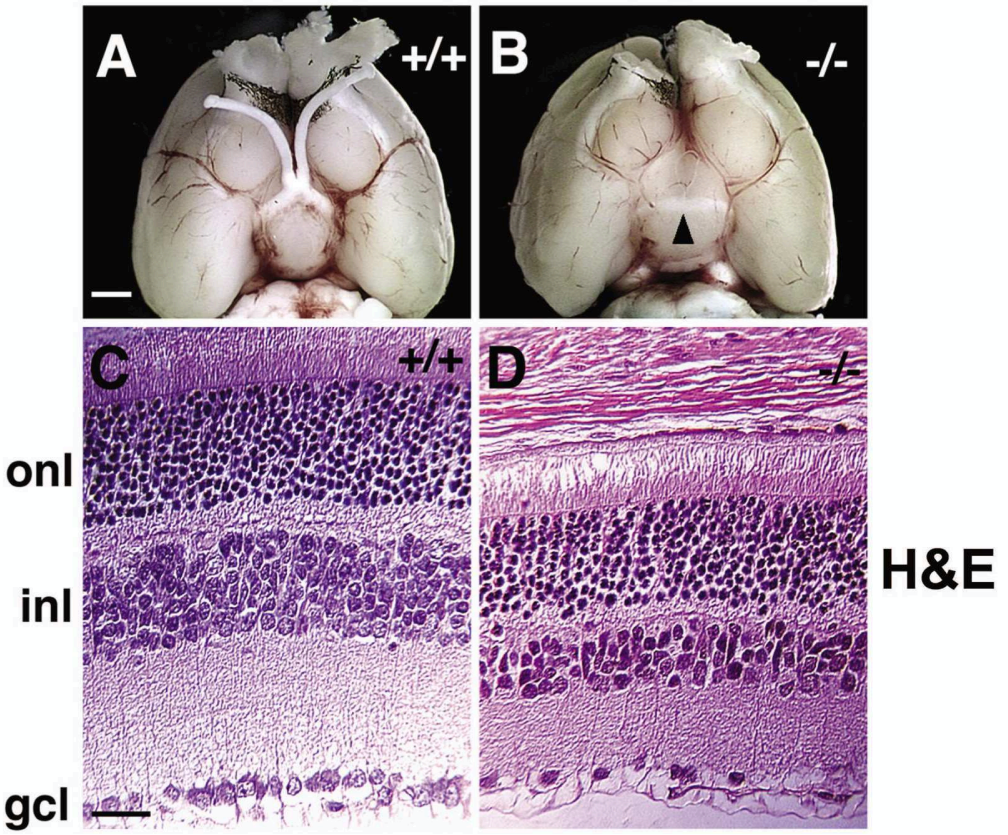

Figure I-3. *Math5* (*Atoh7*) knockout mice have no optic nerves, and severe deficiencies in RGCs. (A-B) Views of the brain of wild-type (A) and *Math5* -/- mice (B). The optic chiasm and nerves are absent in *Math5* -/- mice. (C-D) Hematoxylin and eosin staining of retinal sections from wild-type (C) and *Math5* -/- (D) mice. *Math5* mutant retinas are thinner than wild-type, and have a hypocellular ganglion cell layer that is composed of displaced amacrine cells. Adapted from Brown et al., 2001. onl, outer nuclear layer; inl, inner nuclear layer; gcl, ganglion cell layer.

Figure I-4. Development of the retinal vasculature. (A-H) Vasculature development in wild-type (WT) and *Math5* -/- mice. In wild-type mice (A, C, E, G), intrinsic retinal vasculature (red, arrows) spreads radially following an astrocyte network, while hyaloids vessels (arrowheads) regress over time. In *Math5* -/- mice (B, D, F, H), intrinsic vasculature fails to sprout by angiogenesis from the area of the putative optic nerve (*). Instead, hyaloid vessels proliferate and spread across the inner retina. (I) Models of vascular development in wild-type and *Math5* -/- mice. Images adapted from (Brzezinski, 2005) and (Edwards et al., 2011).

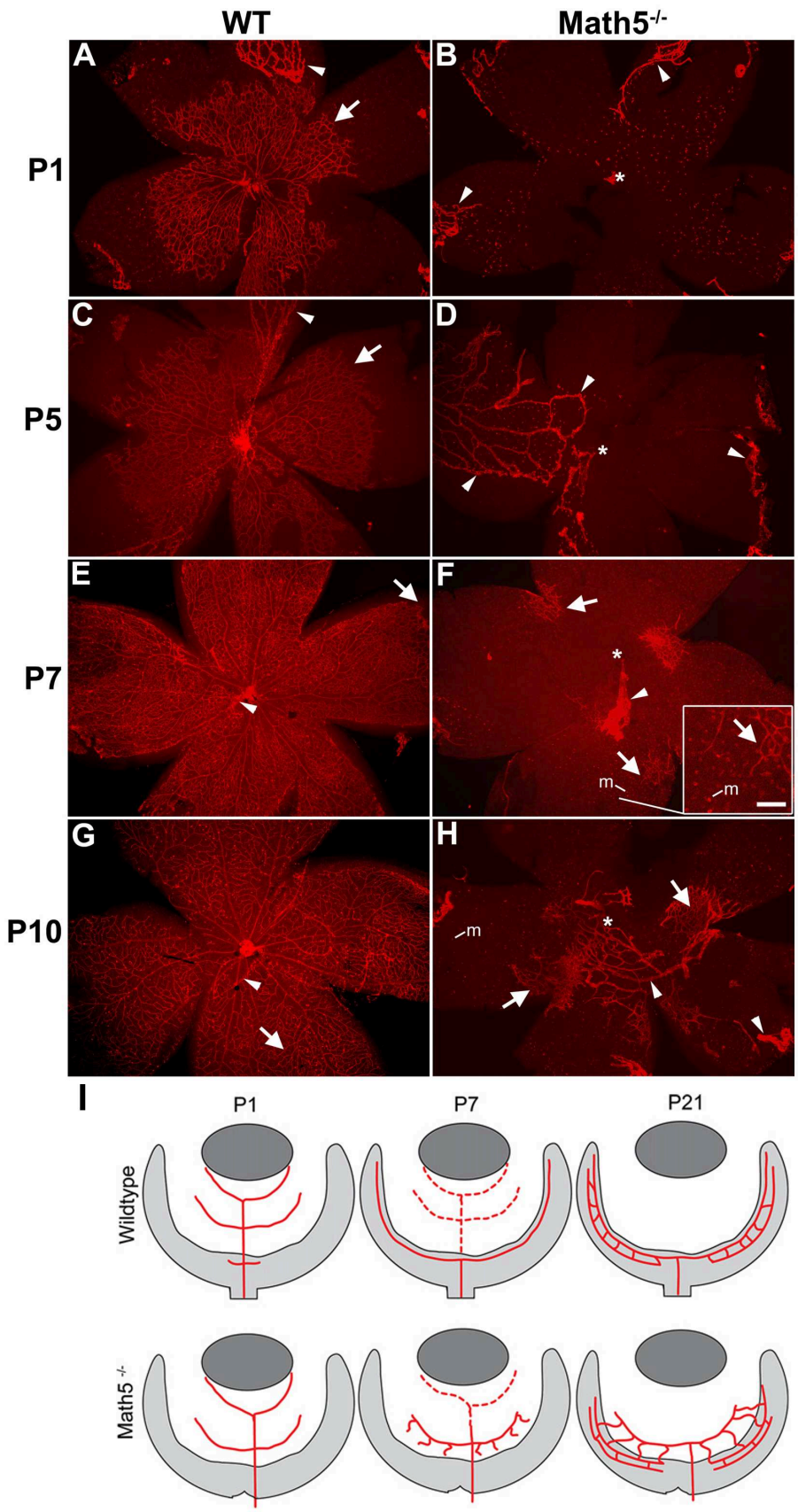
WT
Math5-/-
A
B
P1
C
D
P5
E
F
P7
m
m
G
H
P10
m
I
P1
P7
P21
Wildtype
Math5 -/-

CHAPTER II

A CRITICAL ANALYSIS OF *MATH5 (ATOH7)* mRNA SPLICING IN THE DEVELOPING MOUSE RETINA

Abstract

The *Math5* (*Atoh7*) gene is transiently expressed during retinogenesis by progenitors exiting mitosis, and is essential for ganglion cell (RGC) development. *Math5* contains a single exon, and its 1.7 kb mRNA encodes a 149-aa polypeptide (Brown *et al.* 1998). Mouse *Math5* mutants have essentially no RGCs or optic nerves. Given the importance of this gene in retinal development, we thoroughly investigated the possibility of *Math5* mRNA splicing by Northern blot, 3' RACE, RNase protection assays, and RT-PCR, using RNAs extracted from embryonic eyes and adult cerebellum, or transcribed *in vitro* from cDNA clones. Because *Math5* mRNA contains an elevated G+C content, we used graded concentrations of betaine, an isostabilizing agent that disrupts secondary structure. Although ~10% of cerebellar *Math5* RNAs are spliced, truncating the polypeptide, our results show few, if any, spliced *Math5* transcripts exist in the developing retina (<1%). Rare deleted cDNAs do arise via RT-mediated RNA template switching *in vitro*, and are selectively amplified during PCR. These data differ starkly from a recent study (Kanadia and Cepko 2010), which concluded that the vast majority of *Math5* and other bHLH transcripts are spliced to

generate noncoding RNAs. Our findings clarify the architecture of the *Math5* gene and its mechanism of action.

Introduction

The vertebrate retina develops from a single multipotent progenitor population, which gives rise to seven major cell types – rod and cone photoreceptors; amacrine, bipolar and horizontal interneurons; Muller glia; and retinal ganglion cells (RGCs) (Holt et al., 1988; Turner and Cepko, 1987). These diverse cell types emerge from the mitotic progenitor pool in rough sequential order, with overlapping birthdates (Livesey and Cepko, 2001; Wong and Rapaport, 2009). RGCs are the first-born retinal cell type in every vertebrate examined (Altschuler et al., 1991). These cells transmit all visual information from the eye to the brain, via their axons, which comprise the optic nerves. The gene network regulating retinogenesis is an active area of investigation.

An important clue toward understanding the mechanism of vertebrate retinal fate specification was the discovery of Math5 (Atoh7), a proneural basic-loop-helix (bHLH) transcription factor that is evolutionarily related to *Drosophila* Atonal and mouse Math1 (Atoh1) (Brown et al., 1998; Kanekar et al., 1997). The mouse *Math5* gene is expressed transiently in retinal cells exiting mitosis, from E11.5 until P0, in a pattern that is correlated with the onset of neurogenesis, and it is necessary for RGC fate specification. *Math5* mutant mice lack RGCs and optic nerves (Brown et al., 2001; Wang et al., 2001), and have secondary defects in retinal vascularization (Brzezinski et al., 2003) and circadian photoentrainment

(Brzezinski et al., 2005). In zebrafish, the homologous *lakritz* mutation also causes RGC agenesis (Kay et al., 2001), and in humans, the *ATOH7* gene may be associated with congenital optic nerve disease (Brown et al., 2002). Although the exact mechanism of *Math5* action remains unknown, it is thought to confer an RGC competence state on early retinal precursors (Brzezinski and Glaser, 2004; Yang et al., 2003). A number of potential target genes are misregulated in *Math5* mutant retinas (Mu et al., 2005). Apart from the retina, expression domains have been defined in the hindbrain cochlear nucleus and cerebellum (Saul et al., 2008).

During our initial characterization of *Math5* (Brown et al., 1998), we identified multiple independent retinal cDNA clones, which were colinear and coextensive with mouse genomic DNA. The internal sequence and termini of these clones were consistent with a single-exon transcription unit.

In a recent provocative study, Kanadia and Cepko (2010) report that the vast majority of *Math5* transcripts in embryonic mouse retinas are spliced, with donor and acceptor sites located in the 5' and 3' UTRs, such that the coding sequences are excised. This conclusion, which plainly differs from our previous studies (Brown et al., 2002; Brown et al., 1998), was based largely on the size and abundance of particular RT-PCR products. Similar observations were reported for *Ngn3* (neurogenin, *Neurog3*), a related bHLH factor. If correct, these findings raise important questions regarding the origin, extent and function of noncoding (nc) bHLH-gene RNAs, which may integrate into larger gene regulatory networks during neural development (Mercer et al., 2009), and

suggest that abortive splicing may be utilized as a novel post-transcriptional mechanism to regulate bHLH gene expression. Given the importance of *Math5* for retinogenesis, the central role of bHLH factors in neuronal fate specification (Bertrand et al., 2002), and the possibility that functional coding and noncoding RNAs may be generated in the same orientation by alternative splicing of a single transcription unit (Chooniedass-Kothari et al., 2004), we have systematically evaluated *Math5* mRNA splicing in the developing retina, using RNA hybridization and RT-PCR methods adapted for the extreme G+C content of the transcript.

Our data strongly suggest that the apparently frequent splicing of *Math5* retinal mRNA is a technical artifact, resulting from: (1) profound secondary structure in the mRNA, promoting template switching during reverse transcription *in vitro*, (2) selective amplification of deleted products lacking the internal GC-rich segment; and (3) the existence of very rare mis-spliced molecules, representing less than one percent of *Math5* transcripts. Our results refine the structure of the *Math5* transcription unit, explore the concept of an intronless gene, and provide a cautionary lesson for PCR-based studies of RNA processing.

Materials and Methods

Plasmid clones and oligonucleotides

Math5 clone pJN4C (accession nos. AF071223, AF418923) was derived from a neonatal C57BL/6 retinal cDNA library (Brown et al., 1998). It contains 318 bp 5' UTR, 447 bp coding sequence (CDS) and 390 bp 3' UTR, and terminates at an A-rich stretch in the 3' UTR. Clones JN1 and JN2 extend 55 bp and 279 bp further

in the 5' and 3' directions, respectively (Fig. II-1). Plasmid vector pCR4-TOPO (Invitrogen) was used for TA cloning of RT-PCR products, including the templates used for RPA probes. All custom PCR primers in this study are indicated in Fig. II-1A and listed in Table II-S1.

RNA

Total RNA was isolated from eyes or retinas dissected from CD-1 mouse embryos (ages E14.5 and E15.5) and adult tissues (eyes, cerebral cortex, cerebellum and liver) by the phenol-guanidinium-chloroform (Trizol) extraction method (MacDonald et al., 1987).

Northern analysis

Ten μg total RNA from each tissue was resolved by formaldehyde-agarose gel electrophoresis and transferred to a 0.45 μm pore nitrocellulose membrane as described (Cho and Dressler, 1998). An RNA ladder in the 0.25-9.5 kb range (Gibco-BRL) was co-electrophoresed to accurately determine the size of hybridizing RNAs. After prehybridization, the membrane was probed successively with ^{32}P-radiolabeled 1.2 kb *Math5* and 1.1 kb β-actin (Alonso et al., 1986) mouse cDNAs, washed to 0.1X SSC 65°C stringency, and exposed to Kodak XAR film with an intensifying screen at -80°C for 16 hrs. The autoradiographic images were digitized using a flatbed scanner. The *Math5* probe was gel-purified from clone JN4C after digestion with *Xho*I and *Eco*RI, and was labeled to high specific activity with ^{32}P-[α]-dCTP using the random hexamer (dN_6) priming method (Feinberg and Vogelstein, 1983).

Reverse transcriptase (RT) and genomic PCRs

Total RNA from E14.5 or E15.5 mouse eyes (5 µg) or retinas (3 µg), adult cerebellum (5 µg), or adult liver (3 µg) was treated with 5 U DNaseI (Roche) for 15 min at 37ºC in DNAse buffer (20 mM Tris-HCl, 2 mM $MgCl_2$, 50 mM KCl). To stop the reaction, EDTA was added to 2 mM and the DNaseI was inactivated at 75ºC for 10 min. RNAs were mixed with 500 ng oligo dT or 300 ng dN_6 (Invitrogen) primer, denatured at 65ºC for 10 min, and reverse-transcribed with 10 U Transcriptor^{TM} High Fidelity RT (Roche) at 55ºC for 1 hr. The 20 µL RT reactions contained 50 mM Tris-HCl pH 8.5, 30 mM KCl, 8 mM $MgCl_2$, 5 mM DTT, 1 mM dNTPs, and 10 U RNase Inhibitor (Protector^{TM}, Roche). The RT was inactivated at 85ºC for 5 min. The Transcriptor^{TM} enzyme mixture has RNA-directed DNA polymerase, DNA-dependent DNA polymerase, helicase, RNase H, and 3' $\rightarrow$ 5' exonuclease proofreading activities (Schonbrunner et al., 2006). In the RT (-) controls, this enzyme mixture was replaced with nuclease-free water.

PCRs were performed using 1 µL of the cDNA reactions as template, in 1.5 mM $MgCl_2$, 0.2 mM dNTPs, 20 mM Tris pH 8.4, 50 mM KCl, with 2 nM each primer and 2.5 U hot-start Platinum *Taq* polymerase or 0.5 U conventional *Taq* polymerase (Invitrogen). All PCRs were performed in 12-well strip tubes, in a 96-well MJ thermocycler with heated lid assembly, using specified primers and conditions (Table II-S1, 2). PCR products were separated by electrophoresis through 1.5 % agarose gels, purified by membrane binding (Wizard SV,

Promega) and sequenced or subcloned. Genomic PCRs were performed using 50 ng CD-1 mouse tail DNA.

To melt secondary structure, 10X Masteramp™ (Epicentre) was included in some PCRs, with a final fractional volume in the reaction mixture between 0.0 to 0.3 (v/v), designated 0X to 3X. Although the formulation of this additive is proprietary, equivalent results were obtained with 0.0 to 1.0 M betaine (Sigma B0300).

In vitro transcription

Plasmid DNA (1 µg) from clones pJN4C (Brown et al., 1998) or pCR4-ECO was linearized with *Xho*I or *Not*I, respectively, and transcribed for 2 hr with 40 U bacteriophage T3 RNA polymerase (Roche), in a reaction containing 1 mM NTPs, 40 mM Tris-HCl pH 8.0, 6 mM $MgCl_2$, 10 mM DTT, 2 mM spermidine and 20 U RNase Inhibitor (Protector). The template was then digested with 20 U DNase I for 1 hr at 37ºC, and the resulting RNA was purified using Trizol (Invitrogen) and assessed by 1% agarose gel electrophoresis and UV absorbance (A_{260}). The full length (FL) *Math5* IVT RNA product (10 ng) was mixed with DNaseI-treated mouse liver RNA (3 µg) or used directly (10-200 ng) for RT-PCRs.

Triplex competitive RT-PCR assays

Retinal and cerebellar RT-PCRs (Leygue et al., 1996) were performed in 1X MasterAmp™, with equal molar ratios of competing forward primers (1 nM) and a single fluorescent (6-FAM) reverse primer (LP4) as indicated (Table II-S2), which

were matched for length and G+C content. Products were diluted to 1:50 to 1:200 in formamide and co-electrophoresed with GS-600 LIZ size marker in a 3730XL capillary DNA Analyzer (Applied Biosystems). The fluorescence intensity of each amplimer and the ratio of spliced to unspliced PCR products were calculated using GeneMarker (SoftGenetics), from the sum of major peaks in triplicate experiments.

Rapid amplification of cDNA ends (3' RACE)

First-strand cDNA synthesis was performed from retinal RNA as described above, using 10 pmol adapter primer (AP, Table II-S1). One µL of the cDNA reaction was then used to amplify 3' terminal sequences using primers and conditions in Tables II-S1 and II-S2. To minimize spurious products from unrelated genes, a second round of PCR was performed using nested primers, following a conventional nested 3' RACE strategy (Frohman, 1993).

RNase protection assays (RPA)

RNase protection assays (Melton et al., 1984) were conducted using the RP-III kit (Ambion). Antisense cRNA probes were transcribed from PCR products A and B (Fig. II-5) cloned in pCR4-TOPO. One µg of each plasmid was digested with *Not*I and transcribed with T3 RNA polymerase as described above, except that 125 pmol (75 µCi) or 113 pmol (90 µCi) ^{32}P-[α]-CTP was included in probe A and B reactions, respectively, with 200 pmol CTP and 10 nmol of ATP, GTP and TTP. This yielded 366 and 632 nt cRNA products with 301 nt (A) and 567 nt (B) direct sequence homology to *Math5*. Probes were purified by electrophoresis

through denaturing 6% polyacrylamide gels and eluted for 3-4 hrs at 37ºC. Ten μg of DNaseI-treated E14.5 eye RNA, yeast RNA (Ambion), or yeast RNA spiked with 10 ng *Math5* IVT product (ECO or FL) was precipitated in 2.5 M ammonium acetate 70% ethanol and resuspended in 8 µl hybridization buffer. The RNAs were hybridized with 2 µl probe A (8×10^4 cpm) or probe B (1.2×10^5 cpm) for 13 hr at 42ºC, and digested with RNase A+T1 (1:100) for 30min at 37ºC, and co-precipitated with glycogen and 5 µg yeast carrier RNA. Reactions were electrophoresed through 6% polyacrylamide denaturing gels (0.4 mm) in 6 M Urea and 0.5X TBE. dsDNA size markers were prepared by radiolabeling *Msp*I-digested pBR322 with ^{32}P-[α]-dCTP and Klenow DNA polymerase. The dried gels were exposed to phosphor screens for 12-14 hrs and imaged using a Typhoon scanner (Molecular Dynamics) at 0.2 mm resolution. Yeast RNA controls were included ± RNase, to assess the probe integrity and the completeness of digestion.

Informatics

Sequence alignments, G+C and antigenicity profiles, and PCR primer optimization were performed using MacVector (Accelrys) software and NCBI BLAST servers. *Math5* polyadenylation sites were predicted using the polyADQ (Tabaska and Zhang, 1999) web server (rulai.cshl.org/tools/polyadq/). Scores were calculated for a 6.0 kb sequence extending from the transcription start site (Fig. II-1D), using default threshold values. RNA secondary structures were predicted by free-energy minimization (Mathews et al., 1999; Zuker, 2003) using the M-fold web server (mfold.bioinfo.rpi.edu/). Expressed sequence tags (ESTs)

for mouse and human bHLH cDNAs were accessed through the UCSC genome browser (genome.ucsc.edu/).

Math5 antibodies

Commercial and custom antibodies to Math5 peptides and recombinant proteins are indicated in Fig. II-S2 along with the immunogen, including the Abcam polyclonal reagent (ab13536) cited by Kanadia and Cepko (2010). Custom rabbit polyclonal sera were generated using internal (RCEQRGRDHP) or C-terminal (RLFGFQPEPFPMAS) Math5 peptide haptens coupled to KLH (keyhole limpet hemocyanin) via a cysteine thiol linkage (Research Genetics, Huntsville, AL), and were affinity purified.

Cell transfection and Western analysis

NIH 3T3 fibroblast cultures were transfected with expression plasmid DNA (1 μg per 60 mm plate) for native or N-terminal 6x Myc-tagged versions of mouse or human ATOH7 proteins, or empty vector, using Fugene-6 reagent (Roche), with 0.1 μg pUS2-EGFP as an internal control. These plasmids were prepared by inserting ATOH7 coding regions from genomic phage, plasmid or BAC clones into pCS2 and pCS2MT vectors (Rupp et al., 1994) and verifying the sequence. Mouse pCS2-Math5 and pCS2MT-Math5 plasmids were described previously (Brown et al., 1998). After 48 hrs, cells were harvested in PBS with protease inhibitors (Complete™, Roche), lysed in RIPA buffer (Harlow and Lane, 1988), sonicated, and centrifuged at 13,000 × *g* for 15 min at 4°C. Soluble proteins were electrophoresed through NuPAGE Novex Bis-Tris 4-12 % polyacrylamide gels

(25 μg per lane), transferred to nitrocellulose membranes and stained with Ponceau S. Parallel Western blots were probed with rabbit polyclonal antisera to Math5 peptides (1:200, Fig. II-S2A), full-length human ATOH7 (D01P, 1:500) or GFP (Abcam ab290, 1:2500); or mouse anti-Myc monoclonal (9E10, Zymed, 1:500); and the reactive proteins were visualized using HRP-conjugated anti-rabbit (NEN, 1:5000) or mouse (GE, 1:20,000) IgG secondary antibodies, enhanced chemiluminesence reagents (ECL-Plus, GE), and Kodak MS X-ray film.

Immunostaining and RNA *in situ* hybridization

Mouse E15.5 embryo heads from wild-type and *Math5* knockout (*Atoh7*^{tm1Gla}) littermates (Brown et al., 2001) were fixed in 4% paraformaldehyde PBS for 1 hr at 4^{O}C; processed through a 10-30% sucrose series in PBS; cryoembedded in OCT media (Tissue-Tek, Torrence, CA) and sectioned through the eyes at 5-10 μm. To thoroughly test antibody reactivity, we tried three different antigen unmasking protocols in parallel: 0.1 M Tris pH 9.5 at 95°C for 5 min; 0.05 % trypsin at 37°C for 10 min; and 0.3% Triton X-100 0.1 M Tris pH 7.4 at 25°C for 10 min. Cryosections were then blocked and processed in TST milk as described (Mastick and Andrews, 2001). Slides were incubated overnight at 25°C with a 1:500 dilution of anti-Math5 peptide sera (Abcam no. ab13536, lot no. 610696), followed by a 1:5000 dilution of Alexa 594-conjugated goat anti-rabbit IgG secondary antibody (Molecular Probes). RNA *in situ* hybridization was performed on E15.5 embryonic retinas as described (Wallace and Raff, 1999). A digoxigenin-labeled antisense *Math5* cRNA probe spanning the 3' UTR and CDS

was prepared from *Asc*I-digested plasmid pJN4C with T7 RNA polymerase, hybridized to retinal sections overnight, detected using an AP-conjugated sheep anti-DIG antibody (1:2000, Roche), and visualized using NBT-BCIP histochemistry. Micrographs were imaged using a Zeiss Axioplan 2 microscope, digital camera and Axiovision software.

Results

Math5 transcription unit, defined by cDNA clones, Northern and 3' RACE analysis

During our initial characterization of *Math5* (Brown et al., 1998), we identified four independent retinal cDNA clones, which were colinear with mouse genomic DNA (Genbank accession no. AF418923). The 5' and 3' termini, and internal sequences were consistent with RNA hybridization data suggesting a single-exon transcription unit, with an initiation site 23 bp downstream from a TATAAA box and a polyadenylation (pA) site 669 bp downstream from the TAA stop codon, giving 1.7 kb as the predicted size for polyA+ *Math5* mRNA (Fig. II-1A,D). This major *Math5* transcript was detected by Northern blot analysis of E15.5 mRNA with an 1155 bp radiolabeled cDNA probe (JN4C) that includes 318 bp 5' UTR, 447 bp coding sequence (CDS) and 390 bp 3' UTR (Fig. II-2A). A second, less abundant 4.4 kb transcript was also detected at this age, which is close to the peak time-point for *Math5* expression during embryogenesis (Brzezinski and Glaser, 2004). Careful inspection of the autoradiogram, in relation to the RNA size markers, revealed no smaller *Math5* transcripts,

particularly in the 0.8-1.0 kb size range expected for spliced isoforms lacking the coding region. This pattern resembles Northern data obtained by Kanadia and Cepko with UTR probes (*cf*. Fig.1f and 1f'), but appears inverted compared to the unsized blot hybridized with a CDS probe in their report (*cf*. Fig. 1f"). We cannot explain this discrepancy.

To confirm our identification of the major *Math5* polyadenylation site (Brown et al., 1998) and define the 3' terminus of the longer, 4.4 kb transcript, we first surveyed the 3' *Math5* genomic region for favorable pA signals using the polyADQ weighted statistical algorithm (Tabaska and Zhang, 1999). Among eight potential pA sites downstream from the transcription start site (TSS), two had significant polyADQ scores (nos.1 and 6, Fig. II-2B,C), and these were consistent with the observed transcript sizes. We then looked for mRNAs terminating at pA1 and pA6 in parallel 3' RACE experiments (Frohman, 1993), using E14.5 total eye RNA and nested primers positioned upstream of each site (Figure 2b,d). From the size and sequence of the products (Fig. II-2D-F), and our Northern data, we conclude that there are two principal *Math5* transcripts in the retina, 1.7 kb and 4.4 kb in length, and that both of these transcripts are *unspliced*. This interpretation is further supported by the curation of additional mouse cDNAs, represented as 56 expressed sequenced tags (ESTs) and two Genbank cDNAs in the NCBI database (Fig. II-S1). Only two ESTs and one cDNA, originating from the adult cerebellum, appear to be authentic splice products (see below), and these do not correspond to the retinal isoforms reported by Kanadia and Cepko (2010).

In addition to the coding region, *Math5* mRNA has three notable features relevant to this study (Fig. II-1A). First, the 5' half is highly enriched in G+C nucleotides (Fig. II-1B), with >85% G+C content in the 150 nt segment spanning codons 7 to 57. *Math5* mRNA thus has the potential to form compact, thermodynamically stable secondary structures, owing to the third hydrogen bond in G-C pairs compared to A-U pairs, and the ability of guanine residues to interact with uracil in folded RNA (Mathews et al., 1999). The elevated G+C content is also predicted to affect folding of the (+) and (-) strand cDNA templates, compromising DNA polymerase processivity. Second, the 5' segment of the gene is enriched for specific trinucleotide elements (Py-G-C) that are known to cause DNA polymerase pausing (Mytelka and Chamberlin, 1996) (Fig. II-1C). These account for 15.7% of the trinucleotides in this segment (47 of 300, for both DNA strands), which is 1.73 fold higher than expected from mononucleotide frequencies. Third, mouse *Math5* mRNA contains 30-nucleotide imperfect direct repeats (DRs), located in the 5' and 3' UTRs (Fig. II-1A,E). These UTR repeats are not conserved among mammalian *ATOH7* mRNAs.

Sensitivity of *Math5* PCR to template folding *in vitro*

Our Northern analysis, screening of cDNA libraries, and analysis of ESTs contrasts starkly with the abundant, heterogeneous splicing recently reported for the *Math5* gene (Kanadia and Cepko, 2010). As a first step to resolve this difference, we performed a series of RT-PCR experiments using the same primers (LP8 and LP4, Fig. II-1A and Table II-S1) and similar conditions (Table II-S2) as these authors. Using a thermostable reverse transcriptase (RT)

formulation (Transcriptor™, Roche), E14.5 total mouse retinal RNA as template, and primers located in the 5' and 3' UTRs, we amplified a single 448 bp product (Fig. II-3A) with the same sequence as the ECO cDNA reported by Kanadia and Cepko (2010) (Fig. II-3C), thus technically reproducing their primary observation. In this cDNA, a 639 bp segment encompassing the entire *Math5* coding region has been deleted. The 3' breakpoint abuts the 3' UTR direct repeat.

The extremely high G+C content of the 5' half of the deleted segment (Fig. II-1B) creates the potential for the RNA to form stable secondary structures, which could impede the procession of reverse transcriptase (RT) and DNA polymerases. Given our previous experience working with *Math5*, we repeated this PCR, replacing the water in the reaction mixture with 0 to 3X Masteramp™ (Epicentre). This is functionally equivalent to 0 to 1.0 M betaine (N,N,N-trimethyl glycine) [not shown], which is the principal ingredient in this additive (Henke et al., 1997; Mytelka and Chamberlin, 1996; Weissensteiner and Lanchbury, 1996). In these reactions, betaine interacts with DNA as an isostabilizing agent, equalizing the free energies of A-T and G-C pairs by increasing hydration of the minor groove and flexibility of the double helix (Melchior and Von Hippel, 1973; Rees et al., 1993). It thus melts secondary structures, allowing DNA polymerases to extend through GC-rich segments (Henke et al., 1997; Mytelka and Chamberlin, 1996; Weissensteiner and Lanchbury, 1996). In our experience, ≥ 1 M betaine is required to reliably amplify across the 5' coding sequences of mouse or human *ATOH7*, even when cloned cDNA is used as a template; and relatively high concentrations (~2 M) are tolerated in the PCR. Moreover, in the

absence of betaine, we have observed numerous PCR-generated deletions of *Math5* sequences during molecular cloning projects over several years (not shown).

As the concentration of betaine in the PCR was increased, the apparently spliced 448 bp ECO product vanished, and a strong 1087 bp product appeared, corresponding to full-length, unspliced *Math5* cDNA (Fig. II-3A). The identity of these molecules was verified by sequencing gel-purified PCR products and multiple pCR4-TOPO plasmid clones derived from the PCR products. The effect of betaine on the generation of the 448 bp product suggests that *Math5* splicing either does not occur in nature, within the developing retina, or is an extremely rare event. Indeed, under normal circumstances, the smaller product should have been significantly favored during the amplification steps, with or without betaine. However, since the ECO product cannot be generated by PCR from mouse genomic DNA (Fig. II-3B) (Melchior and Von Hippel, 1973; Rees et al., 1993) and depends on RT, it must be represented in the initial first-strand cDNA pool, albeit at an extremely low level (see below). These molecules could have been generated from rogue, aberrantly spliced mRNAs or by RNA template-switching during the reverse transcription step. Regardless of their origin, these rare cDNA amplicons (448 bp, 52.7 % GC) should have a large selective advantage over the full-length co-terminal cDNA (1087 bp, 60.1 % GC) during subsequent cycles of PCR.

Similar experiments were performed with a second pair of primers (LP6 and LP7), which are separated by 486 bp in genomic DNA and flank the GC-rich

segment (Fig. II-3C,D). In the absence of betaine, these primers did not amplify any product. However, when 2-3X Masteramp™ was included in the PCR, only the expected 486 bp amplimer was observed. When we extended the PCR beyond 35 cycles, preincubated the reaction at 25°C ("cold start") or used crude *Taq* polymerase preparations in the absence of betaine, a heterogeneous group of deleted (lacunar) products was observed (not shown), with a size and sequence distribution (Fig. II-4D, Table II-S3) similar to that reported by Kanadia and Cepko.

Deleted PCR products derived from RNAs transcribed *in vitro*

To determine the origin of the lacunar cDNAs, we performed parallel RT-PCR experiments on RNA templates derived by *in vitro* transcription (IVT). Full-length, sense *Math5* transcripts were synthesized *in vitro* using bacteriophage T3 RNA polymerase and a *Xho*I-cleaved pJN4C DNA template (Fig. II-4A). RT reactions were performed as before, with oligo dT-priming, and 0-200 ng of the *in vitro* RNA transcript as template, alone or diluted into 3 μg total mouse liver RNA. When the PCRs were performed in 3X Masteramp™, full-length 1087 bp and 486 bp products were amplified (Fig. II-4B,C), identical to those generated from E14.5 retinal RNA (Fig. II-3A,C). However, when the betaine was reduced or omitted, we observed a variety of smaller products, with a size distribution (Fig. II-4B-D) and sequence diversity (Table II-S3) similar to that reported by Kanadia and Cepko (2010, *cf*. Table S1), despite the absence of retinal RNA, spliceosomes or other eukaryotic cell components.

Because these products depend on reverse transcriptase, they must have arisen via RNA template-switching during the RT reaction (Biagini et al., 2008), despite the use of a thermostable recombinant enzyme mixture with high fidelity, processivity and proofreading features (Kitabayashi and Esaka, 2003; Schonbrunner et al., 2006). A similar origin seems likely for the majority of apparently spliced *Math5* cDNAs reported by Kanadia and Cepko (*cf*. Table S1). Indeed, most of the deleted products obtained here and in the previous paper (Table II-S3) contain 5-10 nt direct sequence homology at the junctions (Pfeiffer and Telesnitsky, 2001). The only remaining explanation – that *Math5* encodes a nuclear self-splicing mRNA – lacks precedent (Cech, 1986). A possible exception is the ECO cDNA product, which was amplified from embryonic retinal RNA *in less than 1M betaine* (Fig. II-3A) but not from IVT-derived material or genomic DNA.

Critical evaluation of *Math5* splicing by competitive RT-PCR

To further investigate *Math5* splicing *in vivo*, we directly compared the abundance of full-length and ECO (spliced) RNAs in competitive, triplex (3-primer) RT-PCR assays (Fig. II-5). Each reaction contained two alternative forward (sense strand) primers – one located in the 5' UTR and a second, internal primer in the 3' coding region – plus a single reverse (antisense) primer located in the 3' UTR (Fig. II-5A). In this assay, the proportion of the two predicted products should reflect the relative abundance of the corresponding mRNAs in the E14.5 retina. The outer UTR primers and the resulting ECO product are identical to those reported by Kanadia and Cepko (see Table II-S1).

For completeness, we performed two independent competitive RT-PCRs in parallel, with two different internal forward primers (LP13 and LP14), giving full-length products that were larger (567 bp) or smaller (301 bp) than the 448 bp ECO product, respectively. The spliced and unspliced products were also matched for G+C content (Fig. II-5A), so a direct comparison would be reliable. Moreover, these amplicons do not overlap the 5' GC-rich segment of *Math5* that is refractory to RNA and DNA polymerase processivity. Only the full-length (unspliced) *Math5* products were detected in these experiments by ethidium bromide staining of agarose gels (Fig. II-5B). To consider this point more rigorously, and detect extremely rare spliced *Math5* mRNAs, we performed identical competitive RT-PCRs with a common 6-carboxyfluorescein (6-FAM) end-labeled reverse primer, and determined the molar ratio of spliced and unspliced products by fluorescence capillary electrophoresis (Fig. II-5C). We estimate that the ECO isoform represents less than 1.0% of *Math5* transcripts in the E14.5 eye. *Math5* splicing thus does not occur at significant levels in the developing mouse retina.

Direct test of *Math5* splicing by nuclease protection (RPA)

To independently assess *Math5* mRNA splicing in the retina, we performed RNase protection assays (Melton et al., 1984). The nuclease protection method was developed in the 1970s to demonstrate the existence of mRNA splicing (Berget et al., 1978; Berk and Sharp, 1977; Eisenstein, 2005). Unlike PCR, nuclease protection assays do not depend on an exponential amplification process, which is highly sensitive to template secondary structure.

To evaluate the ratio of spliced and unspliced *Math5* transcripts, we hybridized total eye RNA from E14.5 embryos, in parallel, with a molar excess of two ^{32}P-labeled antisense RNAs (Fig. II-6A). These cRNAs were prepared by *in vitro* transcription of two cDNA clones derived from unspliced 301 bp (A) and 567 bp (B) competitive RT-PCR products (Fig. II-5B). After hybridization and RNase digestion, surviving probe RNA molecules were resolved by polyacrylamide gel electrophoresis (Fig. II-6B). Probes A and B were protected by full-length *Math5* mRNA in the embryonic eye, giving 301 nt and 567 nt digestion products. No hybridizing fragments were detected at the size predicted for ECO mRNA (212 nt). The absence of smaller protected fragments in this sensitive assay further indicates that the *Math5* coding segment is not significantly spliced in the embryonic eye.

Coding potential of lacunar *Math5* RNAs

In addition to the ECO product, which lacks the entire coding region, multiple mRNAs were proposed to originate from *Math5* primary transcripts via alternative splicing (Kanadia and Cepko, 2010). In some cases, these contain partial open reading frames and were predicted to encode shorter Math5 isoforms. To test this hypothesis, the authors used commercial Math5 peptide antisera to probe extracts from cells transfected with various splice products (*cf.* Fig. 1H). We independently tested the reactivity of Math5 antibodies to mouse and human proteins expressed at high levels in transfected NIH 3T3 cells, by Western blotting, and to retinal sections from wild-type and *Math5* mutant embryos (Fig. II-S2), following standard precepts (Rhodes and Trimmer, 2006;

Saper and Sawchenko, 2003). We were unable to detect mouse Math5 polypeptide with any of these reagents, including the Abcam antisera (ab13536) used by Kanadia and Cepko (2010).

Spliced *Math5* transcripts in the cerebellum

During our previous characterization of *Math5*, we noted expression in the developing hindbrain and cerebellum, including a single hybridizing *Math5* mRNA detected by Northern analysis (Saul et al., 2008). This 1.7 kb mRNA was consistent with the size of embryonic retinal transcripts (Fig. II-2A). However, three out of six *Math5* clones derived from adult mouse brain RNA in the NCBI database are apparently spliced, cerebellar (Cb) ESTs BY705389 and AV030226, and cDNA AK005214 (Fig. II-S1A). These Cb isoforms are missing 199 nucleotides, and consequently are predicted to encode a truncated polypeptide in which the 22 terminal amino acids of Math5 (VDPEPYGQRLFGFQPEPFPMAS) are replaced by 2 residues (VS). Although the C-terminal amino acids are moderately conserved among amniotes (Fig. II-S3C), the donor splice sites are not.

To evaluate *Math5* splicing in the cerebellum, we performed binary (2-primer) and competitive RT-PCR experiments with total adult cerebellar RNA as template (Fig. II-S3). In the binary PCR, the primers flanked the putative 199 bp intron, giving 567 bp (unspliced) or 368 bp (spliced) products (Fig. II-S3D). In the triplex PCR, the two forward primers were located inside the intron and spanning the exon junction (to amplify unspliced and spliced products respectively), and the common reverse primer was end-labeled (Fig. II-S3E,F).

The reactions involved the terminal portion of the *Math5* coding region and 3' UTR, and the products were similar in size (301 vs. 228 bp) and G+C content (47.8 vs. 52.2 %). In contrast to the embryonic retina, we observed a moderate level of alternative mRNA splicing in the adult cerebellum, involving 11 ± 2 % of *Math5* transcripts. The major (1.7 kb) and minor (1.5 kb) cerebellar splice forms were not previously resolved in Northern blots (Saul et al., 2008), presumably because of the difference in abundance, and the effect of polyA tail heterogeneity (with an expected mean length of 250 adenosines, (Wahle, 1995). This shorter isoform was not detected in the embryonic retina (Fig. II-S3D).

Discussion

We have critically defined the transcriptional anatomy of the *Math5* gene, and characterized alternatively spliced mRNAs. In contrast to the adult cerebellum, *Math5* mRNA is not significantly spliced in the developing retina. This conclusion is supported by six independent lines of evidence: Northern analysis; RT-PCR analysis of natural and IVT-derived RNAs in the presence of graded betaine concentrations; triplex RT-PCR analysis; EST data; and ribonuclease protection assays. Our findings differ sharply from the recent report of Kanadia and Cepko (2010). Three major factors contribute to the technical artifacts observed by these authors: [1] intense secondary structure in the >85% GC-rich segment of *Math5* RNA and cDNA, which blocks the progression of polymerase enzymes, creating a powerful negative selection; [2] RT template switching *in vitro*; and [3] the existence of a vanishingly small population of

aberrantly spliced *Math5* mRNAs (Fig. II-7A). In view of these results, further investigation of *Ngn3* splicing may be warranted (Fig. II-S4).

The GC-rich coding segment of *Math5* (Fig. II-1B) evidently forms a "Gordian knot" of secondary structure (Fig. II-7B,C), so dense that it favors the amplification of minor cDNA products, representing less than 1% of *Math5* molecules. G+C sequence bias is a well known problem in cDNA profiling studies (Blackshaw et al., 2004; Margulies et al., 2001). The folded hairpin structure of *Math5* mRNA is relaxed in the presence of betaine. *In vivo*, local melting is presumably catalyzed by DNA- and RNA-binding proteins, allowing *Math5* replication, transcription and translation. However, the tight RNA secondary structure may have consequences for Math5 protein expression. For example, translation may require specific mRNA unwinding activity, creating another potential mode of post-transcriptional regulation (Gray and Hentze, 1994). Indeed, mRNA hairpins are known to impede ribosome elongation (Baim et al., 1985) and G+C content is inversely correlated with translation efficiency (Kenneson et al., 2001). If translation of the GC-rich *Math5* mRNA were hypersensitive to ribosome functional status, this may contribute to the disruption of RGC development in *Bst*/+ mice, which have a mutation in the *Rpl24* riboprotein gene and severe optic nerve hypoplasia (Oliver et al., 2004).

On the basis of these results, we believe that the most likely explanation for the plethora of deleted *Math5* cDNAs (Fig. II-4) is RNA template-switching during the reverse transcriptase reaction, at points of sequence micro-homology (Fig. II-7A, Table II-S3) (Brincat et al., 2002). Indeed, RT polymerases are

required to switch templates during normal retroviral replication, as part of the first and second transfer steps (Telesnitsky and Goff, 1997). Aberrant switching *in vivo* can generate intramolecular deletions, and the frequency is positively correlated with the amount of RT pausing (Wu et al., 1995) and RNase H activity (Brincat et al., 2002). In practice, template switching and related phenomena are well known hazards in PCR-based expression studies, and have been collectively termed “RT-facts” (Cocquet et al., 2006; Derjaguin and Churaev, 1973; Mader et al., 2001; Roy and Irimia, 2008; Zaphiropoulos, 2002).

The process of eukaryotic splicing produces a variety of functional and nonproductive mRNAs during normal gene expression. While alternative splicing greatly extends the genetic repertoire (Brett et al., 2002), particularly in the nervous system (Li et al., 2007), a significant fraction of Pol-II transcripts are mis-spliced, such that no protein or stable RNA species is synthesized, similar to the ECO isoform. Frequent errors include exon skipping, intron retention, and activation of cryptic splice sites. The resulting aberrant RNAs may outnumber correctly spliced mRNAs among initial spliceosomal products (Jaillon et al., 2008; Mitrovich and Anderson, 2000). For protein-coding genes with multiple exons, the majority of aberrant RNAs contain a premature truncation codon (PTC) and are degraded through the nonsense-mediated decay (NMD) pathway (Baker and Parker, 2004). This is not generally possible for single-exon genes, which require distinct quality control mechanisms to eliminate defective mRNAs (Maquat and Li, 2001). The intronless class represents 5-15% of mammalian genes (Gentles and Karlin, 1999; Sakharkar et al., 2004) and includes histones, GPCRs and

many Zn finger, HMG, and bHLH domain transcription factors.

The process of splice site recognition is also far more complicated than the local pairing of 5' and 3' consensus sequences. It requires the *holo* definition of exon or intron elements in context, with integration of multiple splice enhancer and silencer effects (Berget, 1995; Fox-Walsh et al., 2005; Hertel, 2008; Wang and Burge, 2008). In this way, intronless genes may have selectively acquired sequence features that resist mRNA splicing (Fedorov et al., 2001; Irimia and Roy, 2008; Jeffares et al., 2008). Detailed sequence comparisons of intronless vs. intron-containing human genes has revealed differences in oligonucleotide frequencies and context-dependent codon biases (Fedorov et al., 2001). The most striking characteristic of intronless genes in this analysis was the overrep-resentation of GC-rich 4- to 6-mers, after correcting for base composition. The *Math5* cDNA matches this pattern extremely well (not shown), exhibiting sequence features that are characteristic of intronless genes. Moreover, the GGG triplet, which binds U1 snRNP as an intronic splice enhancer (Engelbrecht et al., 1992; McCullough and Berget, 2000), is depleted within the *Math5* coding region, despite the high G+C content. These global compositional features are not considered by the Spliceport algorithm that was used by Kanadia and Cepko to predict *Math5* splice sites. This web-based tool performs statistical analysis of *k*-mers in a 160 nt window surrounding putative donor and acceptor sites, based on human genome search data (Dogan et al., 2007). The analysis predicted the alternative Cb splice acceptor, which is utilized at low frequency in the adult cerebellum (FGA score = 1.33); however, the Cb donor site was not identified

and statistical support for donor sites in the *Math5* transcript was relatively low (max FGA score = 0.26). Indeed, the mouse genome contains many more weak, potential splice sites than are actually utilized *in vivo*.

Among the numerous *Math5* species reported by Kanadia and Cepko, only one PCR product, termed ECO, is compatible with mRNA splicing. On the basis of our results, we believe this solitary cDNA is derived from an aberrantly spliced transcript, which has escaped normal quality control. First, the RNA encodes no protein and has no demonstrated function. In other contexts, long ncRNAs such as *Xist* and *Air*, have been shown to have regulatory roles (Mercer et al., 2009), and a small number of bifunctional mRNAs have alternate coding and noncoding isoforms (Chooniedass-Kothari et al., 2004). Second, the ECO isoform is very rare, representing less than 1% of *Math5* mRNA, and is thus unlikely to have a significant role in regulating *Math5* function or modulating retinal cell fate determination.

An intriguing result from our study is the discovery that 11% of mature *Math5* transcripts in the adult cerebellum are *bona fide* spliced mRNAs. These are predicted to encode a shorter Math5 protein, which lacks 20 amino acids from the C-terminus and may exhibit unique molecular properties (Fig. II-S3). However, its function is not known, and *Math5* mutants have no overt cerebellar phenotype (Saul et al., 2008).

Despite the intriguing hypothesis advanced by Kanadia and Cepko, our results show splicing of *Math5* mRNA into noncoding isoforms does not occur in the developing retina at levels greater than 1% of transcripts. Further studies are

needed to determine the exact mechanism of *Math5* action, how progenitors are transformed into neurons, and how noncoding RNAs, including microRNAs, may regulate *Math5* expression, RGC development, and the diversification of ganglion cell subtypes.

Acknowledgements

The authors are grateful to John Moran and David Turner for helpful suggestions; to Dellaney Rudolph, Tien Le, Susan Tarlé and the UM sequencing core for technical support; and to John Moran, David Turner, Miriam Meisler, Doug Engel, Chris Chou, and Terri Grodzicker for careful reading of the manuscript. The research was funded by NIH R01 grants to TG (EY14259) and NLB (EY13612) and The Glaucoma Foundation (TG). LP was supported by NIH T32 grants to the University of Michigan Medical Scientist (GM07863) and Vision Research (EY13934) Training Programs.

Figure II-1. Anatomy of the *Math5* transcription unit. (A) Gene map showing the major 1489 nt mRNA species; coding region (red box) and UTRs; direct repeats (DR); major polyA signal (pA) and internal A-rich segment (A_{14}); cerebellar-specific intron (Cb); and PCR primers used in this study (dark red). LP15 spans the Cb intron junction. (B) Plot showing elevated GC content (red) across the *Math5* coding region, compared to the average value (49.98%) for the mouse transcriptome (green) (Stolting et al., 2009). The 150 nt segment with >85% GC and the 536 nt fold encompassing the coding region are indicated (brackets). (C) Concentration of polymerase-refractory YGC trinucleotides in the proximal coding region (both strands). (D) Magnified view of the *Math5* promoter showing the TATAA box, transcription start site (TSS) and 5' termini of cDNA clones (Brown et al., 2002; Brown et al., 1998). (E) Sequence of UTR direct repeats.

A

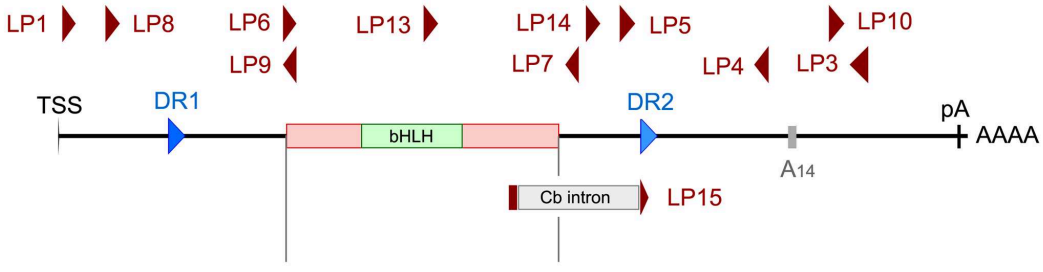

B

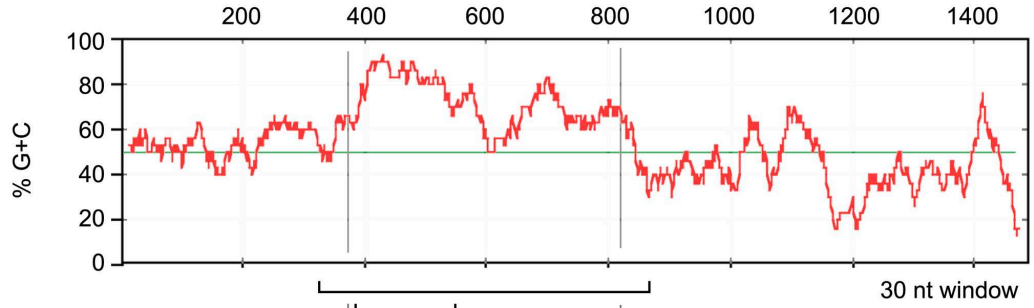

C

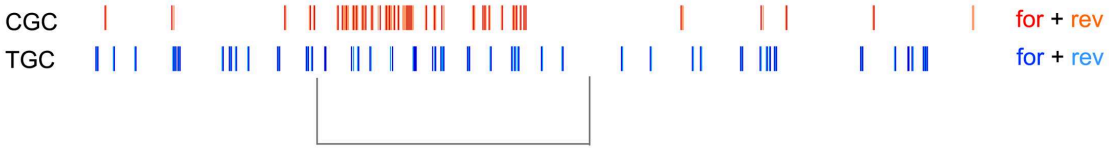

D

```
                                          +1
                                         JN1
GCTATAAATTCTCCTCCCTCATCGCTCTGTCCGACATCTACTGCAAGCTG    20

BC092234                                 JN4   JN6   JN2
TCCAAACGCTCCTGACCTAGCAGAGCTTCTGGGAAGATTTCGTCACCCCG    70
```

E

```
GTTT--GGGGTGGAGTGGGGAGGAATGACTTT    181 - 210    DR1
||||    | |||||     |   ||||||||||
GTTTCATGAGTGGACATCGC--GAATGACTTT    954 - 983    DR2
```

Figure II-2. *Math5* messenger RNAs. (A) Northern blot probed with 1.2 kb *Math5* (JN4C) and 1.1 kb β-actin cDNAs. Two *Math5* mRNAs are visible (left arrowheads), but no hybridizing RNA species is present in the 0.8-1.0 kb size range. The RNA size ladder cross-hybridized to vector DNA in the plasmid probes. (B) Map of the 3' UTR and flanking genomic DNA (6 kb), showing eight potential polyA signals ATTAAA (blue) and AATAAA (green); the internal A_{14} priming site in the UTR (ψpA); interspersed repeats (gray); and the nested 3' RACE primers (dark red) for pA1 and pA6 sites, which have the most favorable sequence context. Clones JN2 and BC092234 terminate at pA1, whereas cDNAs JN1, JN4 and JN6 terminate at ψpA (Brown et al., 2002; Brown et al., 1998). ψpA_2 marks an A-rich genomic site captured in the pA6 assay. (C) polyADQ scores for all potential pA sites, calculated using human genome parameters (Tabaska and Zhang, 1999). Only pA1 and pA6 have scores above threshold. (D) Embryonic eye RT-PCRs with 260 bp and 365 bp 3' RACE products (arrowheads) showing utilization of pA1 and pA6 sites. The 900 bp product was primed from ψpA_2 (open arrowhead). m, marker (1 kb-plus ladder); RT, reverse transcriptase. (E) Sequence of pA1 RACE products originating from the 1.7 kb *Math5* mRNA. (F) Sequence of pA6 RACE products originating from the 4.4 kb *Math5* mRNA.

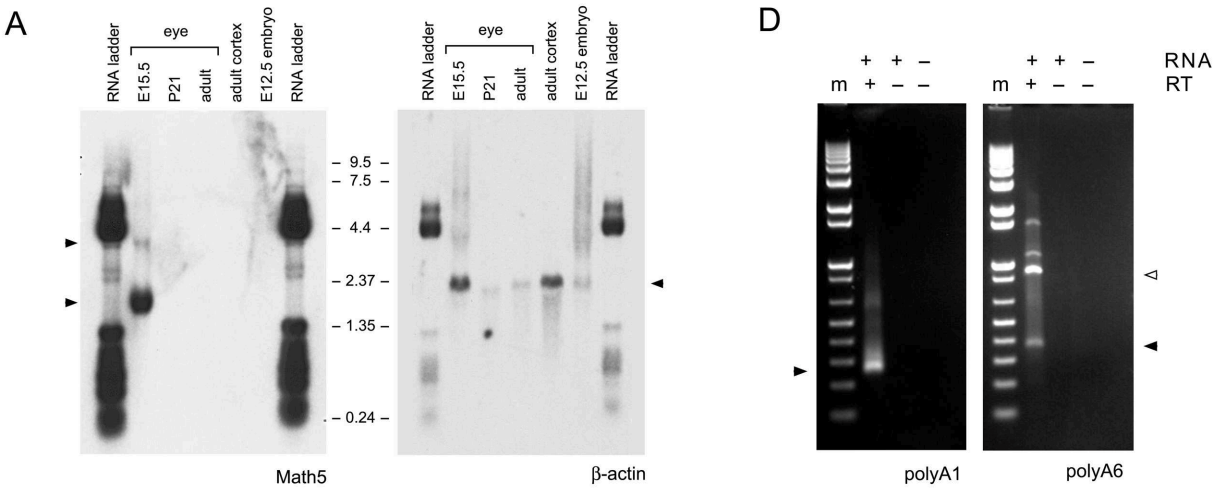

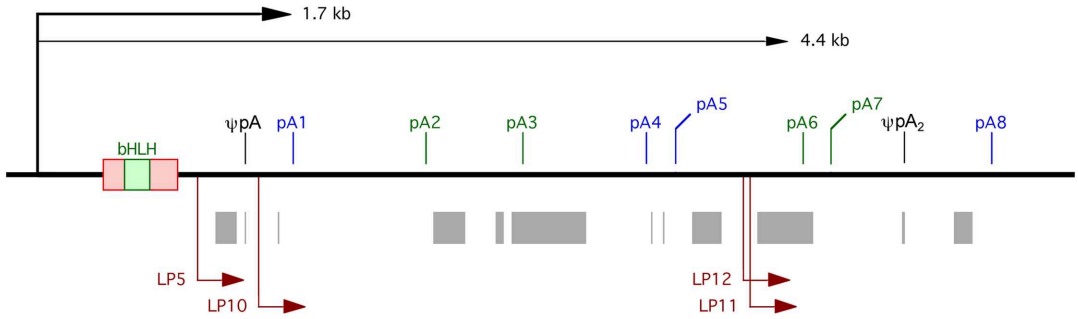

C

Site		Site	Sequence	Score
pA1	**POS**	**1474**	**ATTAAA**	**0.105092**
pA2	neg	2244	AATAAA	0.181400
pA3	neg	2804	AATAAA	0.005023
pA4	neg	3519	ATTAAA	0.000009
pA5	neg	3685	ATTAAA	0.027984
pA6	**POS**	**4424**	**AATAAA**	**0.573270**
pA7	neg	4585	AATAAA	0.068669
pA8	neg	5519	ATTAAA	0.012573

AATAAA cutoff = 0.264746 (default)
ATTAAA cutoff = 0.095796 (default)

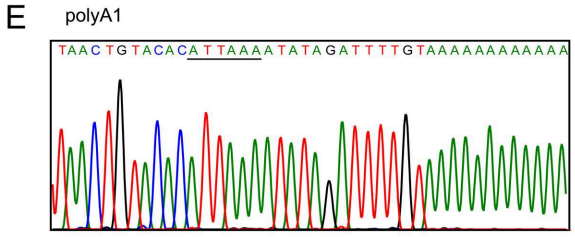

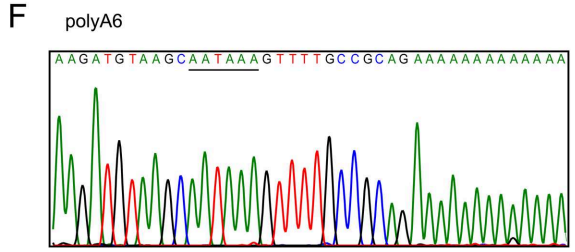

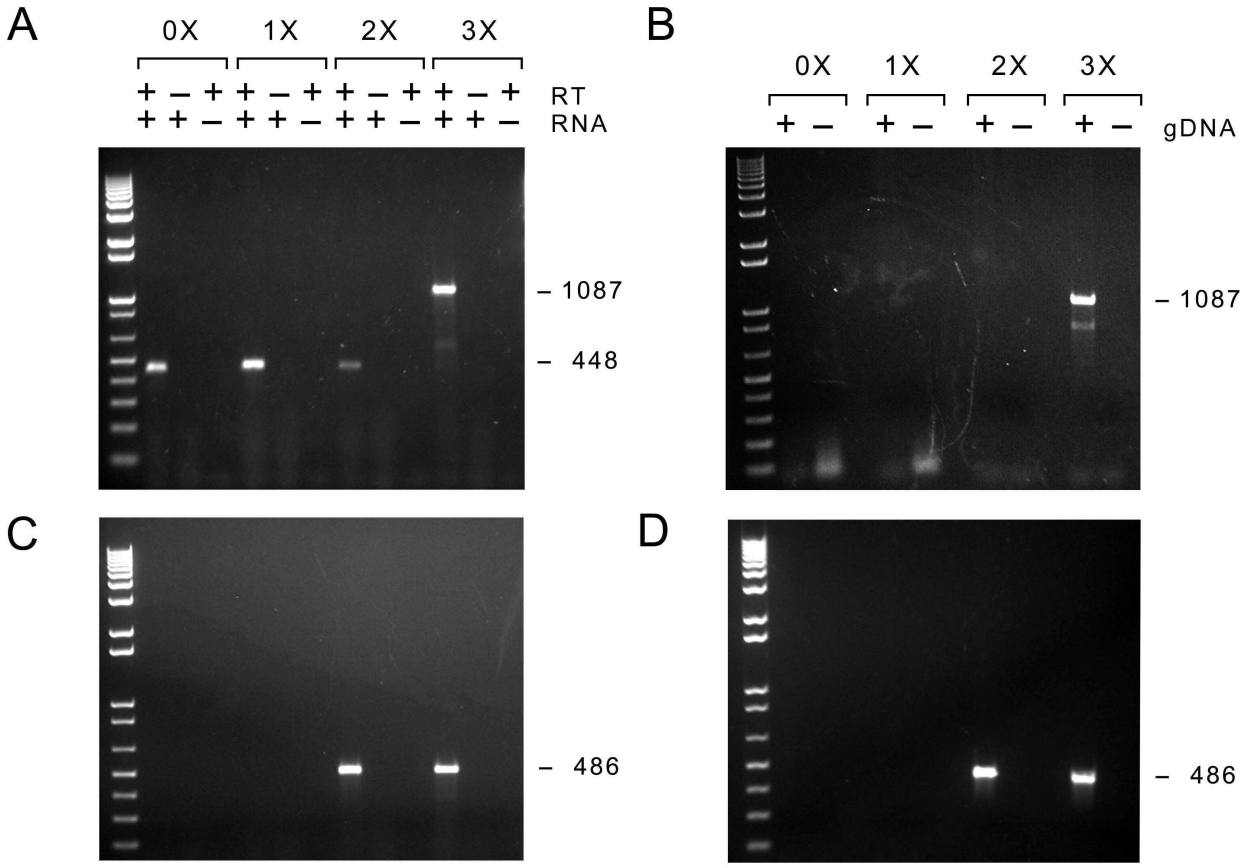

Figure II-3. *Math5* embryonic eye RT-PCRs with increasing amounts of betaine. (A) Agarose gel showing cDNA products amplified from DNase-treated E14.5 eye RNA with UTR primers LP8 and LP4 in the presence of 0X, 1X, 2X and 3X Masteramp™. When the betaine concentration was increased, only the full-length 1087bp *Math5* cDNA product was visible; the 448bp ECO product was absent. No amplimers were observed in the absence (-) of RNA template or RT enzyme. The identity of all PCR products was verified by sequencing. (B) Similar PCR with a mouse genomic DNA template, showing amplification of the identical full-length 1087bp product. (C,D) Parallel PCRs were performed using internal primers LP6 and LP7. A single 486bp *Math5* product was amplified from cDNA or gDNA in 2-3XMasteramp™.

Figure II-4. RT-PCRs of *Math5* RNA transcribed *in vitro*. (A) Diagram and agarose gel showing linearized pJN4C and *Math5* sense RNA generated by T3 polymerase and treated with DNaseI. (B) cDNA products amplified by RT-PCR from IVT-derived RNA with UTR primers LP8 and LP4. Only the full-length 1087 bp *Math5* cDNA product was amplified in the presence of 3X Masteramp (MA, indicated above brackets). In the absence of betaine, a variety of weak products were observed, with a heterogeneous deletion profile, reflecting a low level of RT template switching. This background could be increased by using suboptimal PCR conditions or omitting the mouse liver RNA carrier. IVT, *in vitro* transcribed *Math5* RNA (10 ng); ML, mouse liver RNA (3 μg). (C) Similar RT-PCRs performed using internal primers LP6 and LP7. Only the expected 486 bp cDNA was amplified in 3X MA, while spurious products were amplified at lower MA concentrations. The right three panels in B and C represent adjacent lanes in the same gels, displayed separately for clarity. (D) Alignment of lacunar cDNAs generated from IVT or E14.5 eye RNA templates. The deletion profile is comparable to the distribution reported by Kanadia and Cepko (2010, *cf.* Suppl. Table 1 and Figure 1), using the same primer pairs with no precautions for GC secondary structure. The sequence of breakpoints is given in Table S3, with microhomology at the inferred sites of RT template switching.

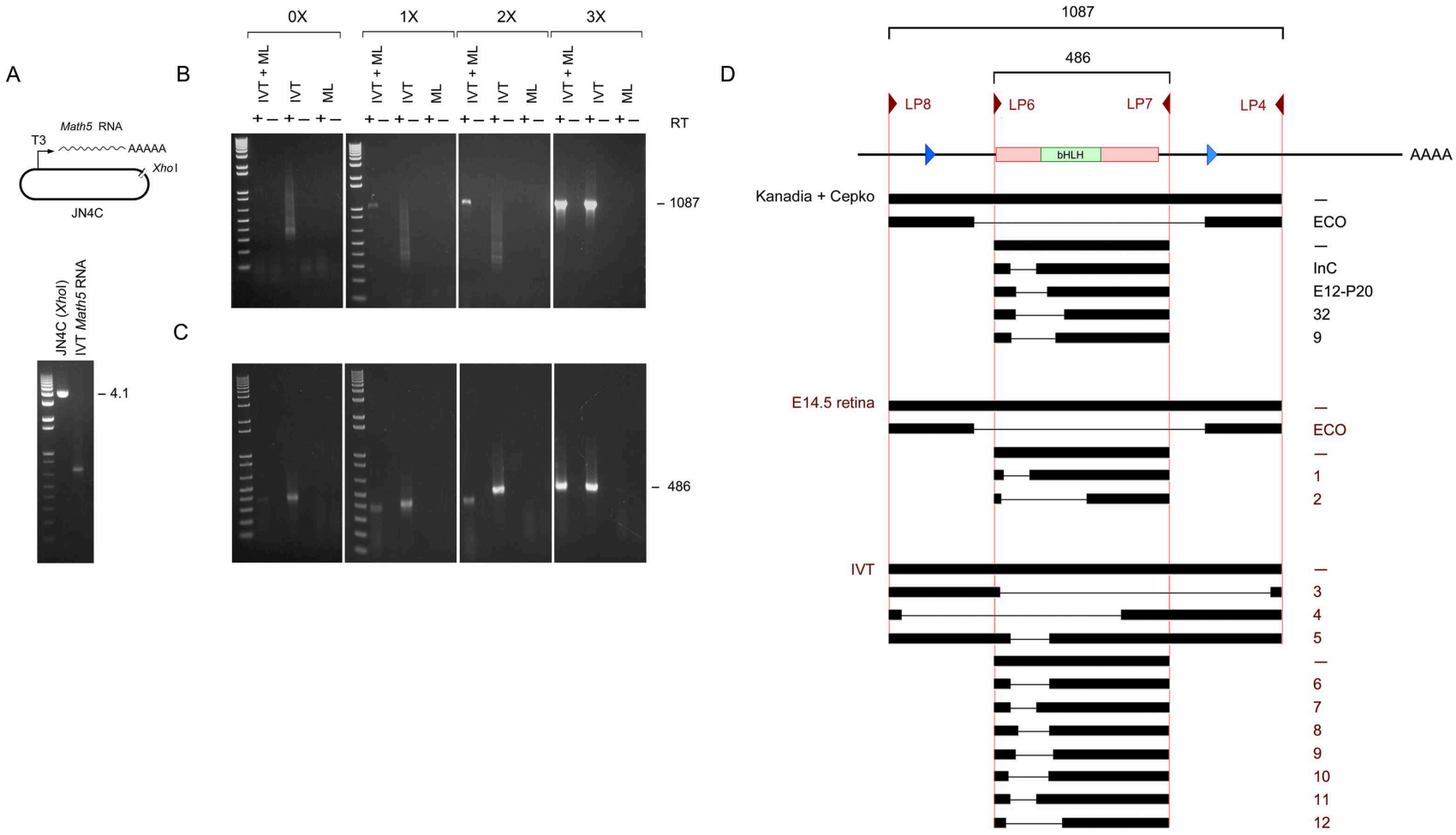
A
Math5 RNA
T3
AAAAA
XhoI
JN4C
JN4C (XhoI)
IVT Math5 RNA
– 4.1
B
0X
1X
2X
3X
IVT + ML
IVT
ML
RT
– 1087
C
– 486
D
1087
486
LP8
LP6
LP7
LP4
bHLH
AAAA
Kanadia + Cepko
ECO
InC
E12-P20
32
9
E14.5 retina
ECO
1
2
IVT
3
4
5
6
7
8
9
10
11
12

Figure II-5. Triplex competitive RT-PCR assay to evaluate trace levels of *Math5* splicing in the embryonic retina. (A) Diagram showing PCR strategy. The length and % G+C of competing amplicons are comparable. (B) Agarose gel stained with ethidium bromide, showing only the unspliced *Math5* cDNA product in each assay. (C). Capillary electrophoresis profiles showing triplex competitive RT-PCR products (top panels) and the ECO product amplified with duplex UTR primers in the presence of 1X MA (bottom panel). The common antisense primer (LP4) was end-labeled with 6-FAM. From the peak areas measured in replicate experiments and mixing controls, we estimate that the ECO product represents 0.4 to 1.0 percent of *Math5* mRNA in the embryonic retina, which is near the detection limit of this assay.

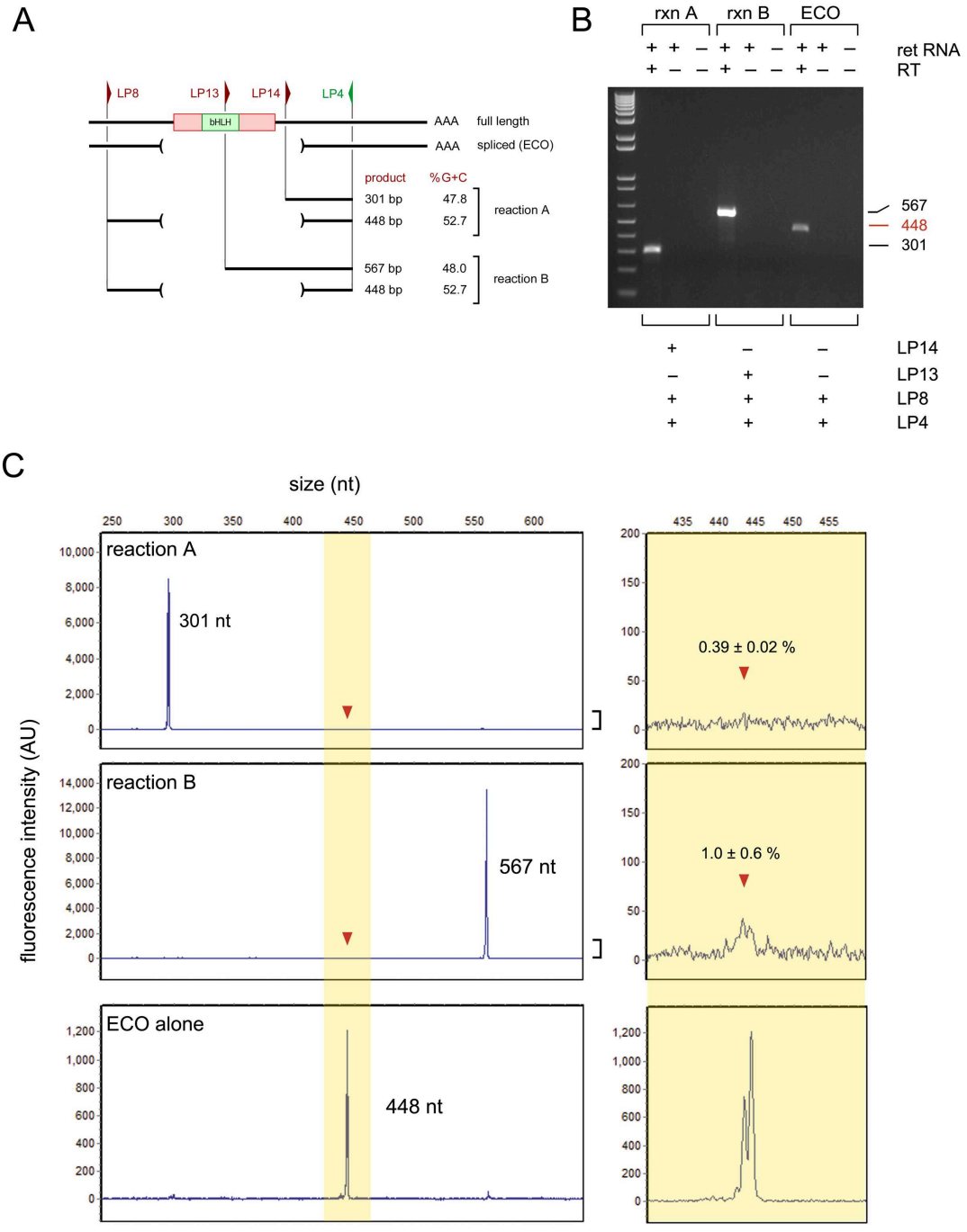
A
LP8
LP13
LP14
LP4
bHLH
AAA
full length
AAA
spliced (ECO)
product
%G+C
301 bp
47.8
448 bp
52.7
reaction A
567 bp
48.0
448 bp
52.7
reaction B
B
rxn A
rxn B
ECO
ret RNA
RT
567
448
301
LP14
LP13
LP8
LP4
C
size (nt)
fluorescence intensity (AU)
reaction A
301 nt
0.39 ± 0.02 %
reaction B
567 nt
1.0 ± 0.6 %
ECO alone
448 nt

Figure II-6. Ribonuclease protection assays. (A) Diagram showing RPA strategy, with *Math5* cDNA, two different antisense cRNA probes, protected fragments expected for FL (full length, unspliced) and ECO (spliced) transcripts, and positive control RNAs generated by sense IVT reactions. (B) Autoradiogram, showing undigested probes *A* and *B* (366 nt and 632 nt) and exclusively *unspliced* fragments protected by E14.5 eye RNA (567 nt and 301 nt). No fragment corresponding to the presumptive ECO transcript (212 nt) was protected by eye RNA using either cRNA probe, although a doublet of this size was protected by the ECO IVT positive control. Background fragments observed with probe *B* (arrowheads) are caused by intrinsic sensitivity of the cRNA-mRNA duplex to RNase cleavage at particular sites and were also present in the full length IVT positive control. The probe (no RNase) and IVT controls were diluted 20- and 10-fold respectively, compared to the E14.5 eye RNA hybridization lanes.

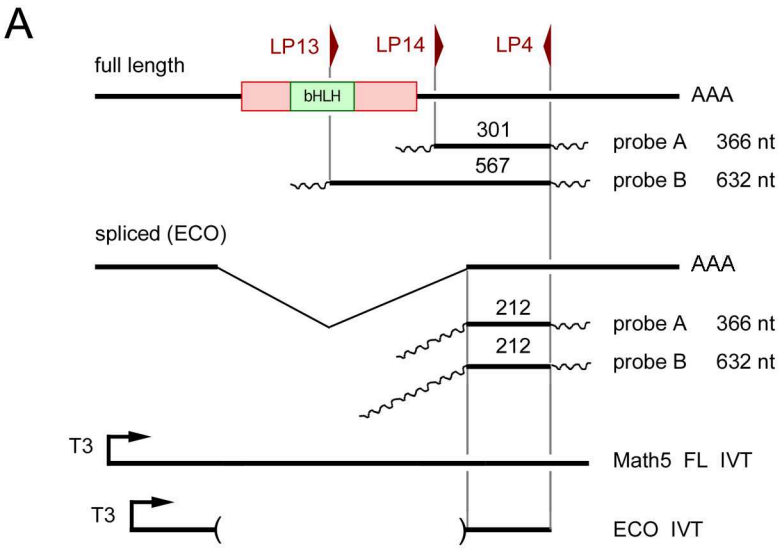
A
full length
LP13
LP14
LP4
bHLH
AAA
301
probe A 366 nt
567
probe B 632 nt
spliced (ECO)
AAA
212
probe A 366 nt
212
probe B 632 nt
T3
Math5 FL IVT
T3
ECO IVT

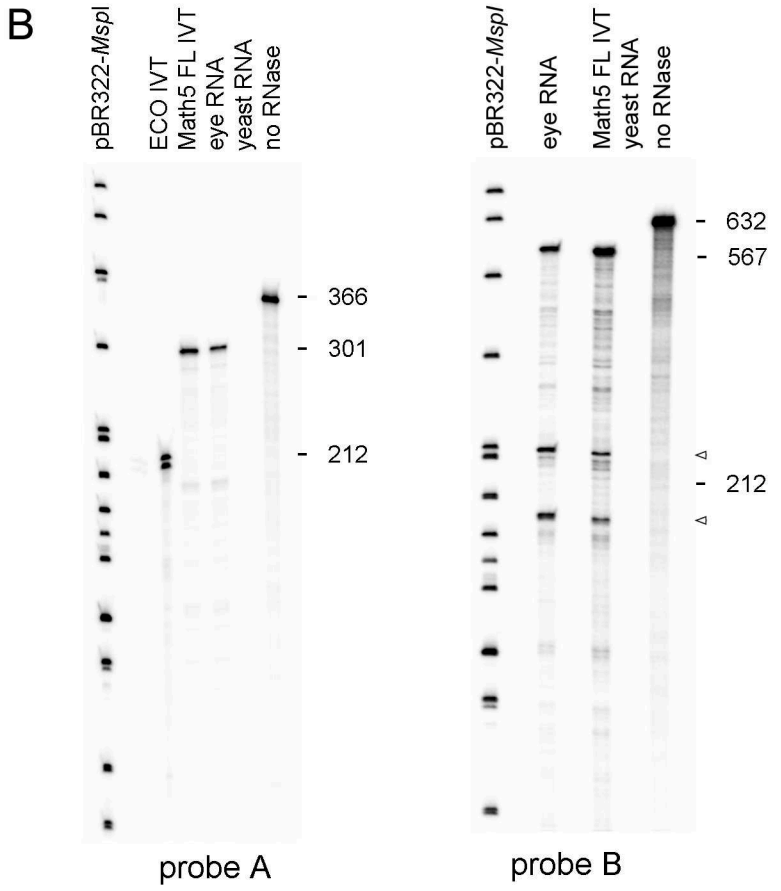
B
pBR322-MspI
ECO IVT
Math5 FL IVT
eye RNA
yeast RNA
no RNase
366
301
212
probe A
pBR322-MspI
eye RNA
Math5 FL IVT
yeast RNA
no RNase
632
567
212
probe B

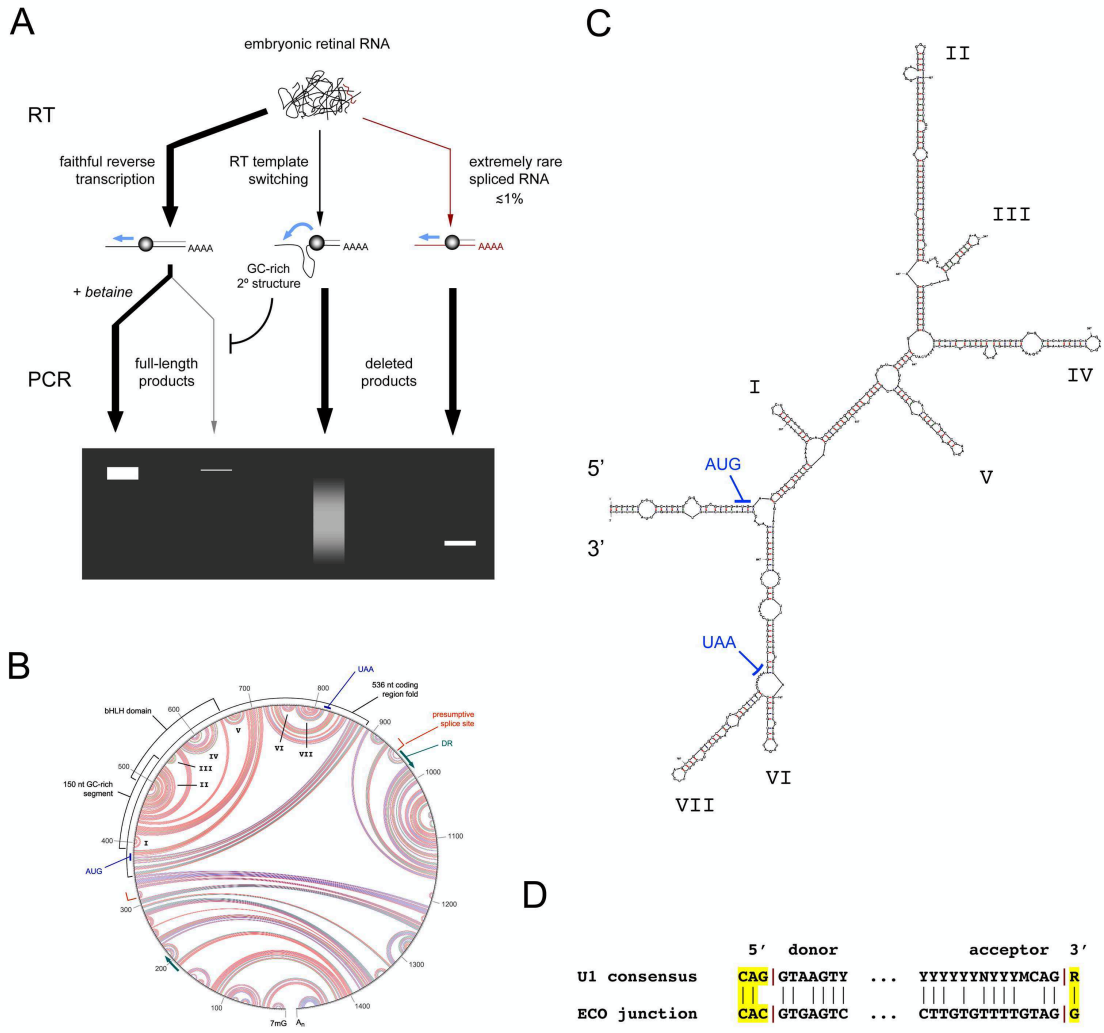

Figure II-7. Model explaining the observed results. (A) Diagram showing the likely origin of heterogeneous deleted *Math5* cDNAs, through combined effects of RT template switching, trace levels of aberrantly spliced ECO mRNA, and powerful PCR selection favoring deletion of GC-rich coding sequences. (B) Secondary structure predicted for the major 1489nt Math5 mRNA. This M-fold circle diagram, generated by free energy (G) minimization, is magnified in Figure S5. Red, blue and green arc lines indicate G-C, A-U and A-G base pairs. The coding region, DRs and presumptive ECO splice sites are labeled. The 150nt segment described in the text with >85% G+C, and the segment expanded in panel C are marked. (C) Stem-loop diagram showing the 536nt fold that encompasses the *Math5* CDS with lowest free energy (ΔG=-258 kcal/mol) and T_m≥82°C. The major structural features in panels B and C are labeled alike. (D) Junctional sequences for the ECO product with presumptive splice sites, compared to the U1 consensus.

Figure II-S1. *Math5* ESTs in the public domain. (A) Diagram modified from the UCSC mouse genome browser (mm9 assembly, chr10 : 62,562,000 - 62,564,300) showing 56 *Math5* ESTs and 2 Genbank cDNAs (BC092234, AK005214), giving a total $n = 58$, with 52 derived from the embryonic retina. Forty-three of these retinal cDNAs cross the presumptive ECO junctions at the 5' or 3' side, and are thus informative for splicing (83 %). Yet none originated from spliced mRNA. Of the remaining six, from adult brain RNA (red), two cerebellar ESTs and one cDNA were spliced at the Cb intron (yellow shading, see Figure S3). Nine 3' ESTs out of 21 terminate at pA1; the remaining 12 were primed from ψpA. (B) Comparable region of the human genome (hg19 assembly, chr10 : 69,992,300 - 69,990,000) showing one full-length Genbank cDNA and 7 unspliced ESTs.

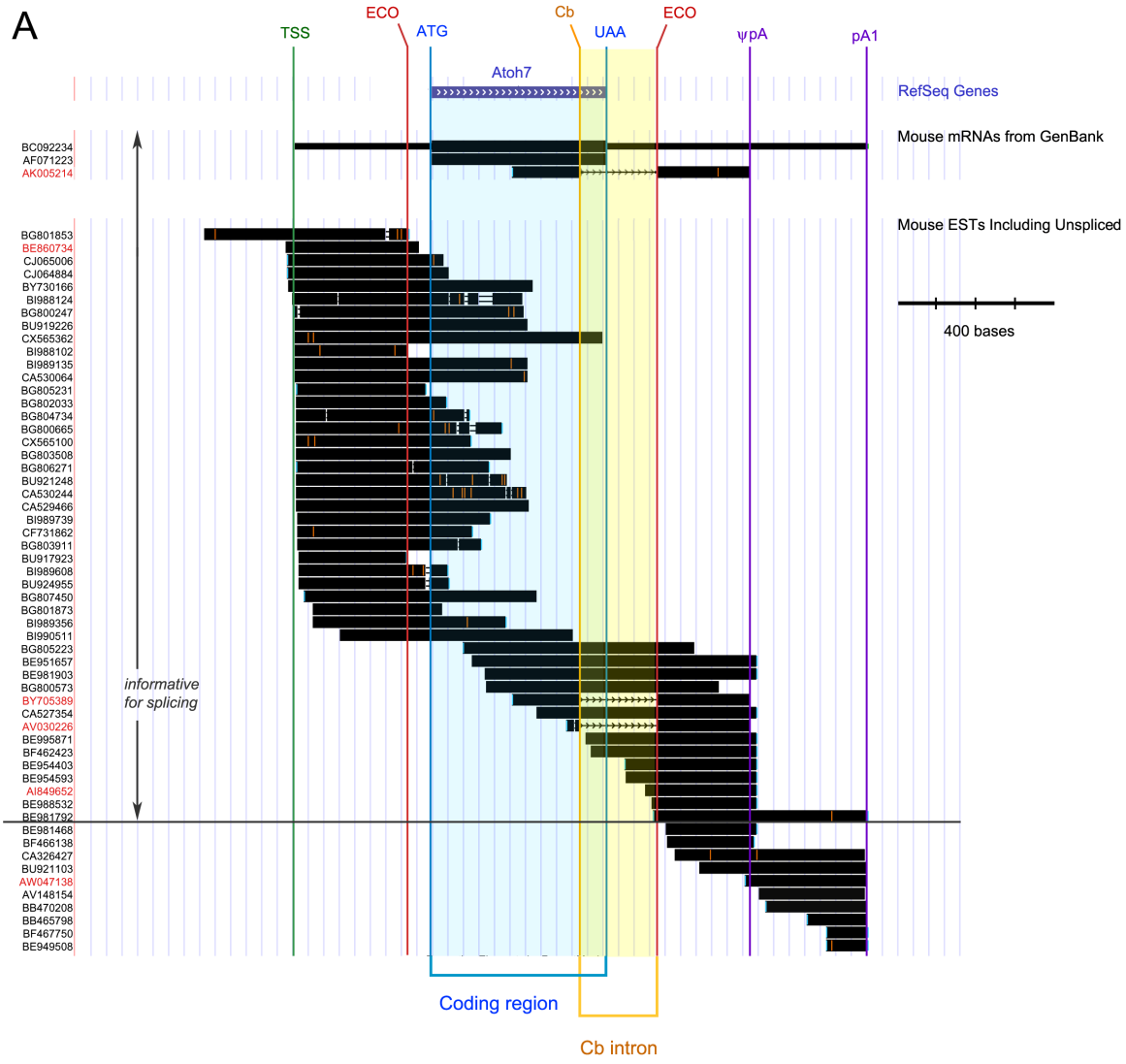
A
TSS
ECO
ATG
Cb
UAA
ECO
ψpA
pA1
Atoh7
RefSeq Genes
Mouse mRNAs from GenBank
Mouse ESTs Including Unspliced
400 bases
informative
for splicing
Coding region
Cb intron
B
ATG
UAG
ATOH7
RefSeq Genes
Human mRNAs from GenBank
Human ESTs Including Unspliced

Figure II-S2. Evaluation of Math5 antibodies. (A) Diagram of the mouse Math5 protein, showing the antigenic index (Jameson and Wolf, 1988) and positions of immunogens used by various sources to prepare antibodies, as follows: *a*,*b* internal and C-terminal peptides (Glaser lab); *c*, ab13536 (Abcam); *d*, AB5694 (Chemicon); *e*, EB07972 (Everest); *f*, 1A5 (multiple vendors). The immunogens for D01P (Abnova) and MAb 1A5 were full-length or partial recombinant human proteins (gray); all others were based on the mouse polypeptide (blue). No immunogen was specified for ab78046 (Abcam). (B) Immunoblots of NIH3T3 cells co-transfected in parallel with pUS2-EGFP and pCS2 expression plasmids for full-length mouse or human Math5 proteins ± six N-terminal Myc epitope tags, or empty pCS2 vector. Five identical blots were probed using antibodies with stated reactivity to mouse (ab13536, ab78046) or human (D01P) Math5; Myc or GFP. The predicted mass for native and 6xMyc mouse Math5 proteins is 16.9 and 27.0 kDa, respectively. Antibody D01P detected the human polypeptides, but not mouse. No other reagent tested was effective, including ab13536 (Abcam) (Kanadia and Cepko, 2010), even when the Math5 proteins were massively overexpressed. (C) Retinal sections from E15.5 embryos immunostained with ab13536 sera. The immunofluorescence pattern was identical between wild-type and *Math5* -/- eyes and is thus nonspecific (Rhodes and Trimmer, 2006; Saper and Sawchenko, 2003). This pattern, which includes lens and RPE nuclei, does not fit the apical distribution of *Math5* mRNA in the neuroblastic retina. The *in situ* hybridization pattern of a *Math5* cRNA probe spanning the 3' UTR and CDS matches our previous reports (Brown et al., 1998; Hufnagel et al., 2010) and both panels provided by Kanadia and Cepko (*cf.* Figure 1j and 1j').

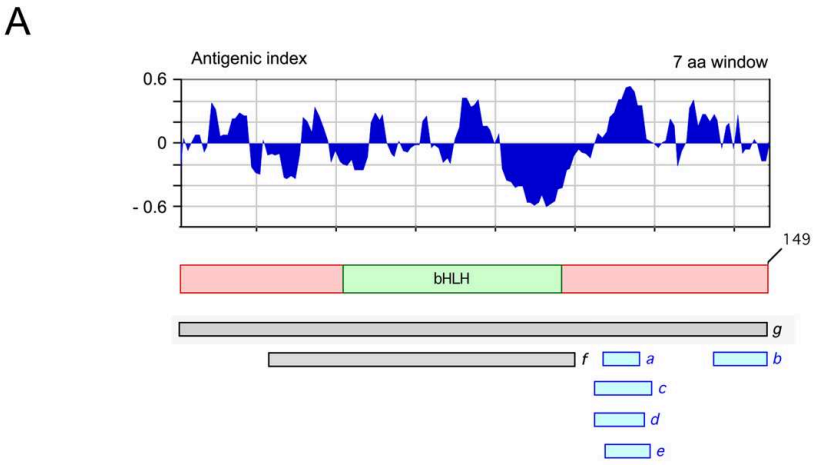
A
Antigenic index
7 aa window
0.6
0
- 0.6
149
bHLH
g
f
a
b
c
d
e

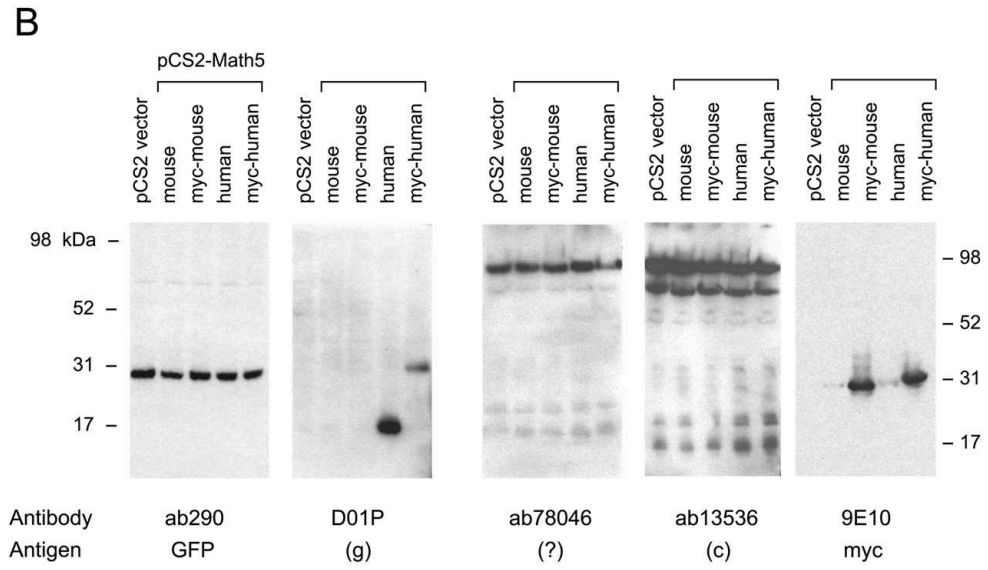
B
pCS2-Math5
pCS2 vector
mouse
myc-mouse
human
myc-human
98 kDa
52
31
17
– 98
– 52
– 31
– 17
Antibody
Antigen
ab290
GFP
D01P
(g)
ab78046
(?)
ab13536
(c)
9E10
myc

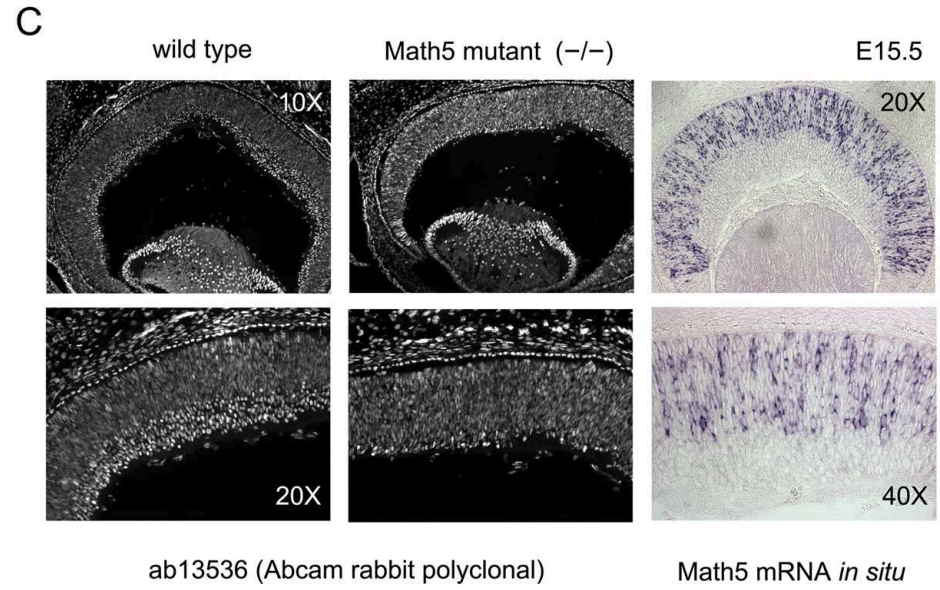
C
wild type
Math5 mutant (−/−)
E15.5
10X
20X
20X
40X
ab13536 (Abcam rabbit polyclonal)
Math5 mRNA *in situ*

Figure II-S3. *Math5* splicing in the cerebellum. (A) Diagram of alternative Cb intron, with PCR primers and products. (B) Sequence of Cb splice junction, corresponding to nucleotides 3524 and 3724 in Genbank acc. AF418923. The acceptor site coincides with the ECO junction (Figure 7D). (C) Spliced cerebellar mRNA encodes a truncated Math5 protein, with 20 fewer amino acids at the C-terminus. The deleted peptide has a similar sequence among amniotes, but the splice junction is not obviously conserved. (D) Agarose gel showing spliced (368 bp) and unspliced (567 bp) RT-PCR products from the adult cerebellar RNA, but not from E14.5 retina. (E) Triplex competitive RT-PCR showing spliced (228 bp) and unspliced (301 bp) products co-amplified from cerebellar cDNA (right lanes). In the duplex control with primers LP15 and LP4, only the Cb form (spliced) was amplified (left lanes). (F) Capillary electrophoresis profiles showing the ratio of spliced (Cb) and unspliced (FL) transcripts in the triplex PCR (top), with Cb duplex product as a control (bottom). The common antisense primer LP4 was labeled with 6-FAM. Approximately 11 ± 2 percent of *Math5* mRNAs are spliced at the Cb site in the adult cerebellum.

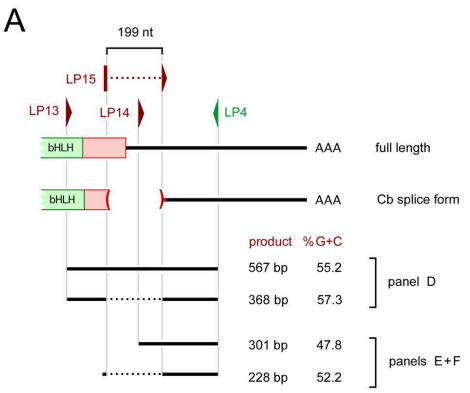
A
199 nt
LP15
LP13
LP14
LP4
bHLH
AAA
full length
bHLH
AAA
Cb splice form
product
%G+C
567 bp
55.2
368 bp
57.3
panel D
301 bp
47.8
228 bp
52.2
panels E+F

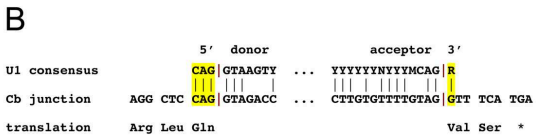
B
5′ donor
acceptor
3′
U1 consensus
CAG|GTAAGTY ... YYYYYYNYYYMCAG|R
Cb junction
AGG CTC CAG|GTAGACC ... CTTGTGTTTTGTAG|GTT TCA TGA
translation
Arg Leu Gln
Val Ser *

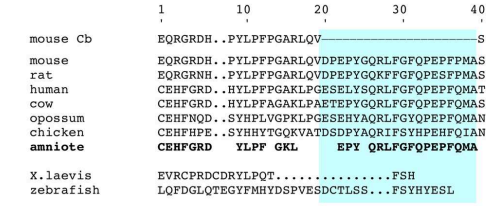
C
1
10
20
30
40
mouse Cb
EQRGRDH..PYLPFPGARLQV
S
mouse
rat
human
cow
opossum
chicken
amniote
EQRGRDH..PYLPFPGARLQVDPEPYGQRLFGFQPEPFPMAS
EQRGRNH..PYLPFPGARLQVDPEPYGQKFFGFQPESFPMAS
CEHFGRD..HYLPFPGAKLPGESELYSQRLFGFQPEPFQMAT
CEHFGRD..HYLPFAGAKLPAETEPYGQRLFGFQPEPFQMAS
CEHFNQD..SYHPLVGPKLPGESEHYAQRLFGYQPEPFQMAN
CEHFHPE..SYHHYTGQKVATDSDPYAQRIFSYHPEHFQIAN
CEHFGRD YLPF GKL EPY QRLFGFQPEPFQMA
X.laevis
zebrafish
EVRCPRDCDRYLPQT.....FSH
LQFDGLQTEGYFMHYDSPVESDCTLSS...FSYHYESL

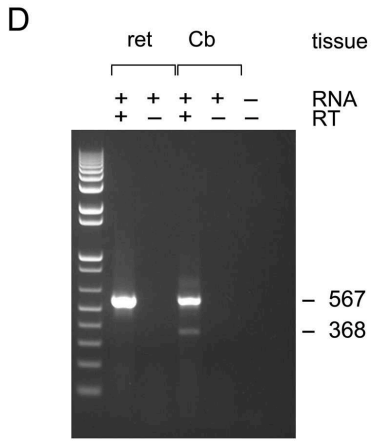
D
ret
Cb
tissue
RNA
RT
567
368

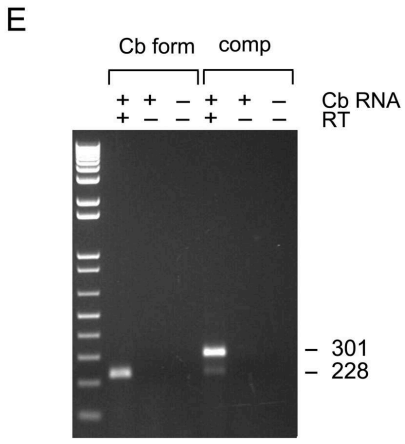
E
Cb form
comp
Cb RNA
RT
301
228

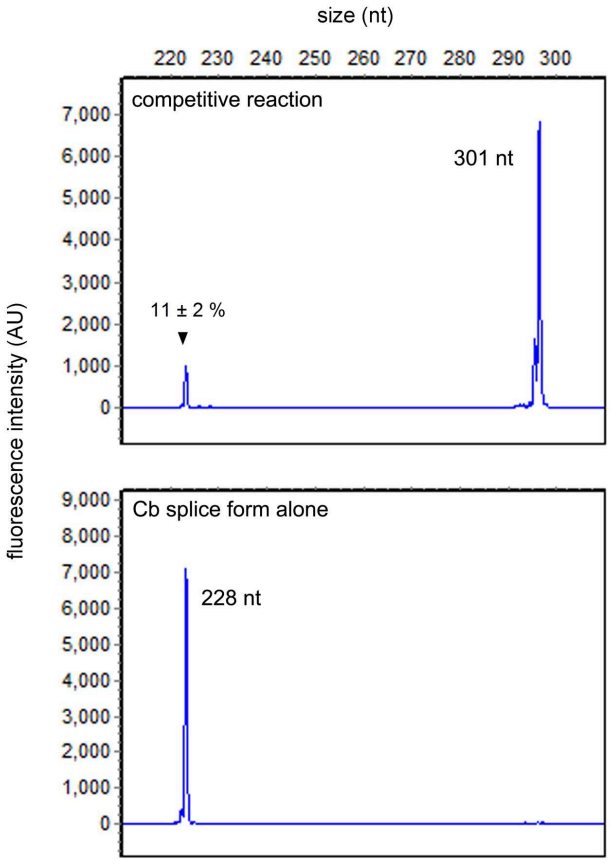
F
size (nt)
220 230 240 250 260 270 280 290 300
competitive reaction
301 nt
11 ± 2 %
fluorescence intensity (AU)
Cb splice form alone
228 nt

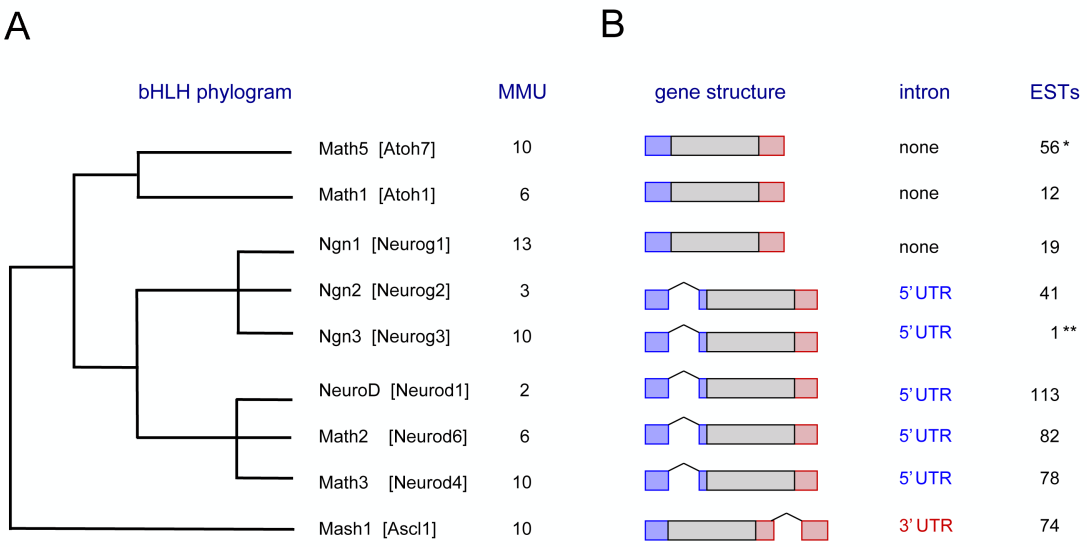

Figure II-S4. Splicing patterns in the mouse Atonal-related bHLH genes. (A) Phylogram of mouse Ato proteins, based on maximum parsimony analysis of the bHLH domain across many taxa (Blackburn et al., 2008; Brown et al., 2002). (B) Exon-intron organization of bHLH genes based on a survey of ESTs in the NCBI database (Brett et al., 2002; Harrington et al., 2004). The eight mouse Ato homologs either have unitary exon structures, or a single intron located in the 5'UTR. The Achaete-Scute homolog *Mash1* (*Ascl1*) has a single intron in the 3'UTR. There is no obvious correlation between splicing patterns and locations in the mouse genome. MMU, mouse chromo ESTs, number of expressed sequence tags supporting the gene structure; *has minor alternative spliced product (Cb); **has overlapping intergenic and antisense RNAs. The intron of one spliced antisense EST (CF104925) for *Ngn3* (*Neurog3*) overlaps the 5'UTR and coding sequence of the sense strand. This antisense RNA is predicted to co-amplify in the RT-PCR and may be mistaken for non-coding sense products.

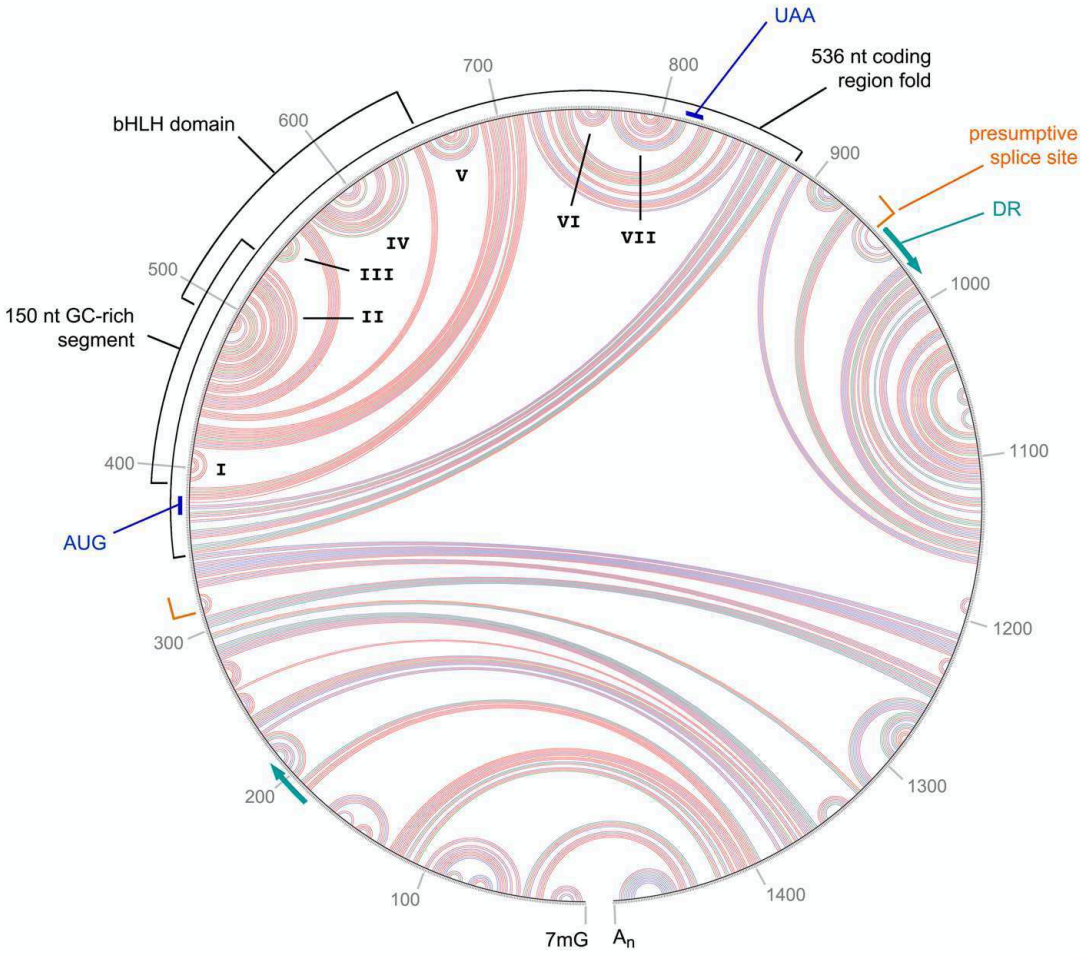

Figure II-S5. Secondary structure for Math5 mRNA. This circle plot was generated by free energy minimization of the 1489nt mRNA, and is enlarged from Fig. II-7. Red, blue and green arc lines indicate G C, A U and A G base pairs. The coding region, DRs and presumptive ECO splice sites are labeled. The 150nt segment with >85% G+C, and 536nt segment spanning the CDS are marked. The CDS contains a high density of G-C base pairs (red arcs), which are deleted in rare, mis spliced RNAs.

Table II-S1. Oligonucleotide primers in this study

				Alternate names‡	
Name	**Ori**	**Sequence (5′→3′)**	**Expt**	**Sup. Fig. 2**	**Sup. Table 2**
LP1	S	TCTACTGCAAGCTGTCCAAACGCTC	RT-PCR	1	
LP2	AS	AACATACAGGCTGTGTTGGTAGCTG	RT-PCR	2	
LP3	AS	GGTAGCTGCTCAGAACATAAACAAGTCACAT	RT-PCR	3	
LP4	AS	GTTTCTCCACCTCCTGAATGACGCT	RT-PCR, triplex PCR†	4	
LP5	S	GCCTCCCTATCTCCACTTCTCTTGTGT	RT-PCR, 3′RACE (pA1)	5	
LP6	S	GTGGATGAAGTCGGCCTGCAAA	RT-PCR	6	
LP7	AS	TTTCTCCCCTAAGACCCAAATGGC	RT-PCR	7	
LP8	S	TCTCAGGCTTTCCCAGAGAACTGGA	RT-PCR, triplex PCR		1
LP9	AS	TTTGCAGGCCGACTTCATCCAC	RT-PCR		2
AP	AS	GGCCACGCGTCGACTAGTACTTTTTTTTTTTTTTTT	3′RACE		
UAP	AS	GGCCACGCGTCGACTAGTAC	3′RACE		
LP10	S	TCCCTATTGGGCGAAGTTGT	3′RACE (pA1)		
LP11	S	AGGGTGAAGTGCTTGCTGGT	3′RACE (pA6)		
LP12	S	GTTACAGGGCCTGCGAAATG	3′RACE (pA6)		
LP13	S	AAGCTGTCCAAGTACGAGACACTGC	RT-PCR, triplex PCR		
LP14	S	CCTTTTCTGCTTAATTTCCTTCCCG	triplex PCR		
LP15	S	GGGTGCTAGGCTCCAG|GTTTC	triplex PCR (Cb)*		

Ori, orientation; S, sense; AS, antisense; AP, adapter primer; UAP, universal amplification primer

*primer sequence spans Cb intron junction

†end-labeled with 6-carboxyfluorescein (6-FAM)

‡used by Kanadia and Cepko (2010)

Table II-S2. PCR conditions used in this study

Experiment	Primers FOR	Primers REV	# cycles†	Product	Size	Figure
RT-PCR, gPCR	LP8	LP4	35 or 40	Math5 full length ECO	1087 448	3a, 3b, 4b
RT-PCR, gPCR	LP6	LP7	35 or 40		486	3c, 3d, 4c
RT-PCR	LP13	LP4	35	unspliced Cb splice	567 368	Suppl 3d
RT-PCR	LP15	LP4*	33	Cb splice	228	Suppl 3e
3'RACE pA1	LP5 LP10	UAP UAP	15 20	initial RACE nested RACE	>591‡ >236‡	2d
3'RACE pA6	LP11 LP12	UAP UAP	15 20	initial RACE nested RACE	>379‡ >342‡	2d
Triplex RT-PCR¶	LP8 LP13	LP4*	33	unspliced ECO	567 448	6b, 6c
Triplex RT-PCR¶	LP8 LP14	LP4*	33 33	unspliced ECO	301 448	6b, 6c
Triplex RT-PCR¶	LP14 LP15	LP4*	33	unspliced Cb splice	301 228	Suppl 3e

Notes:

*End-labeled with 6-FAM (carboxyfluorescein)

†All PCRs had an initial denaturation step (94°C x 3 min); followed by # cycles of 94°C x 30 sec denaturation, 57°C x 45 sec annealing, and 72°C x 60-70 sec extension; with a final extension step (72°C x 7 min)

‡Products include a variable polyA tract

¶Triplex PCRs untilized 3 primers, with 2 FOR primers at 0.1 µM each and 1 REV primer at 0.2 µM.

Table II-S3. DNA sequence flanking deletions in RT-PCR products

No.	5′ sequence	del	3′ sequence
from Kanadia and Cepko (2010)			
ECO	... ACTGACTGCAC|GTGAGTCGCTCCGTC	[639]	TGTTTTGTAG|GTTTCATGAGTGGACATC ...
InC	... CCCTCCGGCGGGAGCT|CGCGGCGCGC	[71]	|CGCGGCGCGCAGGCGTCTGGCGGCCAAC ...
E12P20	... TCGCGGCGCGCCCCCGT|GCGCGGGCG	[85]	|GCGCGAGCGGCGCCGCATGCAGGGGCTG ...
32	... TCGCGGCGCGCCCCCG|TGCGCGGGCG	[134]	|TGCGCAGGGTGGTGCCGCAGTGGGGCCA ...
9	... GGCCCTCCGGCGGGAGCTCGC|GGCGC	[122]	GG|GGCTGAACACGGCGTTCGACCGGCTG ...
from E14.5 retina RT-PCR (•2X MasterAmp™, 40 cycles)			
1	... AAGTCGGCCTGCAAACCCCAC|GGCCC	[70]	|GGCCCGGGCGGCTGGAGAGCGCGGCGCG ...
2*	... ATGAAGTCGGCCTGCAA|ACCCCACG	[235]	CTGCAG|ATGGCGCTCAGCTACATCATCG ...
from RT-PCR of IVT RNA (•2X MasterAmp™)			
3	... CGTGGATGAAGTCGGCCTG|CAAACC	[746]	|TAATCCTAGCGTCATTCAGGAGGTGGA ...
4	... GAAAGGCTTTCTAT|CCCCGACCCCC	[605]	|CCCCTACCTCCCTTTCCCGGGTGCTAG ...
5	... CTCCGGCGGGAGCTC|GCGGCGCGCC	[106]	|GCGGCGCCGCATGCAGGGGCTGAACAC ...
6	... CTCCGGCGGGAGCTC|GCGGCGCGCC	[106]	|GCGGCGCCGCATGCAGGGGCTGAACAC ...
7	... CTCCGGCGGGAGCTC|GCGGCGCGCC	[70]	|CGCGGCGCGCAGGCGTCTGGCGGCCAA ...
8	... CGCGCCCCCGTGCGCGG|GCGCAGCC	[85]	GCGCGA|GCGGCGCCGCATGCAGGGGCT ...
9	... CTCGCGGCGCGCCCCCG|TGCGCGGGC	[103]	|TGCAGGGGCTGAACACGGCGTTCGACC ...
10	... CCCCACGGCCCTCCGGCGG|GAGCTCG	[110]	GCGC|GAGCGGCGCCGCATGCAGGGGCT ...
11	... CCCTCCGGCGGGAGCT|CGCGGCGCGC	[71]	|CGCGGCGCGCAGGCGTCTGGCGGCCAA ...
12	... TGCAAACCCCACGGCCCT|CCGGCGGG	[155]	|CCGGCTGCGCAGGGTGGTGCCGCAGTG ...

Spurious RT-PCR products are numbered to match Figure 5. The highlighted text shows areas of micro-homology, which can promote RT template switching. The size of the deletion [bp] and breakpoints (|) are indicated.

***Product is likely due to mis-priming of LP6.**

CHAPTER III

MATH5 DEFINES THE GANGLION CELL COMPETENCE STATE IN A SUBPOPULATION OF RETINAL PROGENITOR CELLS EXITING THE CELL CYCLE

Abstract

The basic helix-loop-helix (bHLH) transcription factor *Math5* (*Atoh7*) is transiently expressed during early retinal histogenesis and is necessary for retinal ganglion cell (RGC) development. Using nucleoside pulse-chase experiments and clonal analysis, we determined that progenitor cells activate *Math5* during or after the terminal division, with progressively later onset as histogenesis proceeds. We have traced the lineage of *Math5*+ cells using mouse BAC transgenes that express Cre recombinase under strict regulatory control. Quantitative analysis showed that *Math5*+ progenitors express equivalent levels of *Math5* and contribute to every major cell type in the adult retina, but are heavily skewed toward early fates. The Math5>Cre transgene labels 3% of cells in adult retina, including 55% of RGCs. Only 11% of *Math5*+ progenitors develop into RGCs; the majority become photoreceptors. The fate bias of the *Math5* cohort, inferred from the ratio of cone and rod births, changes over time, in parallel with the remaining neurogenic population. Comparable results were obtained using *Math5* mutant mice, except that ganglion cells were essentially

absent, and late fates were overrepresented within the lineage. We identified *Math5*-independent RGC precursors in the earliest-born (embryonic day 11) retinal cohort, but these precursors require *Math5*-expressing cells for differentiation. *Math5* thus acts permissively to establish RGC competence within a subset of progenitors, but is not sufficient for fate specification. It does not autonomously promote or suppress the determination of non-RGC fates. These data are consistent with progressive and temporal restriction models for retinal neurogenesis, in which environmental factors influence the final histotypic choice.

Introduction

The seven major cell types in the vertebrate retina (rod and cone photoreceptors; amacrine, horizontal and bipolar interneurons; Müller glia; and ganglion cells) develop from a common pool of progenitors (Turner and Cepko, 1987; Turner et al., 1990) that are established when the optic vesicles invaginate to form bilayered optic cups (Goldowitz et al., 1996). The inner layer of each optic cup consists of proliferative retinal progenitor cells (RPCs), which are arranged as a pseudostratified epithelium. These RPCs begin to permanently exit mitosis and differentiate around embryonic day 11 (E11) in the mouse. Retinal neurons and glia are fully formed by postnatal day 21 (P21) and are arranged in a highly ordered tri-laminated structure (Rodieck, 1998). The outer nuclear layer (ONL) consists of photoreceptors while the inner nuclear (INL) and ganglion cell (GCL) layers are populated by interneurons, glia and ganglion cells.

The mechanism of cell fate determination – how these diverse cell types are generated from an initially homogeneous progenitor population – remains poorly understood.

Birthdating experiments, in which [^{3}H]-thymidine was used to mark the terminal S phase of progenitor cells, have established a characteristic order for the emergence of different retinal cell types during histogenesis (Carter-Dawson and LaVail, 1979; Rapaport et al., 2004; Sidman, 1961; Young, 1985a). In all vertebrate species examined, retinal ganglion cells are the first-born neurons (Altshuler et al., 1991). In mammals, these are followed by horizontal cells, cones, amacrines, rods, bipolar cells and Müller glia, in descending birth order. There is considerable overlap in the distribution of birthdates among cell types, particularly for rod photoreceptors, which are born over an extended period (E13-P7 in mice) and are most abundant. Moreover, as a subclass, displaced amacrines, located in the mammalian GCL, are born earlier than amacrines in the INL (LaVail et al., 1991; Reese and Colello, 1992).

Lineage tracing experiments in rodents and frogs show that individual retinal progenitors are multipotent, giving rise to clones with heterogeneous cell type composition and size, and that the histogenic potential of the progenitor pool is gradually restricted over time (Holt et al., 1988; Turner and Cepko, 1987; Turner et al., 1990; Wetts and Fraser, 1988; Wong and Rapaport, 2009). The absence of a strict hierarchical relationship among cell types suggests that fate determination in the retina is a stochastic process (Gomes et al., 2011; Livesey and Cepko, 2001). The observation of discordant two-cell clones in rodent

lineage marking studies indicates that at least some cell fate decisions occur during or after the terminal division, and may be subject to environmental influence (Turner and Cepko, 1987). Indeed, multiple extrinsic factors have been shown to alter the ratio of retinal cell types generated from progenitor pools (Altshuler et al., 1991; Ezzeddine et al., 1997; Fuhrmann et al., 1995; Yang, 2004; Young and Cepko, 2004).

Heterochronic mixing experiments, in which early and late retinal cells are co-cultured in unequal ratios, have shown that progenitors have a limited capacity to shift their fate forward or backward in sequence, and suggest that competence is fundamentally a cell-intrinsic property (Belliveau and Cepko, 1999; Rapaport et al., 2001; Reh, 1992; Watanabe and Raff, 1990). Likewise, single-cell dissociation studies have shown that the fates of retinal progenitors, including post-mitotic cells, change over time and are intrinsically programmed (Adler and Hatlee, 1989; Cayouette et al., 2003; Reh and Kljavin, 1989). Thus, it is likely that cell-intrinsic factors, expressed by progenitors in a prescribed temporal order, work in concert with extrinsic factors in the retinal microenvironment to guide cell fate decisions and ensure proper ratios of each cell type.

The basic helix-loop-helix (bHLH) transcription factor Math5 (Atoh7) was identified on the basis of its homology to *Drosophila* Atonal (Brown et al., 1998), which plays a critical role in the specification of R8 photoreceptors in the eye imaginal disc (Frankfort and Mardon, 2002; Hsiung and Moses, 2002; Jarman, 2000; Sun et al., 2003). The mouse *Math5* gene contains a single exon (Prasov

et al., 2010) and is specifically expressed by progenitor cells during retinal histogenesis (Brown et al., 1998), similar to frog, chick, and zebrafish orthologs (Kanekar et al., 1997; Liu et al., 2001; Masai, 2000). *Math5* mutant mice lack retinal ganglion cells (RGCs) and optic nerves (Brown et al., 2001; Wang et al., 2001) and their circadian rhythms are not photoentrained (Brzezinski et al., 2005; Wee et al., 2002). Retinal vascular development (Brzezinski et al., 2003) and electrophysiology (Brzezinski et al., 2005) are also disrupted in these mice. Finally, the relative abundance of other retinal cell types is altered, through a combination of cell autonomous and non-autonomous effects (Brzezinski et al., 2005; Le et al., 2006). RGC genesis similarly fails in *ath5* mutant (*lakritz)* zebrafish (Kay et al., 2001). In humans, *ATOH7* mutations cause optic nerve aplasia (Ghiasvand et al., 2011) and the *ATOH7* locus is a major determinant of normal variation in optic disc size, which reflects RGC number (Khor et al., 2011; Macgregor et al., 2010; Ramdas et al., 2010).

Math5 is likely to trigger a regulatory cascade for RGC development. Expression of the POU domain transcription factor *Brn3b* (*Pou4f2*) appears to be controlled by *Math5* in mice, similar to the orthologous circuit in chick and frog (Hutcheson and Vetter, 2001; Liu et al., 2001; Schneider et al., 2001; Wang et al., 2001). In turn, *Brn3b* and the homeodomain transcription factor *Isl1* form two regulatory nodes that are critical for RGC maturation (Erkman et al., 1996; Gan et al., 1996; Mu et al., 2004; Mu et al., 2008; Pan et al., 2008).

How does *Math5* regulate ganglion cell fate determination? In principle, *Math5* could act either as an *instructive* factor, irreversibly directing competent

progenitors to differentiate into RGCs, or as a *permissive* factor, establishing an RGC competence state within a set of multipotent progenitors, only some of which develop into RGCs (Wessells, 1977). The Cre-lox recombination system provides a powerful tool to distinguish these mechanisms, by indelibly marking descendant cells. In a previous lineage analysis, a *Math5-Cre* knock-in allele was found to mark multiple retinal cell types, suggesting that Math5 acts permissively (Feng et al., 2010; Yang et al., 2003).

In this report, we extend these findings using a Math5>Cre BAC transgene in wild-type and *Math5* mutant mice. This approach, coupled with birthdating analysis, has allowed us to quantitatively assess the cell type distribution and unique fate trajectory of the Math5 lineage over time. Our results show *Math5* is expressed at equivalent levels in a subset of progenitors that are capable of forming all retinal cell types, with a frequency that decreases according to birth order. Although heavily weighted toward early fates, only 11% of these cells develop into RGCs and only 55% of RGCs descend from Math5+ progenitors. In the absence of *Math5* function, lineage-marked cells exhibit a similarly diverse range of fates but do not differentiate as RGCs, suggesting Math5 has both autonomous and non-autonomous roles in RGC development. Using cell cycle markers and nucleoside pulse-chase analysis, we show *Math5* expression is confined to progenitors during or after the terminal division, and does not control cell cycle exit. Finally, using retroviral clone analysis of explanted embryonic retinas, we demonstrate that *Math5*+ cells frequently arise in pairs from symmetric terminal divisions. Our results extend previous observations, but

compel different conclusions. We provide new insights into *Math5* function, ganglion cell development, and the mechanism of retinal fate determination.

Materials and Methods

Quantitative PCR

Eye tissue was collected from 8-12 CD-1 embryos or newborn mice at time-points between E10.5 and P1.5 and homogenized in Trizol reagent (Invitrogen, Carlsbad, CA). Total RNA was purified from pooled homogenates at each time-point. cDNA was synthesized using $d(N)_6$ primer and Superscript II reverse transcriptase (Invitrogen). Quantitative PCR was performed on cDNA using *Math5* and *Hprt* primers (Brown et al., 2001) with the iCycler iQ system (Bio-Rad, Hercules, CA). Seven measurements were made for each cDNA pool. *Math5* RNA levels (critical threshold cycles) were normalized to *Hprt* as described (Livak and Schmittgen, 2001), and are reported relative to the mean P1.5 value.

Math5>Cre BAC transgenic mice

We replaced the *Math5* open reading frame on bacterial artificial chromosome (BAC) clone RP23-328P3 with a 2.0 kb nlsCre-βactin pA cassette using a two-step *recA*-mediated recombination protocol in *E. coli* (Gong et al., 2002; Heintz, 2001). To target the BAC, which contains 110 kb 5' and 103 kb 3' genomic DNA flanking the *Math5* transcription unit (Prasov et al., 2010), we constructed a plasmid vector with short 5' (A, 345 bp) and 3' (B, 378 bp) homology arms flanking Cre-pA. These were amplified by PCR from UTR

sequences of the solitary *Math5* exon (AF418923) and cloned into the *Sal*I and *Xho*I sites of pαGSU-Cre (Cushman et al., 2000). The resulting A-Cre-B cassette was inserted into the *Xho*I site of shuttle plasmid pLD53ΔGFP10 as a 2.4 kb *Sac*I-*Xho*I fragment and verified by DNA sequencing. Shuttle plasmid pLD53ΔGFP10 was derived from pLD53.SC1 by partial *Spe*I digestion and insertion of a *Xho*I linker in place of the 3.5 kb EGFP fragment. We then targeted RP23-328P3 with the Math5>Cre shuttle vector pLD53ΔACreB to obtain ampicillin- and chloramphenicol-resistant cointegrates (Gong et al., 2002). These were resolved by selection on TYE (tryptone-yeast extract) agarose plates with chloramphenicol and 10% (w/v) sucrose. Two recombinant Math5>Cre BAC clones were recovered and verified by PCR and pulsed-field gel electrophoresis (PFGE) Southern analysis.

Purified circular DNA from Math5>Cre BAC clone RP23-328P3-D1-68 was injected into fertilized (SJL/2 × C57BL/6J) F_2 oocytes by the UM Transgenic Animal Core Facility. Nine transgenic founders were identified by Cre-specific and BAC vector-insert junctional PCRs. Transgene copy number was determined by Southern analysis, using an upstream *Math5* genomic probe that hybridizes equally well to 3.5 kb BAC and 6.5 kb mouse chromosomal *Eco*RI fragments. Transgene integrity was evaluated by Southern analysis following *Not*I digestion and PFGE. Transgenic offspring were genotyped using PCR primers within the Cre-pA cassette.

Math5>Cre mice (line 872 or 360) were crossed to Z/AP (JAX stock 003919, (Lobe et al., 1999) and R26*flox*GFP (JAX stock 004077, (Mao et al.,

2001) reporter strains, which express membrane-tethered hPLAP (human placental alkaline phosphatase) or cytoplasmic GFP (green fluorescent protein), respectively, from ubiquitously active promoters, upon Cre-mediated excision of *floxed* upstream stop signals. Tissues from informative double transgenic progeny were collected from E11.5 to 15.5, on P0.5, and at 3-4 weeks of age. To trace lineage in the absence of *Math5* function, we crossed Z/AP; *Math5* -/- mice (*Atoh7*^{tm1Gla}, Brown et al., 2001) to Math5>Cre (line 360); *Math5* +/- mice and compared the patterns of hPLAP staining in 3-4 week-old double transgenic mutants and heterozygous controls.

Histology

Embryonic and adult eyes were fixed overnight in 4% paraformaldehyde (PFA) at 4°C, cryoprotected in phosphate-buffered saline (PBS) with 10 to 30% sucrose, frozen in OCT compound (Tissue-Tek, Torrance, CA), and cryosectioned at 5-10 μm. For Brn3b (Pou4f2) and cyclin D1 epitopes, fixation was 30 min at room temperature in 2% PFA. For immunodetection, cryosections were blocked for 4 hrs at room temperature in PBTx (0.1 M $NaPO_4$ pH 7.3 0.5% Triton X-100) with 10% normal donkey serum (NDS) and 1% bovine serum albumin (BSA). Sections were incubated overnight at 4°C with primary antisera or biotinylated PNA (peanut agglutinin) lectin diluted in PBTx with 3% NDS and 1% BSA. For fluorescence detection, sections were incubated for 2 hrs at room temperature with appropriate secondary antibodies or streptavidin conjugates (Jackson Immunoresearch, West Grove, PA). Nuclei were identified using 100 ng/mL 4',6-diamidino-2-phenylindole (DAPI). For chromogenic detection,

sections were stained using the avidin-biotin complex method (Vector, Burlingame, CA) with HRP (horeseradish peroxidase)-conjugated streptavidin and diaminobenzidine (Brown et al., 2001).

The primary antibodies were mouse anti-β-galactosidase (βgal, monoclonal 40-1A, 1:500, DSHB, Iowa City, IA); rabbit anti-βgal (1:5000, ICN Cappel, Aurora, OH); rat anti-βgal (1:500, (Saul et al., 2008)); rat anti-BrdU (monoclonal BU1/75, 1:100, Harlan Seralab, Indianapolis, IN); mouse anti-calbindin (monoclonal CB-955, 1:500, Sigma, St. Louis, MO); mouse anti-Cre (monoclonal 7.23, 1:300, Covance, Princeton, NJ); mouse anti-cyclinD1 (sc8396, 1:100, Santa Cruz Biotechology, Santa Cruz, CA); rabbit anti-GFP (1:5000, Upstate, Lake Placid, NY); chicken anti-GFP (1:2000, Abcam, Cambridge, MA); mouse anti-hPLAP (monoclonal 8B6, 1:250, Sigma); mouse anti-Ki67 (monoclonal MM1, 1:25, Novocastra, Newcastle, UK); rabbit anti-mGluR2/3 (1:200, Chemicon); goat anti-Neurod1 (sc1084, 1:50, Santa Cruz); rabbit anti-phosphohistone H3 (1:400, Upstate, Lake Placid, NY); rabbit anti-rhodamine (1:500, Invitrogen). Biotinylated PNA (Vector) was used at 1:250.

For simultaneous detection of BrdU (5-bromo-2-deoxyuridine) and other markers, cryosections were fully stained with primary antibodies and lectins, and fluorescent secondary reagents. Sections were then treated with 2.4 N HCl in PBTx for 60-75 min at room temperature, washed, and immunostained for BrdU. EdU (5-ethynyl-2-deoxyuridine) was detected using an azide-alkyne cycloaddition reaction (Buck et al., 2008) and commercial reagents (Click-iT-647, Invitrogen) after immunostaining. For EdU and BrdU co-labeling, BrdU

immunostaining was performed as the final step. For Ki67 immunostaining, sections were unmasked before the blocking step by heating to 95˚C for 10 min in 0.01 M citric acid.

For chromogenic detection of hPLAP activity in retina, 5-10 µm cryosections were heat-treated for 30 min in PBS with 2 mM $MgCl_2$ at 70°C and stained with 5-bromo-4-chloro-3-indolyl phosphate (BCIP) and nitroblue tetrazolium (NBT) substrates (Roche, Indianapolis, IN) for $\leq$ 1.5 hrs (Lobe et al., 1999). To detect hPLAP activity in the brain, adult tissues from transgenic animals were immersion-fixed in 4% PFA, 2 mM $MgCl_2$ at 4°C overnight, heat-treated for 45 min in PBS with 2 mM $MgCl_2$ at 70°C, and embedded in 3% agarose. Thick coronal vibratome sections (250 µm) were stained for hPLAP activity as floating slices in 24-well plates in AP buffer containing 0.01% Na deoxycholate, 0.02% NP-40, 2 mM levamisole, and BCIP/NBT substrate (Roche), for 5-6 hrs at room temperature. Sections were washed in PBS containing 20 mM EDTA, dehydrated through a graded ethanol series, cleared with BABB (1:2 benzyl alcohol : benzyl benzoate) and mounted in Permount (Fisher Scientific, Pittsburgh, PA). Chromogenic detection of β-galactosidase (βgal) activity with 5-bromo-4-chloro-3-indolyl-β-D-galactopyranoside (Xgal) substrate and *in situ* RNA hybridization were performed as described (Brown et al., 2001).

Images were obtained using a Nikon Eclipse E800 epifluorescence microscope and a SPOT digital camera. Low power images of brain sections were captured using a Zeiss Axioimager Z1 microscope with 5X objective.

Confocal images were collected using a Noran OZ Laser Scanning Confocal assembly microscope or Zeiss LSM510 Meta imaging system.

Labeling RGCs by retrograde axonal tracing

To unequivocally identify all RGCs, we performed retrograde axon labeling with a rhodamine dextran tracer (Farah and Easter, 2005; Rachel et al., 2002). Eyes from adult Math5>Cre; R26*flox*GFP mice were rapidly immersed in artificial cerebral spinal fluid (aCSF) (von Bohlen und Halbach, 1999). The optic nerves were transected within 1 mm of the sclerae and pressed against 4 mm cubes of surgifoam (Ethicon, Somerville, NJ) saturated with 3% L-α-lysophosphatidyl choline (LPC, Sigma) and lysine-fixable tetramethyl rhodamine dextran 3,000 MW powder (Molecular Probes, Eugene, OR). Each eye and surgifoam cube was sealed with 1% agarose and incubated in aerated aCSF for 1 hr at room temperature. The eyes were then incubated overnight in fresh aCSF without surgifoam, fixed in 4% PFA for 4-6 hrs at room temperature, cryoprotected in PBS with 10 to 30% sucrose, and frozen in OCT. For P1 mice, the same retrograde labeling procedure was followed, except that eyes were immersed in Hank's balanced salt solution containing calcium, magnesium and 1 mM glucose (Gerfen et al., 2001). After labeling, eyes were fixed in 4% PFA for 1 hr. The dissected retinas were post-fixed for 3 hrs, immunostained and flatmounted for imaging.

Math5 cell cycle analysis

Retinas from *Math5* +/- and *Math5* -/- embryos (carrying the *lacZ* knock-in allele) were co-labeled for βgal, BrdU or EdU (S phase), phosphohistone H3 (M phase, Bradbury, 1992), cyclinD1 (G1 and early S phases, Yang et al., 2006), and Ki67 (S, G2, M and late G1 phases, Key et al., 1993). To label cells in S phase, pregnant dams were given a single intraperitoneal injection of EdU (6.7 µg/g of body mass) or BrdU (100 µg/g) 30-60 min prior to harvest. To test whether *Math5*+ progenitors re-enter the cell cycle, lineage-marked Math5>Cre embryos carrying Z/AP or R26*flox*GFP reporters were similarly pulsed with BrdU or EdU and their retinas co-stained for hPLAP, GFP or Cre and cell cycle markers.

Quantitative lineage analysis

Math5+ descendants were revealed by hPLAP or GFP immunolabeling in ≥200 adult retinal sections. Cell types were identified by laminar position, characteristic morphology, expression of diagnostic markers, and retrograde axon tracing. Lineage-marked cones were distinguished from rods by co-labeling with anti-hPLAP and PNA lectin (Blanks and Johnson, 1983). Because strong hPLAP staining in cone pedicles obscured horizontal cell bodies, we identified these cells using the R26*flox*GFP reporter and calbindin immunostaining (Peichl and Gonzalez-Soriano, 1993). Horizontal cells were surveyed in 58 sections from Math5>Cre; R26*flox*GFP mice (8 eyes). GFP-positive rhodamine-dextran labeled RGCs and DAPI-labeled nuclei (RGCs + displaced amacrines) were counted within the GCL in 33 fields (200X magnification) representing 8

Math5>Cre; R26*flox*GFP adult eyes. For P1 counts, the fraction of lineage-labeled RGCs was determined in retinal flatmounts from 3 eyes. The fraction of each cell type descending from *Math5*+ progenitors, and the fraction of *Math5*+ progenitors giving rise to each cell type, were calculated based on detailed retinal cell counts reported for adult C57BL/6J mice (Jeon et al., 1998). For lineage tracing in the absence of *Math5* gene function, labeled cells were counted in 23 fields (200X magnification) representing 6 adult eyes.

Dual reporter concordance

To assess Math5>Cre efficiency and heterogeneity among *Math5*+ progenitors, we crossed Math5>Cre; Z/AP mice to homozygous R26*flox*GFP mice. Retinal sections from 3-4 week-old triple transgenic offspring (Math5>Cre; Z/AP; R26*flox*GFP) were immunostained for GFP and hPLAP. Single- and double-labeled cones, rods, amacrines and GCL neurons were counted in 18 fields (200X magnification) representing 4 eyes. To calculate concordance, we divided the number of double-labeled cells by the total number of labeled cells. Concordance was evaluated statistically using Cohen's κ test (Cohen, 1960).

Birthdating and window labeling studies

To identify *Math5* descendants exiting mitosis before P0, we performed a cumulative BrdU labeling experiment (Miller and Nowakowski, 1988). Pregnant dams carrying Math5>Cre; Z/AP embryos were given a single BrdU injection (100 μg/g body mass) on day E10.5 and provided with drinking water containing 500 μg/mL BrdU and 1% sucrose (pH 7.0) until birth (Mayer et al., 2000). To

maximize labeling efficiency, water bottles were protected from light and replaced daily. Retinal sections from 3-week-old offspring were immunostained for BrdU and hPLAP.

To monitor how the fates of *Math5*+ progenitors exiting mitosis change during development, we performed birthdating (pulse-labeling) experiments. Pregnant dams carrying Math5>Cre; Z/AP embryos were given a single BrdU injection (as above) on day E14.5, E15.5, E16.5 or E17.5 of development. Eyes from 3-4 week-old mice were stained with BrdU and hPLAP antibodies, and PNA lectin. The total number of cones (PNA+) and the number of hPLAP+ and/or BrdU+ photoreceptors were counted in ≥14 central retinal fields (200X magnification), corresponding to ≥3 eyes for each time-point. For birthdating lineage-marked photoreceptors in the absence of *Math5* function, we followed the same protocol as above. We immunostained Math5>Cre; R26*flox*GFP; *Math5* -/- retinas for BrdU and GFP, and counted ≥7 fields (200X magnification) from 2-4 eyes for each time-point. The fraction of lineage-marked and birthdated cones was calculated directly from cell counts. The fraction of labeled rods was estimated using a 35.2 rod-to-cone ratio for wild-type mice, based on C57BL/6 data (Jeon et al., 1998), and a 12.1 ratio for *Math5* mutants (SEM = 0.8 based on *n* = 5 animals, 71 fields at 200X magnification).

To determine the contribution of *Math5*+ cells to the early-born (EB) cohort of neurons, we performed pulse- and window-labeling experiments at the onset of neurogenesis. For pulse-labeling, gravid dams carrying Math5>Cre; R26*flox*GFP embryos were given a single injection of EdU at day E11, and eyes

from the resulting pups were harvested at P1. Whole retinas were stained for GFP and EdU, flatmounted, and imaged as confocal Z-stacks through the ganglion cell layer. The fraction of early-born cells in the *Math5* lineage (EdU+ GFP+ / EdU+) was determined from 4 eyes representing 4 mice.

For window labeling (Repka and Adler, 1992), pregnant dams carrying *Math5* +/- and -/- embryos were given EdU on day E11, as a single injection or two injections 12 hrs apart. No difference was apparent in the extent of EdU labeling between these schedules. Dams were then given a single injection of BrdU on E12 and provided with BrdU in the drinking water until harvest at E12.5. Early-born cells (EdU+ BrdU-) were counted from 3-4 embryos of each genotype, representing 1-3 litters, and scored for βgal or Brn3b immunoreactivity. Statistical error is reported as the binomial standard deviation. Labeled fractions were compared using Fisher's exact test (Fisher, 1925).

Retinal explants and clonal analysis

Retinal explant culture and retroviral infections were performed using established methods, which favor RGC survival (Hatakeyama and Kageyama, 2002; Wang et al., 2002b). *Math5 lacZ*/+ retinas were dissected from E12.5 or E13.5 eyes, removing sclerae, pigmented epithelium (RPE) and lens tissue, and were flattened onto 5 mm Nucleopore polycarbonate membranes (0.4 μm pore size, GE Healthcare, Piscataway, NJ). These explants were placed on Transwell inserts (Corning) in 2-cm dishes containing neurobasal media (Invitrogen) with 1X B27 and N2 supplements, glutamine (0.4 mM), BDNF (50 ng/mL, Peprotech, Rocky Hill, NJ), CNTF (10 ng/mL, Peprotech), penicillin (50 U/mL), streptomycin

(50 µg/mL), and gentamicin (0.5 µg/mL), and cultured at the gas-media interface at 37°C and 5% CO_2.

MIG retroviral stocks (Van Parijs et al., 1999) were generated by transfecting MSCV-IRES-GFP plasmid DNA into the Phoenix ecotropic packaging cell line (Pear, 2001; Swift et al., 2001) and titered on NIH3T3 fibroblasts. Filtered viral preparations (~$8x10^5$ colony-forming units/mL) containing polybrene (hexadimethrine bromide, 0.8 µg/mL, Sigma Aldrich, St. Louis, MO) were added directly to the explant surface in one drop (25 µL) to infect mitotic cells. After 2 days *in vitro* (DIV), half of the media was replaced with fresh media. After 3 DIV, explants were fixed for 30 min in 4% PFA, cryoprotected in 30% sucrose, and frozen in OCT. Thick (30 µm) sections were immunostained for βgal and GFP. For each time-point, the size and composition of clones was determined by 3-dimensional analysis of confocal Z-stacks. Clones were defined as clusters of GFP+ cells directly apposed to each other (within 2-3 µm) and separated by at least 4 cell bodies from any other GFP+ cells. Only clones containing at least two GFP+ cells and one βgal+ cell were scored. Previous studies have shown that the average progenitor cell cycle length is 14-16 hrs at this stage (Alexiades and Cepko, 1996; Sinitsina, 1971), permitting 4-5 divisions during the 72 hr culture period. Accordingly, the largest clones in each set of explants contained 8-16 cells, reflecting a minimum of 3-4 divisions *in vitro*.

Results

Math5 is transiently expressed by early retinal progenitors during or after their terminal cell cycle

As a first step to determine the mechanism of *Math5* action, we defined the timing of *Math5* expression during retinal development by quantitative PCR (Fig. III-1A). *Math5* mRNA increases rapidly at E11, peaks between E12.5 and E14.5, and declines gradually after E14.5. This temporal profile is consistent with RNA *in situ* hybridization data (Brown et al., 1998) and closely resembles birthdating curves for RGCs (Drager, 1985; Young, 1985a). These data suggest *Math5* acts transiently during early retinal neurogenesis.

The cellular distribution of *Math5* mRNA and *Math5-lacZ* activity across the retinal epithelium (Brown et al., 2001) is consistent with *Math5* transcription in actively proliferating and/or postmitotic cells. Both patterns have been reported for different bHLH genes during neurogenesis (Kageyama and Nakanishi, 1997). Indeed, the closely related gene *Math1* is expressed in mitotic cells in the developing cerebellum (Helms et al., 2000) and in postmitotic cells in the inner ear (Chen et al., 2002). In frog, zebrafish and chick retinas, orthologous *Ath5* genes are expressed in progenitors during their last cell division (Matter-Sadzinski et al., 2001; Perron et al., 1998; Poggi et al., 2005).

To determine the onset of *Math5* expression in individual mouse retinal progenitors, we immunostained E13.5, E15.5, and E16.0 eyes from *Math5* +/- (*lacZ*/+) and/or *Math5* -/- (*lacZ/lacZ*) embryos for β-galactosidase (βgal), the cell

cycle marker phosphohistone H3 (PH3, M phase), cyclin D1 (cycD1, G1/early S phase) (Yang et al., 2006) or Ki67 (late G1, S and M phase), and the thymidine analog EdU or BrdU (S phase) following a 30-60 minute pulse *in vivo*. After the EdU pulse, a small fraction of S phase progenitor cells enter G2 and are detected as EdU+ cycD1−. In contrast, cells remaining in S phase are EdU+ cycD1+. After careful 3-dimensional analysis of confocal Z-stack images, we observed a small number of βgal-expressing cells that had incorporated EdU at E13.5 (18 of 517 = 3.5 ± 0.6% SD) for *n* = 3 sections, Fig. III-1B). These βgal+ cells were exclusively cycD1− (0 of 517, upper limit 95% CI = 0.6%), indicating that *Math5* is expressed after G1 phase at E13.5. Accordingly, βgal+ PH3+ cells (M phase) were observed at E13.5 (Fig. III-1D, (Le et al., 2006)). In contrast, in E15.5 and E16.0 embryos (Fig. III-1C,E,G), few or no cells co-expressed βgal and cell cycle markers EdU, BrdU, cyclinD1, or PH3. The dynamics of *Math5* expression thus change during development. At early stages (<E14), some progenitors initiate *Math5* expression during the last cell cycle, whereas at later stages (>E15), progenitors express *Math5* only after terminal mitosis. Similar results were observed in E15.5 *Math5* knockout embryos (Fig. III-1F,H, (Le et al., 2006)), demonstrating that βgal+ mutant cells do not re-enter the cell cycle. In *Math5* +/- and -/- mice, βgal+ cells span the entire retinal thickness (arrowheads in Fig. III-1G,H), suggesting that radial processes associated with interkinetic nuclear migration may persist transiently, potentially directing the migration of early post-mitotic cells to their final laminar positions (Barnstable et al., 1985; McLoon and Barnes, 1989; Snow and Robson, 1994; Watanabe et al., 1991).

Math5>Cre lineage marking system

We designed an expression fate-mapping system to permanently mark lineal descendants of *Math5*-expressing progenitors and thereby define the range of fates acquired by these cells. The system has two components – transgenic mice expressing Cre recombinase under strict *Math5* regulatory control (Math5>Cre) and reporter mice (Z/AP or R26*flox*GFP) that express a histochemical marker (hPLAP or GFP) wherever Cre excises a *loxP*-flanked stop signal.

The Math5>Cre recombinant BAC (Fig. III-2A,B) includes all likely *Math5* regulatory elements (Ghiasvand et al., 2011; Hutcheson et al., 2005). We generated nine Math5>Cre founders, each of which contains 1-5 copies of the BAC transgene (Fig. III-S1A). Five lines were tested using Z/AP reporter mice, which conditionally express hPLAP under control of the ubiquitous CAG promoter (Lobe et al., 1999). Each line gave a similar staining pattern, which is consistent with the spatiotemporal expression of *Math5* mRNA (not shown). All subsequent experiments were performed with lines 872 and 360, which contain full-length transgene insertions, as determined by diagnostic PCR, Southern and PFGE analysis (Fig. III-S1B).

From the onset of retinal neurogenesis (E11), *Math5* mRNA is expressed in cells near the ventricular (sclerad) neuroepithelial surface, where the majority of progenitors undergo mitosis (Brown et al., 1998). In *Math5-lacZ* knock-in mice, β-galactosidase protein is expressed in a similar pattern but perdures (Echelard et al., 1994) in the differentiating descendants of these cells, including

RGCs (Brown et al., 2001). In double transgenic Math5>Cre; Z/AP embryos, the alkaline phosphatase (hPLAP) marker first appeared at E12.5 in differentiating RGCs and the developing optic nerve (Fig. III-2D), whereas no hPLAP was detected in control embryos carrying Z/AP alone (Fig. III-2C). At later developmental stages, some other cell types were labeled with hPLAP (e.g. photoreceptors at P0.5 in Fig. III-2D, arrowhead). As expected, hPLAP was only detected in the adult retina and brain, in known *Math5* RNA expression domains. In the central nervous system, the hPLAP reporter marks neurons in the auditory hindbrain and cerebellum (Saul et al., 2008) and reveals all known RGC projections (Rodieck, 1998; Simpson, 1984), including those extending to the superior colliculi, lateral geniculate bodies, suprachiasmatic nuclei, and the accessory optic tracts (Fig. III-2E).

In the E15.5 retina, a comparison of the spatial and temporal patterns for *Math5* mRNA, *Math5-lacZ* and hPLAP (Fig. III-2F) is consistent with a direct role for *Math5* in RGC development and highlights the inherent time delay associated with Cre protein synthesis, excisional activation of the Z/AP reporter, and expression of the hPLAP enzyme (Nagy, 2000). Considering the dynamics of retinal interkinetic nuclear migration (Baye and Link, 2008), these results suggest there is a burst of *Math5* expression in progenitors exiting the cell cycle. If *Math5* is exclusively made during the last division, lineage-marked cells should never re-enter S phase. To test this prediction, we analyzed E13.5 Math5>Cre; R26*flox*GFP and E15.5 Math5>Cre; Z/AP embryos exposed to EdU or BrdU for ≤1 hr (Fig. III-2G,H). In E13.5 embryos after a 30 min chase, some Cre+ EdU+

cells were present (33 of 394 Cre+ cells = 8.4 ± 0.4% SD for *n* = 3 sections) and these were restricted to the fresh neurogenic subset (33 of 223 Cre+ GFP– cells = 14.8 ± 1.4% SD). No GFP+ EdU+ cells were observed in the same sections (0 of 309 GFP+ cells, upper limit 95% CI = 0.9%), due to the delay in the Cre-lox system (Fig. III-2G). Likewise, in E15.5 embryos, there was no overlap between hPLAP activity and any cell cycle marker (Fig. III-2H). Together, these results strongly suggest that *Math5* is expressed transiently during or shortly after the terminal cell division. *Math5* lineage cells do not re-enter the cell cycle.

Quantitative *Math5* lineage analysis

To reveal the fates of *Math5*+ progenitors, we crossed Math5>Cre mice to Z/AP and R26*flox*GFP reporter strains and examined mature retinas of 3-4 week old offspring. We observed hPLAP+ cells distributed evenly across the central and peripheral retinas of Math5>Cre; Z/AP mice, but staining was absent in littermates carrying the Z/AP transgene alone (Fig. III-3A,B). Because hPLAP protein is membrane-tethered, we could identify most retinal cell types by morphology and laminar position. As expected, RGCs were abundantly labeled. However, we also observed significant staining among rods, cones, horizontal and amacrine cells (Fig. III-3A,C,D). The inner plexiform layer (IPL) was intensely labeled due to hPLAP localization in RGC and amacrine dendrites. A thorough survey revealed rare hPLAP+ Müller glia and bipolar cells (Fig. III-3C). Importantly, no labeling was observed in retinal cell types that have a separate developmental origin, such as vascular endothelial cells, pericytes, microglia and

astrocytes, or in any other parts of the eye, including the anterior chamber and RPE.

To systematically measure the fraction of lineage-marked retinal cells in each class, we co-stained sections for hPLAP or GFP reporters and cell type-specific markers. Equivalent results were obtained using Z/AP and R26*flox*GFP reporters (see below) and different Math5>Cre lines (data not shown). However, the intensity of expression varied among cell types. Z/AP is strongly expressed in photoreceptors via the CAG promoter, whereas R26*flox*GFP is weakly expressed by photoreceptors but strongly expressed by other cell types. Consequently, we used Z/AP to count hPLAP+ and hPLAP- cones (arrows in Fig. III-3D), and hPLAP+ rods (arrowheads in Fig. III-3D) in the outer nuclear layer (ONL), and PNA lectin to distinguish cones from rods (Blanks and Johnson, 1983). We then counted hPLAP+ bipolar cells and Müller glia (Fig. III-3C) in the inner nuclear layer (INL) of the same sections. The labeled fraction was calculated for each cell type using reference data for cell populations in the adult mouse retina (Jeon et al., 1998). This fraction ranged from 31% for cones to 1% for rods, and <0.1% for bipolar cells and Müller glia (Table III-1).

To evaluate horizontal, ganglion and amacrine cell types, we used the R26*flox*GFP reporter, which co-localizes with cell type-specific markers in the perinuclear cytoplasm. We identified horizontal cells by calbindin immunostaining (Peichl and Gonzalez-Soriano, 1994) and their position at the outer edge of the INL (Fig. III-3E). Twenty-nine percent of horizontals were GFP+ (Table III-1). This value is significantly lower than that reported by Yang et

al. (2003), but consistent with horizontal cell labeling data of Feng et al. (2010, *cf*. Suppl. Fig. 3E) obtained using a *Math5-Cre* knock-in allele. RGCs were distinguished from displaced amacrine cells (Hayden et al., 1980; Perry and Walker, 1980) by retrograde rhodamine-dextran tracing of optic nerve axons. Forty-three percent of neurons in the ganglion cell layer (GCL) were labeled with rhodamine in this experiment (arrows, Fig. III-3F), in close accord with previous data (Jeon et al., 1998). All other cells in the GCL were scored as displaced amacrines (arrowheads, Fig. III-3F). The frequency of GFP labeling in the adult retina was 55% for ganglion cells, 28% for displaced amacrines, and 9% for INL amacrines (Table III-1). To evaluate the *Math5* lineage fraction prior to the normal period of RGC culling (Galli-Resta and Ensini, 1996), we performed a similar analysis in early postnatal retinas, limited to the GCL (Fig. III-3G). The fraction of GFP+ ganglion cells in P1 retinas (53 ± 1%, n = 3, 948/1777 cells) was similar to that observed in the adult (55 ± 2%, Table III-1, Fisher's exact test P = 0.3).

A clear pattern emerges from these data. First, *Math5*+ progenitors have the potential to develop into all seven major retinal cell types. Second, the distribution of *Math5*+ descendents differs from the retina as a whole (Fig. III-3I, χ^2 test with df = 7, $P < 0.0001$). Third, the labeling fraction of each cell type (Table III-1) decreases according to the birth order (Carter-Dawson and LaVail, 1979; Rapaport et al., 2004; Sidman, 1961; Young, 1985a). Early-born cell types – RGCs, cones, horizontal cells and displaced amacrines – frequently descend from *Math5*+ progenitors, whereas late-born bipolar and Müller glial cells rarely

derive from *Math5*+ progenitors. INL amacrines are born during the middle phase of retinal development, prior to the peak of rod births, and these cell types have an intermediate labeling fraction. We estimate that 3% of adult retinal cells descend from *Math5*+ progenitors (Table III-1). Fourth, only one in nine *Math5*+ descendants is a ganglion cell (11%). Because RGCs represent ~0.5% of neuroretinal cells in adult mice (Jeon et al., 1998) and *Math5* status does not affect RGC survival between P1 and adulthood, *Math5* descendants are 50-fold more likely on average to develop as RGCs than the remaining neuroretinal population (approx. 1 in 500). Fifth, 45% of ganglion cells are not marked by the Math5>Cre transgene, suggesting the possibility of a substantial *Math5*-independent RGC subpopulation. Although the fraction of GCL neurons labeled by Math5>Cre (40%, Table III-I) approximates the RGC fraction (43%), this value includes both RGC (24%) and displaced amacrine cell types (16%).

The fate of *Math5* mutant cells

In mutant mice, the *Math5* transcription unit is active, expressing *lacZ* mRNA, but lineage-marked progenitors are blocked from developing as RGCs. To determine the fates of these cells, we examined retinas from adult *Math5* -/- mice carrying Z/AP and Math5>Cre transgenes (Fig. III-3H). The extent of hPLAP labeling in the mutant retina was roughly similar to wild-type (Fig. III-3A). However, the fate profile within the Math5 lineage was different (χ^2 test with df = 7, $P < 0.0001$). First, RGCs were absent, as expected, decreasing the amount of IPL staining. Second, there was an obvious increase in 'late-born' cell types among the hPLAP+ neurons (Table III-S1). For example, rod photoreceptors

increase from 32% to 40% of the Math5 lineage. Labeled bipolar cells and Müller glia were visible in most low power fields (200X magnification) of mutant mice, but were difficult to find in wild-type Math5>Cre; Z/AP retinas (Table III-1), consistent with results observed by Feng et al. (2010). This effect is more striking if one considers that the total number of rods, bipolar cells and Müller glia are decreased in *Math5* mutants (Brown et al., 2001; Brzezinski et al., 2005). In *Math5* mutant mice, the cohort of progenitors expressing Math5>Cre does not differentiate into RGCs, but retains competence to develop into any of the remaining principal cell types.

Math5+ progenitors have equivalent Cre activity

Only a small fraction (11%) of the *Math5* lineage develops into RGCs. In principle, the *Math5*+ population may be heterogeneous, such that one group of progenitors expresses high levels of Math5>Cre and develops as RGCs, while a second group expresses low levels of Math5>Cre and adopts other fates (Fig. III-4A). In this model, the low-level multi-lineage Math5>Cre expression could represent 'priming' (Hu et al., 1997) of the *Math5* gene, or leaky transgene expression, an 'over-reporting' artifact that is not biologically meaningful (Dymecki et al., 2002). Alternatively, all *Math5*+ progenitors may express equivalent levels of Math5>Cre (Fig. III-4B), consistent with a permissive role for *Math5* in retinal development.

To test these alternatives, we examined retinas from triple transgenic (Math5>Cre; Z/AP; R26*flox*GFP) adult mice, using the concordance of hPLAP and GFP labeling in *Math5* descendants as an indirect measure of Cre activity

(Fig. III-4C). In this experiment, we assume that the probability of reporter activation in a particular cell depends on the concentration and stability of intracellular Cre protein, and that neither reporter is saturated at the Cre levels under investigation. Progenitors with strong Cre expression are expected to activate both reporters, while progenitors with weak Cre expression may randomly activate one reporter, Z/AP or R26*flox*GFP, at a low frequency (Fig. III-4A,B). If these events occur independently with equal probability (ρ), then the joint probability of observing both reporters in a single cell (expected concordance) should equal $\rho^2/(2\rho-\rho^2)$, where ρ^2 is the fraction of cells that activate both reporters and $2\rho-\rho^2$ is the fraction of cells that activate at least one reporter. The observed concordance was uniformly high (~80%) for rods, cones, INL amacrines and GCL neurons, and much greater than expected by chance (Cohen's $\kappa > 0.7$, Fig. III-4D, Table III-S2). Thus, the labeling of non-RGC cell types cannot be attributed to differential or leaky Math5>Cre expression.

The fate of the *Math5*+ progenitor population changes over time

The discovery that some rods, bipolars and Müller glia descend from Math5>Cre progenitors (Table III-1) is somewhat surprising because the vast majority of these cell types undergo terminal mitosis (Rapaport et al., 2004; Young, 1985a) after the temporal envelope of *Math5* mRNA expression (Fig. III-1A). To explain these findings, we performed a cumulative labeling experiment, in which Math5>Cre; Z/AP embryos were continuously exposed to BrdU from E10.5 until P0 and analyzed at P21. Retinal progenitors that exit mitosis before P0 should be heavily BrdU-labeled, whereas those that continue to divide after

P0 should be weakly labeled. We found that essentially all hPLAP+ cells in the central retina were heavily labeled with BrdU (98.8%), including rods (arrowheads in Fig. III-5A), cones (arrows in Fig. III-5A), and INL and GCL neurons (Table III-S3). Therefore, *Math5*+ rods, bipolars and Müller glia are born at the 'leading edge' of birthdating curves for these 'late' cell types.

The fate profile of neurogenic cells emerging from the RPC population is known to change over time, in response to intrinsic factors and environmental signals (Livesey and Cepko, 2001; Rapaport et al., 2004; Young, 1985a). This can occur through alterations in the fate bias of individual cells or the composition of the RPC pool (heterogeneity). In principle, the *Math5*+ cohort may behave similarly. The fate profile of these cells may be intrinsically programmed, or it may vary depending on the time that an individual RPC exits mitosis and initiates *Math5* transcription. To test these alternatives, we compared the fates of *Math5*+ progenitors born on different days. Math5>Cre; Z/AP embryos were exposed to a pulse of BrdU on E14.5, E15.5, E16.5 or E17.5 and their adult retinas were examined by hPLAP, PNA, and BrdU staining (Fig. III-5B). A variety of lineage-marked cell types were born on each of these days, including RGCs, rods, cones, amacrines and horizontal cells, as well as rare 'late' cell types (arrowhead in Fig. III-5B). For quantitative analysis, we focused on photoreceptors, which are relatively numerous and could be directly compared within the ONL. At each time-point, we determined the fraction of hPLAP+ and heavily BrdU+ rods and cones in the central retina (arrows in Fig. III-5B, Table III-S4). The fraction of photoreceptors (rods plus cones) that were derived from

Math5+ progenitors decreased between E14.5 and E17.5, from 20.6% to 4.3% (Fig. III-S2, Table III-S4), in parallel with the decrease in the total number of *Math5*+ cells.

The fate of the *Math5*+ cell population also changed significantly between E14.5 and E17.5, together with the retina as a whole. *Math5*+ cells born on E14.5 were >2 times as likely to develop into cones as compared to rods (136 vs. 64), whereas those born on E17.5 were >60 times as likely to develop into rods as compared to cones (122 vs. 2, Table III-S4). The fates of progenitors inside and outside the *Math5* lineage shifted in parallel, as shown by plots of the cone-to-rod ratio (Fig. III-5C), derived from birthdating curves (Fig. III-S2). This shift is primarily determined by the overall decrease in cone births during this interval. *Math5*+ cells appear to follow the same fate trajectory as other progenitors. However, the ratio curves are displaced by one-half day. In comparison to other neurogenic cells (hPLAP-) exiting mitosis on the same day in the same retinal environment, Math5+ progenitors (hPLAP+) were three times more likely to develop into cones. Surprisingly, similar results were obtained in the absence of *Math5* function, in mutant embryos carrying R26*flox*GFP and Math5>Cre transgenes (Fig. III-5D).

These findings support three conclusions. First, the fate profile of *Math5*+ cells changes over time, similar to that of other retinal progenitors. Second, the fate bias of *Math5*+ cells extends beyond RGC specification, influencing the choice among alternative fates (e.g. cone vs. rod). Third, the bias among

alternative fates is independent of *Math5* action, suggesting that upstream or parallel factors are responsible.

Math5 expression in early-born retinal cells

Because *Math5* expression is closely correlated with the onset of retinal neurogenesis (~E11.5) (Hufnagel et al., 2010) and is essential for specification of the earliest born cell type, RGCs (Brown et al., 2001; Wang et al., 2001), we expected that most or all early-born retinal cells would express *Math5* and adopt RGC fates. To test this hypothesis, we performed a series of window-labeling experiments. Embryos were sequentially exposed to EdU at E11 and BrdU at E12 (Fig. III-6A). In this paradigm, cells incorporate EdU if they are in S phase at E11. Because the average cycle length at this stage is less than 24 hrs (Sinitsina, 1971), EdU+ BrdU+ cells scored at E12.5 are interpreted as RPCs that underwent one additional division (and S phase). In contrast, EdU+ BrdU- cells define the early-born (EB) cohort. These cells were in S phase at E11, but exited the cell cycle before E12.5.

To evaluate RGCs within the EB cohort, we counted the fraction of EdU+ BrdU− cells that were Brn3b+ (RGCs) in *Math5* heterozygous and mutant mice (Fig. III-6B). In *Math5* +/- embryos, 75% of the EB cohort expressed Brn3b, confirming that RGCs are the predominant first-born cell type (Farah and Easter, 2005; Rachel et al., 2002). The abundance of EdU+ BrdU- cells was similar in *Math5* -/- and +/- embryos (5.7 vs. 7.1 per 0.001 mm^2 field, respectively) and comparable to previous birthdating results (Le et al., 2006). However, in *Math5* mutant embryos, only 6% EdU+ BrdU- cells expressed Brn3b. This was

expected from the deficiency of RGCs in these mice, and confirms that the loss of RGCs is an early event. We next determined the fraction of EdU+ BrdU- cells that expressed *Math5*, using the *lacZ* allele (βgal) as a short-term lineage tracer (Wang et al., 1999). Surprisingly, only 20% of EdU+ BrdU− cells were βgal+, in both *Math5* +/- and *Math5* -/- mice (Fig. III-6C). To independently test this result, we exposed Math5>Cre; R26*flox*GFP embryos to a single pulse of EdU at E11, harvested their retinas at P1, and determined that 28% of strongly EdU+ cells in the GCL were GFP+ (Fig. III-6D,E). As a third test, we evaluated retinas from early *Math5-lacZ*/+ embryos for coexpression of *lacZ* and Brn3b. The fraction of βgal+ RGCs was relatively low at E11.5, consistent with the EB analysis, but increased from 20% to 60% between E11.5 and E13.5 (Fig. III-7). Taken together, the results from these three experiments suggest that *Math5* is expressed by a subset of early neurogenic cells, and that only a fraction of Brn3b+ RGCs generated at E11-13 derive from the *Math5*+ cohort.

The *Math5*-independent early-born cells may express other proneural bHLH transcription factors in the Atonal family, such as Neurod1 or Neurog2. At E11.5, Neurod1 was detected in a pattern that partially overlaps *Math5-lacZ* (Fig. III-S3), consistent with mRNA *in situ* hybridization data (Hufnagel et al., 2010). A similar overlap has been noted later in development (Kiyama et al., 2011; Le et al., 2006). This may explain the small number of early-born Brn3b+ RGCs present in *Math5 -/-* mice (Fig. III-6B), as *Neurod1* can partially substitute for *Math5* function in RGC fate specification (Mao et al., 2008b).

Symmetry of *Math5* expression in marked retroviral clones

During nervous system development, the mode of progenitor cell divisions changes over time (Gotz and Huttner, 2005; Huttner and Kosodo, 2005; Lu et al., 2000). Prior to neurogenesis, cell divisions predominantly follow the symmetric self-renewing mode (P-P), which expands the progenitor pool. During early neurogenesis, an asymmetric mode is frequently used to generate one mitotic daughter and one differentiating neuron (P-N). During late neurogenesis, most progenitors undergo a symmetric neurogenic mode of division (N-N), in which both daughters permanently exit the cell cycle. The fates adopted by neuronal daughters may also be symmetric (N_a-N_a) or asymmetric (N_a-N_b). In zebrafish, retinal progenitors expressing *ath5-GFP* undergo terminal neurogenic cell divisions (Poggi et al., 2005). These are symmetric with respect to *ath5-GFP* expression (N_{GFP}-N_{GFP}), but the daughters may have different cell fates, depending on the retinal environment.

To examine the mode of RPC division giving rise to *Math5*+ daughter cells in mice, we infected retinal explants from E12.5 or E13.5 *Math5-lacZ/+* embryos with MSCV-IRES-GFP (MIG) retrovirus at low density to mark independent GFP+ clones. After culturing explants for 3 days *in vitro* (DIV), we immunostained 30 µm cryosections for GFP and βgal (*Math5-lacZ*), and determined the size and composition of clones containing at least one βgal+ cell ($N_{\beta gal}$) (Fig. III-8A). These GFP+ clones ranged from 1 to 16 cells. We then focused our analysis on small clones (2-4 cell) containing ≥1 βgal+ cell, as these were most informative for symmetry of βgal+ expression. These clones are likely to represent terminal

lineages, given their small size and time in culture. Indeed, all cells in these small clones were postmitotic, as judged by expression of the cell cycle inhibitor p27Kip1 (Dyer and Cepko, 2001a) (data not shown). Among 23 clones scored, we observed both symmetric ($N_{\beta gal}$-$N_{\beta gal}$) (Fig. III-8B,C) and asymmetric (N-$N_{\beta gal}$, or possibly P-$N_{\beta gal}$) (Fig. III-8D) patterns of *Math5* expression. Of 23 informative neurogenic divisions, 13 (57%) were symmetric with respect to *Math5* expression and 10 were asymmetric (Fig. III-8E). The fraction of symmetric divisions did not differ significantly between the E12.5 and E13.5 explant time-points (0.64 vs. 0.50 respectively, Fisher's exact test $P = 0.7$). Although few symmetric terminal divisions are expected at this age in the retina as a whole, the high frequency observed among the Math5+ cohort ($N_{\beta gal}$-$N_{\beta gal}$) confirms that early progenitors are capable of N-N divisions in mice as in zebrafish (Poggi et al., 2005). Unlike zebrafish, neurogenic divisions can be asymmetric with respect to *Math5* expression in mice. These findings confirm that many retinal progenitors express *Math5* after terminal M phase.

Discussion

Math5>Cre transgene recapitulates endogenous *Math5* expression

We believe that the Math5>Cre transgene is expressed in the same pattern as endogenous *Math5* mRNA for several reasons. First, the BAC transgenes that we examined are intact and contain >100 kb flanking *Math5* genomic DNA on both sides of the Cre cassette, while core regulatory elements for *Math5* retinal expression are located within 25 kb of the transcriptional start

site (Ghiasvand et al., 2011; Hutcheson et al., 2005). Second, the spatiotemporal pattern of Z/AP activation is congruent with *Math5* mRNA and *Math5-lacZ* expression during retinal development. Third, all lineage-marked adult cells are born during the normal period of *Math5* expression, including rare 'late' cell types. Fourth, similar results were observed with independent BAC transgenic lines, suggesting that chromosomal position effects are minimal or nonexistent. Apart from the retina and RGC projections, hPLAP staining was only noted in the cerebellum and in bushy cells of the cochlear nucleus, tissues that are known to express *Math5* mRNA (Saul et al., 2008). Fifth, the dual reporter concordance experiment provides no evidence for leaky or ectopic Cre expression. Sixth, a similar overall retinal pattern has been observed using a targeted Cre insertion (knock-in allele) in the *Math5* locus (Feng et al., 2010; Yang et al., 2003).

Our quantitative analysis significantly extends these previous studies and allows us to reach different conclusions regarding: [1] the size of the *Math5*-independent cohort of RGCs, [2] the relationship between *Math5* expression and cell cycle exit, [3] the role of *Math5* in determining non-RGC fates, and [4] the diversity of cell types within the Math5 lineage.

Math5>Cre does not mark all RGCs

Since *Math5* is necessary for RGC development, and functions as an intracellular factor, we expected all ganglion cells to be labeled by Cre, as descendants of *Math5*+ progenitors. However, after carefully excluding displaced amacrine cells, we found that only 55% of RGCs were marked by the Math5>Cre

transgene. A similar fraction of RGCs is likely to be labeled by the *Math5-Cre* knock-in allele (Feng et al., 2010, *cf.* Suppl. Fig. 5D), although this finding was not originally appreciated (Yang et al., 2003). These *Math5* descendants project to all known target sites for RGCs in the brain (Fig. III-2E), suggesting that they represent the ganglion cell population as a whole. There are two possible explanations for the incomplete marking of RGCs: [1] inefficiency of the *Cre-lox* system, and [2] the existence of a sizeable *Math5*-independent population of RGCs.

In principle, inefficient Cre reporting may account for a substantial fraction of unlabeled RGCs in the birthdating and lineage tracing experiments. RGCs descending from *Math5*+ precursors may escape detection for two reasons. First, the absolute level or duration of Cre expression in individual cells may not be sufficient to catalyze robust recombination. The Cre polypeptide must assemble into tetramers for enzymatic activity and has a short half-life in mammalian cells (Nagy, 2000). Generally speaking, Cre transgenes that are continuously active in differentiated cells are expected to be more efficient than those that are made briefly in a progenitor population. *Math5* is transiently expressed during retinal development (Fig. III-1A) and may be transcribed for only a few hours in individual cells (Fig. III-2F) (Fu et al., 2009). Consequently, in the dual concordance experiment, Math5>Cre activated only one reporter in 20% of marked cells (Fig. III-4). However, because concordance was relatively high among all cell types (Table III-S3), this effect cannot fully explain the incomplete labeling of RGCs. Second, some cells may epigenetically silence the Math5>Cre

transgene or the *Math5-lacZ* allele, or may be otherwise globally resistant to Cre recombination. Indeed, we have observed rare mice with reduced or elevated RGC labeling (data not shown). In these retinas, the extent of labeling varied coordinately across different cell types, consistent with a clonal epigenetic effect. A similar variation has been noted among Tie1>Cre transgenic mice in the efficiency of endothelial cell labeling (Enge et al., 2002). Nonetheless, among the vast majority of Math5>Cre retinas, there was relatively little variation in the RGC labeling fraction (Table III-1). Taken together, Cre inefficiency and epigenetic silencing are unlikely to explain the incomplete labeling of RGCs that we observed.

Alternatively, a subset of RGCs may develop independently of *Math5*. Detailed analysis of *Math5* -/- retinas has revealed a small population of widely dispersed ganglion cells, approximately 4% of wild-type, that survive to adulthood (Lin et al., 2004) and may project to the superior colliculi and laterial geniculate nuclei (Triplett et al., 2011). Moreover, recent data show that a related bHLH factor, Neurod1, can partially substitute for Math5 and allow RGC development (Mao et al., 2008b). Indeed, we observed that fewer early-born cells express *Math5-lacZ* than Brn3b (Fig. III-6B,C) and that many Brn3b+ RGCs at E11-E13 do not express *Math5-lacZ* (Fig. III-7). A subset of nascent ganglion cells may develop from Neurod1+ precursors (Fig. III-S3), without *Math5*. Consistent with this idea, mutant mice lacking both factors mice have even fewer RGCs than *Math5* -/- mice (Kiyama et al., 2011).

The fraction of unmarked RGCs (~45%, Table III-1) is 10-fold greater than the number of RGCs that survive in *Math5* -/- mice (~4%)(Lin et al., 2004). Apart from Cre inefficiency (noted above), there are two possible explanations for this discrepancy. First, RGCs derived from *Math5*+ progenitors may have a survival advantage during neonatal period (P0-P10) of ganglion cell apoptosis (Young, 1984). However, the deficiency of *Math5*-independent RGCs in *Math5* mutants was clearly evident early in retinal histogenesis, at E12.5 (Fig. III-6B,C), well before the neonatal period of RGC culling. In addition, the fraction of *Math5*+ RGCs in P1 and adult retinas was the same, making this mechanism unlikely. Second, *Math5* lineage cells may have a substantial non-autonomous role in RGC fate specification or early differentiation. These cells may represent 'pioneering' neurons (Pittman et al., 2008; Raper and Mason, 2010), which promote axon pathfinding and fasciculation within the retina (Erskine and Herrera, 2007; Oster et al., 2004) and survival of *Math5*-independent RGCs. In the absence of *Math5*, cells in the inner retina undergo apoptosis during midgestation and surviving RGCs have severe pathfinding defects (Feng et al., 2010; Kiyama et al., 2011; Moshiri et al., 2008); Chapter V). Most likely, *Math5*+ progenitors may favor the formation or survival of other RGCs by para- or juxtacrine signaling. Further work is needed to clarify molecular differences between the *Math5*+ cohort and other cells in the early retina.

Math5 is made by progenitors exiting the cell cycle

We have determined the precise relationship between onset of *Math5* expression and the cell cycle status of retinal progenitors (Fig. III-9A). At early

stages (<E14), *Math5-lacZ* was detected in some G2/M phase progenitors but was otherwise present only in non-proliferating cells. Based on the length of G2 phase (~ 2 hrs) (Sinitsina, 1971) and our analysis of retinal cell cycle kinetics in E13.5 Math5>Cre; R26*flox*GFP embryos, following a 30 min EdU pulse (Fig. III-2G), we conclude that at least 15% (and up to 60%) of newly Math5+ cells (Cre+ GFP-) initiate expression before terminal M phase. During later stages (>E15), *Math5* was exclusively expressed in post-mitotic cells. *Math5* lineage cells did not re-enter the cell cycle at any stage, regardless of the *Math5* genotype. This comprehensive analysis reconciles previous disparate observations regarding the timing of *Math5* expression (Brown et al., 1998; Le et al., 2006; Yang et al., 2003), including RNA profiling of single retinal cells (Trimarchi et al., 2008). In recent studies, an HA epitope-tagged *Math5* allele was expressed with similar kinetics in early E12.5-E14.5 embryos, but was detected in more S, G2, and M phase cells than our *Math5-lacZ* allele (Feng et al., 2010; Kiyama et al., 2011; Wu et al., 2012). This is comparable to zebrafish, where *ath5-GFP* expression initiates during terminal S/G2 (Poggi et al., 2005), and is consistent with results obtained in frog and chick (Kay et al., 2001; Matter-Sadzinski et al., 2001; Perron et al., 1998; Poggi et al., 2005).

The variable timing of *Math5* expression was supported by detailed clonal analysis. We observed symmetric *Math5-lacZ* expression in 13 of 23 informative divisions (56%, N_{Math5}-N_{Math5}) and asymmetric expression in the remaining clones (P/N-N_{Math5}). This frequency is convergent with cell cycle kinetic data discussed above. Together, these findings suggest that early progenitors giving rise to

Math5+ cells are heterogeneous in their intrinsic properties and/or responses to the retinal microenvironment. By comparison, zebrafish *ath5* is expressed symmetrically in terminal neurogenic divisions ($P_{ath5} \rightarrow N_{ath5}$-$N_{ath5}$), but resulting daughters often adopt different fates (Poggi et al., 2005). This difference may be correlated with the accelerated pace of retinal neurogenesis in zebrafish compared to mice. Further studies are needed to determine how the timing of *Math5* expression influences the fate choice of daughter cells in mice.

Math5 is unlikely to autonomously regulate the decision to exit the cell cycle for two reasons. First, it is variably expressed during or after the terminal division (Figs. 1B-D, 2G,H). Second, *Math5* lineage cells exhibit similar *lacZ* and Cre reporter expression kinetics in mutant and wild-type mice (Fig. III-1E-H). Instead, this binary choice must be made upstream or in parallel with *Math5* transcription. However, *Math5* may affect progenitor cycling indirectly. For example, differentiating RGCs secrete sonic hedgehog (Shh), which acts as a mitogen for RPCs and promotes rod and Müller glial fates (Jensen and Wallace, 1997; Levine et al., 1997; Wang et al., 2005; Yu et al., 2006). Accordingly, *Math5* mutants have thinner retinas with fewer rods and glia compared to wild-type mice (Brown et al., 2001), which may reflect a general loss of late-born cells. In zebrafish, *ath5* and *syu* (Shh) mutants exhibit similar defects in retinal cell mitosis, involving a delay in switching polarity of division, from central-peripheral (proliferative) to circumferential (neurogenic) modes (Das et al., 2003). This likewise suggests that nascent RGCs, not the *ath5* product *per se*, affect progenitor cell cycle dynamics.

Math5 establishes an RGC competence state

The expression fate mapping (Fig. III-3) and dual concordance (Fig. III-4) experiments support six conclusions. First, only a small fraction (3%) of the retina derives from *Math5*+ progenitors. Second, *Math5*+ progenitors are multipotent. They retain the potential to generate all seven major retinal cell types. Third, *Math5*+ progenitors contribute differentially to each cell type. The labeling frequency for a given cell type depends on the histogenic birth order and the temporal expression profile for *Math5* (Fig. III-9B). Similar overall results were observed in a previous *Math5* lineage study (Feng et al., 2010; Yang et al., 2003). However, bipolars and Müller glia were not identified in the wild-type *Math5* lineage, presumably because fewer cells were sampled. Fourth, *Math5*+ progenitors express uniform levels of *Math5* and may represent a developmental equivalence group, similar to *ato*+ progenitors in the fly eye imaginal disc (Dokucu et al., 1996). Fifth, the fates of the *Math5*+ and *Math5*- populations change over time with parallel trajectories. The *Math5* lineage cells are biased in their selection of non-RGC fates, compared to other neurogenic cells in the same environment, but this difference does not depend on *Math5* activity. Sixth, the diversity of retinal cell fates within the *Math5* lineage was similar in mutant and wild-type mice, apart from the deficiency of RGCs (Fig. III-9C). However, there were modest increases in the labeling fraction of rods, bipolar cells and Müller glia (Fig. III-3I). The most parsimonious explanation for these quantitative effects is a difference between wild-type and mutant mice in the fractional distribution of cell types, creating a *denominator problem*. As noted above, *Math5* -/- retinas

have significantly fewer late-born cells, presumably due to loss of Shh. Because all *Math5* lineage cells retain early birthdates in these retinas (Fig. III-6C, Fig. III-S2), this cohort appears expanded and skewed toward late cell fates. Taken together, we conclude *Math5* does not directly control the acquisition of multiple retinal cell fates (Feng et al., 2010). Instead, *Math5* has an active role in RGC fate specification, as a competence (permissive) factor, and a passive or minor role in the selection of alternative (non-RGC) fates.

Mechanisms of fate determination in the mouse retina

Retinal cell fate choice, differentiation and survival are jointly controlled by intrinsic and extrinsic factors (Livesey and Cepko, 2001). As a nuclear bHLH protein, Math5 is an intrinsic factor. It is necessary but not sufficient for RGC development. During retinogenesis, nine-fold more *Math5*+ cells are produced than develop into RGCs (Fig. III-3, Table III-1). These cells have a different fate bias than other neurogenic cells in the same environment (Fig. III-5). This property is conferred upstream of *Math5*. The development of RGCs from Math5+ cells may require the presence of positive cofactors or the absence of inhibitors. Soluble factors and cell-cell signaling are known to negatively regulate RGC genesis, including factors secreted by nascent RGCs (Austin et al., 1995; Belliveau and Cepko, 1999; Waid and McLoon, 1998; Zhang and Yang, 2001), and these may act on *Math5*+ cells. Together, our data suggest that the *Math5*+ cohort is influenced by intrinsic and extrinsic factors.

Our finding that *Math5*+ progenitors born on the same day can give rise to early or late cell types (Fig. III-5) is consistent with a progressive restriction

model for retinal neurogenesis, in which the progenitor pool is initially multipotent, but gradually loses competence to form early cell types (Pearson and Doe, 2003; Shen et al., 2006). This model is favored by heterochronic co-culture experiments (Reh, 1992; Watanabe and Raff, 1990) and *Ascl1* (*Mash1*) lineage analysis. Mouse *Ascl1*+ progenitors form all retinal cell types except RGCs (Brzezinski et al., 2011) and may represent the first competence-restricted state. However, our results are also consistent with a temporal restriction model, in which progenitors proceed *unidirectionally* in time through a relatively fixed series of competence states (Wong and Rapaport, 2009).

The reservoir of neurogenic cells that are competent to form RGCs greatly exceeds the final number. Likewise, the period of RGC competence extends beyond the normal time envelope for RGC births in rat and chick (James et al., 2003; Silva et al., 2003). This excess capacity, which includes *Math5*+ and *Math5*- cells, and the fate plasticity of *Math5*+ cells may serve to enhance the robustness of RGC development and ensure an appropriate histotypic profile in the mammalian retina.

Acknowledgements

The authors are grateful to Thom Saunders, Maggie van Keuren and the UM transgenic animal model core for generating the BAC transgenic animals; to Sue Tarlé and Dellaney Rudolph for technical support; to Nadean Brown for *in situ* hybridization data; to Nathaniel Heintz for BAC targeting plasmids and strains; to Sally Camper for the nlsCre plasmid; and to Sean Morrison for the MIG retroviral construct. The authors thank Chris Edwards, the UM microscopy

and image analysis laboratory staff, Rafal Farjo and Mohammad Farah for technical advice. The authors are grateful to Nadean Brown, Chris Chou, David Turner, Matt Wilken, Julia Pollak, Anna La Torre, and Yumi Ueki for valuable discussions and critical reading of the manuscript. This research was funded by National Institutes of Health (NIH) R01 grant EY14259 (TG). JAB and LP were supported by NIH T32 grants EY13934 (JAB, LP), GM07544 (JAB), and GM07863 (LP).

Figure III-1. *Math5* is expressed by early retinal progenitors during or shortly following their terminal cell cycle. (A) Time course of *Math5* mRNA expression in developing eyes. *Math5* mRNA levels peak at E14, with a profile that resembles RGC birthdating curves (Young 1985; Rapaport *et al.* 2004). (B-C) Sections from E13.5 (B) or E16.0 (C) *Math5* +/- embryos co-stained for βgal (*Math5-lacZ* allele), EdU (following a 30 min chase), and cyclin D1 (marks G1/early S phase). Upper and lower panels show single- and double-labeled confocal projection images of 10 (B) or 3 (C) 1-μm optical slices. Insets show a βgal+ cell in G2 (EdU+ cyclinD1−). At E13.5, some βgal+ EdU+ cells are present (arrows, 18 of 517 βgal+ cells), but none are cyclinD1+ (0 of 517). At E16.0, few or no βgal+ cells are EdU+ or cycD1+. (D-H) Retinal sections from *Math5* +/- (D, E, G) and *Math5* -/- (E, G) mice co-stained for βgal and cell cycle markers. *Math5-lacZ* is occasionally co-expressed with M-phase marker PH3 at E13.5 (arrow in D, inset), but does not overlap with PH3 (arrows in E,F) or BrdU (1 hr chase) (arrows in G,H) at E15.5. Therefore, *Math5-lacZ* expression initiates during terminal G2 phase at E13.5, but after terminal M phase at E15.5 and E16.0 in both *Math5* +/- and -/- retinas. M5, *Math5*; βgal, *E. coli* β-galactosidase; cycD1, cyclinD1; PH3, phosphohistone H3. Scale bar, 50 μm.

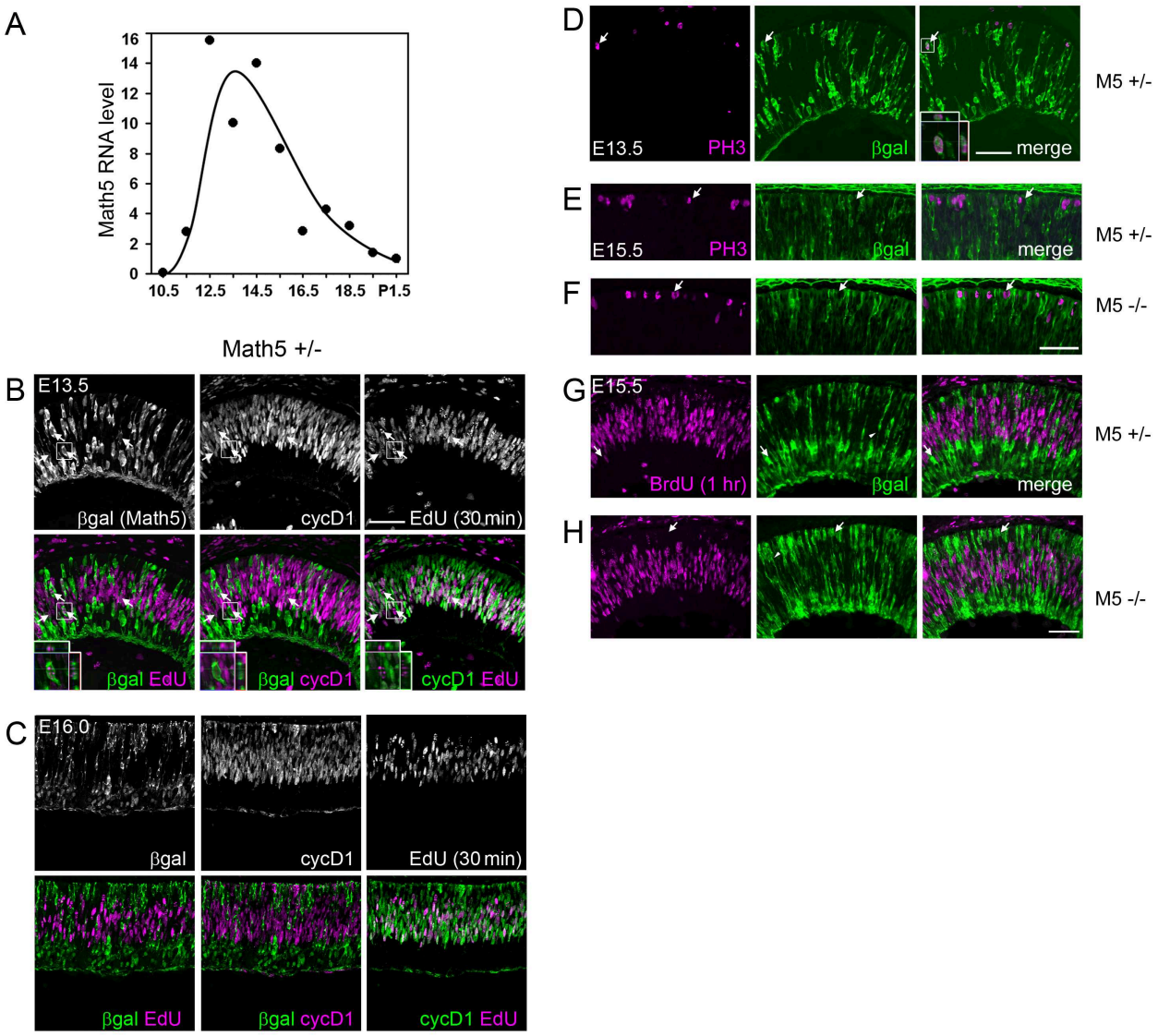
A
Math5 RNA level
16
14
12
10
8
6
4
2
0
10.5
12.5
14.5
16.5
18.5
P1.5
Math5 +/-
B
E13.5
βgal (Math5)
cycD1
EdU (30 min)
βgal EdU
βgal cycD1
cycD1 EdU
C
E16.0
βgal
cycD1
EdU (30 min)
βgal EdU
βgal cycD1
cycD1 EdU
D
E13.5
PH3
βgal
merge
M5 +/-
E
E15.5
PH3
βgal
merge
M5 +/-
F
M5 -/-
G
E15.5
BrdU (1 hr)
βgal
merge
M5 +/-
H
M5 -/-

Figure III-2. Construction and expression of the Math5>Cre transgene. (A) Math5>Cre BACs were generated in *E. coli* by a two-step homologous recombination procedure. The single-exon *Math5* open reading frame was precisely replaced with a nlsCre-pA cassette, using "A" and "B" homology arms derived from 5' (red box) and 3' (cyan box) UTRs. The pLD53 shuttle vector contains *recA* recombinase, positive (*amp*) and negative (*sacB*) selection cassettes, and the R6Kγ origin of replication. The pBACe3.6 vector (gray box) contains the chloramphenicol resistance gene (*Cm*) and P1 origin (*ori*). (B) Confirmation of recombinant BAC structure using diagnostic (dx) PCRs 1-6 indicated in panel A (assembled from multiple gels). (C-F) Developmental expression pattern. Math5>Cre mice were crossed to mice carrying the Z/AP transgene, which permanently reports Cre activity. Alkaline phosphatase (hPLAP)-positive RGCs (purple, arrows) are first observed at E12.5 in double transgenic embryos (D), while control littermates (C) containing only the Z/AP transgene are negative. hPLAP activity increases from E13.5 to E15.5 as RGCs develop and form the optic nerve. By P0.5, hPLAP activity is abundant in RGCs (arrow) and can be detected in some photoreceptors (arrowhead); however most of the retina is unlabeled. (E) Composite images of 250 µm coronal vibratome sections through the adult thalamus and optic chiasm (inset) show the axonal projections of RGCs derived from *Math5*+ precursors. Lower panels show sections through the accesory optic system (left) and superior colliculus (right). Labeled RGCs project to all major ganglion cell target sites in the CNS. No significant staining was observed in the cerebral cortex or hippocampus. (F) Kinetics of *Math5* expression in the E15.5 retina. *Math5* mRNA (*in situ* hybridization) is expressed in retinal progenitor cells, while the cytoplasmic *Math5-lacZ* knock-in allele labels progenitors (sclerad) and developing RGCs (vitread), which have recently transcribed *Math5* (β-galactosidase activity). hPLAP activity in Math5>Cre; Z/AP mice is localized to developing RGCs on the vitread side of the retinal epithelium. These patterns demonstrate the spatiotemporal progression of *Math5* expression, if one considers the perdurance of β-galactosidase, the delay associated with Cre excision, and interkinetic nuclear migration. *Math5* is expressed transiently in progenitors that become RGCs. (G-H) Math5>Cre retinas co-stained for lineage tracers and cell cycle markers. Cre is expressed with the same kinetics as *Math5*, whereas GFP or hPLAP reporters are expressed with a delay. (G) At E13.5, Cre+ EdU+ cells are present (30 min chase, arrows, 33 of 394 Cre+ cells), but no GFP+ EdU+ cells are observed (0 of 309 GFP+ cells). (H) At E15.5, no hPLAP+ cells (arrows) are co-labeled with BrdU (1 hr chase), PH3, or Ki67 (marks late G1 through M phase). Together, these results indicate that cells in the *Math5* lineage do not re-enter the cell cycle. pA, polyadenylation signal; SC, superior colliculus; BSC, brachium of the superior colliculus; LGB_d, lateral geniculate body, pars dorsalis; LGB_v, lateral geniculate body, pars ventralis; LTN, lateral terminal nucleus ; AOT, accessory optic tract; OT, optic tract; TV, third ventricle; SCN, suprachiasmatic nucleus; OC, optic chiasm; H, hippocampus; PN, pons. Scale bars, 100 μm in C-F; 50 μm in G-H.

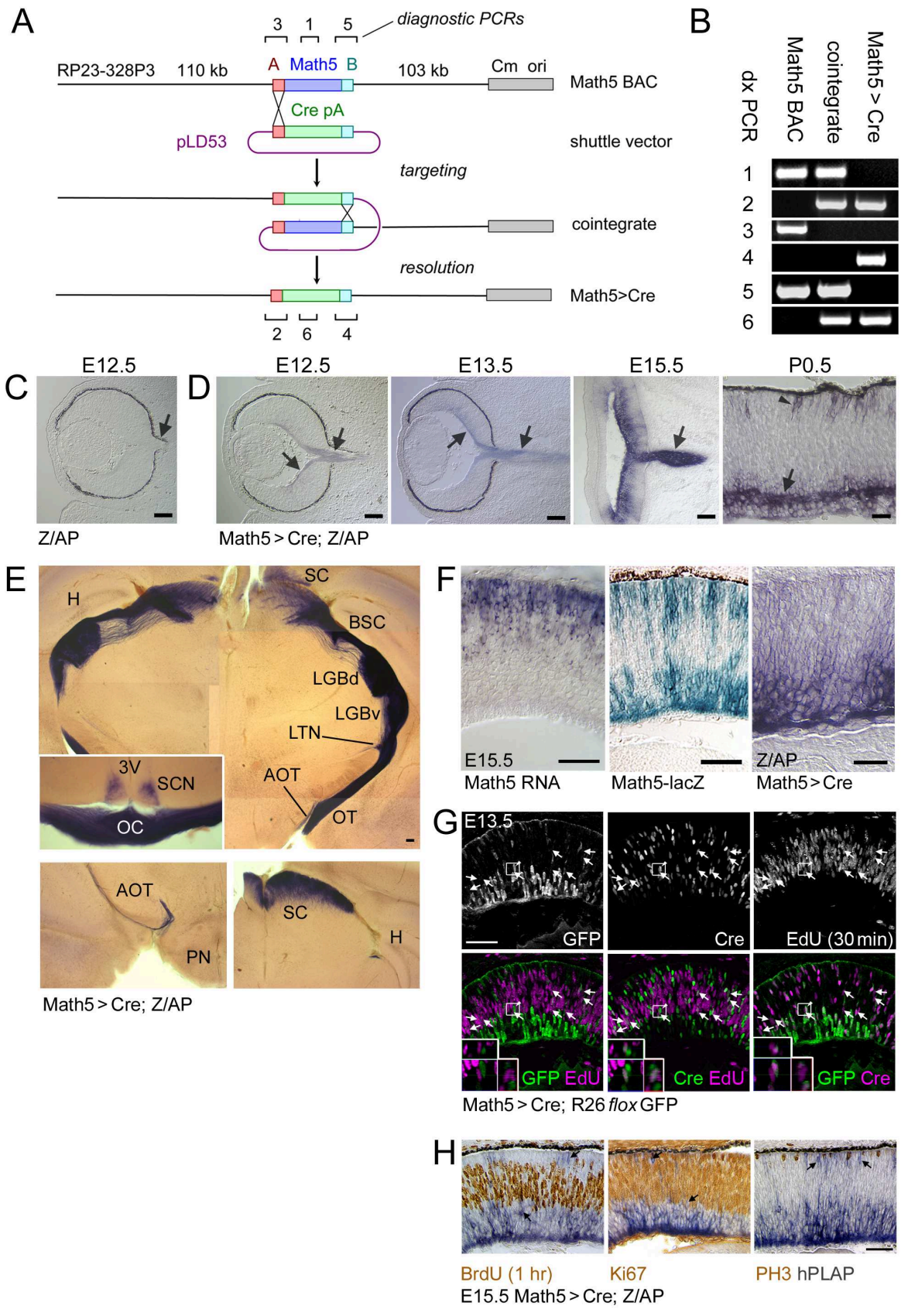
A
3 1 5
diagnostic PCRs
RP23-328P3
110 kb
A Math5 B
103 kb
Cm ori
Math5 BAC
Cre pA
pLD53
shuttle vector
targeting
cointegrate
resolution
Math5>Cre
2 6 4
B
dx PCR
Math5 BAC
cointegrate
Math5 > Cre
1
2
3
4
5
6
C
E12.5
Z/AP
D
E12.5
E13.5
E15.5
P0.5
Math5 > Cre; Z/AP
E
H
SC
BSC
LGBd
LGBv
LTN
3V
SCN
OC
AOT
OT
AOT
PN
SC
H
Math5 > Cre; Z/AP
F
E15.5
Math5 RNA
Math5-lacZ
Z/AP
Math5 > Cre
G
E13.5
GFP
Cre
EdU (30 min)
GFP EdU
Cre EdU
GFP Cre
Math5 > Cre; R26 flox GFP
H
BrdU (1 hr)
Ki67
PH3 hPLAP
E15.5 Math5 > Cre; Z/AP

Figure III-3. *Math5*+ progenitors contribute differentially to all retinal cell types. Math5>Cre mice were crossed to Z/AP (A-D) or R26*flox*GFP reporter (E-G) strains. (A) In Math5>Cre; Z/AP mice, hPLAP+ descendants of *Math5*+ progenitors represent 3% of adult retinal cells (see Table III-1) and are present in every cell layer. (B) Z/AP-only control retinas have no hPLAP activity. (C) *Math5*+ descendants, detected by hPLAP immunostaining, include horizontal (h), ganglion (rgc), displaced amacrine (da), INL amacrine (a), bipolar (b), rod (r), cone (c) and Müller glial (m) cells. (D) *Math5*+ cone (arrows) and rod (arrowheads) photoreceptors are distinguished by co-labeling with anti-hPLAP and cone-specific PNA lectin. Non-specific labeling of pigment epithelium and choroid reflects mouse IgG crossreactivity. (E-G) In Math5>Cre; R26*flox*GFP mice, Math5+ horizontal cells (E, arrows) are marked by GFP and calbindin immunoreactivity. The arrowhead shows a solitary *Math5*+ bipolar cell. (F-G) *Math5*+ RGCs (arrows) and displaced amacrines (arrowheads) in the GCL are shown in adult retinal sections (F) or P1 retinal flatmounts (G). RGCs are distinguished by retrograde labeling of optic nerve axons with rhodamine dextran. There is no difference in the GFP+ fraction of rhodamine dextran-labeled RGCs between these two ages. (H) The fate of Math5>Cre- expressing progenitors in *Math5* -/- mice. hPLAP+ cells are distributed throughout the retina, but RGCs are lacking. Vitreal hemorrhages (arrowhead) are common in *Math5* -/- mice. (I) The distribution of cell fates in the entire retina (from Jeon et al., 1998), in the *Math5* lineage of wild-type mice, and in the *Math5* lineage of knockout mice. The *Math5* lineage is biased toward early-born cell types (RGC, horizontal, cone), although rods are the most common fate adopted by *Math5*+ cells. In the *Math5* knockout, lineage-derived cells adopt all retinal fates except for RGCs. hPLAP, human placental alkaline phosphatase; o, outer nuclear layer; i, inner nuclear layer; g, ganglion cell layer. Scale bars, 100 μm in A-B, H; 50 μm in C-G.

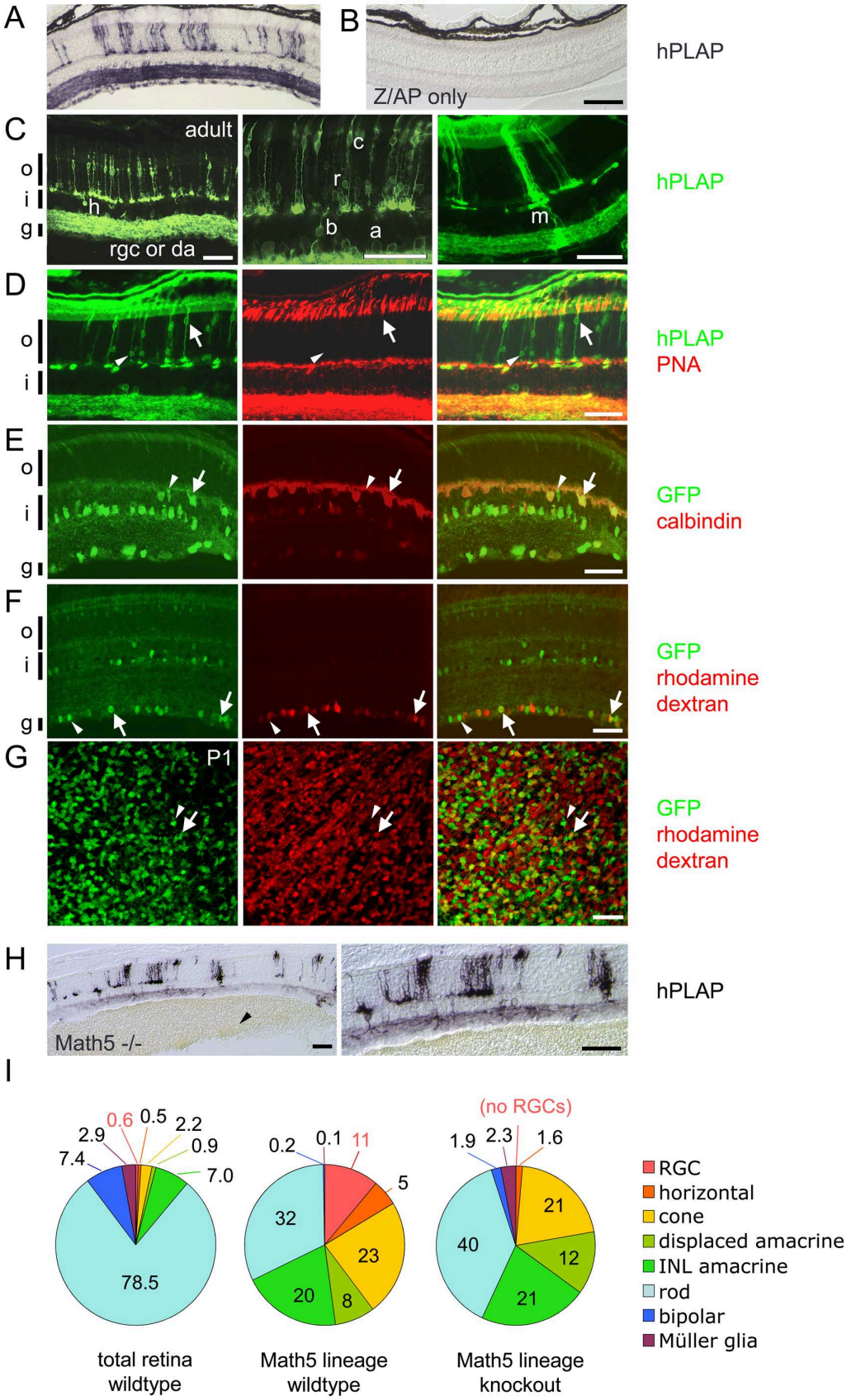
A
B
Z/AP only
hPLAP
C
adult
o
i
g
h
rgc or da
c
r
b
a
m
hPLAP
D
hPLAP
PNA
E
GFP
calbindin
F
GFP
rhodamine
dextran
G
P1
GFP
rhodamine
dextran
H
Math5 -/-
hPLAP
I
0.6
0.5
2.2
2.9
0.9
7.4
7.0
78.5
0.2
0.1
11
5
32
23
20
8
(no RGCs)
1.9
2.3
1.6
21
40
12
21
RGC
horizontal
cone
displaced amacrine
INL amacrine
rod
bipolar
Müller glia
total retina
wildtype
Math5 lineage
wildtype
Math5 lineage
knockout

Figure III-4. All Math5>Cre progenitors express similar levels of Cre, regardless of cell fate. Math5>Cre lineage analysis was performed using Z/AP and R26*flox*GFP reporters simultaneously, to evaluate the heterogeneity of *Math5* expression among progenitors. This analysis assumes that the probability of reporter activation in a given cell is determined by the cumulative amount of Cre recombinase expressed by that cell. (A-B) Two models for *Math5* (Cre) expression. (A) Bimodal expression. In this model, *Math5*+ progenitors giving rise to non-ganglion cell types express Cre weakly (left peak), so reporter activation in these cells is inefficient, and consequently few of their descendants co-express GFP and hPLAP. RGCs in the same retinas express Cre strongly (right peak) and are expected to have high concordance. (B) Uniform expression. In this model, every *Math5*+ progenitor expresses Cre strongly, so concordance is very high for all cell types (B, right). (C) Retinas of adult Math5>Cre; Z/AP; R26*flox*GFP mice immunostained for hPLAP and GFP. Double-labeled cells (arrows) greatly outnumber single-labeled cells (arrowheads). (D) The observed concordance between hPLAP and GFP reporters was ~80%, which is significantly greater than expected by chance (Cohen's $\kappa > 0.7$). This value was similar for all cell types, indicating that *Math5* is expressed at uniform levels by a subpopulation of progenitor cells, only some of which develop as RGCs. The labeled fractions (ρ) are based on data in Table III-1. GCL includes RGCs and displaced amacrines; INL Am, inner nuclear layer amacrine. Scale bar, 50 μm.

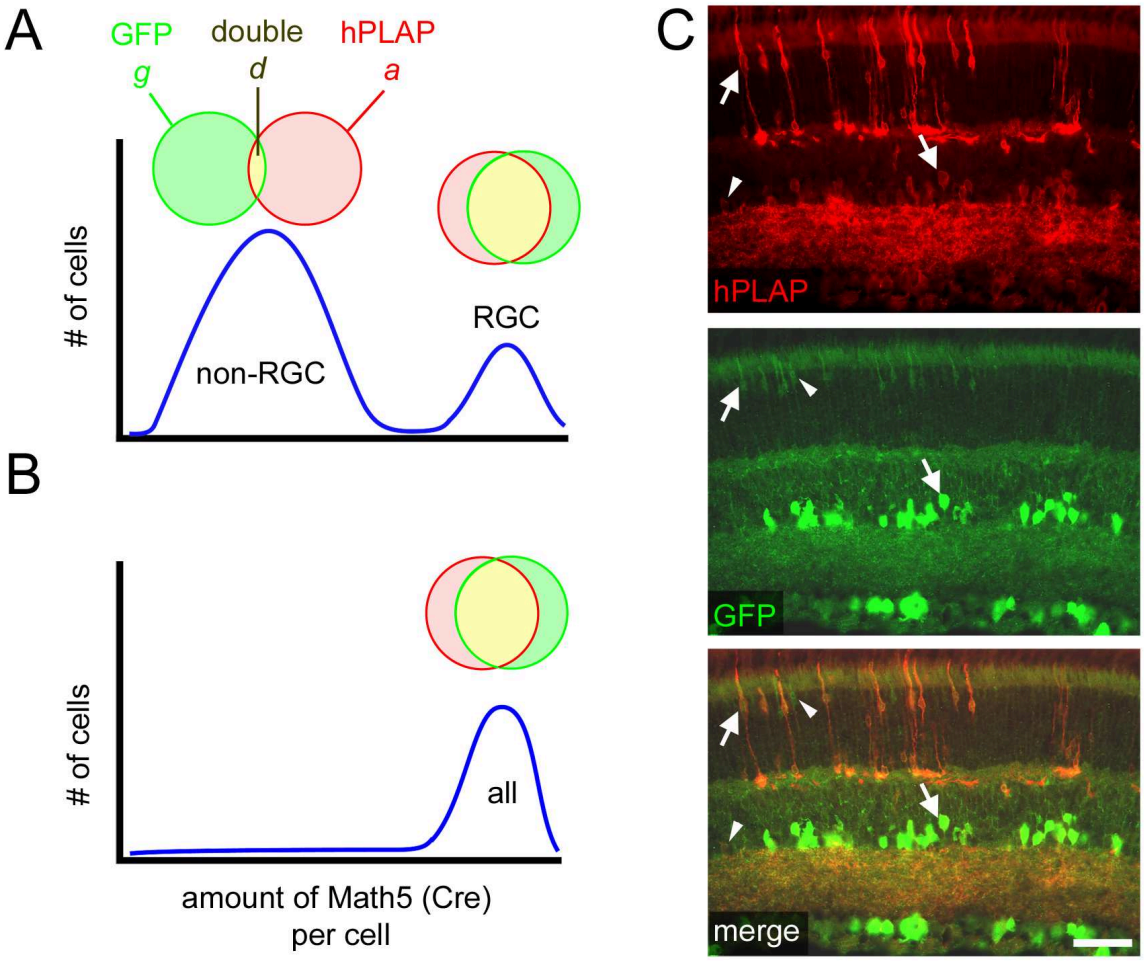

D

	labeled fraction		reporter concordance		
cells	single (ρ)	joint (ρ^2)	expected*	observed¥	Cohen's κ
GCL	0.40	0.16	0.25	0.77	0.70
cone	0.31	0.095	0.18	0.84	0.80
INL Am	0.09	0.007	0.04	0.80	0.79
rod	0.012	0.0001	0.006	0.82	0.82

$$* \text{ expected} = \frac{\rho^2}{(2\rho - \rho^2)} \qquad ¥ \text{ observed} = \frac{d}{a + g - d}$$

Figure III-5. The fate distribution of *Math5*+ progenitors changes over time. (A) Cumulative BrdU labeling experiment. Math5>Cre; Z/AP embryos were continuously exposed to BrdU from E10.5 to P0 and their retinas were collected at P21. Nearly all *Math5*+ descendants (hPLAP+) are heavily labeled with BrdU, indicating that the majority exited mitosis before P0, including lineage-labeled cones (arrows) and rods (arrowheads). There is a distinct gradient of BrdU labeling (birthdates) within the inner and outer nuclear layers, such that cells with nuclei closest to the lens have earlier birthdates (brightest BrdU signal). (B) Pulsed BrdU labeling experiment. Math5>Cre; *ZAP* embryos were transiently exposed to BrdU at E15.5. Adult retinas were stained with hPLAP and BrdU antibodies and PNA lectin. *Math5*+ cone (hPLAP+ PNA+ BrdU+, arrow) and bipolar (hPLAP+ BrdU+, arrowhead) cells are indicated. (C) Cone-rod ratio plots for birthdated hPLAP+ (red), hPLAP− (blue) and combined (black) photoreceptor groups. The ratio of cone-to-rod births decreases steadily between E14.5 and E17.5 for hPLAP+ and hPLAP− populations. The curves are parallel, indicating that the fate of *Math5*+ cells changes over time, similar to other retinal progenitors. However, the cone-to-rod ratio is 3-fold higher for *Math5*+ progenitors at every time point, suggesting that these cells have a fixed cone vs. rod bias, or are shifted by 0.5 days, compared to other neurogenic cells (hPLAP−) in the same retinal environment. (D) Cone-rod ratio plot for birthdated GFP+ (red), GFP− (blue) and combined (black) photoreceptor groups in *Math5* -/-; Math5>Cre; R26*flox*GFP mice. Scale bar, 50 μm.

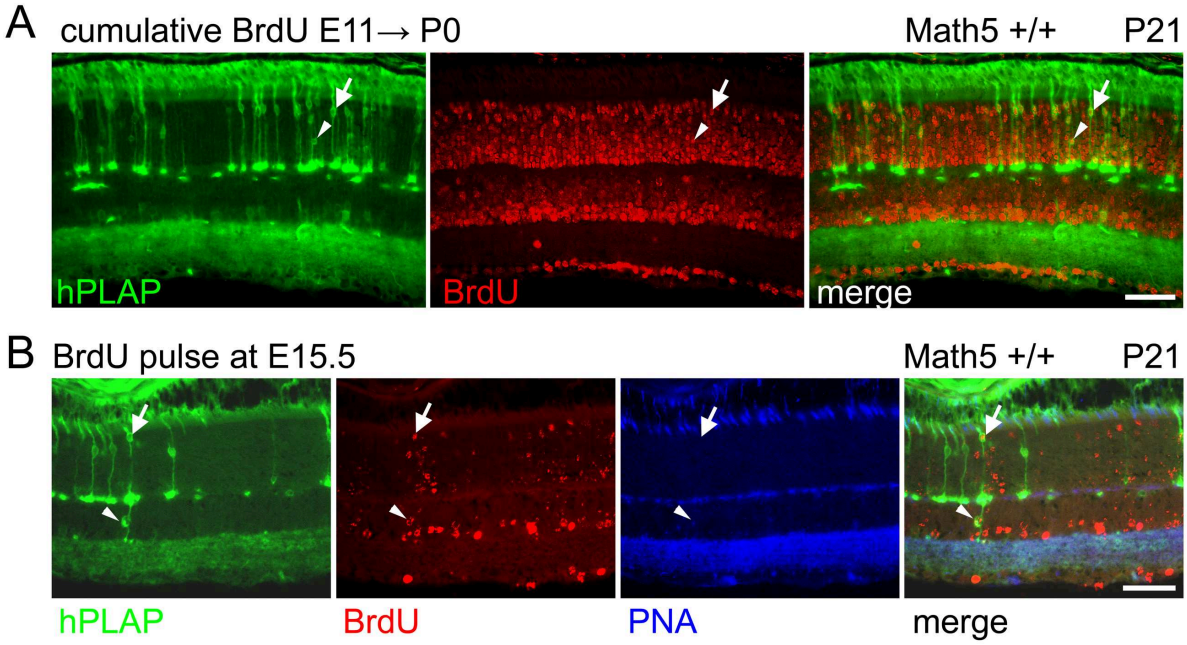
A
cumulative BrdU E11→ P0
Math5 +/+
P21
hPLAP
BrdU
merge
B
BrdU pulse at E15.5
Math5 +/+
P21
hPLAP
BrdU
PNA
merge

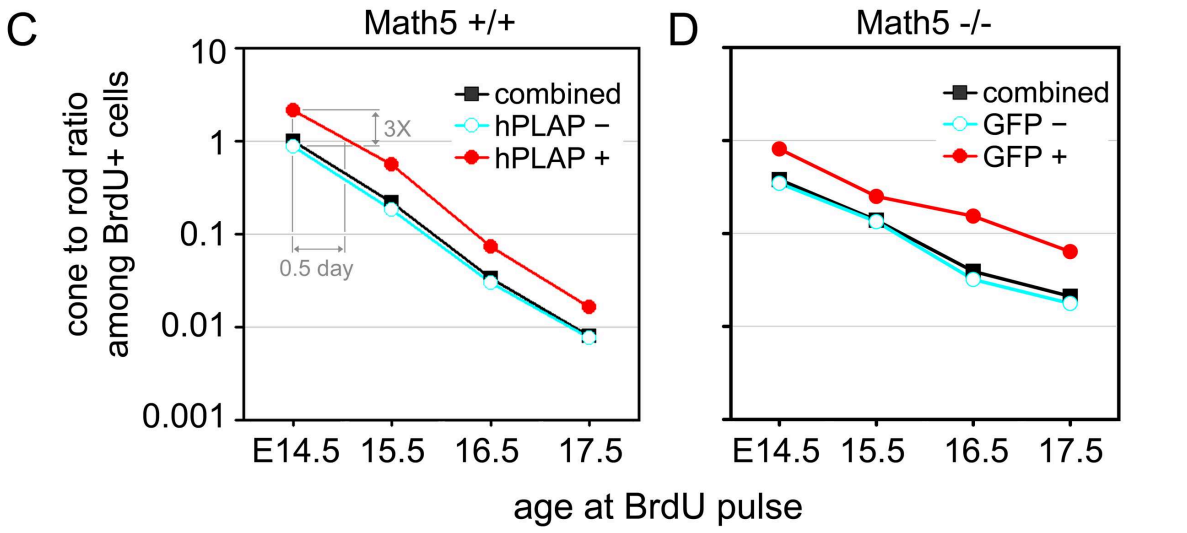
C
Math5 +/+
cone to rod ratio among BrdU+ cells
10
1
0.1
0.01
0.001
3X
0.5 day
combined
hPLAP −
hPLAP +
E14.5
15.5
16.5
17.5
D
Math5 -/-
combined
GFP −
GFP +
E14.5
15.5
16.5
17.5
age at BrdU pulse

Figure III-6. *Math5* marks many of the earliest born cells in the retina. (A-C) Window labeling analysis. (A) Embryos were exposed to pulses of EdU at E11 (onset of neurogenesis) and E11.5, and to continuous BrdU from E12 to E12.5. Progenitors (RPCs) that continue to cycle through E12.5 are EdU+ BrdU+, while cells that have exited mitosis between E11 and E12 are EdU+ BrdU−, and represent the earliest born cohort of retinal neurons. (B-C) Sections through the neural retina (brackets). (B) Most early-born cells in *Math5 +/-* mice adopt RGC fate (EdU+ BrdU- Brn3b+, arrows). The Brn3b- cells in this cohort are likely to include horizontal cell precursors (arrowheads). Few Brn3b+ RGCs (arrows) are present in Math5 -/- embryos, and the abundance of non-RGC fates increases accordingly (arrowheads). (C) Early-born *Math5-lacZ* (EdU+ BrdU- βgal+, arrows) and βgal− (arrowheads) cells are shown in *Math5 +/-* (top) and *Math5 -/-* (bottom) mice. Only ~20% of the early-born cohort expresses the *Math5* transcription unit (βgal+), in both genotypes. (D-E) Birthdating analysis. (D) E11 Math5>Cre; R26*flox*GFP embryos were exposed to a single EdU injection and analyzed at P1. (E) Flatmounted retinas were stained for EdU and GFP and imaged through the GCL. Strongly EdU+ cells mark the earliest born retinal neurons. Confocal projection image (6-10 μm) shows EdU+ GFP+ (arrow) and EdU+ GFP− (arrowhead) cells. Only 28% of the GCL cells born at E11 are in the Math5+ lineage. i.p., intraperitoneal; EB, early-born. Error bars represent the binomial standard deviation. Scale bar, 50 μm.

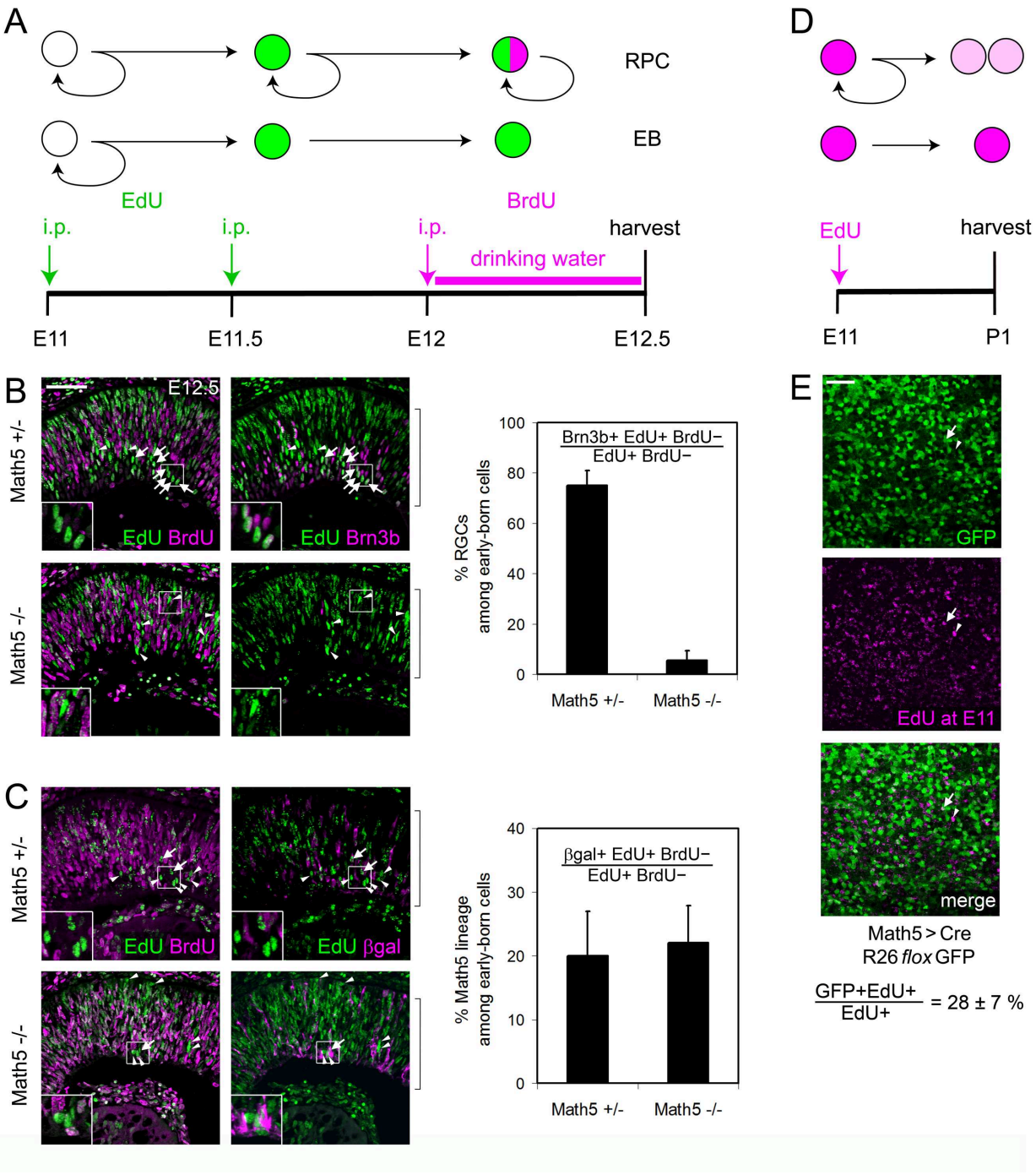
A
RPC
EB
EdU
BrdU
i.p.
i.p.
i.p.
harvest
drinking water
E11
E11.5
E12
E12.5
D
EdU
harvest
E11
P1
B
E12.5
Math5 +/-
Math5 -/-
EdU BrdU
EdU Brn3b
Brn3b+ EdU+ BrdU−
EdU+ BrdU−
% RGCs among early-born cells
100
80
60
40
20
0
Math5 +/-
Math5 -/-
C
EdU BrdU
EdU βgal
βgal+ EdU+ BrdU−
EdU+ BrdU−
% Math5 lineage among early-born cells
40
30
20
10
0
Math5 +/-
Math5 -/-
E
GFP
EdU at E11
merge
Math5 > Cre
R26 flox GFP
GFP+EdU+ / EdU+ = 28 ± 7 %

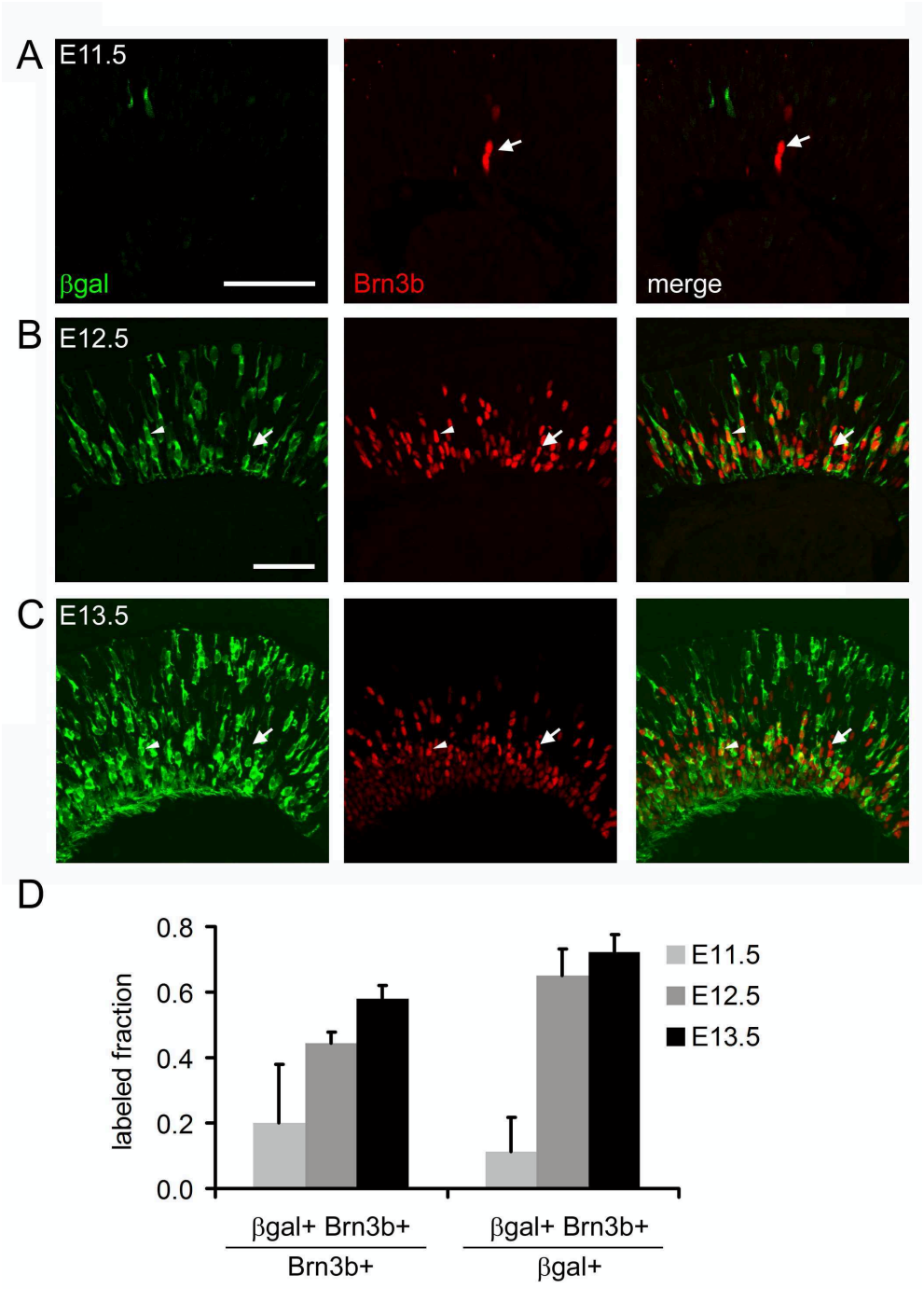

Figure III-7. A subset of Brn3b+ RGCs derives from the *Math5* lineage. (A-C) Sections from embryonic *Math5-lacZ*/+ retinas co-stained for βgal and Brn3b. At E11.5, relatively few Brn3b+ cells are βgal+ (A, arrow). The fraction of Brn3b+ cells expressing *Math5-lacZ* (arrowheads) increases from E12.5 (B) to E13.5 (C). However, there are many *Math5*-independent RGCs (arrows) at each age. (D) Histograms showing the fraction of *Math5*+ cells among Brn3b+ RGCs and the fraction of Brn3b+ RGCs within the *Math5*+ cohort. Error bars show the standard deviation (*n* = 3 sections). The total number of cells counted at E11.5, E12.5 and E13.5 was 13, 228 and 667, respectively. Scale bar, 50 μm.

Figure III-8. Retrovirally marked clones exhibit symmetric and asymmetric patterns of *Math5* expression. (A) E12.5 or E13.5 retinas were explanted from *Math5 lacZ/+* embryos, flattened on polycarbonate membranes, infected at low density with a retroviral stock to mark clonal lineages (green), and cultured for 3 days *in vitro* (DIV). The micrograph shows a cross-section from a representative explant (bracket) co-stained for cytoplasmic βgal (magenta) and GFP (green). The diagram shows hypothetical 2-cell clone with βgal+ cells. Each clone reflects one informative terminal division: a symmetric [S] division which gave rise to two *Math5*+ daughters (left); or an asymmetric [A] division, which gave rise to one *Math5*+ and one *Math5*− daughter (right). (B-D) Confocal Z-stack projections and drawings showing representative clones that are symmetric (B, C) or asymmetric (D) with respect to *Math5* expression. (E) Summary of observed clones containing at least one *Math5*+ cell. Informative divisions have a unique interpretation, and give rise to one [A] or two [S] *Math5*+ daughters. Both types of divisions were identified. MIG, MSCV-IRES-GFP virus. Scale bars: 10 μm in A; 5 μm in B-D.

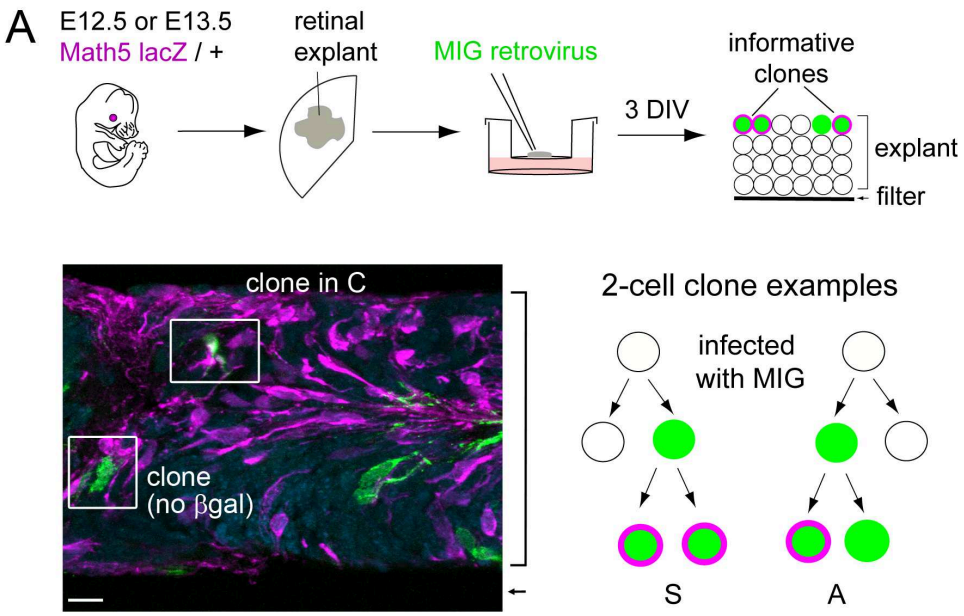

E

clone properties		Math5 informative divisions	clones scored			informative divisons observed		
size	pattern		E12.5	E13.5	total	S	A	total
8 cell	●○○○○○○○	A	1	0	1	0	1	1
4 cell	●●●●	S + ?	3	1	4	4	0	4
	●●●○	A + ?	0	1	1	0	1	1
	●○○○	A	3	2	5	0	5	5
2 cell	●●	S	4	5	9	9	0	9
	●○	A	0	3	3	0	3	3
		sum	11	12	23	13	10	23

Figure III-9. Natural history of the *Math5* lineage. (A) The timing of *Math5* expression shifts during retinal histogenesis. RPCs (white) shift from a proliferative (P-P) mode of division to stem (N-P) or terminal (N-N) modes, giving rise to neurogenic cells (gray). These express *Math5* (red) either during (S, symmetric) or after (A, asymmetric) final mitosis. During early retinal development (<E14), *Math5* is frequently expressed during G2 phase of the last cell cycle, generating two *Math5*+ daughters. During later stages (>E15), *Math5* is exclusively expressed by post-mitotic cells. (B) The size of the neurogenic (birthdated) population and proportion of *Math5*+ cells changes during development. At the onset of neurogenesis (E11), *Math5* is expressed by 20-30% of newborn cells. The number of *Math5*+ cells peaks during midgestation (E14) and rapidly diminishes (E16), while the neurogenic population as a whole continues to expand. The temporal profile for RGC birthdates follows similar kinetics, and reflects *Math5*+ and *Math5*– populations. (C) The fate spectrum of *Math5* lineage (red) and other neurogenic (gray) cells in wild-type and mutant mice. The thickness and shading of arrows denotes the relative demographic contribution of these cohorts to the mature retina.

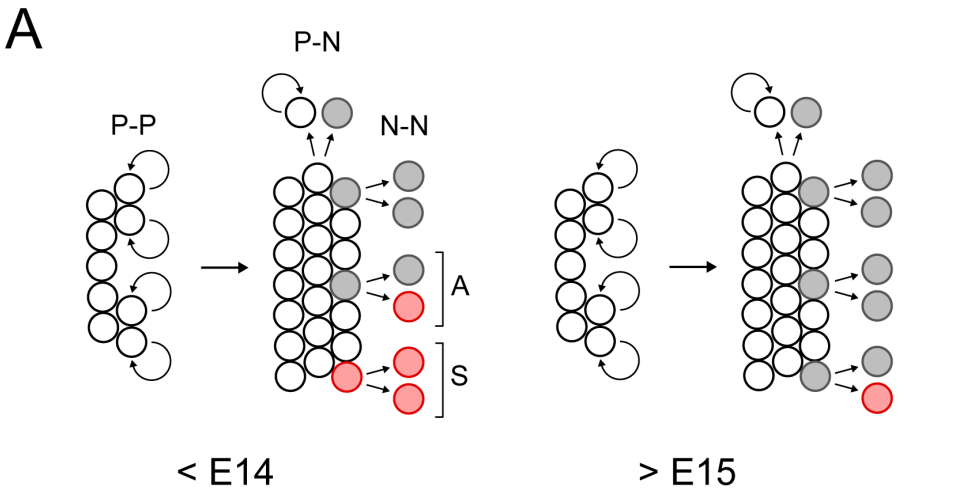
A
P-N
P-P
N-N
A
S
< E14
> E15

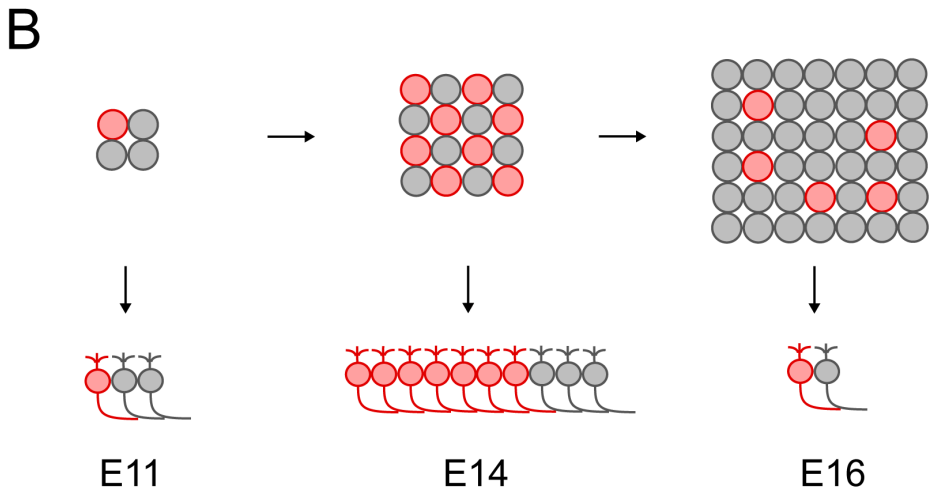
B
E11
E14
E16

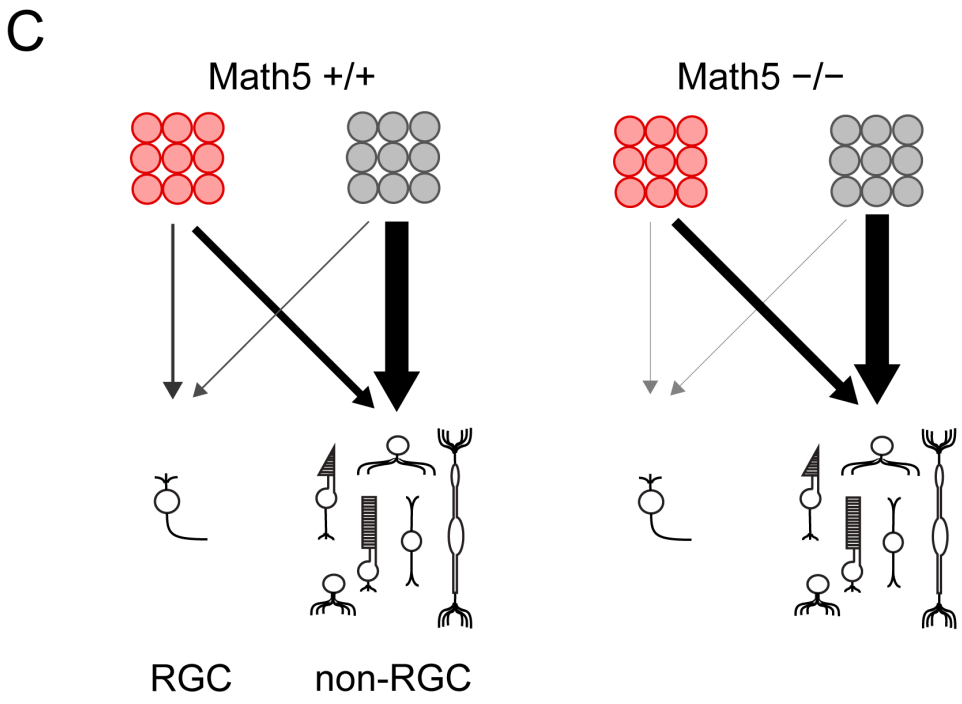
C
Math5 +/+
Math5 −/−
RGC
non-RGC

Table III-1. Cell type distribution of Math5 lineage descendants in wild-type Math5>Cre transgenic retinas

	cells counted					
	Math5 lineage	total	Math5 lineage (% of cell type)[§]	cell type[†] (% of retina)	Math5 lineage (% of retina)	cell type[‡] (% of Math5 lineage)
CELL TYPE	(*a*)	(*b*)	(*a*/*b*) x 100	(*c*) x 100	(*a*/*b*)(*c*) x 100	(*a*/*b*)(*c*/*f*) x 100
RGC	700	1,265[#]	55[§]	0.6	0.3	11
cone	1,515	4,914	31	2.2	0.7	23
horizontal	1,041	3,592	29	0.5	0.2	5
amacrine	1,665	15,570*	11	7.9	0.8	29
INL	1,198	13,920*	9	7.0	0.6	20
displaced	467	1,648[#]	28	0.9	0.2	8
rod	2,085	173,000*	1	78.5	0.9	32
bipolar	12	12,900*	< 0.1	7.4	< 0.005	< 0.2
Müller glia	5	8,800*	< 0.1	2.9	< 0.002	< 0.1
TOTAL				**100.0**	**2.9 (*f*)**	**100**

RGCs, displaced amacrines, and INL amacrines were counted in 33 fields (200 X, 8 eyes, 6 mice, R26*flox*GFP reporter). Horizontal cells were counted in 58 sections (8 eyes, 6 mice, R26*flox*GFP reporter). All other cell types were counted in 50 to 70 fields (200 X, 16 eyes, 12 mice, Z/AP reporter). Math5+ descendants detected using the Cre lineage system comprise 2.9% of the adult retina (*f*).

* Estimated using cell type ratios reported by Jeon *et al.* (1998) for adult C57BL/6J mice. The total number of cones counted in surveyed fields was multiplied by 35.2 to give the number of rods, and by 3.32 for bipolar cells and 1.3 for Müller glia. The total number of GCL neurons surveyed (RGC and displaced amacrines) was multiplied by 4.78 to estimate the number of inner nuclear layer (INL) amacrines.

[#] RGCs (identified by retrograde axon labeling) represent 43% of GCL neurons (1265/2913 cells). The remaining GCL cells were scored as displaced amacrines.

[§] Among *n* = 8 eyes, the mean RGC labeling fraction ± SEM was 54 ± 2%, with a range between 46 and 63%. The overall labeling fraction for the GCL was 40% (1167/2913 cells), which represents 24% RGCs (700/2913 cells) and 16% displaced amacrines (467/2913 cells).

[†] Calculated from Jeon *et al.* (1998) and shown in Fig. 3I (left pie chart)

[‡] These values are shown in Fig. 3I (middle pie chart).

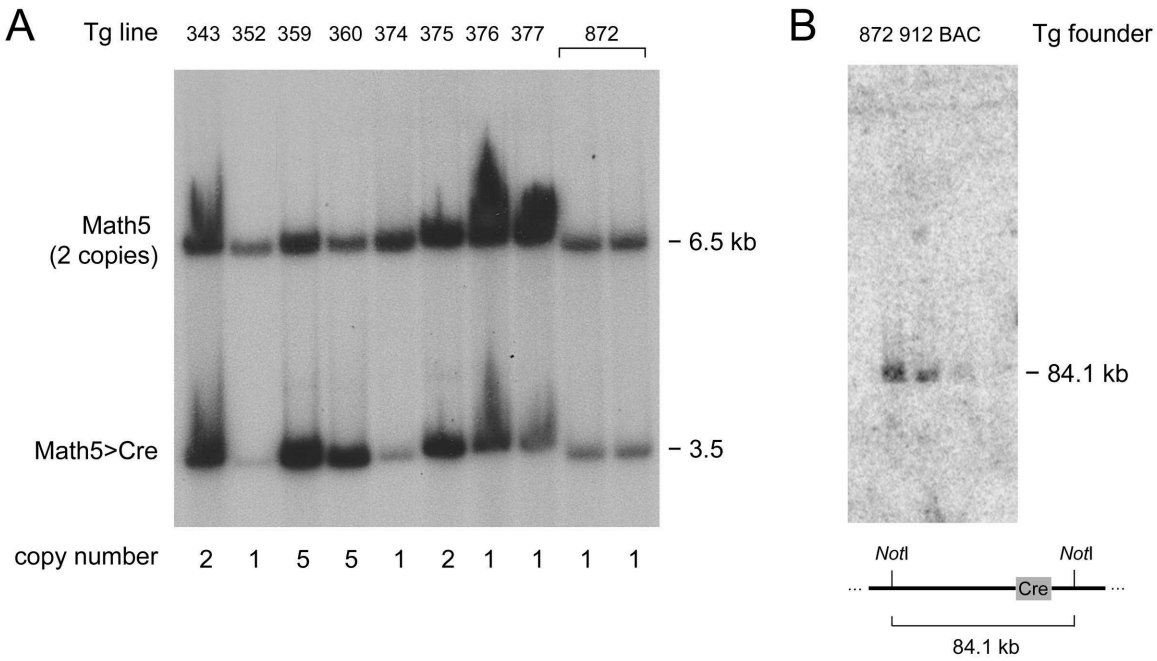

Figure III-S1. Copy number and integrity in Math5>Cre transgenes. (A) Southern blot of *Eco*RI-digested DNA from nine independent transgenic lines, hybridized with a 5' *Math5* genomic probe labeled with ^{32}P. The Math5>Cre BAC fragment (3.5 kb) is smaller than the endogenous *Math5* fragment (6.5 kb) due to the presence of an *Eco*RI site in the Cre cassette. Transgene copy number was estimated from the relative intensity of these fragments, as determined by densitometry. (B) Pulsed-field gel Southern analysis. Genomic DNA from Math5>Cre transgenic founders 872 and 912, and purified episomal DNA from BAC clone RP23-328P3-D1-68 were digested with *Not*I, separated by PFGE, and hybridized with a Cre probe. Both founders had the predicted 84.1 kb *Not*I fragment, indicating that this segment is intact. Tg, transgenic.

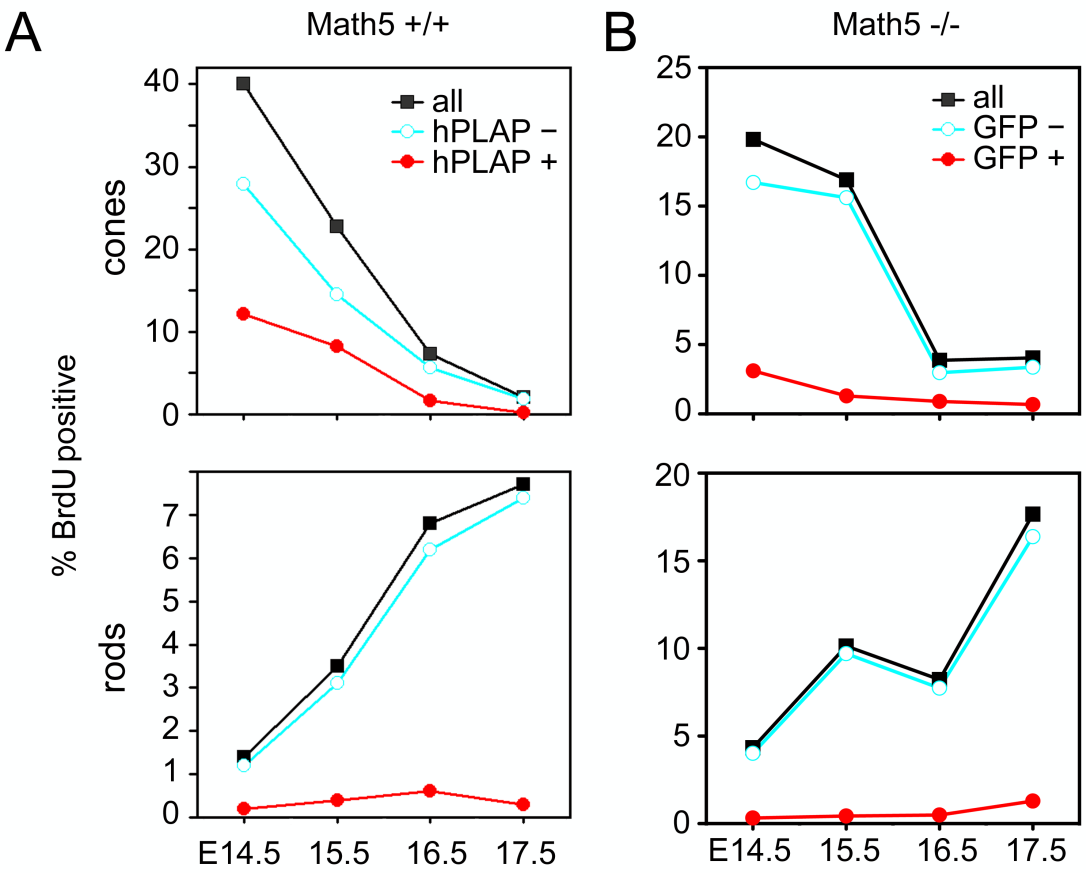

Figure III-S2. Birthdating curves for cones (top graphs) and rods (bottom graphs) in (A) wild-type Math5>Cre; Z/AP and (B) mutant Math5>Cre; R26*flox*GFP mice between E14.5 and E17.5 (see Table III-S4). Single BrdU injections were given to pregnant dams on the indicated days, and photoreceptors were analyzed in the adult retinas. Curves show the percentage of each photoreceptor type that is BrdU+ for the hPLAP+ or GFP+ (red), hPLAP− or GFP− (blue), and combined (black) progenitor groups. The difference in scale between panels A and B reflects the relative deficiency of late-born rods (>E17) and relative excess of early-born cones (<E14) in *Math5* -/- mice.

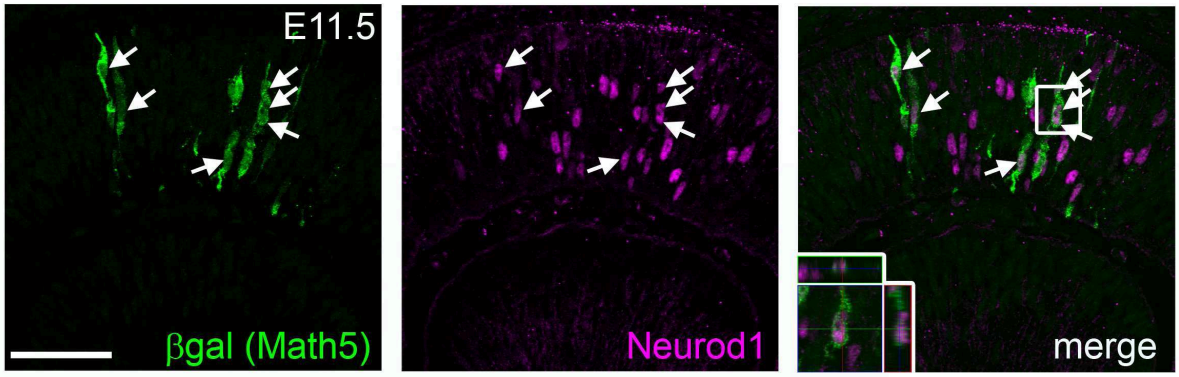

Figure III-S3. Proneural bHLH factors Neurod1 and Math5 are expressed in overlapping subsets of progenitor cells during early retinal neurogenesis. E11.5 *Math5-lacZ/+* retinal sections were immunostained for βgal and Neurod1. Approximately half of the βgal+ cells co-express Neurod1 (arrows, inset). Scale bar, 50 μm.

Table III-S1. Cell type distribution of Math5 lineage descendants in Math5 mutant mice

	Math5 lineage cells counted	cell type (% of Math5 lineage)
CELL TYPE	**(*a*)**	**(*a*/*b*) x 100**
cone	189	21
horizontal	14	1.6
amacrine	295	33
INL	187	21
displaced	108	12
rod	358	40
bipolar	17	1.9
Müller glia	21	2.3
TOTAL	**894 (*b*)**	100

All labeled cells were identified and counted in 23 fields (200X, 6 eyes, Z/AP reporter). All cells in the GCL were assumed to be displaced amacrine cells, as no cells in Math5 mutant retinas were positive for RGC markers Brn3a or Brn3b.

Table III-S2. Dual reporter concordance for Math5>Cre labeled retinal cells

	cells counted[†]			concordance (%)[#]	
cell type	hPLAP+ GFP+ (*d*)	total hPLAP (*a*)	total GFP (*g*)	$\frac{d}{a+g-d}$	SEM[‡]
rods	334	376	390	77	3
cones	257	274	289	84	1
INL amacrines	330	376	368	80	4
GCL neurons*	257	287	284	82	3
TOTAL	1178	1313	1331	80	1

All single and double labeled cells were counted in 18 fields (200X) representing 4 eyes from 3 Math5>Cre; Z/AP; R26*flox*GFP mice. hPLAP, alkaline phosphatase; GFP, green fluorescent protein.

*RGCs and displaced amacrines.

[†]There was no significant difference in the number of cells labeled by each reporter in the fields surveyed (paired *t* test, $P > 0.1$).

[#]The incomplete concordance (<100%) in this experiment validates our assumption that Cre levels are not saturated.

[‡]Standard error of the mean (SEM) calculated from concordance for $n = 4$ eyes. There was no significant difference among cell types (one-way ANOVA, $P > 0.15$).

Table III-S3. Cumulative BrdU labeling experiment (E10.5 to P0)

	Math5 lineage cells counted		
cell type	**BrdU+**	**total**	**% BrdU+**
rods	70	70	100
cones	53	53	100
INL neurons	62	65	95
GCL neurons	53	53	100
TOTAL	238	241	99

Table III-S4. Birthdates of Math5 lineage retinal descendants

Math5 +/+ mice

		cones counted (% of combined total)			rods counted (% of combined total)		
time of pulse		**hPLAP+**	**hPLAP−**	**combined**	**hPLAP+**	**hPLAP−**	**combined**
E14.5	**BrdU+**	136 (12.1)	314 (27.9)	450 (40.0)	64 (0.2)	455 (1.1)	519 (1.3)
	BrdU−	243 (21.6)	431 (38.4)	674 (60.0)	315 (0.8)	38,700* (97.8)	39,100* (98.7)
	total	379 (33.7)	684 (66.3)	1,124 (100.0)	379 (1.0)	39,200* (98.9)	39,600* (100.0)
E15.5	**BrdU+**	79 (8.3)	141 (14.5)	220 (22.7)	140 (0.4)	1,073 (3.1)	1,213 (3.5)
	BrdU−	214 (22.0)	537 (55.3)	751 (77.3)	317 (0.9)	32,600* (55.3)	33,000* (96.5)
	total	293 (30.2)	678 (69.8)	971 (100.0)	457 (1.3)	33,700* (69.8)	34,000* (100.0)
E16.5	**BrdU+**	28 (1.6)	100 (5.7)	128 (7.3)	383 (0.6)	3,881 (6.2)	4,264 (6.8)
	BrdU−	513 (29.1)	1,124 (63.6)	1,637 (92.7)	480 (0.8)	57,400* (92.4)	57,900* (93.2)
	total	541 (30.7)	1,224 (69.3)	1,765 (100.0)	863 (1.4)	61,300* (98.6)	62,100* (100.0)
E17.5	**BrdU+**	2 (0.2)	20 (1.9)	22 (2.1)	122 (0.3)	2,729 (7.4)	2,851 (7.7)
	BrdU−	300 (28.5)	732 (69.4)	1,032 (97.9)	264 (0.7)	34,000* (91.6)	34,300* (92.3)
	total	302 (28.7)	752 (71.3)	1,054 (100.0)	386 (1.0)	36,700* (99.0)	37,100* (100.0)

For the E14.5 pulse, 16 fields (200X) were counted (3 eyes, 3 mice). For the E15.5 pulse, 14 fields (200X) were counted (4 eyes, 2 mice). For the E16.5 pulse, 24 fields (200X) were counted (5 eyes, 4 mice). For the E17.5 pulse, 15 fields (200X) were counted (4 eyes, 3 mice).

* Combined rod totals were estimated by multiplying the combined cone counts by 35.2 (Jeon *et al.* 1998).

Math5 -/- mice

		cones counted (% of combined total)			rods counted (% of combined total)		
time of pulse		**GFP+**	**GFP−**	**combined**	**GFP+**	**GFP−**	**combined**
E14.5	**BrdU+**	21 (3)	113 (17)	134 (20)	26 (0.3)	326 (4)	352 (4)
	BrdU−	87* (13)	455* (67)	542* (80)	83* (1)	7,699* (95)	7,782* (96)
	total	108 (16)	568* (84)	676* (100)	109 (1.3)	8,025* (99)	8,134* (100)
E15.5	**BrdU+**	8 (1)	97 (16)	105 (17)	32 (0.4)	1,066 (14)	1,098 (15)
	BrdU−	27* (4)	490* (79)	517* (83)	40* (0.5)	6,337* (85)	6,377* (85)
	total	35 (6)	587* (94)	622* (100)	72 (1.0)	7,403* (99)	7,475* (100)
E16.5	**BrdU+**	10 (1)	33 (3)	43 (4)	65 (0.5)	692 (5)	757 (6)
	BrdU−	14* (1)	1,054* (95)	1,068* (96)	58* (0.4)	12,548* (94)	12,606* (94)
	total	24 (2)	1,087* (98)	1,111* (100)	123 (0.9)	13,240* (99)	13,363* (100)
E17.5	**BrdU+**	5 (1)	25 (3)	30 (4)	115 (1)	1,461 (16)	1,576 (18)
	BrdU−	73* (10)	639* (86)	712* (96)	138* (2)	7,212* (81)	7,350* (82)
	total	78 (11)	664* (89)	742* (100)	253 (3)	8,673* (97)	8,926* (100)

For the E14.5 pulse, 14 fields (200X) were counted (2 mice). For the E15.5 pulse, 7 fields (200X) were counted (2 mice). For the E16.5 pulse, 9 fields (200X) were counted (2 mice). For the E17.5 pulse, 10 fields (200X) were counted (2 mice).

* Combined rod and cone totals were estimated by multiplying the measured number of inner nuclear layer nuclei by 0.326 for cones or 3.92 for rods. These ratios were determined empirically in Math5 -/- mice (data not shown).

CHAPTER IV

DYNAMIC EXPRESSION OF GANGLION CELL MARKERS IN RETINAL PROGENITORS DURING THE TERMINAL CELL CYCLE

Abstract

The vertebrate neural retina contains seven major cell types, which arise from a common multipotent progenitor pool. During neurogenesis, these cells stop cycling, commit to a single fate, and differentiate. The mechanism and order of these steps remain unclear. The first-born type of retinal neurons, ganglion cells (RGCs), develop through the actions of Math5 (Atoh7), Brn3b (Pou4f2) and Islet1 (Isl1) factors, whereas inhibitory amacrine and horizontal precursors require Ptf1a for differentiation. We have examined the link between these markers, and the timing of their expression during the terminal cell cycle, by nucleoside pulse-chase analysis in the mouse retina. We show that G2 phase lasts 1-2 hours at embryonic (E) 13.5 and E15.5 stages. Surprisingly, we found that cells expressing Brn3b and/or Isl1 were frequently co-labeled with EdU after a short chase (<1 hr) in early embryos (<E14), indicating that these factors, which mark committed RGCs, can be expressed during S or G2 phases. However, during late development (>E15), Brn3b and Isl1 were exclusively expressed in post-mitotic cells, even as new RGCs are still generated. In contrast, Ptf1a and amacrine marker AP2α were detected only after terminal

mitosis, at all developmental stages. Using a retroviral tracer in embryonic retinal explants (E12-E13), we identified two-cell clones containing paired ganglion cells, consistent with RGC fate commitment prior to terminal mitosis. Thus, although cell cycle exit and fate determination are temporally correlated during retinal neurogenesis, the order of these events varies according to developmental stage and final cell type.

Introduction

The vertebrate neural retina is populated by seven major cell types, which are generated in an invariant histotypic order from a common progenitor pool (Livesey and Cepko, 2001; Wong and Rapaport, 2009). Individual cell fates are specified by intrinsic transcriptional programs and the retinal microenvironment. At the onset of retinal neurogenesis, on embryonic day 11 (E11) in the mouse, the first neurons exit the cell cycle and differentiate as retinal ganglion cells (RGCs), whose axons form the optic nerves. Mouse RGC birthdates extend from E11 to P0 with a peak at E14 (Drager, 1985; Young, 1985a). This temporal profile significantly overlaps the distribution of birthdates for cone photoreceptor, horizontal and amacrine cells. Rod photoreceptors, bipolar cells and Müller glia generally have later birthdates.

RGC development is controlled by a complex transcriptional network. *Math5* (*Atoh7*) is expressed transiently in multipotent precursors (Brzezinski et al., 2012; Yang et al., 2003) and is necessary for RGC fate specification (Brown et al., 2001; Wang et al., 2001). The *Brn3b* (*Pou4f2*) and *Islet1* (*Isl1*)

homeodomain genes form two regulatory nodes that are downstream of *Math5* in the RGC differentiation hierarchy (Mu et al., 2008; Pan et al., 2008). Both factors are thought to be expressed in newly post-mitotic cells, and are abundant in differentiated ganglion cells (Pan et al., 2008; Pan et al., 2005; Xiang, 1998). Brn3b appears to mark committed RGC precursors, as it is expressed exclusively in RGCs and required for terminal differentiation (Erkman et al., 1996; Gan et al., 1996; Qiu et al., 2008; Xiang, 1998). *Isl1* is also required for RGC development (Mu et al., 2008; Pan et al., 2008), but is expressed in a wider population of cells (Elshatory et al., 2007a). The *Brn3b*+ population is essentially contained within the *Isl1* lineage (Pan et al., 2008). Amacrine and horizontal neurons are specified in part by *Ptf1a*, a transiently expressed factor that acts downstream of *FoxN4* (Fujitani et al., 2006; Li et al., 2004). Brn3b and Ptf1a are likely to assemble in opposing transcriptional complexes that regulate RGC or amacrine/horizontal cell differentiation, respectively (Fujitani et al., 2006; Qiu et al., 2008).

The sequential birth order of different retinal cell types reflects a shift in the fate bias of progenitors during development (Livesey and Cepko, 2001). In addition, the progenitor cell cycle length increases progressively (Alexiades and Cepko, 1996; Sinitsina, 1971; Young, 1985b). Because neurons do not divide, and differentiation occurs after the final division, it is generally thought that cell cycle exit is strictly coupled to fate specification. However, it remains unclear how cycle length, terminal division, and neurogenic fate are linked, and precisely when fate commitment occurs (Dyer and Cepko, 2001b; Ohnuma and Harris,

2003). To explore these questions, we have determined the onset of expression of three key regulators of RGC, horizontal and amacrine cell fate specification (Brn3b, Isl1 and Ptf1a), relative to the terminal cell cycle. Unexpectedly, during early development (E11.5-E13.5), we found that Brn3b and Isl1, unlike Ptf1a, can be coexpressed *prior* to cell cycle exit, during late S or G2 phases. Retroviral lineage analysis revealed multiple two-cell clones containing paired RGCs, suggesting that these terminal progenitors represent committed ganglion cell precursors that undergo a final mitosis. Surprisingly, the timing changes significantly during late embryonic stages (after E15), such that Brn3b and Isl1 are expressed exclusively in post-mitotic cells. Our findings suggest that cell fate commitment can occur before or after cell cycle exit. The order of these events is not rigidly fixed.

Materials and Methods

Pulsed EdU/BrdU and cell cycle labeling

All mouse studies were approved by the University of Michigan Committee on the Use and Care of Animals (UCUCA). Pregnant dams were injected with 5-bromo-2-deoxyuridine (BrdU, 100 µg/g body mass) or 5-ethynyl-2-deoxyuridine (EdU, 6.7 µg/g body mass) on embryonic (E) day 11.5, 13.5, 15.5 or 16.0. BrdU is rapidly absorbed within minutes after an intraperitoneal injection (Kriss and Revesz, 1962). Embyros were harvested after a variable chase period, between 0.5 to 12 hours, in order to follow cells after they complete DNA synthesis (S phase). The time of onset of a particular transcription factor expression was

defined by the first chase period in we detected cells positive for the particular marker and EdU/BrdU.

Histology

Embryonic eyes were fixed for 0.5-1 hour in 2-4% paraformaldehyde (PFA) at 22ºC, cryoprotected with 30% sucrose in phosphate-buffered saline (PBS), and frozen in OCT compound (Tissue-Tek, Torrance, CA). Short fixation was critical for immunodetection of Brn3b and cyclinD1. Cryosections (10 μm) were blocked with 10% normal donkey serum (NDS) and 1% bovine serum albumin (BSA) in PBTx (0.1 M $NaPO_4$ pH 7.3, 0.5% Triton X-100) for 4 hours at 22ºC. Sections were incubated overnight at 4°C with primary antisera diluted in PBTx with 3% NDS, 1% BSA. Sections were then washed in PBS 0.5% BSA, incubated for 2 hours at 22ºC with Dylight 488- (1:1000), Dylight 549- (1:1000), or Dylight 649- (1:500) conjugated secondary antibodies (Jackson Immunoresearch, West Grove, PA), mounted in Prolong Gold Antifade media (Invitrogen, Carlsbad, CA), and imaged using the Zeiss LSM510 Meta confocal microscope at the University of Michigan Microscopy and Image Analysis Core Facility (MIL).

The primary antibodies were: mouse anti-AP2α (1:1000, 3B5, DSHB, Iowa City, Iowa); rat anti-BrdU (1:100, BU1/75, Harlan Seralab, Indianapolis, IN); rabbit anti-βgal (1:5000, ICN Cappel, Aurora, OH); rat anti-βgal (1:500) (Saul et al., 2008); mouse anti-Brn3a (1:50, 14A6, Santa Cruz Biotechnology, Santa Cruz, CA); goat anti-Brn3b (1:200, sc31987, Santa Cruz); mouse anti-cyclin D1 (1:100, A-12, Santa Cruz); chicken anti-GFP (1:2000, Abcam, Cambridge, MA);

mouse anti-Isl1 (1:200, 39.4D5, DSHB); rabbit anti-phosphohistone H3 (1:200, Upstate, Lake Placid, NY); rabbit anti-Ptf1a (1:800) (Fujitani et al., 2006).

Following immunostaining, EdU was detected using an azide-alkyne cycloaddition reaction (Buck et al., 2008) (Click-iT-647, Invitrogen). For detection of BrdU and other markers, cryosections were fully stained with primary and secondary antibodies for the marker protein. Sections were then treated with 2.4 N HCl in PBTx for 1 hour at 22ºC, washed, and immunostained for BrdU.

Quantitative analysis of Brn3b onset

The percentage of EdU+Brn3b+ cells among the Brn3b+ cohort was determined for eight different EdU chase times, at E13.5 (0.5, 1, 2, 4, 12 hrs) and E15.5 (1, 4, 12 hrs). Double-positive cells were definitively identified by visual examination of 3-dimensional confocal Z-stacks (225 µm x 225 µm x 8-12 µm). Two to six sections were analyzed for each time point, from at least 2 embryos, representing 440 to 930 Brn3b+ cells. Error is reported as the standard deviation among sections. The total Brn3b+ population represents both newly neurogenic cells and existing ganglion cells. To selectively analyze neurogenic cells, we also normalized percentages to the 12-hr chase value at E13.5. At this stage, 12 hrs is sufficient time for any EdU-labeled neurogenic cell to progress from S to G0 phase. This single EdU pulse thus captures all newly Brn3b+ cells born within a 5-6 hr period (length of S phase). The normalized value at 1-2 hrs reflects new Brn3b+ cells that initiate Brn3b expression in terminal G2 phase.

Retroviral clone analysis in retinal explants

Retinal explant cultures and retroviral infections were performed as described (Brzezinski et al., 2012), using established methods (Hatakeyama and Kageyama, 2002; Wang et al., 2002b). Briefly, *Math5-lacZ*/+ retinas were dissected from E12.5 or E13.5 embryos, flattened onto Nucleopore polycarbonate membranes (0.4 µm pore size, GE Healthcare, Piscataway, NJ), and placed into Transwell culture dishes containing neurobasal media (Invitrogen) with B27 and N2 supplements, glutamine (0.4 mM), brain-derived neurotrophic factor (BDNF, 50 ng/mL, Peprotech, Rocky Hill, NJ), ciliary neurotrophic factor (CNTF, 10 ng/mL, Peprotech), penicillin (50 U/mL), streptomycin (50 µg/mL), and gentamicin (0.5 µg/mL).

MIG retroviral stocks were prepared in advance by calcium phosphate transfection of the Phoenix ecotropic packaging cell line (Pear, 2001; Swift et al., 2001) with pMSCV-IRES-GFP plasmid DNA (Van Parijs et al., 1999). Filtered viral preparations containing polybrene (hexadimethrine bromide, 0.8 µg/mL, Sigma Aldrich, St. Louis, MO) were titered on NIH3T3 fibroblasts and diluted to ~$8x10^5$ colony-forming units per mL. One drop of retrovirus (25 µL) was added on top of each fresh explant to sparsely mark dividing cells (Roe et al., 1993) and their descendants.

Retinal explants were cultured for 3 days at the gas-media interface at 37ºC under 5% CO_2. After 2 days, half of the media was replaced with fresh media. On day 3, explants were fixed for 30 minutes in 4% PFA, and processed for cryosectioning or stained directly as wholemounts. Thick (30 µm) sections, or wholemount retinas, were immunostained for GFP and Brn3a/3b, and imaged by

confocal microscopy. The size and composition of clonal clusters were determined by 3-dimensional analysis of Z-stacks. A clone was defined as a group of directly apposed GFP+ cells that were separated by at least 4 cell bodies from other GFP+ cells. For assessing symmetry of fate, only clones with at least one Brn3+ RGC were scored.

Results

G2 phase is 1-2 hours long in most retinal cells

The eukaryotic cell cycle is anchored by M phase, when cytokinesis occurs, and S phase when DNA synthesis occurs. These are separated by G1 and G2 'gap' phases, respectively (Fig. IV-1A) (Nurse, 2000). As a first step to evaluate the timing of the transcription factor expression relative to cell cycle exit, we systematically determined the onset of M phase in cycling progenitors at different developmental stages using EdU or BrdU pulse-chase experiments. In this experimental paradigm, cycling progenitors incorporate nucleoside analogs EdU or BrdU during DNA replication (S phase), and these labeled progenitors are then followed as they progress through G2 and M phases (Fig. IV-1A). To assess the onset of M phase, we co-stained embryonic sections for phosphohistone H3 (PH3) and EdU or BrdU to identify the shortest chase that yielded double-labeled cells. Histone H3 is transiently phosphorylated for the entire duration of M phase (Bradbury, 1992) No EdU+ PH3+ cells were detected after a 1 hr EdU chase, while most PH3+ had punctate EdU labeling after a 2 hr chase (Fig. IV-1B). These results suggest that M phase initiates at 1-2 hrs after

the end of S phase, in the majority of progenitors. Similar results were observed at E15.5 (Fig. IV-1C), and are consistent with measurements of G2 length at other embryonic times (Sinitsina, 1971; Young, 1985b).

Expression of Brn3b and Isl1, but not Ptf1a or AP2α, prior to cell cycle exit

Using the pulse-chase paradigm, it is possible to unambiguously identify the onset of expression relative to the end of S phase. Previous lineage analysis and marker co-staining have shown that Brn3b is restricted to RGCs (Badea et al., 2009; Qiu et al., 2008; Xiang et al., 1995), and that Ptf1a is confined to inhibitory horizontal and amacrine cells (Fujitani et al., 2006). As a first step in this analysis, we tested whether Brn3b and Ptf1a truly mark mutually exclusive populations of committed precursors during early retinal development, by co-staining sections from E13.5 retinas for Brn3b, Ptf1a, and the amacrine marker AP2α (Bassett et al., 2007). We observed no overlap of Ptf1a or AP2α with Brn3b (Fig 2A) consistent with previous results observed during late gestation (Bassett et al., 2007; Fujitani et al., 2006; Qiu et al., 2008). As expected, many AP2α-expressing cells were contained within the Ptf1a population, and are presumed to be precursors of inhibitory amacrine neurons.

We next determined the onset of Brn3b, Ptf1a and AP2α with respect to the terminal cell cycle as outlined (Fig. IV-1A). At both E13.5 and E15.5, we observed no overlap between Ptf1a or AP2α and EdU after a 4 hr chase (Fig. IV-2B,C), but Ptf1a+ EdU+ cells were apparent after a 12 hr chase (Fig. IV-2D,E). Although Ptf1a is transiently expressed and vital for development of horizontal and amacrine cells, its actions are apparently delayed until after cell cycle exit,

most likely during cell migration. In contrast, at E13.5, we found that Brn3b+ EdU+ cells were present after a 1 hr chase (2-5 per high-power field, Fig. IV-3A). All Brn3b+ cells were cyclinD1− (cycD1), including the EdU+ cohort, whereas the vast majority of EdU+ cells (>95%) were cycD1+ (Fig. IV-3A). In most cycling cells, cycD1 is made during G1 and down-regulated during S phase, and it controls the G1/S transition. CycD1 is reactivated in G2 (Stacey, 2003), except in terminally mitotic cells (Yang et al., 2006). In the developing retina, cycD1 can be detected in all cells, except for post-mitotic neurons (G0) and a small subpopulation of G2 cells that are likely represent the neurogenic cohort (Barton and Levine, 2008). Accordingly, we interpret the Brn3b+ EdU+ cycD1- precursors at E13.5 as neurogenic cells in late S or G2 phase of the terminal division. Consistent with interpretation, we observed rare Brn3b+ cells at the scleral margin (apex), in M phase (PH3+, arrows) or in adjacent pairs (arrowheads) suggestive of a recent division (Fig. IV-3B). Furthermore, Brn3b+ EdU+ cells can be followed through the cell cycle, with symmetric Brn3b segregation (Fig. IV-3B), and migration into the GCL with a 12 hr chase at E13.5 (Fig. IV-3C). Many of the resulting Brn3b+ EdU+ cells are in close proximity, as presumptive daughter pairs. At E15.5, essentially no Brn3b+ EdU+ cells were observed after 1- or 4-hr chase periods, but were readily detected throughout the retina after a 12 hr chase (1-4 per high-power field, Fig. IV-3D). Although new Brn3b+ cells continue to be generated throughout the retina, Brn3b is expressed exclusively in post-mitotic cells at this stage. Quantitative analysis revealed that only 4.8 ± 0.9% of Brn3b+ cells at E13.5, and 1.2 ± 0.6% at E15.5, were EdU+

after a 12 hr chase (Fig. IV-3E). These cells represented the sum of neurogenic cells initiating Brn3b expression during S/G2 and G0 phase. To estimate the fraction of Brn3b+ cells at E13.5 that initiate expression during S/G2, we normalized the Brn3b+EdU+ fractions observed after a 0.5-4 hr chase to the 12 hr chase value (Fig. IV-3E). This analysis revealed that 50-60% of new Brn3b+ cells (accounting for mitotic doubling) initiated expression prior to cell cycle exit (<4 hr chase).

To confirm these observations regarding the timing of RGC marker expression relative to terminal M phase, we evaluated a second regulator of RGC differentiation, Islet-1 (Isl1). We co-stained sections for Brn3b, Isl1 and EdU following a 30 min chase. We observed numerous Brn3b+ Isl1+ cells that were EdU+ at E11.5 or E13.5 (Fig. IV-4A,B), whereas no Brn3b+ Isl1+ cells were EdU+ at E16.0 (Fig. IV-4C). These results indicate that at least two key regulators of RGC fate are expressed prior to cell cycle exit during early (<E14), but not during late (>E15), developmental stages.

RGC fate symmetry in marked clones

If progenitors express Brn3b and Isl1 before terminal M phase, they should give rise to paired RGCs. To test this hypothesis, we performed a clonal analysis. Retinal explants from E12.5 or E13.5 embryos were infected with MSCV-IRES-GFP (MIG) retrovirus at low density to generate independent clones. After culturing 3 days *in vitro (*DIV), we scored the resulting GFP+ clones for their size and number of RGCs, using Brn3a or 3b immunoreactivity and cellular morphology to identify ganglion cells (Fig. IV-5A). The Brn3a paralog is

functionally interchangeable with Brn3b at the protein level (Pan et al., 2005) and its spatiotemporal expression pattern is highly overlapping with Brn3b and Brn3c (Xiang et al., 1995; Xiang et al., 1993).

In 12 explanted retinas, we observed approximately 250 GFP+ clones, which were 1-16 cells in size. Fourteen (~5%) included at least one Brn3+ RGC. Among these informative clones, we observed two-cell clones with paired (Fig. IV-5B,C) or single (Fig. IV-5D) RGCs. Of the 12 neurogenic divisions that could unambiguously be scored among 14 clones, six were symmetric, resulting in paired RGCs (Fig. IV-5E). In principle, paired RGCs could arise if both daughter cells independently adopt the RGC fate, stochastically or in response to the local retinal environment. Given the very small number of GFP+ ganglion cells observed in these explants ($n = 24$), and the high frequency of symmetric fating (6 of 12 divisions), this pattern is unlikely to reflect independent events paired by chance ($\chi^2 > 40$, $df = 2$, $P < 0.001$ for a Poisson distribution). Instead, this statistical clustering, and the expression of definitive RGC markers in G2 and through cytokinesis (Fig. IV-3), strongly argue that many RGCs arise in pairs and descend from progenitors that commit to the ganglion fate during their final cell cycle, prior to terminal mitosis.

Discussion

The kinetics of the retinal progenitor cell cycle have been extensively characterized in rodents and other vertebrate species by window and cumulative nucleoside labeling, cell counting, and percent labeled mitosis (PLM) methods

(Alexiades and Cepko, 1996; Fujita, 1962; Li et al., 2000; Sinitsina, 1971; Young, 1985b). In addition, a variety of nuclear factors responsible for generating histotypic diversity in the retina have been identified through loss- and gain-of-function genetic analysis, and expression studies (Ohsawa and Kageyama, 2008; Swaroop et al., 2010). However, the basic question of when the cell fate decision is made relative to the terminal cell cycle has remained largely unanswered. In this paper, we have integrated expression and cell cycle analysis to determine the precise time that transcription factors controlling RGC, amacrine and horizontal fates appear during the last (neurogenic) cell cycle.

RGC fate commitment can occur before cell cycle exit

At early developmental times (<E14), we detected Isl1 and Brn3b in many cells during late S or G2 phases of the terminal cell cycle (Figs. 3,4), similar to *Math5-lacZ* (Brzezinski et al., 2012), and in contrast to previous reports (Pan et al., 2008; Xiang et al., 1993). This interpretation is based on three convergent results: the precise timing of PH3 (Fig. IV-1), Brn3b and Isl1 (Fig. IV-4) onset relative to the end of S phase, the mutually exclusive pattern of cycD1 and Brn3b expression (Fig. IV-3A), and the presence of Brn3b+ M phase cells (Fig. IV-3B).

There are three possible explanations for the observation of RGC markers in dividing cells. First, the immunopositive cells may reflect low-level leaky transcription of Brn3b or Isl1 that is not biologically meaningful. This seems unlikely given that the expression in S/G2 phase progenitors is often as strong as that observed in post-mitotic cells (e.g. arrows in Fig 4A,B). Second, Isl1 and Brn3b may not accurately mark committed RGC precursors. Indeed, Isl1 is also

expressed in differentiating amacrine and bipolar precursors, and has a role in the development of both of these interneuron classes (Elshatory et al., 2007a; Elshatory et al., 2007b). In contrast, Brn3b is not co-expressed with Ptf1a or AP2α, which mark nascent horizontal and amacrine interneurons, and it is made in most, but not all RGCs (Fig. IV-2A). Complementary co-expression and lineage analyses, using Cre recombinase or stable histogenic reporters, have also demonstrated that Brn3b is made only in RGCs (Badea et al., 2009; Bassett et al., 2007; Fujitani et al., 2006; Qiu et al., 2008). In the absence of Brn3b, progenitors adopt non-RGC fates (Badea et al., 2009; Qiu et al., 2008). Overexpression of Brn3b in progenitors promotes RGC fate and suppresses amacrine differentiation (Feng et al., 2011; Liu et al., 2000; Qiu et al., 2008). Taken together, these results strongly suggest that Brn3b identifies committed RGCs, and does not label multipotent progenitors. Third, the RGC fate decision may precede terminal mitosis, and occur during G2. According to this interpretation, Brn3b+ Isl1+ EdU+ cells represent progenitors committed to develop as RGCs. In general, progenitors may undergo symmetric or asymmetric divisions to generate one or two post-mitotic daughters, respectively (Huttner and Kosodo, 2005). Our pulse-chase (Fig. IV-3) and clonal analyses (Fig. IV-5) suggest that many divisions giving rise to RGCs are symmetric and terminal. This observation is somewhat surprising considering that the retina is rapidly expanding during the period of early development. However, G2 fate commitment may be necessary for prompt deployment of RGCs, which establish a pioneering scaffold for axon pathfinding (Pittman et al., 2008; Raper and

Mason, 2010). Alternatively, the relatively early onset of Brn3b expression may reflect the position of RGCs as the first sampled fate in the histogenetic sequence (Wong and Rapaport, 2009).

Our clonal data are generally consistent with previous observations of terminal divisions in the early retina. In rodent and frog lineage analysis, many two-cell clones have been observed during early development, but typically these cells have discordant fates (Holt et al., 1988; Turner et al., 1990; Wong and Rapaport, 2009). Notably, among 114 two-cell clones analyzed in these reports, only one contained paired RGCs (Holt et al., 1988). During early zebrafish development, most ath5-expressing progenitors, monitored by time-lapse imaging of mosaic *ath5-GFP* embryos, undergo a terminal division and give rise to at least one ganglion cell (Poggi et al., 2005). The daughters typically have discordant fates, but paired RGCs may arise from wild-type cells in an *ath5* mutant environment.

Similar to our finding of mitotic Brn3b+ cells (Fig. IV-3B), RA4+ cells were observed in terminal mitotic anaphase in the chick retina (Waid and McLoon, 1995), and migrating in pairs shortly after mitosis (McLoon and Barnes, 1989). Although originally interpreted as RGC precursors, it is no longer clear that the RA4 neurofilament antigen marks ganglion cells exclusively (Gutierrez et al., 2011). Beyond these observations, there is precedent for G2 commitment during neurogenesis of other cell types. In the chick retina, committed horizontal cell precursors typically arrest in G2 and undergo a final non-apical mitosis (Boije et al., 2009), which may explain the presence of paired horizontal cell clones of a

single subtype (Rompani and Cepko, 2008). In the ferret cerebral cortex, progenitors lose their competence to respond to environmental signals following terminal G2 phase (McConnell and Kaznowski, 1991). Similarly, heterochronic analysis of dissociated rat retinal cells suggests that progenitors commit to the amacrine fate (VC1.1+) during G2/M of the last cell cycle (Belliveau and Cepko, 1999).

Post-mitotic fate plasticity in the retina

In this study, the amacrine marker Ptf1a was only detected in post-mitotic cells, at both E13.5 and E15.5 (Fig. IV-2B-E). In *Ptf1a* mutant mice carrying Cre knock-in alleles, many lineage-marked cells expressed Brn3b and adopted RGC fates (Fujitani et al., 2006). Taken together, these results suggest a degree of post-mitotic plasticity, such that some amacrine cells solidify their identity after the terminal division. Likewise, photoreceptor and bipolar precursors retain the ability to switch fates after cell cycle exit (Adler and Hatlee, 1989; Brzezinski et al., 2010; Ng et al., 2011; Oh et al., 2007). Indeed, the bZIP factor NRL, which instructs rod photoreceptor fate, initiates expression soon after terminal M phase, throughout development (Akimoto et al., 2006); data not shown).

We observed a gradual restriction in the expression of Brn3b and Isl1, as well as *Math5-lacZ* (Brzezinski et al., 2012), to post-mitotic cells during late gestation (Fig. IV-3D). At these ages (>E15), many RGCs are still generated, including migrating EdU+ Brn3b+ cells (Drager, 1985; Young, 1985a). In the early (<E14) retina, we observed both symmetric and asymmetric patterns of RGC marker expression among daughter cells in clones, suggesting that some

cells commit to the RGC fate after terminal mitosis in the early retina (Fig. IV-5E) (Brzezinski et al., 2012). The difference in the timing of RGC marker onset between the early and late retina cannot be explained by a change in the length of G2, which is relatively static (Fig. IV-1), or by the progressive lengthening of the cell cycle during development (Alexiades and Cepko, 1996; Sinitsina, 1971; Young, 1985b). Indeed, if transcription initiates after G1 or S phase with a fixed time delay, then the onset of expression following terminal S phase should be advanced (closer to S), rather than delayed as we observed during the course of development. It is more likely that progenitor fate decisions occur before or after cell cycle exit, depending on the lineage or developmental stage.

What could explain these shifts in expression kinetics? Environmental signals elaborated by differentiating neurons, such as Delta ligand or Shh, increase as RGCs accumulate (Ahmad et al., 1997; Wang et al., 2005; Yang, 2004; Yu et al., 2006) and could delay the onset of RGC transcription factor expression. Alternatively, the onset may be intrinsically programmed to shift over time, and is potentially regulated by the same upstream cascades that control cell cycle exit. Further studies are needed to distinguish these mechanisms. Nonetheless, it is clear that cell fate determination and cell cycle exit, though correlated, are not strictly causally related events.

Acknowledgements

The authors are grateful to Dellaney Rudolph and Melinda Nagy for technical support; to Helena Edlund for Ptf1a antisera; to Chris Edwards, and the UM microscopy and image analysis laboratory staff, for technical advice; to Sean

Morrison for the MIG retroviral construct; to Joe Brzezinski, Nadean Brown, Chris Chou, Sally Camper and David Turner for valuable discussions and critical reading of the manuscript. This research was funded by National Institutes of Health (NIH) R01 grant EY14259 (TG). LP was supported by NIH T32 grants EY13934 and GM07863.

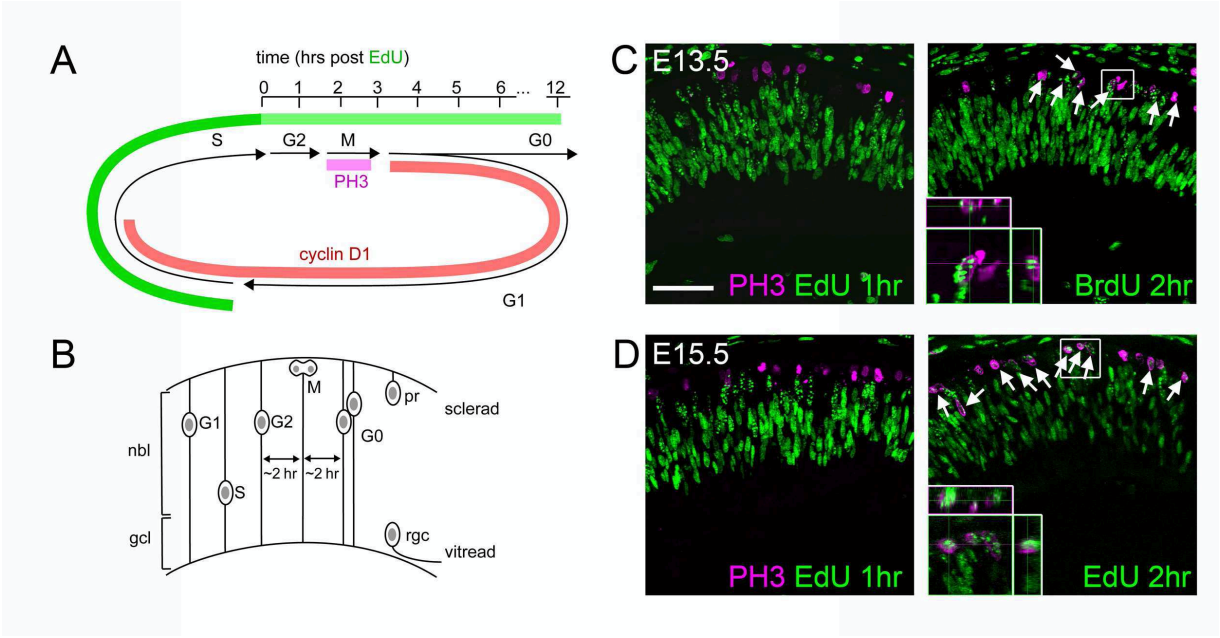

Figure IV-1. Timing of cell cycle progression in the mouse retinal neuroepithelium at E13.5 and E15.5. (A) EdU pulse-chase experiments. Phosphohistone H3 (PH3) is expressed during M phase, while cyclin D1 is primarily expressed during G1 and early S phases. After an EdU pulse, labeled S phase cells progress into G2, M and G1/G0 phases. (B) Diagram of interkinetic nuclear migration, showing the positions of progenitor nuclei at each stage of the cell cycle. Following terminal M phase, G0 daughters segregate vertically according to their cell fate. Ganglion cells (rgc) migrate toward the base (vitread), while photoreceptors (pr) migrate toward the apex (sclerad). (C-D) E13.5 and E15.5 embryos stained for PH3 and EdU or BrdU following a 1-2 hour chase. No PH3+ cells are EdU+ after a 1 hour chase, but most are EdU+ or BrdU+ after a 2 hour chase. Therefore, M phase initiates at 1-2 hours after S phase in most cells, at both of developmental stages. nbl, neuroblastic layer; gcl, ganglion cell layer. Scale bar, 50 µm.

Figure IV-2. Co-expression and onset analysis of amacrine and horizontal markers Ptf1a and AP2α. (A) Developing horizontal or amacrine neurons do not express Brn3b. Sections from E13.5 retinas coimmunostained for Brn3b, AP2α and Ptf1a. Although many Brn3b+ cells are present, none co-label with the horizontal and inhibitory amacrine marker Ptf1a, or the pan-amacrine marker AP2α, suggesting that Brn3b specifically marks RGCs during early development. (B-E) Sections from E13.5 (B,D) or E15.5 (C,E) embryos co-stained with Ptf1a, AP2α and EdU following a 4 hr (B,C) or 12 hr (D,E) chase. No Ptf1a+ or AP2α+ cells are EdU+ after a 4 hr chase, suggesting that these factors are expressed exclusively in post-mitotic (G0) cells. Many Ptf1a+ EdU+ cells are apparent after a 12 hr chase at both E13.5 and E15.5 (arrows, insets), indicating that this factor initiates expression in migratory cells. Many AP2α+ cells are Ptf1a+ (arrowheads), marking the inhibitory amacrine population. Scale bar, 50 μm.

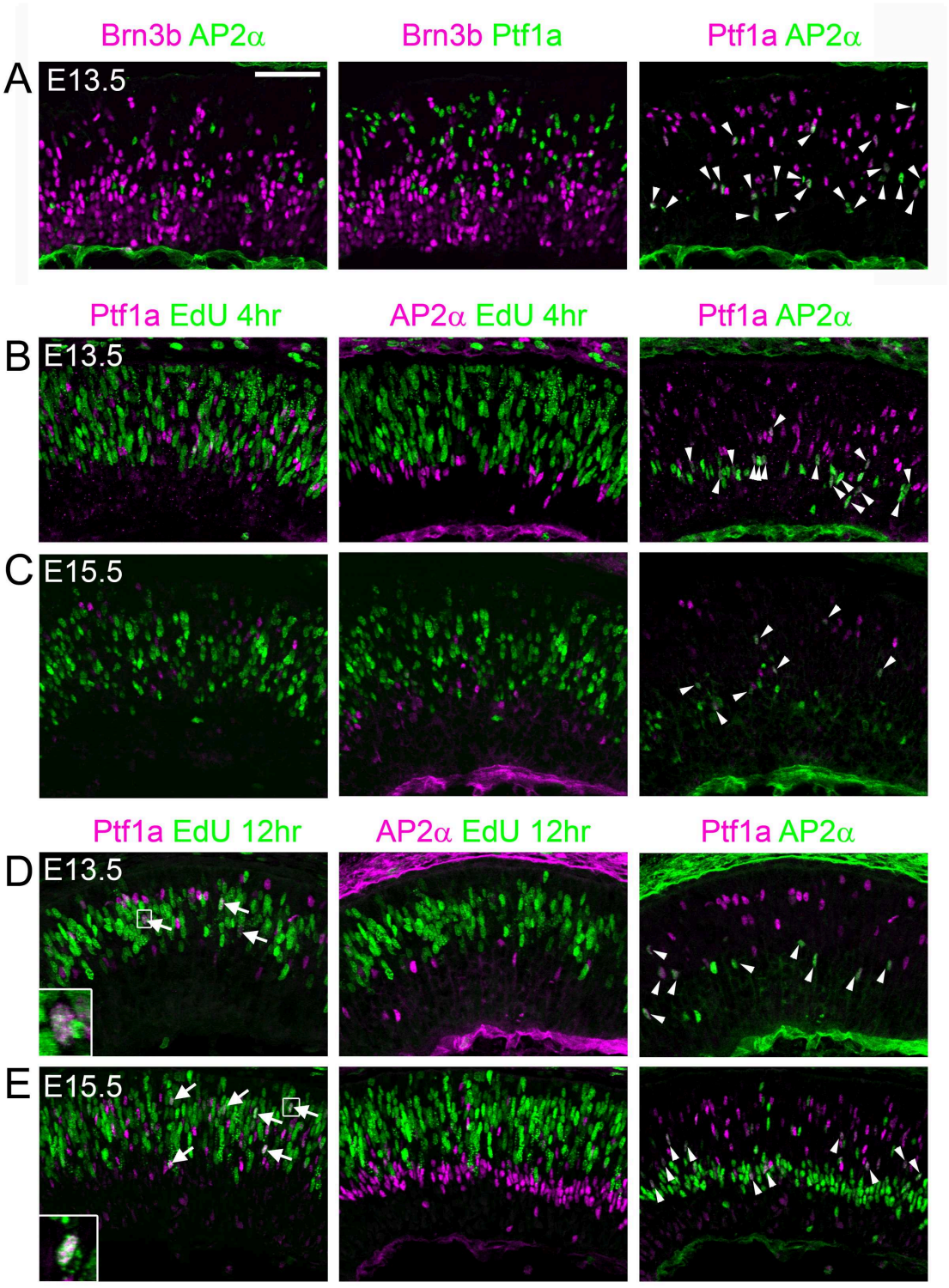
Brn3b AP2α
Brn3b Ptf1a
Ptf1a AP2α
A
E13.5
Ptf1a EdU 4hr
AP2α EdU 4hr
Ptf1a AP2α
B
E13.5
C
E15.5
Ptf1a EdU 12hr
AP2α EdU 12hr
Ptf1a AP2α
D
E13.5
E
E15.5

Figure IV-3. The onset of Brn3b and Isl1 expression within individual cells is progressively delayed during retinal development. (A) Sections from E13.5 embryos co-stained for Brn3b, cyclinD1 (cycD1) and EdU following a 1 hr chase. In some cells, Brn3b is co-localized with EdU (arrows), but not with the G1/early-S phase marker cycD1, indicating that Brn3b expression initiates in late S or G2 phase. Insets show two cells that are Brn3b+ EdU+ cyclinD1−. One has a punctate EdU staining pattern, indicating incorporation in late-replicating DNA regions at the end of S phase. (B) Sections from E13.5 embryos stained for Brn3b and the mitotic marker PH3 or the nuclear counterstain DAPI. Brn3b+ cells in M phase (arrows) and presumptive daughter pairs (arrowheads) are indicated. (C-D) Sections from E13.5 or E15.5 embryos co-stained for Brn3b and EdU following the indicated chase period. At E13.5 (C), many newly generated Brn3b+ cells are co-labeled with EdU after a 2, 4 or 12 hr chase. By 12 hrs, some EdU-labeled cells migrate to the nascent GCL, and many Brn3b+ EdU+ cells are in close proximity as presumptive daughter pairs. At E15.5 (D), no Brn3b+ EdU+ cells are observed after 1 hr chase, and very few are detected after a 4 hr chase, but Brn3b+ EdU+ are readily detected after a 12 hr chase (arrows). (E) Quantitative analysis of Brn3b and EdU co-labeling. The abundance of co-labeled cells is plotted as a percentage of all Brn3b+ cells (left scale) or neurogenic Brn3b+ cells (right scale, normalized to the 12 hr chase value at E13.5). Approximately 30% of newly Brn3b+ cells initiated expression prior to cell cycle exit at E13.5 (gray line). In contrast, few Brn3b+ cells are co-labeled with EdU prior to 12 hrs at E15.5, indicating that RGCs are specified later at this developmental stage. Scale bar, 50 μm.

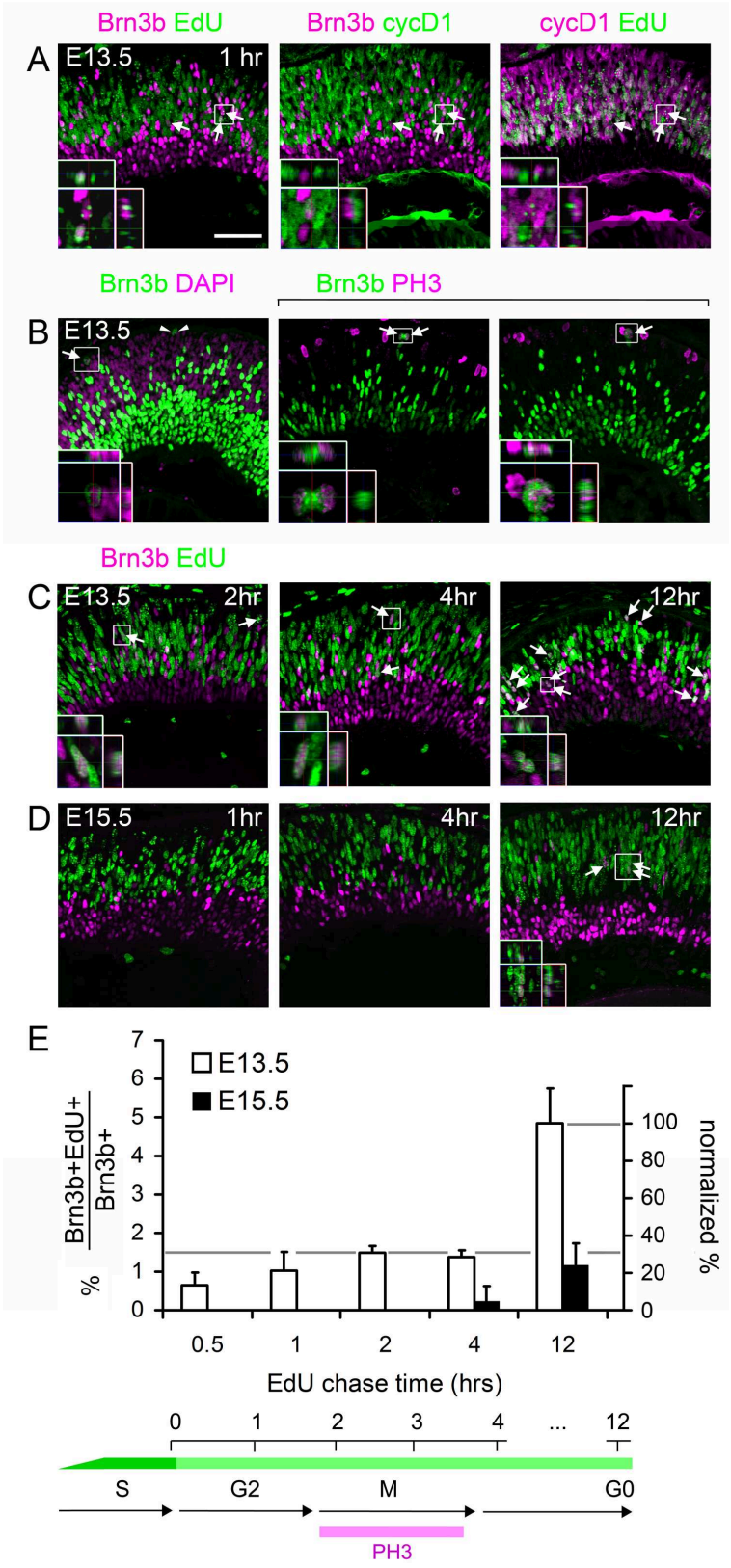
Brn3b EdU
Brn3b cycD1
cycD1 EdU
A
E13.5
1 hr
Brn3b DAPI
Brn3b PH3
B
E13.5
Brn3b EdU
C
E13.5
2hr
4hr
12hr
D
E15.5
1hr
4hr
12hr
E
E13.5
E15.5
Brn3b+EdU+ / Brn3b+ %
normalized %
EdU chase time (hrs)
0.5
1
2
4
12
0
1
2
3
4
...
12
S
G2
M
G0
PH3

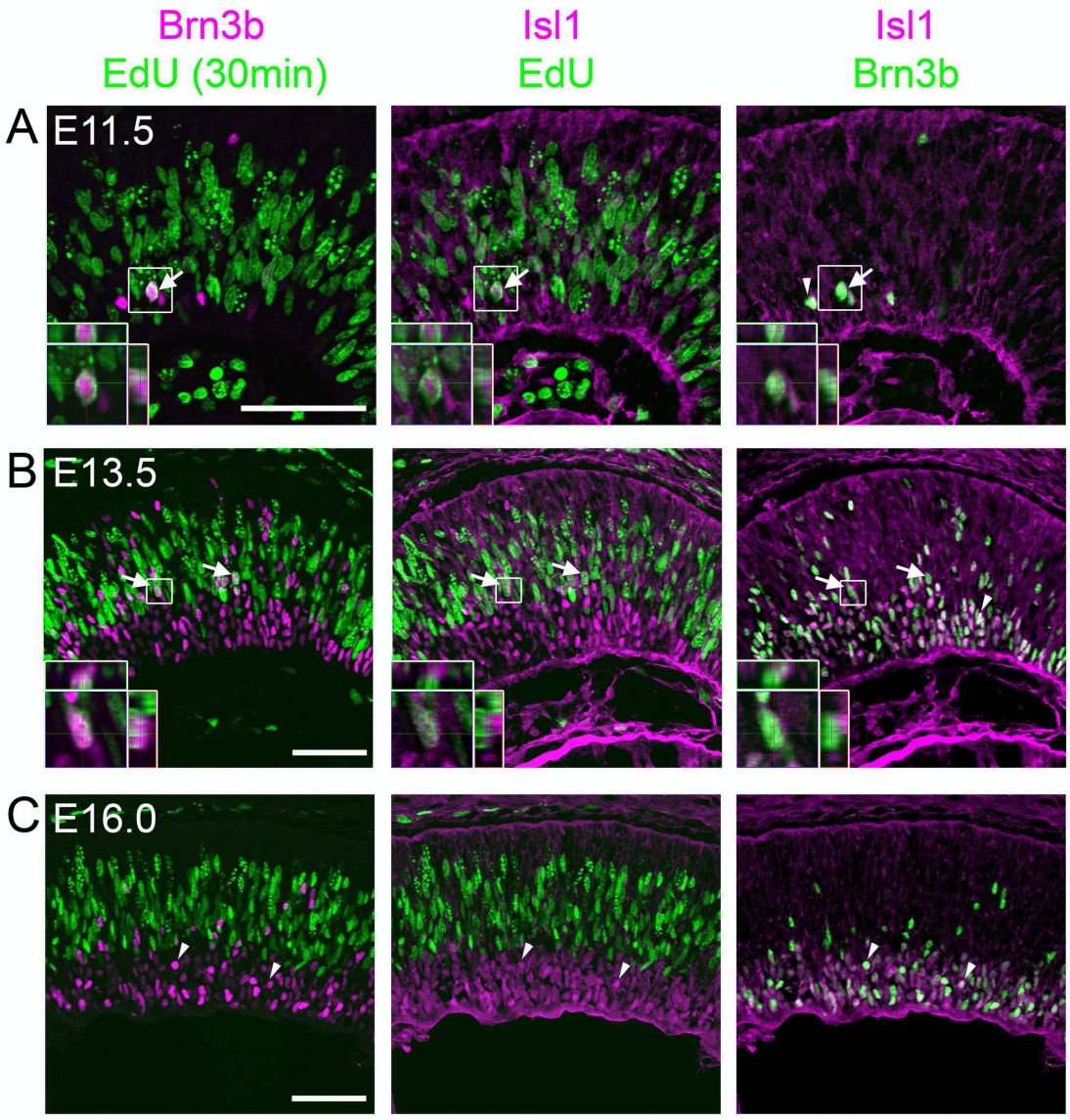

Figure IV-4. Co-expression of Brn3b and Isl1 during or shortly after the terminal cell cycle. (A-C) Sections from E11.5, E13.5, and E16.0 embryos co-stained for Brn3b, Isl1 and EdU following a 30 min chase. At E11.5 (A) and E13.5 (B), multiple Brn3b+ Isl1+ EdU+ cells are observed (arrows), indicating that RGC markers can initiate expression prior to cell cycle exit, in late S or G2 phase. In contrast, at E16.0 (C), all Brn3b+ Isl1+ cells are EdU– (examples marked by arrowheads in D-F). The insets show orthogonal Z-stack views of magnified Brn3b+ Isl1+ EdU+ cells. Scale bar, 50 μm.

Figure IV-5. Paired ganglion cells can be generated from retinal progenitors by symmetric terminal division. (A) Retinas were explanted from E12.5 or E13.5 embryos, infected at clonal density with MSCV-IRES-GFP (MIG) retrovirus (green), and cultured for 3 days *in vitro* (DIV). The micrograph shows a cross-section from a representative explant (bracket) coimmunostained for Brn3a (magenta) and GFP (green). The schema shows informative two-cell GFP+ clones: a symmetric [S] clone containing two Brn3+ RGCs, and an asymmetric [A] clone with one Brn3+ RGC. (B-D) Confocal Z-stack projections and drawings from representative symmetric (B, C) or asymmetric (D) clones containing RGCs. Most Brn3+ cells have long processes (arrows), confirming that they are differentiated RGCs. (E) Summary of observed clones containing at least one Brn3+ cell. In these experiments, RGCs were identified using Brn3a (12 clones) or Brn3b (2 clones) antisera interchangeably. Among 12 informative divisions, an equal number with symmetric and asymmetric fates was observed. Scale bars, 10 μm in A; 5 μm in B-D.

A

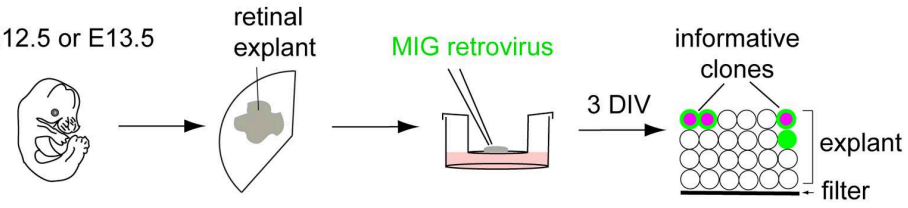

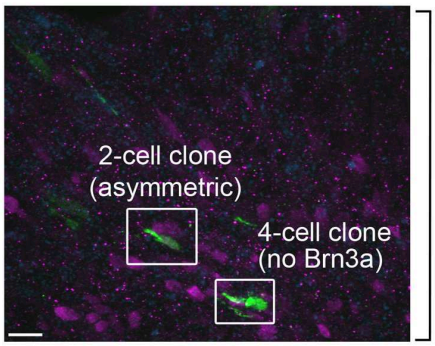

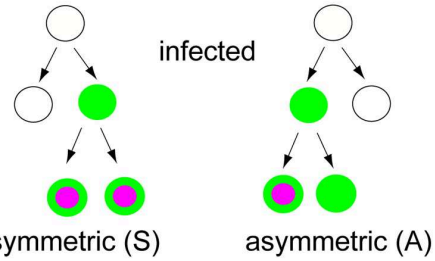

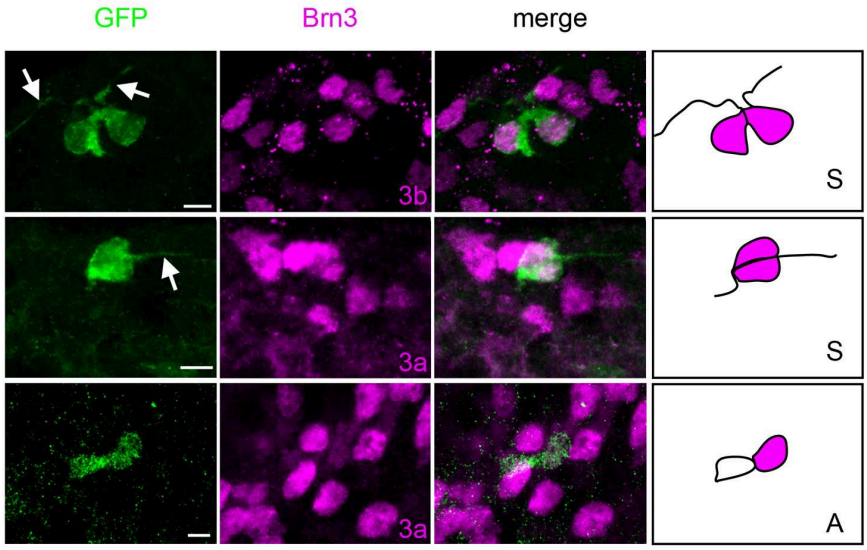

E

clone properties				informative divisions scored		
size	pattern	RGC symmetry	# clones	S	A	total
6 cell	●●●○○○	A + ?	1	0	1	1
4 cell	●○○○	A	1	0	1	1
3 cell	●●○	?	2	0	0	0
2 cell	●●	S	6	6	0	6
	●○	A	4	0	4	4
		sum	14	6	6	12

CHAPTER V

PUSHING THE ENVELOPE OF RETINAL GANGLION CELL GENESIS: CONTEXT DEPENDENT FUNCTION OF *MATH5* (*ATOH7*)

Abstract

The basic-helix-loop helix factor Math5 (Atoh7) is required for retinal ganglion cell (RGC) development. However, only 10% of Math5-expressing cells adopt the RGC fate, and most become photoreceptors. In principle, Math5 may *actively* bias progenitors towards RGC fate or *passively* confer competence to respond to instructive factors. To distinguish these mechanisms, we misexpressed Math5 in a wide population of precursors using a *Crx* BAC or 2.4 kb promoter, and followed cell fates with Cre recombinase. In mice, the *Crx* cone-rod homeobox gene and *Math5* are expressed shortly after cell cycle exit, in temporally distinct, but overlapping populations of neurogenic cells that give rise to 85% and 3% of the adult retina, respectively. The Crx > Math5 transgenes did not stimulate RGC fate or alter the timing of RGC births. Likewise, retroviral Math5 overexpression in retinal explants did not bias progenitors towards the RGC fate or induce cell cycle exit. The Crx>Math5 transgene did reduce the abundance of early-born (E15.5) photoreceptors two-fold, suggesting a limited cell fate shift. Nonetheless, retinal histology was grossly normal, despite widespread persistent Math5 expression. In an RGC-deficient (*Math5* knockout)

environment, Crx>Math5 partially rescued RGC and optic nerve development, but the temporal envelope of RGC births was not extended. The number of early-born RGCs (before E13) remained very low, and this was correlated with axon pathfinding defects and cell death. Together, these results suggest that Math5 is not sufficient to stimulate RGC fate. Our findings highlight the robust homeostatic mechanisms, and role of pioneering neurons in RGC development.

Introduction

The vertebrate retina is a highly ordered structure composed of six major types of neurons and one type of glia. These originate from a common progenitor pool (Holt et al., 1988; Turner and Cepko, 1987; Turner et al., 1990) and include retinal ganglion cells (RGCs), rod and cone photoreceptors, amacrine, horizontal and bipolar interneurons, and Müller glia. At the onset of retinal neurogenesis, embryonic day 11 (E11) in mice, multipotent retinal progenitor cells (RPCs) begin to exit the cell cycle and differentiate.

Birthdating studies, in which nucleoside analogs are used to identify progenitors exiting the cell cycle, have defined a fixed, but overlapping, order for the generation of these major cell classes in vertebrates (Rapaport et al., 2004; Sidman, 1961; Young, 1985a). RGCs are the first to exit the cell cycle, at E11 in mice, with peak birthdates at E14 and termination by P0 (Drager, 1985). This early temporal profile overlaps significantly with those of cone, horizontal, and amacrine neurons. Rods, Müller glia and bipolar cells have characteristically later birthdates. In mice, the distribution of rod births peaks in the neonatal period, but the tails of the distribution extend across most of the histogenic

period, from E12.5 to P10 (Carter-Dawson and LaVail, 1979; Swaroop et al., 2010), because rods compose ~80% of the mature retina (Jeon et al., 1998).

Heterochronic co-culture and transplantation experiments, in which early embryonic and late RPCs were cultured in unequal ratios, have suggested that fate determination is largely a cell intrinsic process (Belliveau and Cepko, 1999; Rapaport et al., 2001; Reh, 1992; Watanabe and Raff, 1990). Indeed, progenitors cultured at low density can develop into each of the major cell classes, with similar diversity and proportions as the intact retina, in the absence of environmental feedback signals (Adler and Hatlee, 1989; Cayouette et al., 2003; Reh and Kljavin, 1989). However, extrinsic signals can influence progenitor cell cycle dynamics and override fate decisions *in vivo* (Cepko, 1999; Ezzeddine et al., 1997; Kim et al., 2005; Yang, 2004). Collectively, these observations are consistent with a temporal, or serial, competence model for retinal development (Cepko et al., 1996; Livesey and Cepko, 2001; Reh and Cagan, 1994; Wong and Rapaport, 2009). According to this model, RPCs pass through discrete competence states over time, in which they can adopt a limited number of cell fates. Within each state, the decision to exit the cell cycle and the final histotypic choice are influenced by extrinsic signals.

Two prototypical intrinsic factors important for development of mouse RPCs into specific types of neurons are the cone-rod homeodomain (HD) factor Crx and the basic-helix-loop-helix (bHLH) factor Math5 (atonal homolog Atoh7). Crx, and closely related factor Otx2, are expressed in during or shortly after the terminal cell cycle in tripotential precursors that give rise to photoreceptors and

bipolar cells (Furukawa et al., 1997; Muranishi et al., 2011). The precise role of Crx remains unclear. In mice, Crx expression initiates at E12.5 and is necessary for proper development of photoreceptors, and may be partially redundant with Otx2 in conferring competence for photoreceptor specification (Chen et al., 1997; Furukawa et al., 1999; Nishida et al., 2003; Sato et al., 2007). Crx works in concert with other transcription factor to regulate photoreceptor gene expression (reviewed in (Hennig et al., 2008; Swaroop et al., 2010)), and Crx is abundant in adult rods, cones and bipolar cells. The 5' regulatory DNA for Crx has been extensively characterized, and a critical 2.4 kb promoter region is thought to faithfully recapitulate the endogenous *Crx* pattern. This segment has been used to drive Cre, *lacZ*, and regulators of rod photoreceptor specification in transgenic mice (Cheng et al., 2006; Furukawa et al., 2002; Koike et al., 2005; Nishida et al., 2003; Oh et al., 2007).

Like Crx, the role of Math5 in fate specification has not been fully elucidated. *Math5* (*Atoh7*) is a single-exon gene that is transcribed by retinal progenitors in a spatiotemporal pattern that mirrors RGC births (Brown et al., 1998; Brzezinski et al., 2012; Prasov et al., 2010). This factor is transiently expressed by RPCs during or after their terminal cell cycle (Brzezinski et al., 2012; Feng et al., 2010; Kiyama et al., 2011) and is required for RGC development. *Math5* mutant mice have very few RGCs (<5%) and lack optic nerves (Brown et al., 2001; Wang et al., 2001). Apart from the deficiency of RGCs, all other retinal cell classes are preserved (Brown et al., 2001; Brzezinski et al., 2005). The mRNA profiles of *Math5* mutant retinas are altered, with

downregulation of genes associated with RGC differentiation (Mu et al., 2005). Lineage tracing experiments have established that *Math5*-expressing cells contribute to 3% of the adult retina, and every major cell class (Brzezinski et al., 2012; Feng et al., 2010; Yang et al., 2003). Together, these data suggest Math5 acts as an essential competence factor for RGC development. Orthologous genes in zebrafish, chicken, and frog have similar functions, lineage properties, and expression patterns (Kanekar et al., 1997; Kay et al., 2001; Liu et al., 2001; Matter-Sadzinski et al., 2001; Poggi et al., 2005), and mutations in human *ATOH7* have been linked to optic nerve aplasia and retinal vascular disease (Ghiasvand et al., 2011; Khan et al., 2011; Prasov et al., 2012).

Despite these expression and phenotypic analyses, the precise role of Math5 in RGC development remains unclear. Gain-of-function studies in frog and chick, and mouse embryonic stem cells, have yielded mixed results. In these systems, Math5 biases proliferating progenitors towards RGC fates when over-expressed during *early* developmental stages (Brown et al., 1998; Kanekar et al., 1997; Liu et al., 2001; Moore et al., 2002; Yao et al., 2007), but promotes other cell fates when expressed during *late* development, or in a cross-species context (Brown et al., 1998; Moore et al., 2002). In general, the interpretation of these experiments is confounded by the tendency of proneural bHLH factors to drive cell cycle exit when overexpressed (Farah et al., 2000).

To circumvent these limitations and critically assess the role of Math5 in biasing RGC development, we generated transgenic mice that ectopically express Math5 in a large number of retinal progenitors and newly post-mitotic

neurons, under control of a mouse *Crx* promoter fragment (Crx>Math5 Tg) or bacterial artificial chromosome (Crx>Math5 BAC), with a bicistronic Cre lineage tracer. Although endogenous *Crx* and *Math5* genes mark overlapping populations, and appear to be co-expressed in some cells, profound overexpression of transgenic Math5 did not stimulate RGC production or alter the profile of RGC births. Instead, the number of early-born photoreceptors was reduced. Despite sustained high-level expression of Math5 in photoreceptors and bipolar cells, retinal histology and cell type distribution were grossly normal. Likewise, no substantial RGC bias was observed in retinal explants infected with a Math5-expressing retrovirus. In mutant mice, the Crx>Math5 transgenes rescued RGC development. However, because endogenous *Crx* expression initiates somewhat later that *Math5*, early-born RGCs were scarce, and some rescued ganglion cells exhibited pathfinding defects or apoptosis during development. These results suggest that Math5 action is context dependent. Our findings also warrant a re-examination of previous results obtained using conventional *Crx* transgenes.

Materials and Methods

Conventional and Bacterial Artifical Chromosome (BAC) transgenes

To ectopically express *Math5* in a wide population of retinal cells, we generated a conventional Crx>Math5-IRES-Cre bicistronic transgene. We assembled mouse *Math5* cDNA and Cre recombinase coding sequences, separated by an internal ribosomal entry site (IRES2) and followed by a SV40

polyA signal. The mouse *Crx* promoter and proximal regulatory region were amplified by PCR and inserted upstream as a 2.4 kb *Xho*I-*Sal*I fragment (Furukawa et al., 2002; Oh et al., 2007). A matched Crx>Cre transgene was then generated from the Crx>Math5-IRES-Cre plasmid by precise deletion of *Math5* and IRES sequences using the single-strand oligonucleotide (ss oligo) recombineering method (Thomason et al., 2007), with a 70 nt antisense oligo (Suppl. Table 1) and *Asc*I selection.

To faithfully express *Math5* in the endogenous *Crx* pattern, we generated BAC transgenes by λRED recombineering (Lee et al., 2001). The targeting construct was assembled, with short (400 bp) 5' and 3' homology arms (H) flanking a Math5-IRES-Cre-FRT-amp-FRT cassette. This was equivalent to the conventional transgene, but included an FRT-*amp*-FRT selection cassette (Gene Bridges, Heidelberg) downstream of the SV40 polyA signal. The 5' homology arm extends from *Crx* intron 1 to the exon 2 initiation (ATG) codon, while the 3' homology arm contains sequence from *Crx* intron 2. A matched control (Cre-FRT-amp-FRT) was then generated by ss oligo recombineering, with the 70 nt antisense oligo (Suppl Table 1) and *Asc*I selection.

Linearized targeting plasmids were used in parallel to target mouse BAC clone RP23-81H17 by λRED-mediated homologous recombination in strain SW105 (Warming et al., 2005) after heat induction. This 219 kb BAC contains 134 kb 5' and 69 kb 3' DNA flanking the *Crx* gene. Targeted BAC clones were selected on ampicillin and chloramphenicol plates at 30°C, and verified by junctional PCR and DNA sequencing. The *amp* seletion cassette was then

deleted by arabinose induction of *Flpe* recombinase, leaving a solitary FRT site (Andrews et al., 1985). Homogeneity and integrity of the resulting clones was verified by ampicillin sensitivity, junctional PCRs, restriction mapping, and pulsed-field gel electrophoresis.

Purified circular DNA from BAC transgene constructs or linearized plasmid DNA from conventional constructs was injected into fertilized (C57BL/6J × SJL/2) F2 or R26*flox*GFP (JAX stock 004077 reporter strain, (Mao et al., 2001)) x B6SJLF1/J oocytes by the UM Transgenic Animal Core. Founders were identified by transgene-specific PCR genotyping (Suppl. Table 1), and lines were maintained by crossing to C57BL/6J or R26*flox*GFP reporter strains. We analyzed 2 founders and 2 lines for each conventional transgene (Crx>Cre Tg and Crx>Math5 Tg), and ≥3 lines for each BAC transgene. The most extensively characterized transgenes in this report were Crx>Math5 Tg 251, Crx>Cre Tg 352 control, Crx>Math5 BAC 60, and Crx>Cre BAC 764 control.

RNA analysis

Duplex and competitive triplex RT-PCRs were performed as described (Prasov et al., 2010) to compare the levels of transgene-derived and endogenous mRNAs. Total RNA was extracted from embryonic eyes (E14.5) or adult (P21) tissues of transgenic or wild-type animals using Trizol reagent (Invitrogen, Carlsbad, CA). First-strand cDNA was generated by high-fidelity reverse transcription (RT, Transcriptor™, Roche) at 50°C and used as template for PCR, with primers and conditions in Suppl. Table 1. Triplex competitive RT-PCRs used a common 6-carboxyfluorescein (FAM)-labeled forward primer in *Crx* exon

1, and two reverse primers (Suppl. Table 1). Dual products were closely matched for size and G+C content, and analyzed using a 3730XL capillary electrophoresis unit (Applied Biosystems, Carlsbad, CA) and Gene Marker software (SoftGenetics, State College, PA).

Quantitative RT-PCRs were performed using custom Taqman probes and Universal Taqman Mastermix (Applied Biosystems), and were analyzed on the ABI 7600 Real Time PCR System. Critical cycle threshold levels were normalized to *Gapdh* internal controls, using two-fluorophore (VIC and FAM) detection. Fold activity was calculated using the ddCt method (Livak and Schmittgen, 2001) and reported relative to the Crx>Math5 BAC expression level. Expression copy-number levels were calculated for conventional and BAC transgenes by normalizing to endogenous *Crx* values, using the mean ratio determined in triplex competitive RT-PCRs (*k*). Measurements were obtained using independent RNA pools from 2-5 mice of each genotype.

Histology

For section immunostaining, eyes or embryonic heads were fixed in 2-4% paraformaldehyde (PFA) 0.1 M $NaPO_4$ pH 7.3 for 30-60 min at 22ºC, processed through a 10-30% graded sucrose series, embedded in OCT (Tissue-Tek, Torrence, CA) and cryosectioned at 10 μm. For flatmount preparations, eyes of P1 or adult mice were removed and fixed in 4% PFA for 5 min. The optic nerves were then transected, and the retinas were teased apart from other ocular tissues, fixed in 4% PFA for 25 min. After immunostaining, retinas were incised

with 6-8 radial cuts and flattened with the ganglion cell layer (GCL) facing upward.

For immunodetection, slides or whole retinas were blocked in a solution of 10% normal donkey serum (NDS), 1% bovine serum albumin (BSA) in PBTx (0.1 M $NaPO_4$ pH 7.3 0.5% Triton X-100) for 1-4 hrs. To reduce mouse-on-mouse background associated with mouse monoclonal primary antibodies, donkey anti-mouse IgG Fab fragments were added at 0.8 mg/mL to some blocking reactions. Primary antibodies were applied overnight at 4°C and diluted in 3% NDS 1% BSA in PBTx. Sections or retinas were then washed in PBS, incubated for 2 hrs at 22ºC with Dylight-conjugated secondary antibodies and 4',6-diamidino-2-phenylindole (DAPI), and mounted in Prolong Gold Antifade (Invitrogen, Grand Island, NY). Slides were imaged using the Zeiss LSM510 Meta confocal system or an Olympus BX-51 epifluorescence microscope.

The primary antibodies were mouse anti-AP2α (1:1000, DSHB, Iowa City, IA); rabbit anti-βgal (1:5000, ICN Cappel, Aurora, OH); rat anti-β-galactosidase (1:500, (Saul et al., 2008)); rat anti-BrdU (BU1/75, 1:100, Harlan Seralab, Indianapolis, IN); mouse anti-calbindin (CB-955, 1:500, Sigma, St. Louis, MO); rabbit anti-cleaved-caspase 3 (1:100, Cell Signaling, Beverly, MA); sheep anti-Chx10 (1:250, Exalpha, Shirley, MA); mouse anti-Cre (clone 7.23, 1:300, Covance, Princeton, NJ); rabbit anti-Crx (1:1000, (Zhu and Craft, 2000)); chicken anti-GFP (1:2000, Abcam, Cambridge, MA); mouse anti-hPLAP (monoclonal 8B6, 1:250, Sigma); mouse anti-PKC (MC5, 1:100, Sigma); rabbit anti-mCar (1:500, Millipore, Billerica, MA); mouse anti-syntaxin (HPC-1, 1:1000,

Sigma); rabbit anti-M-opsin (1:1000, Millipore); rabbit anti-S-opsin (1:5000, (Applebury et al., 2000)); rabbit anti-phosphohistone H3 (1:400, Upstate, Lake Placid, NY); rabbit anti-rhodamine (1:500, Invitrogen); rabbit anti-Sox9 (1:250, Millipore); rabbit anti-TuJ1 (MRB-435P, 1:2000, Covance). The Crx antibody appears to cross-react weakly with Otx2 antigen (Brzezinski et al., 2010), most likely through a shared LDYKDQ sequence in the Crx 14-residue peptide immunogen (Zhu and Craft, 2000).

For detection of BrdU (5-bromo-2-deoxyuridine) and other antigens, cryosections were fully stained with primary and secondary antibodies to the other markers. Sections were then treated with 2.4 N HCl in PBTx for 1hr at 22°C, and immunostained for BrdU. Likewise, EdU (5-ethynyl-2-deoxyuridine) was detected after immunostaining, using an azide-alkyne cycloaddition reaction (Buck et al., 2008) and with Click-iT-647 reagents (Invitrogen).

For fine histology, mice were perfused transcardially with 2% PFA and 1.25% glutaraldehyde. The eyes were removed, post-fixed overnight at 22°C, dehydrated, embedded in glycol methacrylate plastic resin (JB-4, Polysciences, Warrington, PA), sectioned at 4 μm with a Leitz 1512 rotary microtome, and stained with basic fuchsin and methylene blue. Paraffin or cryosections (5-10 μm) of eyes or optic nerves were stained with hematoxylin and eosin as described (Brown et al., 2001).

Retrograde axon labeling of RGCs

RGCs were definitively marked by retrograde axon labeling with rhodamine dextran (Brzezinski et al., 2012; Rachel et al., 2002). Eyes from adult

or P1 mice were removed and immersed in Hank's balanced salt solution containing calcium, magnesium and 1 mM glucose (HBSSG). Optic nerves were transected within 1 mm of the sclera, and lysine-fixable tetramethyl rhodamine dextran 3,000 MW powder (Molecular Probes, Eugene, OR) was applied directly to the cut site. The eyes were positioned with severed optic nerves facing downward against cubes of surgifoam (Ethicon, Somerville, NJ) saturated with 3% L-α-lysophosphatidyl choline (LPC, Sigma) and rhodamine dextran. These were sealed with 1 % agarose, and incubated *en bloc* in aerated HBSSG for 1 hour at 22ºC. The surgifoam was then removed, and the eyes were incubated overnight in HBSSG under the same conditions. Rhodamine-labeled eyes were fixed in 4% PFA for 4 hrs at 22ºC and processed for sectioning or stained as whole retina preparations. In some experiments, the signal was enhanced by indirect immunofluorescence staining with anti-rhodamine antibody.

Cre lineage and dual reporter concordance analysis

To trace the descendants of cells expressing Cre recombinase, transgenic mice were crossed to R26*flox*GFP or Z/AP (JAX stock 003919, (Lobe et al., 1999)) reporter strains, which activate cytoplasmic GFP (green fluorescent protein) and membrane-tethered hPLAP (human placental alkaline phosphatase), respectively, after excision of *floxed* upstream stop signals. Retinal sections or flatmounts were co-stained for histotypic antigen markers, hPLAP and/or GFP. Cell types were identified by characteristic laminar position, morphology, and marker co-localization. RGCs were clearly distinguished from displaced amacrines by retrograde axon labeling. To assess the heterogeneity in

the level of *Crx* transgene (Cre) expression among progenitors giving rise to different cell types, we conducted dual reporter concordance experiments, as described (Brzezinski et al., 2012). Coexpression of GFP and hPLAP was scored in the outer nuclear (ONL), inner nuclear (INL) and ganglion cell (GCL) layers of adult triple transgenic mice (Crx>Math5 BAC or Crx>Cre BAC; Z/AP; R26*flox*GFP).

Quantitative assessment of RGCs in transgenic mice

Retinal ganglion cells were counted in Crx>Math5 Tg and non-transgenic littermates at P0 and P22, using Brn3a or retrograde axon labeling to mark RGCs. The fractional contribution of RGCs to the GCL (DAPI nuclei) was determined from 20 sections (400X) representing $n = 2$ eyes of each P22 genotype, and 12-22 sections (200X) representing $n = 4$-6 eyes for each P0 genotype.

To evaluate transgenic rescue of RGC development in mutants, Crx>Math5 Tg or Crx>Math5 BAC mice were crossed to *Math5* knockout (KO) mice (*Atoh7*^{tm1Gla}, (Brown et al., 2001)) for two or more generations. Eyes from informative embryonic, neonatal and adult littermates were immunostained as sections or flatmounts. Retinal cell death was assessed at E16.5 using activated Caspase-3 staining (Gown and Willingham, 2002). RGCs and apoptotic cells were counted in 18 sections (200X) representing $n = 6$ eyes of each genotype.

EdU pulse-chase and birthdating analysis

To evaluate the overlap between *Crx*+ and *Math5*+ cell populations, and compare the timing of *Crx* and *Math5* expression, pregnant dams carrying E13.5 or E15.5 *Math5-lacZ*/+ embryos were given to a single intraperitoneal injection of EdU (6.7 µg/g body mass). Embryos were harvested after a 4-hr chase and their retinas were stained for Crx, βgal and EdU. For other short-term labeling experiments, a single pulse of EdU or BrdU was given to pregnant dams 1 hr prior to harvest.

To assess alterations in the fate distribution of neurogenic cells exiting mitosis on different days, pregnant dams carrying Crx>Math5 Tg (line 251) and non-transgenic control embryos were given a single injection of BrdU (100 µg/g body mass) on E12.5, E13.5 or E15.5. Retinal sections from the resulting mice were stained for BrdU at P21, and the distribution of strongly BrdU+ cells among GCL, INL and ONL layers was determined. For the E15.5 pulse, we counted 24 sections (200X) from $n = 6$ eyes of each genotype, representing a total of 816 birthdated cells in Crx>Math5 Tg mice and 1005 birthdated cells in control mice. To evaluate late-stage RGC births, dams carrying Crx>Math5 BAC (line 60) and control embryos were pulsed with EdU at E17.5 and harvested at P22. Likewise, Crx>Math5 Tg (line 251) pups with *Math5* KO and heterozygous (het) genotypes, and non-transgenic littermates, were pulsed with BrdU at P1 and harvested at P22.

RGC birthdating curves were generated for rescued and control littermates by giving single EdU pulses at E11 and E12, E13.5, E15.5, or E17.5. The resulting pups (four genotypes) were harvested at P1 and their retinas were

stained for Brn3a and EdU as flatmounts. Two 0.05 mm^2 areas in the central retina were imaged as confocal Z-stacks through the GCL for each flatmount preparation. The density of RGCs (Brn3a+ cells per mm^2) and birthdated RGCs (Brn3a+ EdU+ cells per mm^2) was determined by direct counting. The normalized RGC birth fraction was calculated by dividing the number of RGCs born at each time point by the sum of RGCs born in all four time points (E11-E12, E13.5, E15.5, E17.5).

Statistics

Comparisons were made using a two-tailed Student's *t*-test in Microsoft Excel in cases where equal variance was observed. The Welch *t*-test was used for comparisons among groups of unequal variance. Errors are reported for biological replicates as SDM (standard deviation of the mean) unless otherwise noted. Jitter plots were generated with Prism software (Graphpad, La Jolla, CA).

Clonal analysis in retinal explants

Retinal explant cultures and retroviral infections were performed as described (Brzezinski et al., 2012) using standard methods (Hatakeyama and Kageyama, 2002; Wang et al., 2002b). Briefly, retinas were dissected from E13.5 wild-type embryos, flattened onto Nucleopore polycarbonate membranes (0.4 µm pore size, GE Healthcare, Piscataway, NJ) and transferred to Transwell culture dishes containing neurobasal media (Invitrogen) with B27 and N2 supplements, glutamine (0.4 mM), BDNF (50 ng/mL, Peprotech, Rocky Hill, NJ),

CNTF (10 ng/mL, Peprotech), penicillin (50 U/mL), streptomycin (50 µg/mL), and gentamicin (0.5 µg/mL).

The Math5-IRES-GFP retroviral plasmid was constructed by inserting a Math5 cassette in the bicistronic MSCV-IRES-GFP (MIG) retroviral vector (Van Parijs et al., 1999). MSCV-IRES-dnMAML^{GFP} was generated by replacing the GFP cassette in MIG with dnMAML^{GFP}. This encodes a fusion protein with residues 12-72 of mouse MAML1 (mastermind-like) at the N-terminus and GFP at the C-terminus (Maillard et al., 2004). Retroviral stocks were prepared in parallel by calcium phosphate transfection of the Phoenix ecotropic packaging cell line (Pear, 2001; Swift et al., 2001) with plasmid vectors. Polybrene (hexadimethrine bromide, 0.8 µg/mL, Sigma Aldrich, St. Louis, MO) was added to filtered media containing infectious particles. These viral stocks were titered on NIH3T3 cells and diluted to ~8×10^5 CFU (colony forming units) per mL. Transductions were performed by pipetting one drop (~25 µL) on top of each fresh explant, to sparsely mark dividing cells (Roe et al., 1993) and their descendants.

Infected explants were cultured for 7 days at the gas-media interface at 37ºC under 5% CO_2. Half of the media was replaced with fresh media on days 2, 4 and 6. After one week in culture, explants were fixed in 4% PFA for 30 min and processed for cryosectioning. Serial thick (30 µm) cryosections were immunostained for GFP and Brn3a, and imaged as 3-dimensional confocal Z-stacks. Clones were scored for size (number of GFP+ cells) and composition (number of Brn3a+ RGCs). A clone was defined as an isolated group of directy

apposed GFP+ cells, separated by at least 4 cell bodies from other GFP+ cells. We scored 3-4 explants per virus, giving a total number of 70 (IRES-GFP), 60 (Math5-IRES-GFP) and 52 (IRES-dnMAML) clones, respectively.

Results

Crx and Math5 are expressed in comparable neurogenic cell populations

Crx and Math5 progenitor cell populations give rise to 85% (rods, cones and bipolar cells) and 3% of the mouse adult retina (Brzezinski et al., 2012; Furukawa et al., 1997; Jeon et al., 1998), respectively (Fig. V-1A). To compare these factors directly, we examined their overlap and onset of expression relative to the terminal S phase, using a *lacZ* allele (*Atoh7*^{tm1Gla}, (Brown et al., 2001)) as a proxy for Math5. We found that Crx and βgal are expressed in distinct, but overlapping, cohorts of cells at both E13.5 and E15.5 (Fig. V-1B,C), consistent with the lineage profile of *Math5* descendants, over half of which are photoreceptors (Brzezinski et al., 2012). Using EdU or BrdU pulse-chase analysis at these time points, we determined that a small number of Crx and βgal double-positive cells at E13.5 and E15.5 were also labeled with EdU after a 4-hr chase (Fig. V-1). At these developmental stages, four hours is sufficient time for some cells progress through S, G2, and M phases and enter G0 (Prasov and Glaser, 2012; Sinitsina, 1971; Young, 1985b). Given that both of these factors are expressed during or after the terminal division (Brzezinski et al., 2012; Muranishi et al., 2011); and data not shown), these results suggest that *Crx* and *Math5* can be made in the same cells, simultaneously or sequentially, at the time

when cell fate is determined. While *Math5* is short-lived, *Crx* expression persists in a broad population of differentiated photoreceptor and bipolar cells (Brzezinski et al., 2012; Furukawa et al., 2002; Furukawa et al., 1997).

Crx>Math5 conventional and BAC overexpression systems

To critically assess the role of *Math5* in biasing progenitor cell fate, we generated transgenic mice with ectopic Math5 expression. Given the overlap of endogenous *Crx* and *Math5* expression, and the similar nature of these neurogenic cells, we chose the *Crx* promoter to broadly express *Math5* in a large population of early post-mitotic precursors. The 2.4 kb Crx promoter has been extensively characterized and is thought to drive specific expression in photoreceptor precursors, and mature rods, cones and bipolar cells (Furukawa et al., 2002). However, to limit position effects and ensure faithful Crx expression, we also built a BAC transgene containing 134 kb regulatory DNA upstream of the Crx start site (exon 1), and 69 kb downstream of the polyadenylation signal (exon 3). We then generated conventional and BAC transgenic mice, termed Crx>Math5 Tg and Crx>Math5 BAC, respectively (Fig. V-2A). The transgenes express Math5 and Cre from bicistronic transcripts. The Cre recombinase allowed us to trace the fate of cells expressing transgene-derived Math5 using the R26*flox*GFP reporter (Mao et al., 2001), which makes GFP after excision of a *loxP*-flanked stop signal. In parallel, we generated matched Crx>Cre and Crx>Cre BAC control transgenic mice to confirm the *Crx* lineage, and isolate Math5 effects.

Multiple independent insertions (≥4) of each transgene were analyzed for GFP and Cre expression, after crossing to R26*flox*GFP reporter mice (Fig. V-2B). These patterns were consistent, indicating that position effects were minimal in the vast majority of the transgenic lines (Fig. V-S1 and data not shown). For subsequent analysis, we chose a single representative line for each of transgene.

To evaluate transgene fidelity, we co-immunostained sections from adult and embryonic mice for GFP, Cre, and Crx antigens (Fig. V-2B). In both Crx>Math5 Tg mice (line 251) and Crx>Cre Tg mice (line 352), we observed cumulative expression (GFP) throughout the neural retina, RPE (retinal pigmented epithelium), and ciliary body, but not in lens or scleral tissue (Fig. V-2B, Fig. V-S2). GFP expression was also evident in the pineal gland (Fig. V-S2), and in embryonic forebrain regions (data not shown). Within the retina, all cell layers, and the vast majority of cells, were labeled with GFP by both conventional transgenes. In contrast, the patterns of Cre and Crx immunostaining were much more restricted. Cre antigen was completely co-extensive with Crx in adult photoreceptors and bipolar cells, although the relative expression levels varied among INL cells. Likewise, in the embryonic retina, all Cre+ cells were Crx+ (Fig. V-2B and data not shown). These results indicate that the Crx 2.4 kb promoter drives strong expression in photoreceptor and bipolar precursors, but is also active in multipotent progenitors or in other post-mitotic cells. Together, these patterns are most consistent with high-level expression in Crx domains (Chen et al., 1997; Furukawa et al., 1997), and leaky expression in the domains of closely

related homeodomain factor Otx2 (Bovolenta et al., 1997; Simeone et al., 1993). In Crx>Cre BAC mice (line 60) and Crx>Math5 BAC mice (line 764), cumulative transgene expression (GFP) was confined to the retina (Fig. V-2B), and was not observed in the RPE or ciliary body as noted with the conventional transgenes (Fig. V-S2). Again, Cre+ cells were co-extensive with the Crx population of cells at both adult and embryonic time points (Fig. V-2B). Within the adult retina, only a few scattered cells were labeled with GFP in the inner INL and GCL by the Crx>Cre BAC and Crx>Math5 BAC transgenes, as expected. Overall, the patterns of BAC and conventional transgene expression were very different, suggesting that the *Crx* 2.4 kb promoter is active beyond the endogenous *Crx* domain.

To further characterize the BAC and conventional transgenes, we assessed the distribution and level of *Math5* mRNA expression by RT-PCR. In the Crx>Math5 Tg, transcripts were evaluated in various tissues using primers specific to transgenic (Tg) or endogenous *Math5* (Fig. V-2B). Both species were confined largely to the eye, with a low level of endogenous *Math5* mRNA in the brain (Saul et al., 2008). Only transgenic *Math5* was detected in the adult retina, consistent with the known patterns of *Math5* and *Crx* expression (Brown et al., 1998; Brzezinski et al., 2012; Chen et al., 1997; Furukawa et al., 1997). To quantitatively compare the levels of BAC and conventional Crx>Math5 transgene expression, we first determined the ratio of Crx>Math5 BAC and endogenous *Crx* transcripts using a triplex competitive RT-PCR assay (Prasov et al., 2010) with a common end-labeled forward primer located in Crx exon 1 (Fig. V-S3). We found

that BAC-derived *Math5* transcripts were present at 53 ± 3% (*k*) the level of endogenous *Crx* transcripts in the adult retina, or approximately single-copy expression levels. We next measured *Math5* (*a*) and *Crx* (*b*) RNAs relative to *Gadph* in Crx>Math5 BAC, Crx>Math5 Tg and control adult retinas by TaqMan quantitative PCR. We found that *Math5* levels in Crx>Math5 Tg retinas were 16-fold higher than those in BAC transgenic retinas. As expected, *Math5* was not detected in controls and the level of *Crx* mRNA did not vary between genotypes. In the adult Crx>Math5 Tg retinas, the level of *Math5* expression was thus 8-fold higher than endogenous *Crx* ($a \times k/b$). The differences observed between BAC and conventional transgenic mice (Fig. V-2B) may thus reflect differences in the pattern and/or level of expression.

Lineage analysis of Crx>Math5 transgenes

To determine whether ectopic Math5 biases progenitors towards particular cell fates, we evaluated the distribution of cell types in Crx>Math5 BAC and Crx>Math5 Tg retinas compared to control Crx>Cre BAC and Crx>Cre Tg retinas, by examining GFP staining pattern of double transgenic mice carrying the R26*flox*GFP reporter. As expected, each transgene labeled all photoreceptors and bipolar cells. Persistent Math5 expression did not grossly alter the subtype distribution of cones or bipolar cells (Fig. V-S4).

In addition to rods, cones and bipolar cells, the Crx>Math5 BAC and Crx>Cre BAC control transgenes marked a small number of ganglion, horizontal and amacrine neurons, with frequency that varied from region to region in the retina and among cell types (Fig. V-3). Early cell types, particularly horizontal

neurons, were rarely marked by Crx>Cre BAC or Crx>Math5 BAC transgenes (Fig. V-3E,F), consistent with the onset of *Crx* expression at E12.5 (Chen et al., 1997; Furukawa et al., 1997). Likewise, in conventional Crx>Math5 Tg and Crx>Cre Tg mice, the vast majority of retinal cells were marked with GFP, including all major cell types. As noted with the BAC transgenes, fewer RGCs and horizontal cells were marked compared to other cell types (Fig. V-S5 and data not shown).

In principle, the labeled RGCs, horizontal and amacrine cells in BAC transgenic mice could represent one of three classes: [1] lineal descendents of proliferating progenitors that expressed low or high levels of the transgene, [2] rare *Crx*+ precursors that adopted non-photoreceptor or bipolar fates, [3] cells whose fate was shifted due to the action of *Math5*. To distinguish these mechanisms, we used two approaches. First, we assessed the heterogeneity of Cre expression levels among cells using a dual-reporter concordance paradigm (Brzezinski et al., 2012). Adult triple transgenic Crx>Math5 BAC or Crx>Cre BAC mice, carrying R26floxGFP and Z/AP (Lobe et al., 1999) reporters, were immunostained for GFP and hPLAP (Fig. V-S6). Among photoreceptors in the ONL and bipolar cells in the outer INL, concordance for GFP and hPLAP was uniformly high for each transgene (nearly 100%). However, among neurons in the inner INL and GCL, concordance was low (<40%), indicating that these cell types expressed a low level of Cre, and thus recombined stochastically at only one reporter locus. Second, we analyzed the cycle kinetics and spatial distribution of informative cells in E15.5 embryos carrying Crx>Math5 BAC and

R26*flox*GFP. After a 1 hr EdU pulse, no Cre+ EdU+ cells were detected (Fig. V-S7A). However, many EdU+ cells were observed in GFP+ vertical stripes (Fig. V-S7B), where most labeled Brn3b+ RGCs were localized (Fig. V-S7C). These findings are consistent with the general clustering of GFP+ cells in the adult retinas, and suggest a clonal origin (Reese et al., 1999; Turner and Cepko, 1987). Similar patterns were observed for the Crx>Math5 Tg embryos, but the relative abundance of GFP+ progenitors was a much greater (data not shown).

Crx>Math5 expression does not stimulate RGC genesis

Given the limitations of using the Cre lineage reporter to assess cell fate, we employed other metrics to assess the effects of broad Math5 overexpression on the overall fate distribution. We focused primarily on ganglion cells for these experiments, because *Math5* is necessary for RGC development, and we used Crx>Math5 Tg, because this transgene is expressed at much higher levels than the BAC counterpart (Fig. V-2D). We observed a similar abundance of Brn3a+ or rhodamine dextran-labeled RGCs in Crx>Math5 Tg and control mice throughout development (Fig. V-4A-C). At P0, prior to the neonatal culling of RGCs (Erkman et al., 2000; Farah and Easter, 2005; Galli-Resta and Ensini, 1996; Young, 1984), 56 ± 5% SD of GCL neurons in Crx>Math5 Tg retinas were RGCs (Brn3a+), similar to controls (59 ± 5% SD, $P = 0.4$, Fig. V-4D). Likewise, at P22, no significant difference was observed in the fraction of RGCs (rhodamine dextran-labeled) in the GCL between the two genotypes (41.1 ± 0.1% SD for wild-type, 43 ± 8% SD for Crx>Math5 Tg, $P = 0.8$ Fig. V-4D) or previous reports (41 ± 4% SD (Jeon et al., 1998)). We conclude that broad ectopic *Math5*

expression does not promote RGC fate, alter the survival of RGCs, or drive Brn3 expression in a *Math5* wild-type retina.

Crx>Math5 expression alters the distribution of early born cell types

Given the persistent high level of expression of the Crx>Math5 Tg in rods, cones and bipolar cells, we assessed overall retinal histology in plastic sections (Fig. V-4E). The morphological features of photoreceptor nuclei, inner and outer segments, and other layers were not affected at this level. However, subtle fate shifts might occur during development, which are counterbalanced by homeostatic feedback mechanisms. To assess these effects, we used a birthdating approach. Embryos were exposed to single BrdU pulses at E12.5, E13.5, or E15.5 and their retinas were analyzed at P22. At each time point, fewer birthdated nuclei were observed in the ONL of Crx>Math5 Tg mice than controls (Fig. V-5A, Suppl. Fig 8). For quantitative analysis, we focused on the E15.5 time point, as these litters contained a sufficient number of animals of each genotype for statistical comparisons. We counted the number of strongly BrdU+ nuclei in ONL, INL and GCL layers. We observed a 2-fold decrease in the fraction of birthdated photoreceptors (ONL cells) in Crx>Math5 Tg retinas ($21 \pm 3\%$ SD) compared to controls ($43 \pm 2\%$ SD, *t*-test $P < 10^{-3}$), with a corresponding increase in the INL and to lesser extent GCL (Fig. V-5A).

In principle, the loss of early-born photoreceptors could be due to cell death from persistent Crx>Math5 Tg expression or a small, *bona fide* fate shift. To distinguish these mechanisms, we evaluated Crx>Math5 Tg and control retinas for apoptosis by activated Caspase-3 immunostaining. At multiple time

points between E13.5 and P0, we observed 1-2 apoptotic cells per field (200X) in both Crx>Math5 Tg and control retinas (Fig. V-S9), consistent with previous studies of cell death in the embryonic retina (Vecino et al., 2004). Crx>Math5 Tg is thus unlikely to induce cell death in photoreceptor precursors. Instead, ectopic *Math5* appears to shift the fates of some early rod and cone photoreceptors.

Crx>Math5 expression does not extend the temporal profile of RGC births

In Crx>Math5 Tg mice, the expression of *Math5* is extended through postnatal development, whereas endogenous *Math5* mRNA is downregulated by P0 (Brown et al., 2001; Brzezinski et al., 2012). To test whether prolonged expression in neurogenic cells extends the profile of RGC births, we pulsed Crx>Math5 Tg mice with BrdU at P1 and harvested eyes at P22. In the central two-thirds of the retina, no BrdU+ cells were detected in the GCL of either genotype (Fig. V-5B), consistent with the completion of displaced amacrine and RGC genesis in these areas by P1 (Farah and Easter, 2005; LaVail et al., 1991; Reese and Colello, 1992; Voinescu et al., 2009; Young, 1985a). Similarly, in flatmounts of adult Crx>Math5 BAC retinas that were exposed to an EdU pulse at E17.5, we observed very few, if any,EdU+ RGCs (Fig. V-5C). Therefore, the envelope of RGCs births is not extended by prolonged *Math5* expression.

Retroviral Math5 does not induce RGC fate or cell cycle exit in retinal explants

We also tested whether Math5 can bias proliferating progenitors towards RGC fate, using a retroviral vector to transduce cultured retinal explants. E13.5

retinas were infected at low density *ex vivo* with MIG vectors. The resulting single-copy proviruses express Math5 and GFP, or GFP alone from the potent MSCV LTR promoter (Hawley, 1994) (Fig. V-6A). After 7 days in culture, we counted the number of Brn3a+ RGCs (Fig. V-6B-C). Among 70 clones infected with the IRES-GFP retrovirus, 4/272 GFP+ cells were Brn3a+ ($1.5 \pm 0.7\%$ binomial SD, Fig. V-6D), in accord the fraction of RGCs produced by *in vivo* clonal analysis (Turner et al., 1990). Among 60 clones infected with Math5-IRES-GFP retrovirus, 6/262 GFP+ cells were Brn3a+, which is not different from those transduced with GFP alone ($2.2 \pm 0.9\%$ binomial SD, Fisher's exact $P = 0.34$). Because overexpression of bHLH factors can promote cell cycle exit and differentiation (Farah et al., 2000), we also evaluated clone size. We found that the size distribution did not vary significantly between explants infected with these viruses (Fig. V-6E, χ^2 test $P = 0.6$ for $df = 4$), indicating that high-level single-copy expression of Math5 does not significantly promote cell cycle exit. As a positive control, we also analyzed explants infected with an MSCV-IRES-dnMAML^{GFP} retrovirus. The dnMAML^{GFP} fusion protein autonomously blocks Notch signaling by interfering with the NICD-CSL transcriptional complex (Maillard et al., 2004). Inhibition of Notch activity is associated with premature cell cycle exit and stimulation of RGC fate among early progenitors (Austin et al., 1995; Nelson et al., 2007). Among 52 clones, we detected a modest increase in the fraction of Brn3a+ RGCs (Fig. V-6D, 3/60 GFP+ cells, $5 \pm 3\%$, $P = 0.11$). We also observed a significant reduction in clone size, with all cells deriving from one- or two-cell clones (Fig. V-6E, χ^2 test $P < 10^{-8}$ for $df = 4$). These results

confirm that blockade of Notch signaling by dnMAML^{GFP} drives cell cycle exit, and that our explant system is sufficiently robust to detect this effect. Ectopic Math5 expression in progenitors does not stimulate cell cycle exit or significantly promote RGC fate in this system, consistent with our transgenic overexpression findings (Fig. V-4).

Crx>Math5 expression partially rescues the RGC deficiency in *Math5* KO mice

Although Crx>Math5 Tg does not stimulate RGC genesis in the wild-type environment, cells expressing ectopic Math5 may be prevented from adopting the RGC fate by strong negative feedback from nascent RGCs (Austin et al., 1995; Belliveau and Cepko, 1999; Waid and McLoon, 1998; Wang et al., 2005; Zhang and Yang, 2001). Indeed, we have observed that many Brn3a+ are generated in E13.5 Math5 KO retinal explants transfected with human ATOH7 (Prasov et al., 2012). We therefore crossed Crx>Math5 Tg and Crx>Math5 BAC transgenes onto the *Math5* KO background to examine the potential of *Crx*-driven Math5 to stimulate RGC genesis, heterochronically and heterotopically (Fig. V-1A), in a deficient environment.

We evaluated retinal flatmounts for the density of mature RGC cell bodies, axons and fascicles (Fig. V-7A-C). In *Math5* heterozygous mice, the vast majority of axons made radial projections to the optic disc and were fasciculated (Fig. V-7A,B), and the GCL contained many Brn3a+ RGCs (Fig. V-7C). In contrast, *Math5* KO retinas had vastly reduced axon density, in accord with previous estimates (Lin et al., 2004). The residual axons were largely

unfasciculated and exhibited pathfinding defects similar to those in *Brn3b* -/- mice (Badea et al., 2009; Gan et al., 1999) (Fig. V-7B and Fig. V-S10). Among 10 flatmounts examined from *Math5* KO eyes, no Brn3a+ cells were observed in any area (Fig. V-7C). The Crx>Math5 Tg transgene, and to a lesser extent the Crx>Math5 BAC, were variably capable of rescuing axons and preventing fasciculation defects in *Math5* KO retinas. However, rescue was less pronounced with successive generations of mice, ostensibly due to epigenetic reductions in transgene expression levels (Garrick et al., 1998). The Crx>Math5 Tg, but not the Crx>Math5 BAC, transgene was capable of restoring Brn3a expression among some adult ganglion cells. As expected, all rescued Brn3a+ ganglion cells were derived from progenitors that expressed the Crx>Math5 Tg transgene (GFP+), whereas only ~40% of Brn3a+ cells were GFP+ in the wild-type (Fig. V-7D). Finally, we observed small optic nerves in rescued mice carrying the Crx>Math5 Tg (Fig. V-7E), but not in *Math5* KO controls. Together, these results suggest that the Crx>Math5 Tg transgene, which expresses high levels of Math5 in early post-mitotic precursors and low levels in progenitors, can partially rescue RGC genesis and axonal guidance defects in *Math5* KO mice.

Crx>Math5 expression alters the RGCs birth profile in Math5 KO mice

Given the differences in the timing of *Crx* and endogenous *Math5* expression, we tested whether the rescued RGCs were born within the same temporal envelope as native RGCs, which are only generated prenatally. We first exposed P1 pups to a single pulse of BrdU, and stained their retinas at P21.

Few, if any, GCL cells were birthdated at P1 in *Math5* KO mice carrying Crx>Math5 Tg (Fig. V-7F).

To fully explore the temporal profile of RGC births and the extent of RGC genesis in rescued mice, we generated partial birthdating curves (Young, 1985a) for Crx>Math5 Tg; *Math5* KO mice and littermate controls (Fig. V-8). Crx>Math5 Tg; *Math5* KO mice were crossed to *Math5* heterozygotes and the pregnant dams were given two injections of EdU at E11 and E12 to mark the earliest born RGCs (Fig. V-8A), or a single injection of EdU at E13.5, E15.5, or E17.5 (Fig. V-8B-D). Retinas were harvested from the resulting pups and stained as flatmounts for Brn3a and EdU at P1, a time point before the neonatal RGC culling period (Farah and Easter, 2005), but after all RGCs have been generated (Figs. 5B and 7F). In *Math5* KO and Crx>Math5 Tg; *Math5* KO mice, very few Brn3a+ RGCs were born during early development (Fig. V-8A). In all 4 genotypes, the majority of RGCs were born between E13.5 and E15.5 (Fig. V-8B,C), consistent with RGC birthdating curves for wild-type retinas (Drager, 1985; Farah and Easter, 2005; Young, 1985a). Furthermore, no E17.5 birthdated Brn3a+ cells were detected in any of these mice, after careful examination of confocal Z-stacks through the GCL (Fig. V-8D).

The birthdating data and RGC counts reveal four important trends (Fig. V-8E,F). First, the curves for *Math5* heterozygous (het) and Crx>Math5 Tg; *Math5* het mice were nearly identical, suggesting that Crx>Math5 Tg does not alter the profile of RGC births (χ^2 test $P = 0.26$ for $df = 2$). Second, the normalized distribution of RGC births for Crx>Math5 Tg; *Math5* KO and *Math5* het mice

differed significantly (χ^2 test $P = 0.01$ for $df = 2$). In particular, very few RGCs were generated in the rescued mice (Crx>Math5 Tg; *Math5* KO) at the earliest developmental times, and a larger number of RGCs were born at E15.5. Third, RGCs were generated within the same temporal envelope in all 4 genotypes, suggesting that this time window is fixed. It does not depend on Math5, and cannot be shifted by protracted or elevated Math5 expression.

Fourth, the absolute number of rescued RGCs at P1 in Crx>Math5 Tg; *Math5* KO mice was increased 2.3-fold in comparison to control *Math5* KO mice (Welch *t*-test $P = 0.02$, Fig. V-8G), but this effect was variable, and the number of RGCs was low in comparison to *Math5* hetetozygotes (12%, 1160 ± 250 Brn3a+ cells per mm^2, $P < 10^{-8}$). The Crx>Math5 transgene did not increase the RGC density in *Math5* hets ($10{,}400 \pm 400$ Brn3a+ cells per mm^2 vs. $10{,}800 \pm 600$, Student's *t*-test $P = 0.54$), consistent with the results above (Fig. V-4). Likewise, the number of RGCs was significantly reduced in control *Math5* KO mice compared to heterozygotes (5%, 500 ± 50 Brn3a+ cells per mm^2, $P < 10^{-8}$), as previously reported (Lin et al., 2004).

Increased cell death and optic nerve defects in rescued Crx>Math5 Tg mice

The variability and incomplete rescue of RGCs in Crx>Math5 Tg mice on the *Math5* KO background was surprising. To explore the mechanism underlying this variability, we analyzed optic nerve development during early embryogenesis, using TuJ1 to identify RGC axons. At E15.5 and E17, we observed coalescence of TuJ1+ fibers and formation of optic nerves in Crx>Math5 Tg; *Math5* KO, but not in *Math5* KO retinas (Fig. V-9A,B). These

rescued optic nerves were much thinner than wild-type controls. In some cases, these nerves exhibited severe pathfinding defects as they exited the retina, and formed large 'knot' structures (Fig. V-9A, arrowhead). Because RGCs that fail to properly establish connections in the CNS are eliminated (O'Leary et al., 1986), we evaluated cell death by activated Caspase-3 immunostaining at E16.5, near the end of RGC genesis. We observed a significant increase in cell death in *Math5* KO mice compared heterozygous controls (Fig 9C-D, 9 ± 1 vs. 1.1 ± 0.2 Casp3+ cells per field, Welch *t*-test $P < 0.001$), consistent with previous reports (Feng et al., 2010). In Crx>Math5 Tg; *Math5* KO mice, there was a further increase in cell death compared to *Math5* KO retinas (12.9 ± 0.6 Casp3+ cells per field, $P = 0.016$). The vast majority of dying cells were located in the GCL (Fig. V-9C), suggesting that aberrant RGCs are eliminated. We also observed knots of RGC axons in Crx>Math5 BAC; *Math5* KO mice, consistent with the small degree of rescue by this transgene (Fig. V-9E).

Discussion

The patterns of Crx>Cre BAC and Crx 2.4 kb transgene expression

The Crx 2.4 kb promoter has been used to drive Cre, *lacZ*, Nrl or Nr2e3 expression (Cheng et al., 2006; Furukawa et al., 2002; Koike et al., 2005; Nishida et al., 2003; Oh et al., 2007), and Crx BACs have been used to drive GFP, hPLAP or *lacZ* expression (Muranishi et al., 2010; Samson et al., 2009). From these studies, it is clear that both types of transgenes are expressed at high levels in photoreceptors and bipolar cells, and their precursors. However,

thorough lineage data reflecting cumulative transgene expression are lacking. In this study, as control for *Math5* overexpression, we characterized the cumulative expression of Crx 2.4 kb promoter and Crx>Cre BAC transgenes using R26*flox*GFP and Z/AP reporters. At the level of Cre immunodetection (Fig. V-2), both transgene formats recapitulated endogenous *Crx* expression throughout development, and were restricted to known *Crx* domains in the eye and pineal gland (Fig. V-2, Fig. V-S2) (Chen et al., 1997; Furukawa et al., 1997). However, when Cre activity was assessed using highly sensitive reporters, the Crx 2.4 kb promoter and, to a much lesser extent the Crx>Cre BAC, were found to mark all major cell types in the retina, contrary to previous reports (Koike et al., 2005; Nishida et al., 2003). Multiple independent insertions gave similar results (Fig. V-S1 and data not shown), so the ectopic patterns cannot be attributed to chromatin position effects.

There were notable differences between conventional and BAC transgenes. First, the GFP reporter was detected in the RPE, ciliary body and embryonic brain with conventional, but not with BAC transgenes (Fig. V-S2 and data not shown), and GFP was more broadly expressed within the neural retina. These differences are likely to reflect leaky expression of the Crx 2.4 kb promoter in *Otx2* domains. Otx2 and Crx are evolutionary paralogs (Plouhinec et al., 2003), and Otx2 is expressed in the RPE, ciliary body, retinal progenitors, and embryonic forebrain (Bovolenta et al., 1997; Brzezinski et al., 2010; Muranishi et al., 2011; Simeone et al., 1993). Given their structural and functional similarity, common evolutionary origin, and overlapping expression in photoreceptors and

the pineal, at least some transcription factors are likely to regulate both genes, and bind within this 2.4 kb sequence. Indeed, the zebrafish *Crx* ortholog is expressed in proliferating retinal progenitors (Shen and Raymond, 2004), and it has been suggested that bovine Crx, along with Otx2, regulate gene expression in the RPE (Esumi et al., 2009). Second, the level of expression was significantly higher (16-fold) from the conventional transgene (Fig. V-2 and Fig. V-S3). Together, the qualitative and quantitative differences we observed can explain the greater abundance of GFP+ cells in Crx>Cre Tg mice compared to Crx>Cre BAC mice.

We believe the patterns of cumulative transgene expression reflect dichotomous low-level or leaky activity in proliferating RPCs, and high-level activity in photoreceptor and bipolar precursors, for four reasons. First, Cre immunoreactivity closely matched endogenous *Crx* expression, in adult and embryonic retinas (Fig. V-2). Second, high-level *Crx* or Cre expression was observed only in post-mitotic cells (Fig. V-S7 and data not shown) (Muranishi et al., 2011). Third, GFP reporter expression was distributed in radial stripes in BAC transgenic mice (Figs. 2-3 and Suppl Figs. 1,7), suggesting a clonal origin. Fourth, low concordance (<40%) was observed between R26*flox*GFP and Z/AP reporters in the GCL and inner INL of Crx>Math5 BAC and Crx>Cre BAC mice, but high concordance (~100%) was observed in photoreceptor and bipolar neurons. This dichotomy contrasts starkly with the uniformly high concordance observed for a Math5>Cre BAC transgene (Brzezinski et al., 2012), and

demonstrates the utility of this approach to distinguish populations with heterogeneous levels of Cre.

Our analysis suggests that some previous results obtained using conventional Crx>Cre transgenes should be reinterpreted. Notably, Nishida *et al.* (Nishida et al., 2003) ablated *Otx2* using a Cre transgene driven by a 12 kb *Crx* promoter segment. Paradoxically, this resulted in complete loss of *Crx* mRNA at E18.5 (*cf.* Fig. 4C,D) despite the inherent time delay required for Cre protein expression, excision of *Otx2* genomic sequences, and decay of existing pools of *Otx2* and *Crx* mRNA and protein (Nagy, 2000). Thus, the ablation of Otx2 in this experiment must have occurred earlier, in retinal progenitors, well before the onset of *Crx* trancription. Likewise, Koike *et al.* (Koike et al., 2005) conditionally ablated atypical protein kinase C (aPKC) and observed a major disruption in retinal organization. On this basis, they concluded that photoreceptors were critical for proper lamination of the retina. Instead, we believe a more parsimonious explanation is that aPKC function in RPCs is critical for lamination and epithelial polarity, as has been demonstrated for other neural progenitors (Cui et al., 2007; Wodarz et al., 2000).

Ectopic expression of *Math5* does not stimulate RGC fate

After establishing the patterns of Crx BAC and Crx 2.4 kb transgenic expression, we were able to test the effects of massive Math5 overexpression on the fate trajectory of retinal cells. Our findings show that Math5 overexpression does not significantly bias RGC fate in the wild-type environment for three reasons. First, the fraction of RGCs within the GCL was not increased in

Crx>Math5 Tg mice at any point during development (Fig. V-4). It is likely that negative feedback from nascent RGCs (Austin et al., 1995; Belliveau and Cepko, 1999; Waid and McLoon, 1998; Wang et al., 2005; Zhang and Yang, 2001) restricts Math5 from inducing supernumerary RGCs. Second, the temporal profile of RGC births was not extended by Crx>Math5 Tg expression (Figs. 5 and 8), despite abundant Crx expression in early post-mitotic precursors during the post-natal period.

Third, retroviral expression of Math5 did not significantly promote RGC fate or cell cycle exit in cultured embryonic retinal explants. These results differ from previous studies in chick and frog, in which overexpression of Math5 orthologs favored RGC fate (Kanekar et al., 1997; Liu et al., 2001). In these studies, effects on cell cycle dynamics and cell fate could not be completely isolated. By itself, any experimental manipulation that forces cell cycle exit during early neurogenesis can cause RPCs to adopt early fates, by effectively stopping progression of the 'histogenetic clock' (Ohnuma et al., 2002). Indeed, high-level expression of proneural bHLH factors induces cell cycle exit *in vitro* (Farah et al., 2000), and Xath5 overexpression reduces clone size *in vivo* (Moore et al., 2002). Furthermore, misexpression of other bHLH factors, such as Neurod1, during early frog development promotes RGC fate, whereas overexpression of Xath5 during late developmental stages favors non-RGC fates (Moore et al., 2002). In mice, Math5 is unlikely to be a major determinant of cell cycle exit, because it is variably expressed, during or after the terminal division, and lineage-marked cells do not re-enter the cell cycle in *Math5* KO mice

(Brzezinski et al., 2012). These disparate gain-of-function results may reflect differences between species in the timing, level or unique post-translational regulation of the endogenous Math5 ortholog, or the effective dose of bHLH protein delivered in these experiments.

Our transgenic and retroviral clone analyses separate cell cycle and fate effects. In the explant experiments, the level of proviral Math5 expression in transduced RPCs was not sufficient to promote cell cycle exit (Fig. V-6E) and RGC fate was not favored (Fig. V-6D). In contrast, the dnMAML retrovirus, which blocks Notch signaling, drove RPCs out of the cell cycle and increased RGC abundance, consistent with previous results (Austin et al., 1995; Nelson et al., 2007; Ohnuma et al., 2002). Some RGC fate effects attributed to Ath5 orthologs may be explained by premature cell cycle exit. When expressed at eight times the level of endogenous Crx (Fig. V-2D), ectopic Math5 does not significantly bias progenitors or post-mitotic precursors towards the RGC fate in a wild-type environment, supporting its role as a competence factor. However, ectopic Math5 does favor RGC development in a deficient environment (*Math5* KO). We observed partial rescue of RGC and optic nerve formation in adults and embryos (Figs. 7-9). These findings are generally consistent with the stimulation of ganglion cell fate by Math5 transfection in neurosphere cultures (Yao et al., 2007) or by electroporation of human ATOH7 in *Math5* KO retinal explants (Prasov et al., 2012).

In the wild-type environment, we did observe one relatively minor fate effect of transgenic Math5. The number of early-born photoreceptors was

significantly reduced (2-fold at E15.5) in Crx>Math5 Tg mice. However, adult retinal histology and photoreceptor morphology were grossly unaffected (Fig. V-4E). Furthermore, widespread Math5 expression is not sufficient to stimulate ectopic Brn3b immunoreactivity (Fig. V-S11), a known downstream target (Liu et al., 2001; Mu et al., 2005). Finally, the co-expression of Crx and *Math5-lacZ* in some progenitors (Fig. V-1) and the persistent expression of transgenic Math5 in mature adult photoreceptors (Fig. V-2) show that downregulation of Math5 is not an essential step in the specification of these cell types.

Math5 is not the sole determinant of RGC competence

Our birthdating analyses (Figs. 5-8) provide novel insights into the window of RGC competence and the role of *Math5*. The timing of Math5 expression closely mirrors the RGC birthdating curve and Math5 is required for RGC competence (Brown et al., 1998; Brown et al., 2001; Brzezinski et al., 2012; Wang et al., 2001). Thus, in principle, the pattern of Math5 expression may be the sole factor temporally restricting RGC specification. Indeed, in *Gdf11* mutant mice, an overproduction of RGCs during development is correlated with a spatiotemporal increase in *Math5* expression (Kim et al., 2005). Our results, however, suggest that prolonged expression of Math5 in Crx>Math5 Tg mice does not extend the profile of RGC births, even when few nascent RGCs are present, in the *Math5* KO rescue. In the rescued mice, the peak of RGC birthdates was shifted by approximately two days (Fig. V-8), consistent with the later onset of *Crx* expression, but this modest heterochronic effect occured within the normal envelope for RGC genesis. Furthermore, the profile of residual RGC

births in *Math5* KO mice closely matches wild-type birthdating curves, except for the extremely low RGC abundance (Fig. V-8). Together, these findings suggest that the pattern of *Math5* expression is not the sole factor restricting RGC competence. Instead, a complex network of interactions, including Math5, is likely to determine the spatiotemporal pattern of RGC genesis. For example, the envelope of RGC genesis also appears to be shaped by other transcription factors, Notch signaling, and microRNAs (Elliott et al., 2008; Georgi and Reh, 2010; Silva et al., 2003).

A pioneering model for RGC fate specification

In Crx>Math5 Tg; *Math5* KO and *Math5* KO mice, the loss of early-born RGCs (Fig. V-8) is correlated with pathfinding defects in remaining RGCs (Fig. V-9 and Fig. V-S10). These observations can be explained in two ways. First, the residual and rescued RGCs may follow an aberrant RGC differentiation pathway. In adult *Math5* KO mice, residual RGCs form dendritic arbors with normal size and spacing (Lin et al., 2004), but these cells fail to express Brn3b and Brn3a (Fig. V-7 and data not shown), which are critical for axon pathfinding, dendritic stratification, and cytodifferentiation (Badea et al., 2009; Gan et al., 1999). It is thus possible that Crx>Math5 Tg derived RGCs are intrinsically defective and express an aberrant set of RNA transcripts. Alternatively, the pathfinding defects in these RGCs may result indirectly, from a deficiency of early-born ganglion cells, which may limit the extent of rescue overall. Nascent RGCs are known to elaborate signals, such as sonic hedgehog (Shh), which promote intraretinal axon pathfinding generally (Erskine and Herrera, 2007; Oster et al., 2004). In

zebrafish, the establishment of early RGC axons is necessary and sufficient for pathfinding and survival of later RGCs (Pittman et al., 2008), and this community effect may be widespread in the nervous system (Raper and Mason, 2010). In *Math5* KO mice, residual RGC axons are poorly fasciculated, and often branched (Fig. V-7), and do not extend radially toward the central retina (Fig. V-S10). In Crx>Math5 Tg; *Math5* KO animals the extent of fasciculation is roughly correlated with the number of surviving RGCs (data not shown). Thus, isotypic interactions are likely to be critical for proper pathfinding and fasciculation of the transgene-rescued RGCs. These *pioneering* effects are not limited to intraretinal pathfinding, as knots of tangled fibers were apparent behind the retinas of rescued Crx>Math5 Tg and BAC animals (Fig. V-9). These defects appear to be resolved by apoptosis, although a small number of ganglion cells survive, and are likely to make synaptic connections in the brain (Triplett et al., 2011). Our results highlight the robust pathfinding mechanisms that operate in the retina, and the strong homeostatic mechanisms that balance the ratio of diverse cell types during development.

Acknowledgements

The authors are grateful to Thom Saunders, Maggie van Keuren and the UM transgenic animal model core for generating conventional and BAC transgenic animals; to Sue Tarlé, Dellaney Rudolph, Christine Brzezinski and Melinda Nagy for technical support; to Cheryl Craft for *Crx* antisera; to Sean Morrison and Ivan Malliard for the MIG and dnMAML retroviral constructs, respectively; to Mitchell Gillett for assistance with histology; to Anand Swaroop and Edwin Oh for Crx 2.4

kb promoter plasmid; to Chris Edwards, and the UM microscopy and image analysis laboratory for technical advice. The authors thank Nadean Brown, Chris Chou, David Turner, and Joe Brzezinski for valuable discussions and critical reading of the manuscript. This research was funded by National Institutes of Health (NIH) R01 grant EY14259 (TG). LP was supported by NIH T32 grants EY13934 and GM07863.

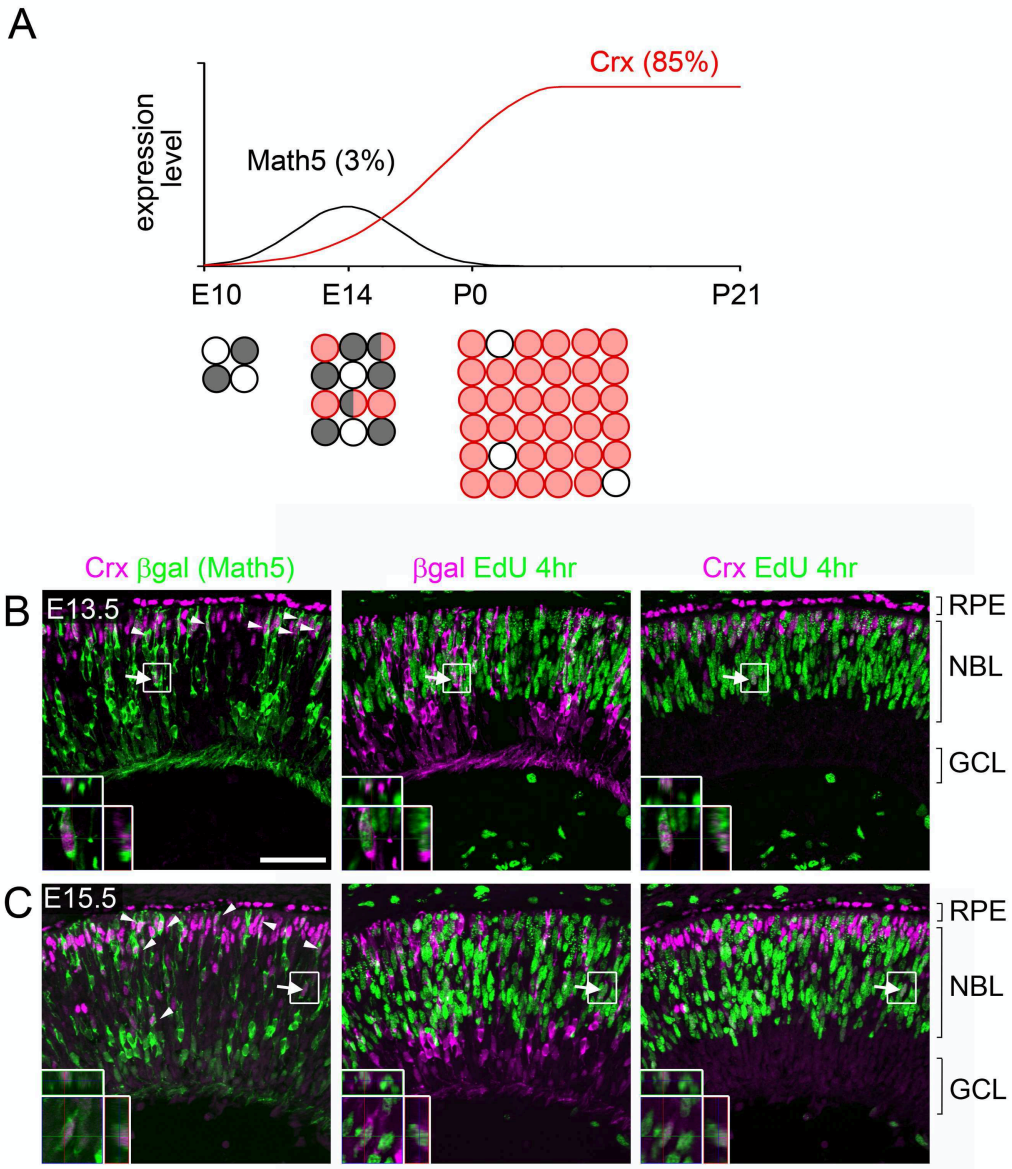

Figure V-1. Crx and Math5 (βgal) are expressed in overlapping subsets of cells shortly after cell cycle exit. (A) Schema comparing the termporal expression patterns and cellular abundance of Crx (red) and Math5 (black) in the retina. (B-C) Sections from E13.5 (B) or E15.5 (C) *Math5-lacZ*/+ embryos costained for βgal (*Math5-lacZ* allele), Crx, and EdU following a 4 hour chase *in vivo*. Many cells coexpress Math5 and Crx (arrowheads), and both factors are expressed in some cells shortly after cell cycle exit (EdU+, arrows). Cells initiating expression of Crx or Math5 reflect similar populations of progenitors. RPE, retinal pigmented epithelium; NBL, neuroblastic layer; GCL, ganglion cell layer. Scale bar, 50 μm.

Figure V-2. Characterization of the Crx>Math5-IRES-Cre and Crx>Cre conventional and BAC transgenic mice. (A) Map of conventional and BAC transgenes. In conventional transgenes, Math5-IRES-Cre pA and control Cre pA cassettes are positioned downstream of the 2.4 kb *Crx* promoter fragment, as Crx>Math5 Tg and Crx>Cre Tg, respectively. In BAC transgenes, equivalent cassettes were precisely inserted in BAC clone RP23-81H17, at the first ATG of the *Crx* gene, in exon 2, as Crx>Math5 BAC and Crx>Cre BAC. (B) Expression patterns of Crx>Math5 BAC, Crx>Cre BAC, Crx>Math5 Tg, and Crx>Cre Tg mice carrying R26*flox*GFP reporters. In adult and embryonic retinas for each transgene (right, far right), Crx and Cre are coextensive, suggesting faithful recapitulation of the endogenous *Crx* pattern. In Crx>Math5 BAC and Crx>Cre BAC retinas, reporter expression (R26*flox*GFP) is largely confined to the photoreceptor and bipolar precursors in the neural retina. In Crx>Math5 Tg and Crx>Cre Tg, the GFP reporter is widespread throughout the neural retina, and is apparent in the RPE and ciliary body. (C) RT-PCR of RNA from P21 Crx>Math5 Tg tissues, P21 wild-type (WT) retinas, and E14.5 wild-type eyes. The products show total, endogenous (endo), and transgenic (Tg) *Math5* mRNA expression, and βactin control. Endogenous *Math5* is expressed in the embyonic retina, and at low levels in the brain, but is not detected in other tissues (including the adult retina). In contrast, transgenic Math5 is strongly expressed in P21 retinas, and is restricted to eye tissue. No PCR products are detected in the absence of reverse transcriptase (− RT). (D) Taqman qRT-PCR comparing the relative abundance of *Math5* and *Crx* transcripts in P21 Crx>Math5 BAC (BAC 60), Crx>Math5 Tg (Tg251), and wild-type retinas. *Math5* (*a*) and *Crx* (*b*) expression levels are normalized to *Gapdh*, with expression reported relative to Crx>Math5 BAC (left). *Math5* expression is also reported relative to endogenous *Crx* levels (right), calculated using triplex competitive PCR data (*k*) from Crx>Math5 BAC to normalize expression levels (Fig. V-S3). *Math5* expression in Crx>Math5 Tg retinas is 16-fold higher than Crx>Math5 BAC retinas, and 8-fold higher than endogenous *Crx*. Ex, exon; IRES, internal ribosome entry site; FRT, Flipase recognition target; on, optic nerve; cb, ciliary body; IS, inner segment; ONL, outer nuclear layer; INL, inner nuclear layer. Scale bar, 50 μm.

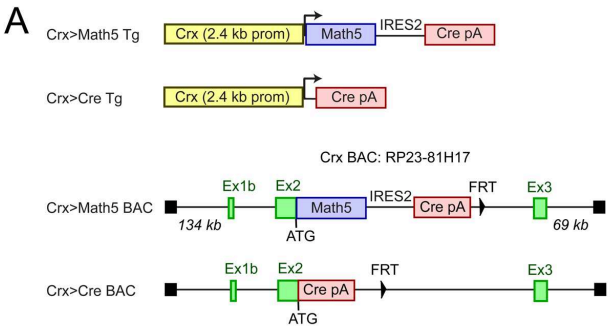
A
Crx>Math5 Tg
Crx (2.4 kb prom)
Math5
IRES2
Cre pA
Crx>Cre Tg
Crx (2.4 kb prom)
Cre pA
Crx BAC: RP23-81H17
Crx>Math5 BAC
Ex1b
Ex2
Math5
IRES2
Cre pA
FRT
Ex3
134 kb
ATG
69 kb
Crx>Cre BAC
Ex1b
Ex2
Cre pA
FRT
Ex3
ATG

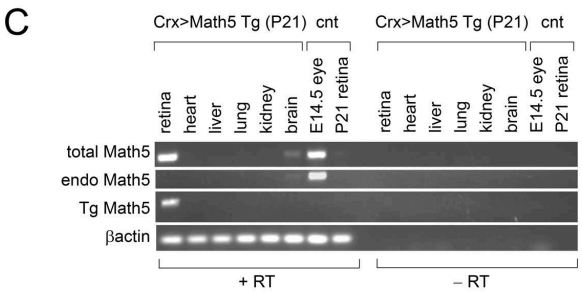
C
Crx>Math5 Tg (P21)
cnt
Crx>Math5 Tg (P21)
cnt
retina
heart
liver
lung
kidney
brain
E14.5 eye
P21 retina
retina
heart
liver
lung
kidney
brain
E14.5 eye
P21 retina
total Math5
endo Math5
Tg Math5
βactin
+ RT
– RT

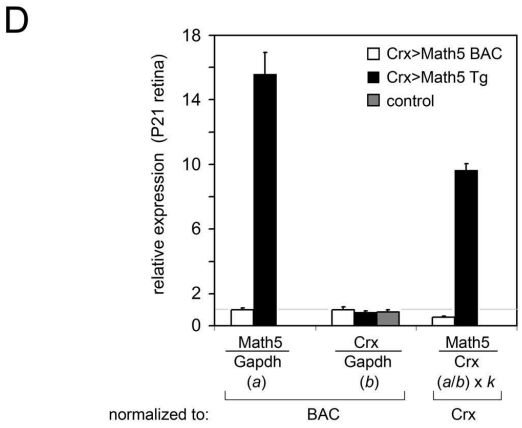
D
relative expression (P21 retina)
18
14
10
6
2
0
Crx>Math5 BAC
Crx>Math5 Tg
control
Math5
Gapdh
(a)
Crx
Gapdh
(b)
Math5
Crx
(a/b) x k
normalized to:
BAC
Crx

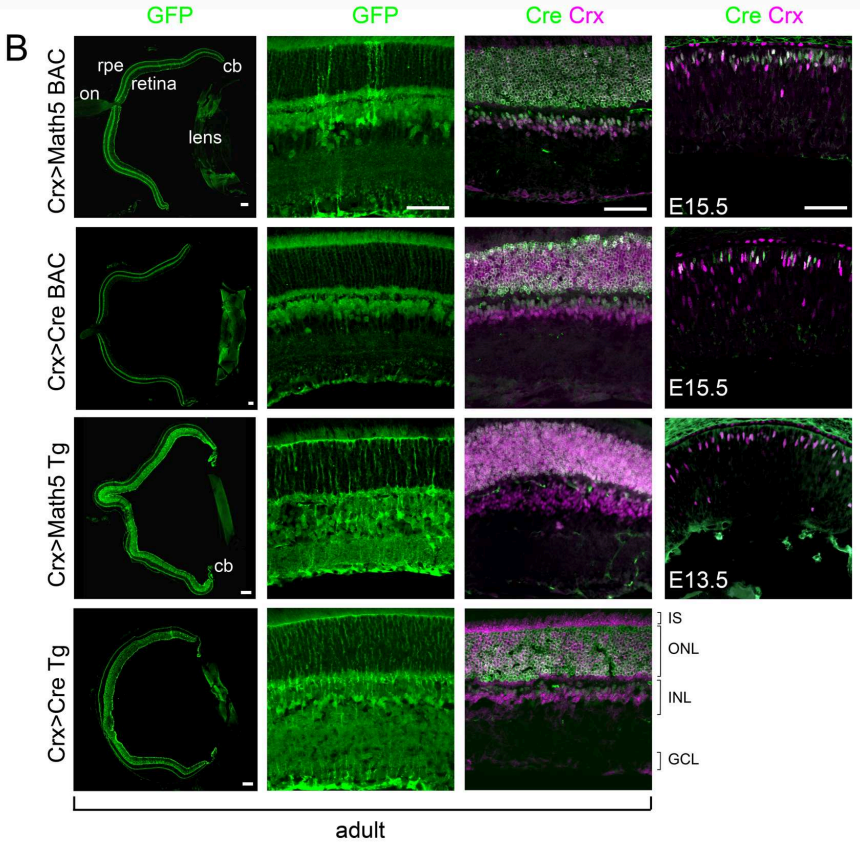
B
GFP
GFP
Cre Crx
Cre Crx
Crx>Math5 BAC
rpe
on
retina
cb
lens
E15.5
Crx>Cre BAC
E15.5
Crx>Math5 Tg
cb
E13.5
Crx>Cre Tg
IS
ONL
INL
GCL
adult

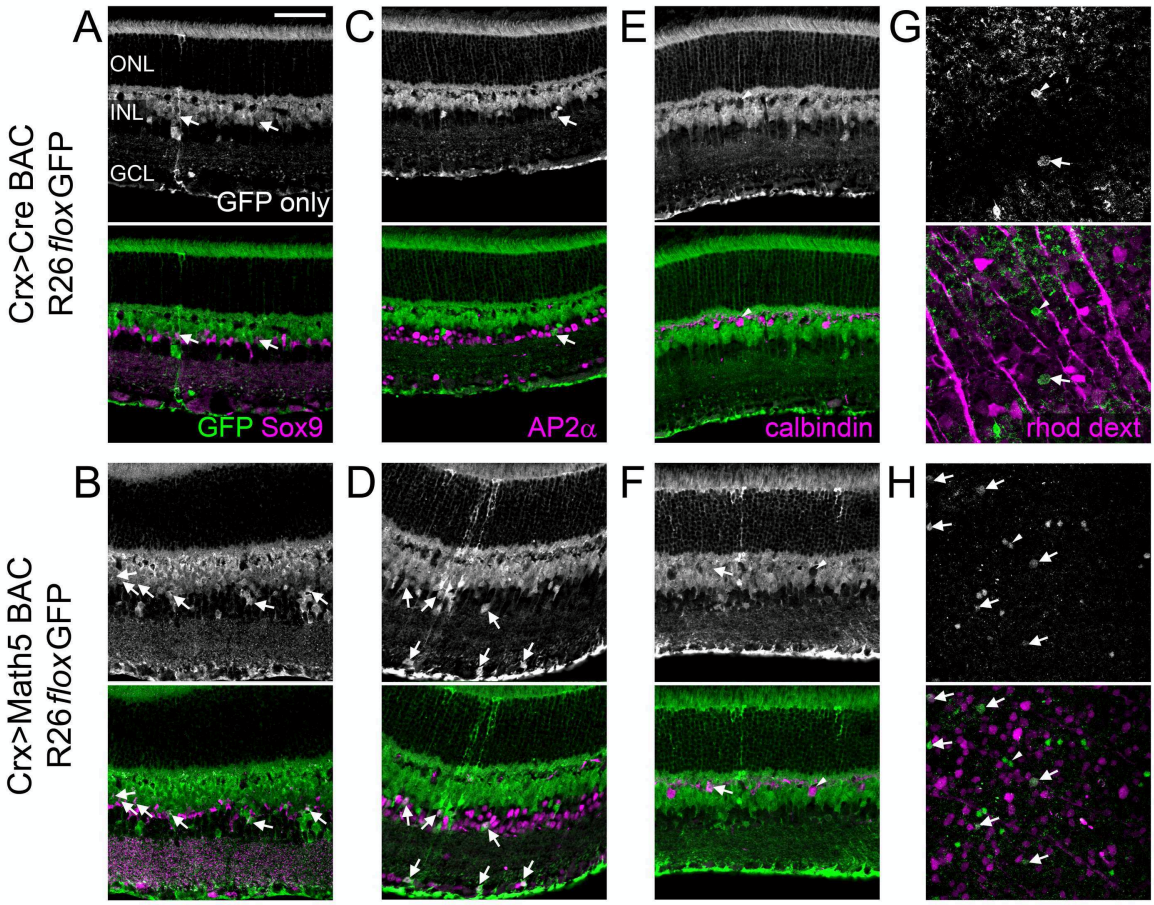

Figure V-3. Widespread Crx>Math5 expression has little effect on cell fate decisions in the retina**.** (A-F) Sections from adult Crx>Math5-IRES-Cre BAC (shortened as Crx>Math5 BAC) or matched Crx>Cre BAC control transgenic mice carrying R26floxGFP reporters were coimmunostained with GFP and informative markers. GFP and marker costaining (bottom) and GFP alone (top) are indicated (arrows). Müller glia were identified by Sox9 (A,B), amacrines by AP2α (C,D) and horizontal neurons by calbindin (E,F). Arrowheads in E and F mark calbindin+ horizontal cells that are GFP–. (H-I) Flatmounts of adult Crx>Math5 BAC and Crx>Cre BAC retinas with rhodamine dextran labeled RGCs. Some lineage-marked RGCs (arrows) and displaced amacrine cells (arrowheads) are indicated. While both transgenes mark essentially all photoreceptors and bipolar cells (Fig. V-S2), a small fraction of other cell types was also labeled in each case. The fate spectra are similar, with or without Math5. Rare horizontal cells were labeled in Crx>Math5 BAC Tg mice, but not in Crx>Cre BAC Tg controls, most likely due to differences in transgene expression level. Scale bar, 50 μm.

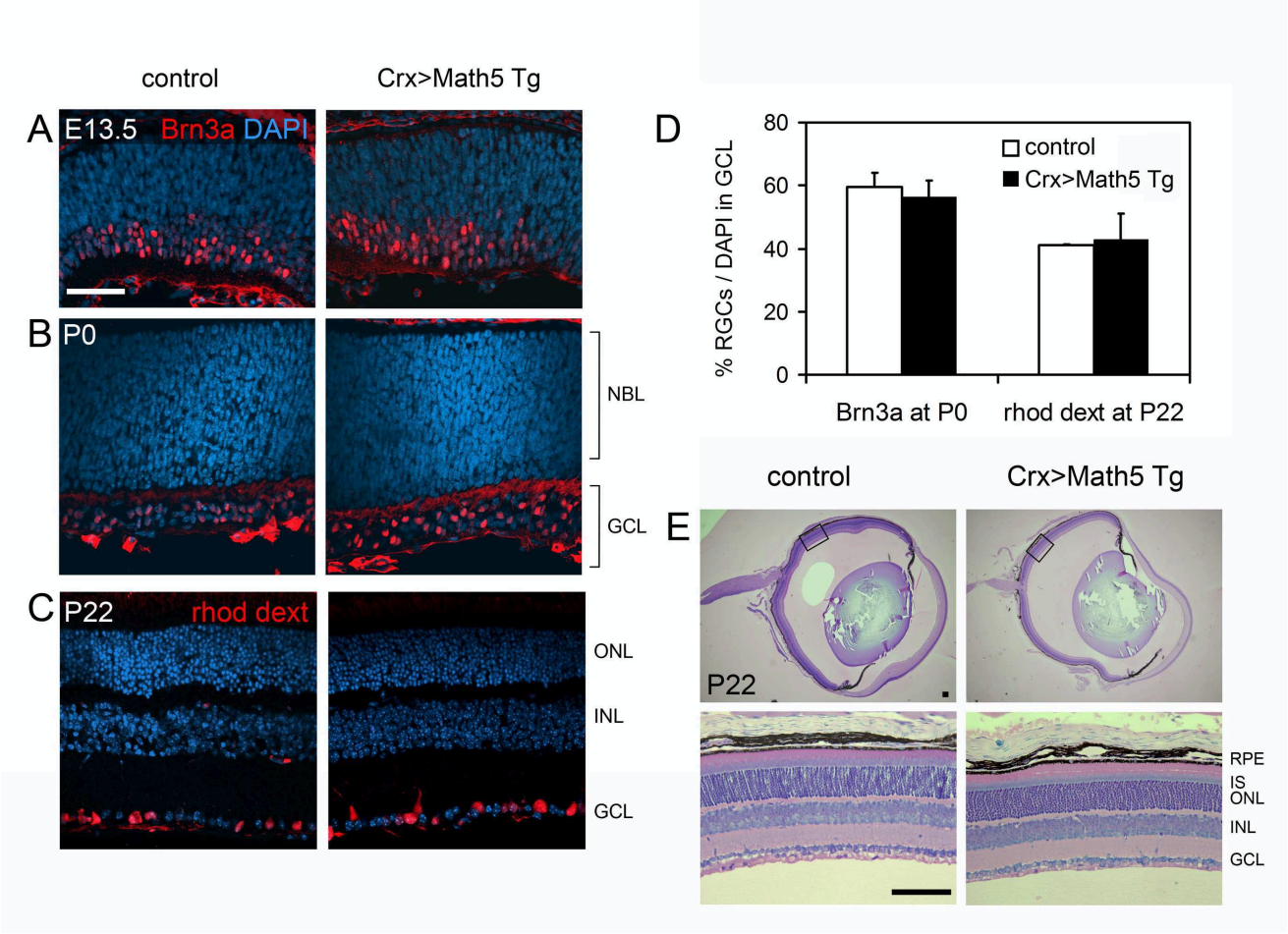

Figure V-4. Widespread Crx>Math5 expression does not alter RGC abundance or retinal histology. (A-C) Sections from E13.5 (A), P0 (B) and P22 (C) control or Crx>Math5-IRES2-Cre transgenic (Crx>Math5 Tg) retinas stained for Brn3a (A,B) or rhodamine dextran (C) to mark RGCs, and counterstained with DAPI to mark nuclei. (D) RGC fraction among GCL neurons at P0 and P22. There is no significant difference in the RGC fraction between transgenic (Tg) and contol retinas. (E) Low (top) and high (bottom) magnification views of basic fuchsin- and methylene blue-stained plastic sections. The retinal histology is similar in Crx>Math5 Tg and control mice. Scale bar: 50 µm in A-C; 100 µm in E.

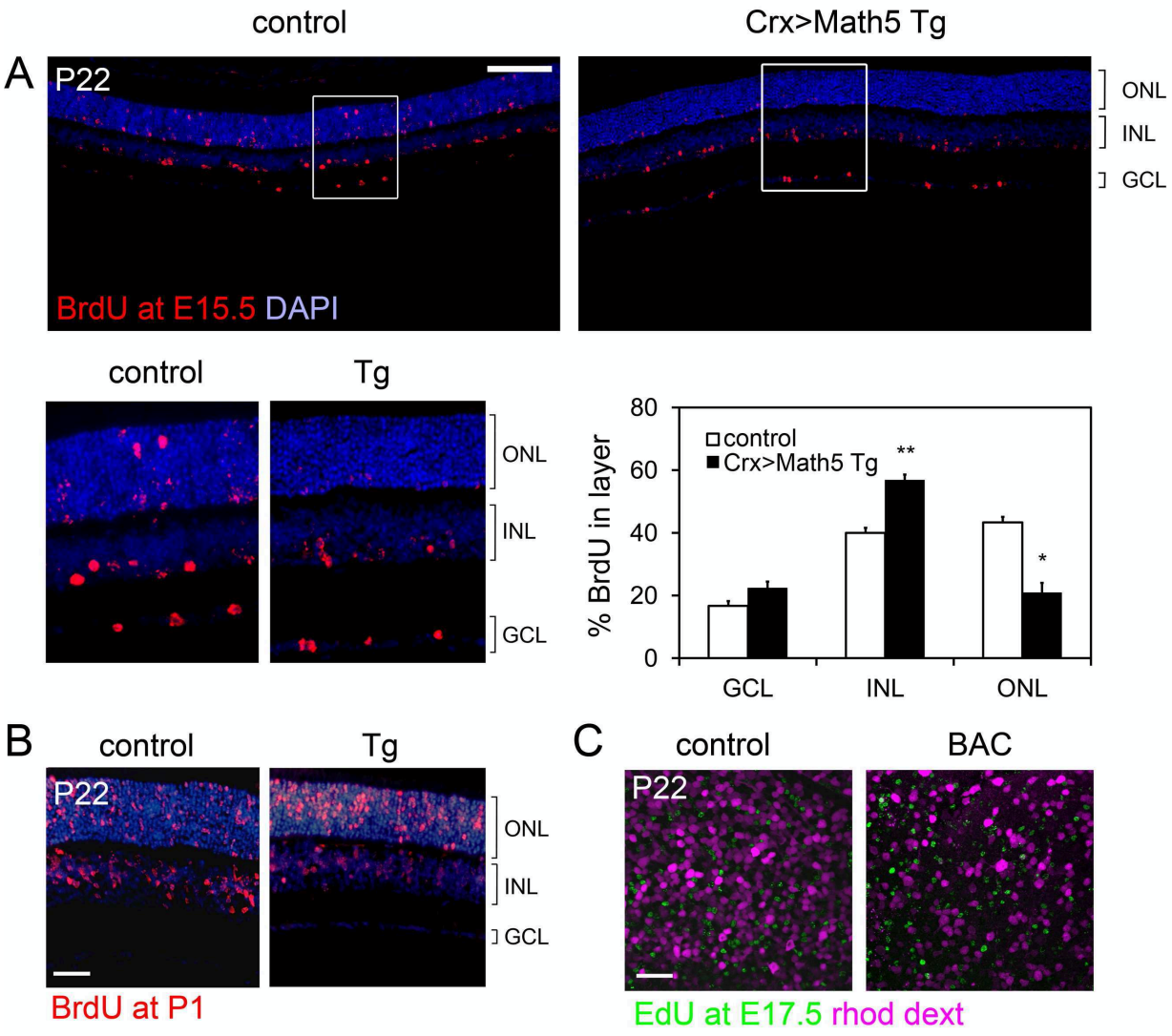

Figure V-5. Widespread Crx>Math5 expression does not extend the profile of RGC births, but decreases the numbers of early-born photoreceptors. (A) Birthdating of Crx>Math5-IRES-Cre transgenic (Crx>Math5 Tg) and littermate control retinas. Embryos were exposed to BrdU at E15.5 and analyzed at P22. There were 2-fold fewer E15.5 birthdated cells in the ONL (photoreceptors) of Crx>Math5 transgenic animals compared to controls, and corresponding increases in the INL and GCL. (B) Crx>Math5 Tg pups were similarly exposed to BrdU at P1 and harvested at P22. Few, if any, GCL cells were labeled with BrdU in transgenic or control mice. (C) Crx>Math5-IRES-Cre BAC (BAC) embryos were exposed to EdU at E17.5, and their RGCs were labeled with rhodamine dextran at P22. No EdU+ RGCs were detected in central flatmounts of BAC or control retinas. Prolonged transgenic expression of *Math5* does not extend the RGC birthdating profile. Scale bar: 100 µm in A-B; 50 µm in C.

Figure V-6. Retroviral *Math5* overexpression does not stimulate RGC fate or cell cycle exit in retinal explant cultures. (A) Experimental design. Retinas were explanted from E13.5 embryos, flattened on polycarbonate membranes, infected at low density with the indicated MSCV retrovirus, and cultured for 7 days *in vitro* (DIV). Isolated GFP+ clones were scored for RGC number by Brn3a immunoreactivity and clone size. (B-C) Example clones from explants infected with IRES-GFP (B) or Math5-IRES-GFP (C) retroviruses. (D) Plot showing the fraction of GFP+ cells that developed as Brn3a+ RGCs in transduced explants. There was no significant difference in the RGC fraction of explants transduced with Math5-IRES-GFP or IRES-GFP control. A modest increase in RGCs was observed when Notch signaling was autonomously blocked in clones with the IRES-dnMAML virus. Error bars show binomial standard deviation. (E) Clone size distribution. There was no difference between Math5-IRES-GFP and IRES-GFP explants, but clone size was significantly reduced in explants infected with IRES-dnMAM. Scale bar, 50 μm.

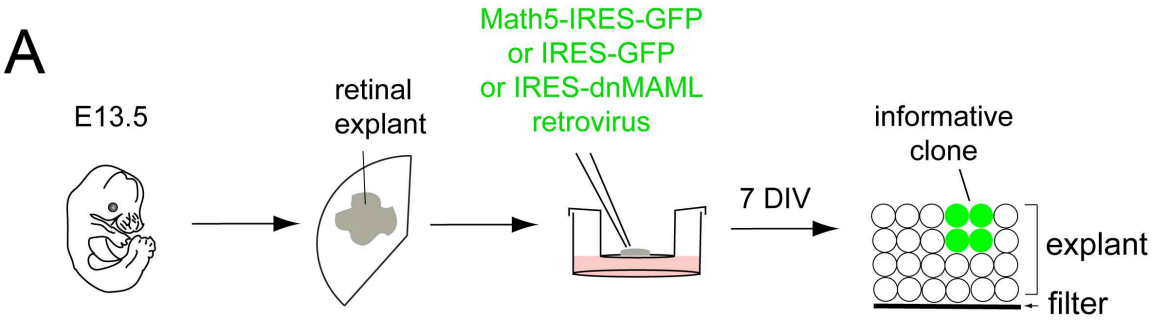
A
E13.5
retinal
explant
Math5-IRES-GFP
or IRES-GFP
or IRES-dnMAML
retrovirus
7 DIV
informative
clone
explant
filter

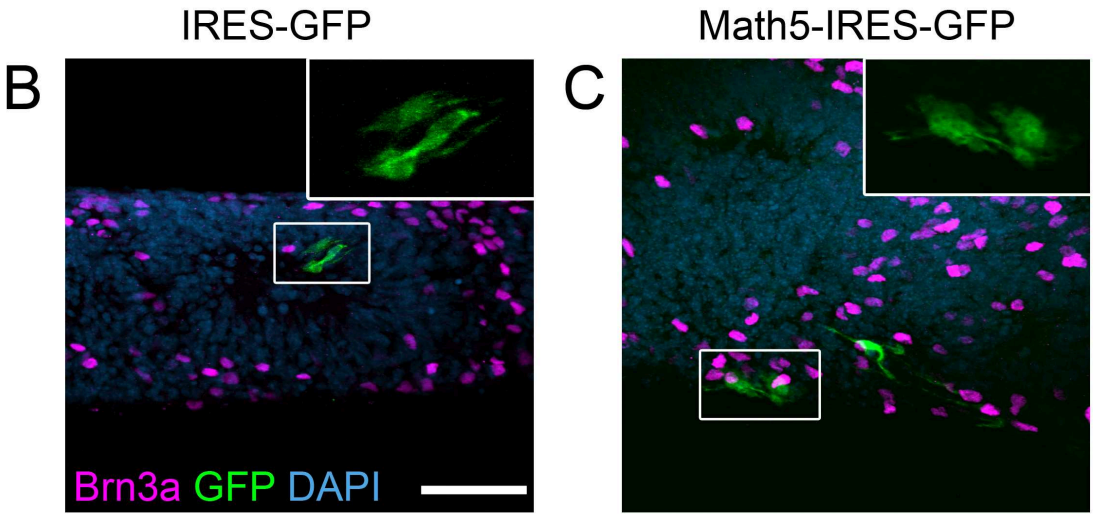
IRES-GFP
Math5-IRES-GFP
B
C
Brn3a GFP DAPI

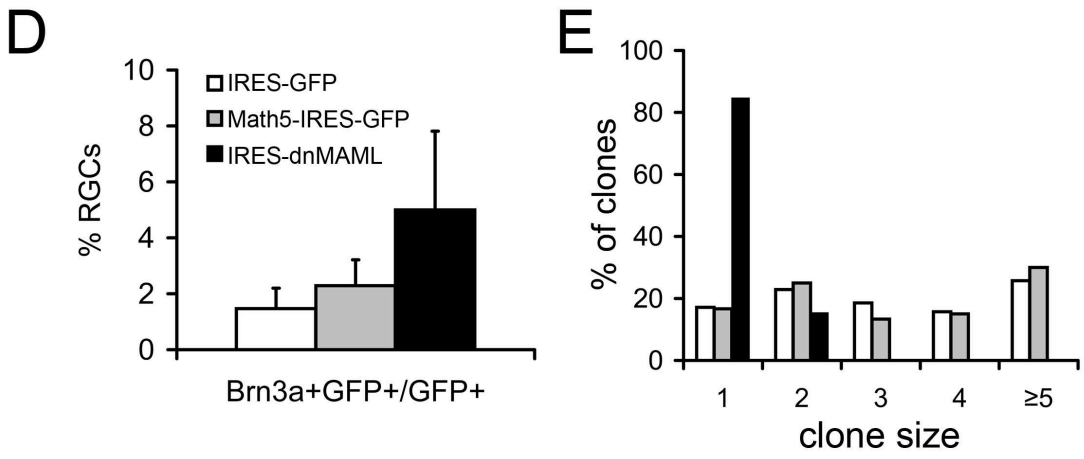
D
E
IRES-GFP
Math5-IRES-GFP
IRES-dnMAML
% RGCs
Brn3a+GFP+/GFP+
% of clones
clone size

Figure V-7. Crx>Math5 expression partially rescues RGC fate specification and optic nerve development in *Math5* knockout (KO) mice. (A-C) Flatmounts of adult retinas from the indicated genotypes stained for TuJ1 (A, B) to mark axons, and Brn3a (C) to mark cell bodies of mature RGCs. In *Math5* heterozygous mice (het), RGC axons fasciculate and project to the optic disc (OD), and their cell bodies are reactive for Brn3a. In *Math5* KO mice, RGC axons are very sparse, meander and do not fasciculate, and their cell bodies not express Brn3a; and the presumptive optic disc (POD) is not fully developed. The Crx>Math5 Tg – and to a much lesser extent Crx>Math5 BAC – transgene is able to partially rescue RGC density (Brn3a+), pathfinding and fasciculation defects in *Math5* KO mice. (D) Sections from adult retinas of the indicated genotypes, stained for GFP and Brn3a. In heterozygous mice, the Crx>Math5 Tg marks ~40% of the Brn3a+ RGC population. In contrast, rescued Brn3a+ RGCs derive exclusively from the Crx>Math5 Tg lineage (arrows). (E) Optic nerves of adult *Math5* het and Crx>Math5 Tg; *Math5* KO mice, stained with H+E. The rescued nerve is much thinner than the control. (F) Birthdating transgenic and control *Math5* KO retinas. Pups were exposed to a pulse of BrdU at P1 and harvested at P22. Few, if any, GCL cells were labeled with BrdU in either genotype, indicating that rescued RGCs are born prior to P1. P, proximal; D, distal. Scale bar, 50 μm.

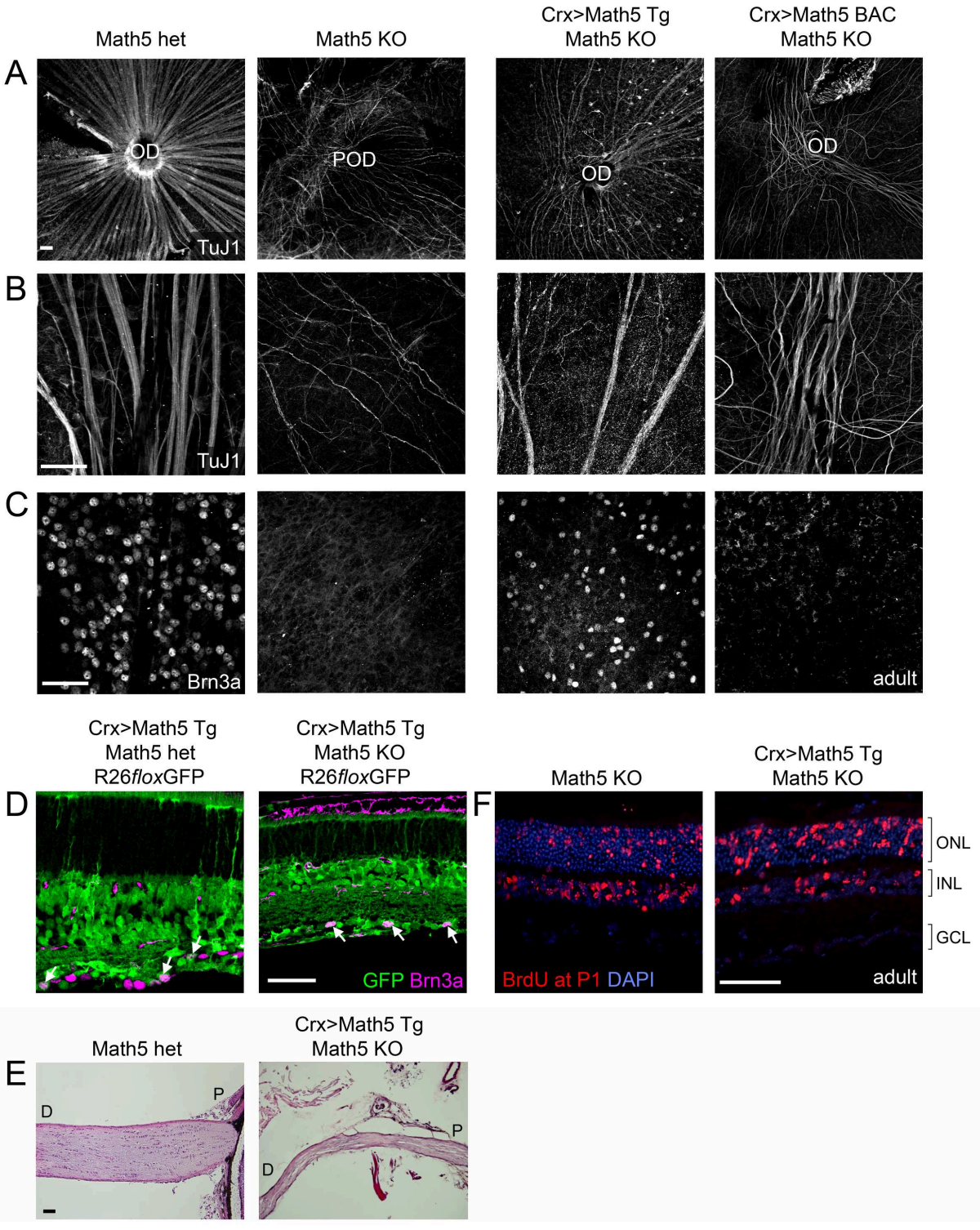
Math5 het
Math5 KO
Crx>Math5 Tg
Math5 KO
Crx>Math5 BAC
Math5 KO
A
OD
POD
OD
OD
TuJ1
B
TuJ1
C
Brn3a
adult
Crx>Math5 Tg
Math5 het
R26floxGFP
Crx>Math5 Tg
Math5 KO
R26floxGFP
D
GFP Brn3a
F
Math5 KO
Crx>Math5 Tg
Math5 KO
ONL
INL
GCL
BrdU at P1 DAPI
adult
Math5 het
Crx>Math5 Tg
Math5 KO
E
D
P
D
P

Figure V-8. RGC birthdates in transgenic, *Math5* KO and rescued animals. Embryos with the four indicated genotypes were exposed to a single pulse of EdU at E11 and E12, E13.5, E15.5 or E17.5, and are compared as littermates. (A-D) GCL confocal views of P1 birthdated retinal flatmounts, stained for Brn3a (magenta) and EdU (green). (E) RGC birthdating curves for each genotype. No Brn3a+ RGC births were detected in any genotype after E17. The overall number of RGC births is substantially reduced in *Math5* KO and Crx>Math5 Tg (Tg) rescued mice. (F) Normalized RGC birthdating curves for each genotype. Because virtually all RGCs are born between E11 and E17, the total number of RGCs was summed across the 4 time points for each genotype, and the RGC birth fraction at each time is plotted relative to this total. The normalized curves are quite similar. However, very few, if any, Brn3a+ RGCs were born during early neurogenesis (E11-E12) in *Math5* knockout (KO) or rescued (Tg; *Math5* KO) mice. In the rescued mice, a larger fraction of RGCs were born during mid-gestation (E15.5). (G) Brn3a+ RGC density jitter plots for each genotype. Each data point represents a single eye. The Crx>Math5 transgene (Tg) partially rescues the RGC deficiency in *Math5* KO mice, which have significantly more Brn3a+ RGCs than *Math5* KO controls, although this effect is variable. The Crx>Math5 Tg does not significantly affect RGC density in heterozygotes. Scale bar, 50 μm.

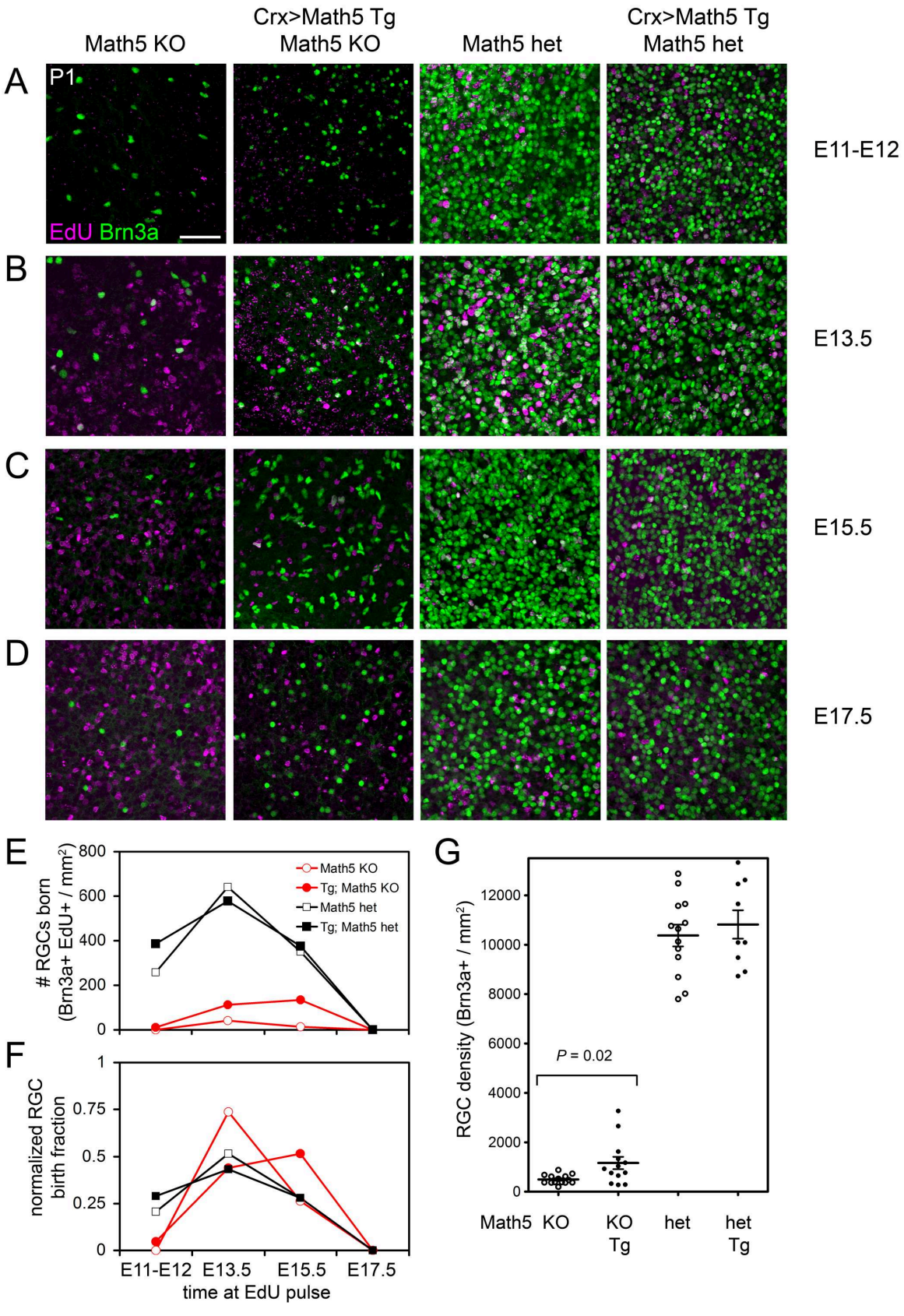
Math5 KO
Crx>Math5 Tg
Math5 KO
Math5 het
Crx>Math5 Tg
Math5 het
A
P1
EdU Brn3a
E11-E12
B
E13.5
C
E15.5
D
E17.5
E
RGCs born
(Brn3a+ EdU+ / mm²)
800
600
400
200
0
Math5 KO
Tg; Math5 KO
Math5 het
Tg; Math5 het
F
normalized RGC
birth fraction
1
0.75
0.5
0.25
0
E11-E12
E13.5
E15.5
E17.5
time at EdU pulse
G
RGC density (Brn3a+ / mm²)
12000
10000
8000
6000
4000
2000
0
P = 0.02
Math5 KO
KO Tg
het
het Tg

Figure V-9. Survival and generation of late-born RGCs are inhibited in rescued animals. (A-B) βIII-tubulin (TuJ1) staining of rescued (Crx>Math5 Tg; *Math5* KO) rescued retinas at E15.5 and E17, compared to *Math5* heterozygous littermates (het, A,C) or *Math5* wild-type (WT) control (E17.5, B). *Math5* KO (left) retinas form a nerve fiber layer, but there is no clear coalescence of axons into an optic nerve. Crx>Math5 Tg rescued retinas have thin optic nerves, and these occasionally form axon knots in the optic stalk (arrowhead, inset). (C-D) Rescued and control sections stained for cleaved Caspase-3 (arrows) at E16.5 to mark apoptotic cells. Dying cells primarily reside in the forming ganglion cell layer. Crx>Math5 Tg rescued animals (Tg; KO) exhibit increased levels of apoptosis as compared to *Math5* KO mice, which have much higher levels of cell death than heterozygous animals. (E) TuJ1 staining of E15.5 Crx>Math5 BAC; *Math5* KO mice, shows partial rescue of optic nerve development and the appearance of a similar RGC axon knot (arrowhead). Scale bar, 50 μm.

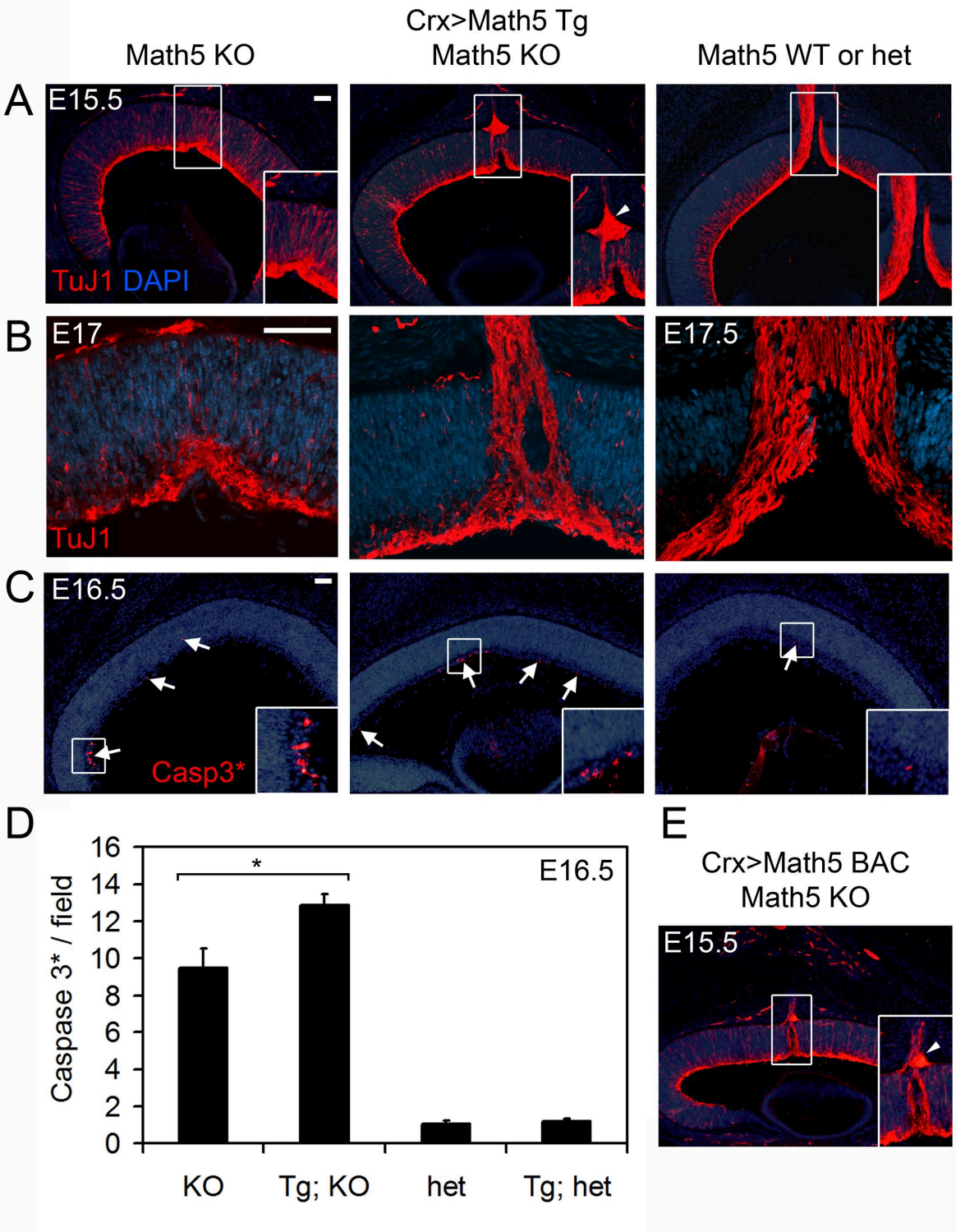
Math5 KO
Crx>Math5 Tg
Math5 KO
Math5 WT or het
A
E15.5
TuJ1 DAPI
B
E17
TuJ1
E17.5
C
E16.5
Casp3*
D
E16.5
Caspase 3* / field
16
14
12
10
8
6
4
2
0
*
KO
Tg; KO
het
Tg; het
E
Crx>Math5 BAC
Math5 KO
E15.5

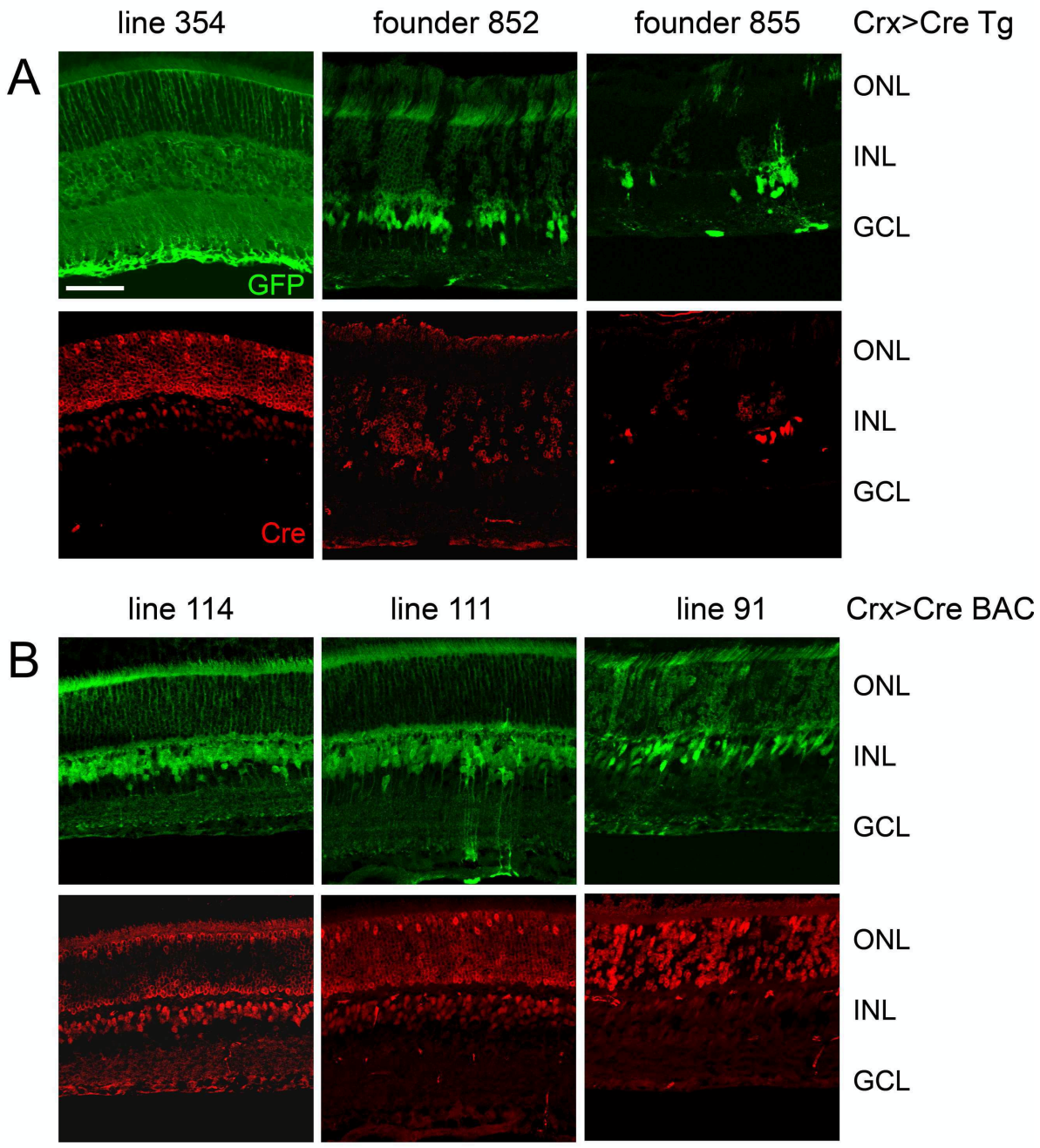

Figure V-S1. Consistent retinal expression patterns for multiple, independent Crx>Cre Tg and Crx>Cre BAC transgene insertions. Adult retinas from founders or offspring carrying the R26floxGFP reporter were immunostained for GFP and Cre. Although each transgenic line gave a similar pattern, some expression was variegated due to mosaicism (Crx>Cre Tg founder 852 and 855) or epigenetic silencing (Crx>Cre BAC line 91). (A) In conventional Crx>Cre Tg mice, Cre is confined to photoreceptors and bipolar cells, while GFP is evident in every retinal layer. (B) In Crx>Cre BAC mice, Cre and GFP are restricted to the ONL and outer INL, with occasional stripes of GFP+ cells (line 111). ONL, outer nuclear layer; INL, inner nuclear layer; GCL, ganglion cell layer. Scale bar, 50 µm.

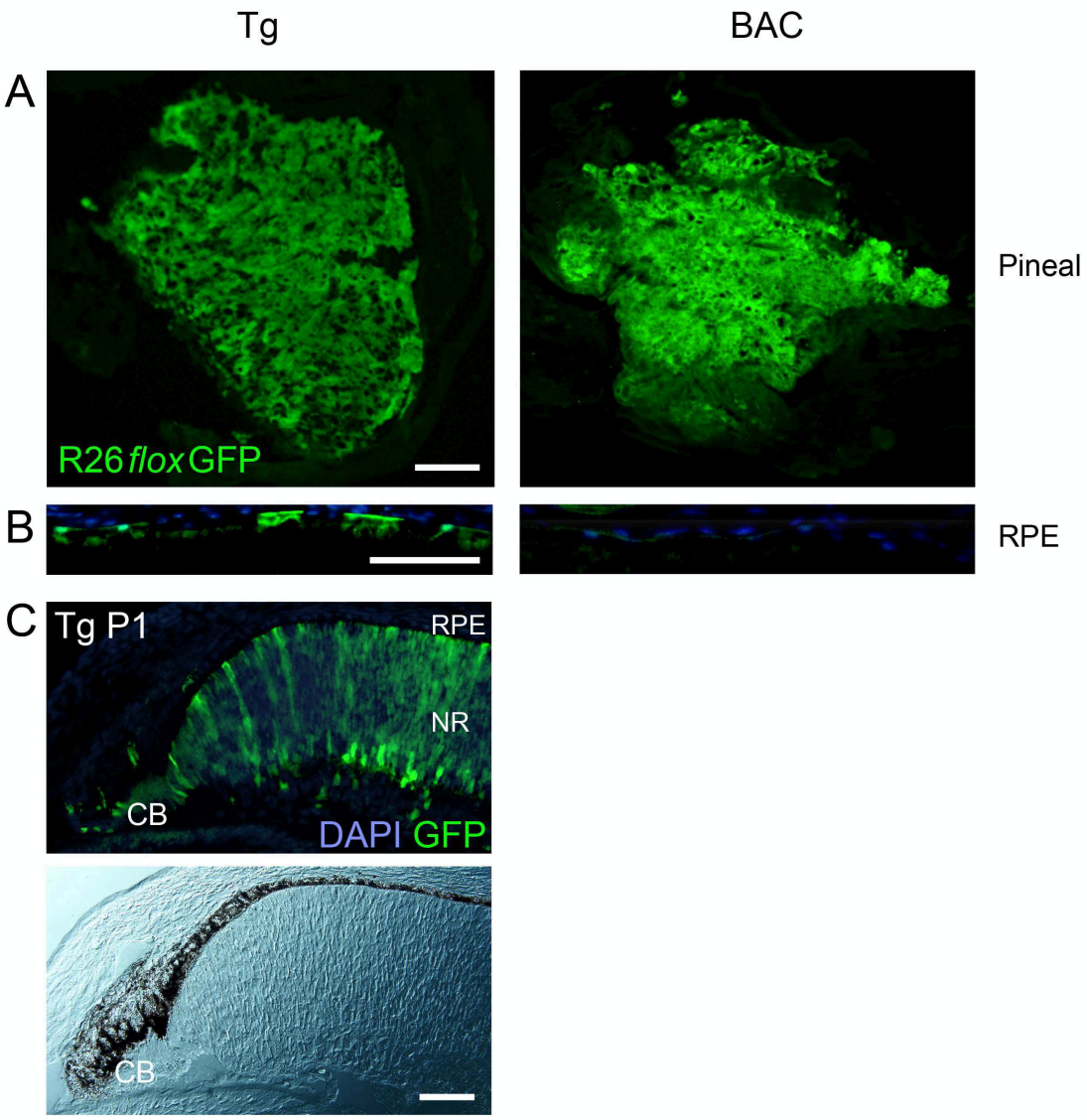

Figure V-S2. Crx transgenic and BAC expression patterns in the pineal gland, retinal pigmented epithelium, and ciliary body. (A) Pineal gland sections from Crx>Math5 Tg and Crx>Math5 BAC mice stained for R26*flox*GFP reporter expression. GFP is evident in the pineal gland, but absent in surrounding connective tissue. (B) Sections of adult retinal pigmented epithelium (RPE) from transgenic mice stained for the GFP reporter. Although the signal is partially obscured by melanin, GFP is abundant in conventional, but not in BAC transgenic mice. (C) Immunofluorescence (top) and differential interference contrast (bottom) images of P1 peripheral retina from a Crx>Math5 Tg; R26*flox*GFP pup. GFP expression was apparent in both pigmented and unpigmented ciliary body (CB) epithelial cells. NR, neural retina.
Scale bar, 50 µm.

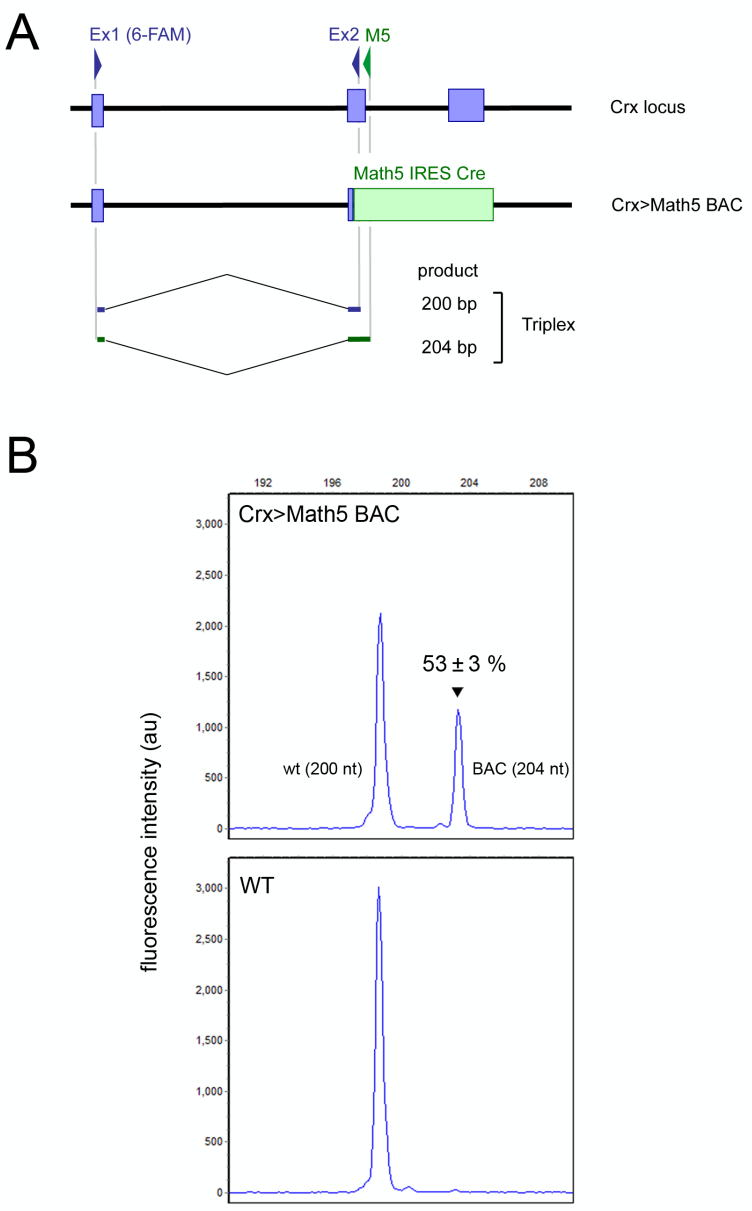

Figure V-S3. Direct comparison of Crx>Math5 BAC and endogenous *Crx* transcript levels. (A) Diagram of the triplex competitive RT-PCR strategy. Primers and expected product sizes are shown within the *Crx* locus and Crx>Math5 BAC. A common forward primer labeled with 6-FAM (Ex1) was used in the PCR. Reverse primers in *Crx* exon 2 (Ex2) or in *Math5* (M5) were used in an equal molar ratio. (B) Capillary electrophoresis profiles of triplex competitive PCR products amplified from Crx>Math5 BAC (top) or wild-type (WT, bottom) adult retinal RNA templates. In Crx>Math5 BAC retinas (n = 5), the molar ratio of transgenic *Math5* and endogenous *Crx* transcripts, inferred from the ratio of PCR products, was 53±3%, consistent with single-copy expression. This value (k) was used to normalize qRT-PCR measurements (Fig. V-2D).

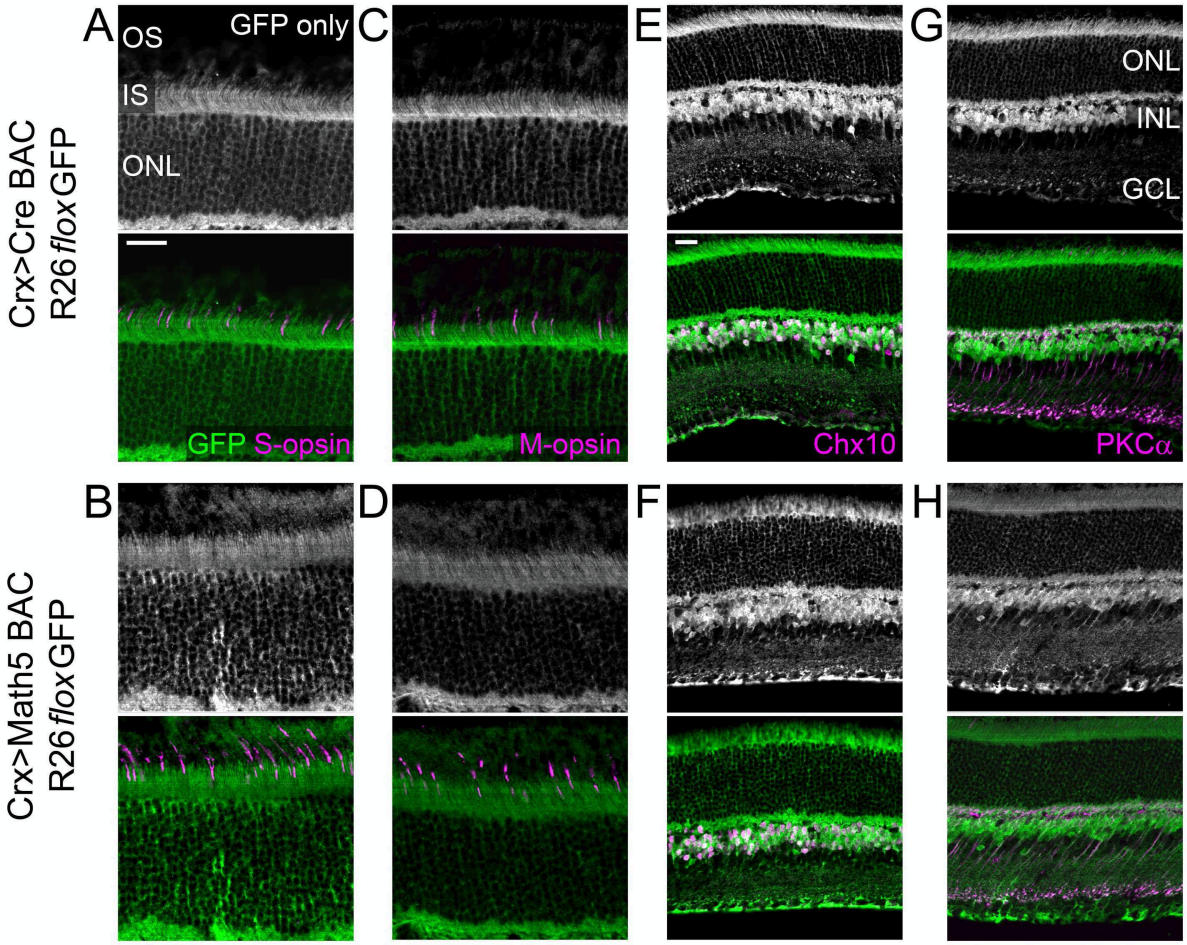

Figure V-S4. Math5 does not grossly alter secondary fate choices of photoreceptors and bipolar cells. (A-H) Sections from adult Crx>Math5-IRES-Cre BAC (Crx>Math5 BAC) or matched Crx>Cre BAC control transgenic (Crx>Cre BAC) mice carrying the R26*flox*GFP reporter were coimmunostained for GFP and indicated photoreceptor or bipolar marker. In the ONL, cone subtypes were identified by M- or S-opsin staining, and rods by the absence of staining (A-D). In the INL, bipolar cells were identified by Chx10 staining (E-F), and rod bipolar subtypes were identified by PKC staining (G-H). Virtually all photoreceptors and bipolar cells are contained within the *Crx* lineage (GFP+). There is no apparent difference in the distribution of these subtypes between transgenes. Scale bar, 50 μm.

Figure V-S5. Cell fate spectrum of the conventional Crx>Math5 transgene. Adult Crx>Math5 Tg; R26*flox*GFP eyes were immunostained for GFP and cell type specific markers. Descendants of Crx>Math5 Tg expressing cells contribute to all major cell types, including Müller glia (A, Sox9), amacrines (B, syntaxin), horizontal neurons (C, calbindin), RGCs (D, retrograde rhodamine dextran labeling), bipolar cells (E, Chx10), rods (F, rhodopsin) and cones (G, mCar). Some examples of double-positive cells are marked by arrows. Scale bars, 50 μm.

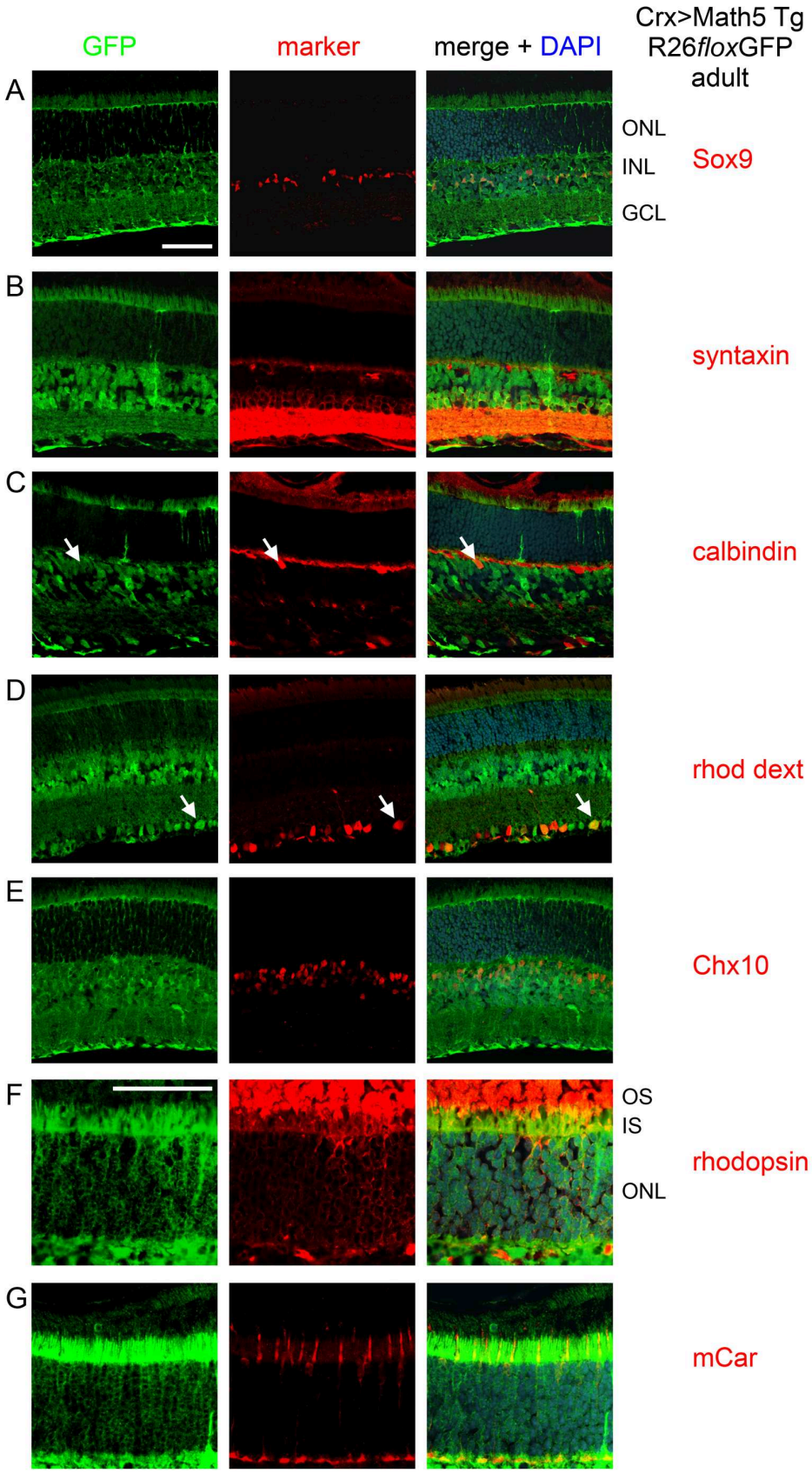
GFP
marker
merge + DAPI
Crx>Math5 Tg
R26floxGFP
adult
A
ONL
INL
GCL
Sox9
B
syntaxin
C
calbindin
D
rhod dext
E
Chx10
F
OS
IS
ONL
rhodopsin
G
mCar

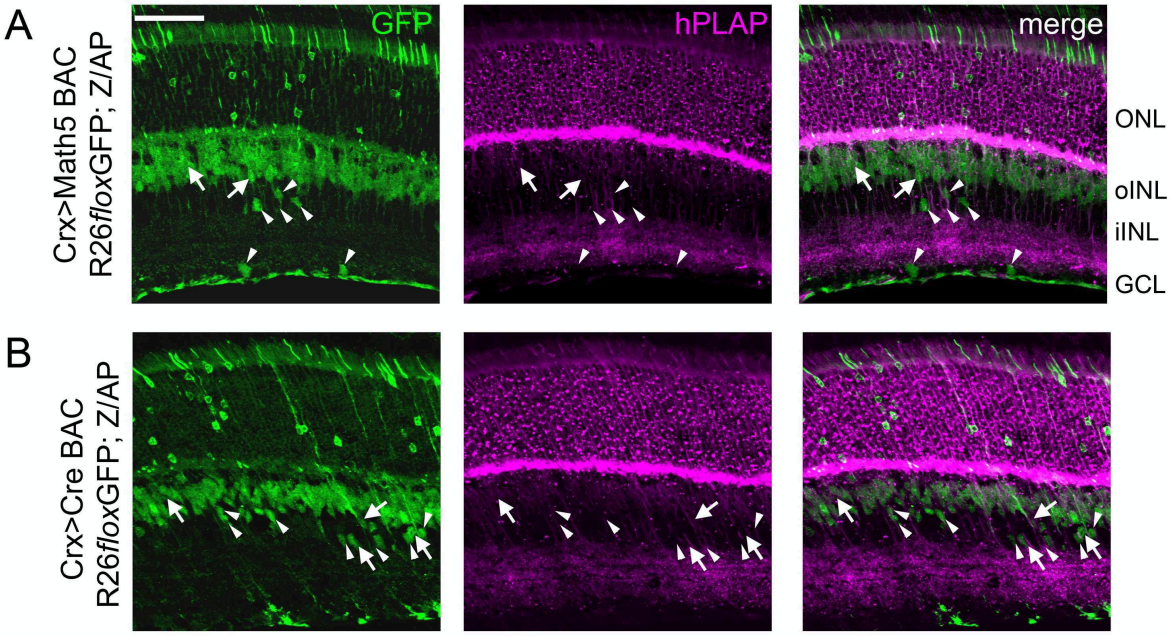

Figure V-S6. Dual-reporter concordance experiment. (A-B) Lineage analysis was performed in Crx>Math5-IRES-Cre BAC (A) or Crx>Cre BAC (B) mice carrying both Z/AP and R26*flox*GFP reporters. In photoreceptors and bipolar cells, the concordance between reporters is nearly 100%, suggesting that these cell types express high levels of Cre. In other cell types, the concordance is low (<40%), as few cells express GFP and PLAP (arrows). Instead, most lineage-marked cells in the GCL or inner INL express a single reporter (arrowheads). The labeling of these cell types in the adult retina (Fig. V-3 and Fig. V-S5) can thus be attributed to low-level or leaky Cre expression. oONL, outer half of the inner nuclear layer (bipolar domain); iINL, inner half of the inner nuclear layer (amacrine domain). Scale bar, 50 µm.

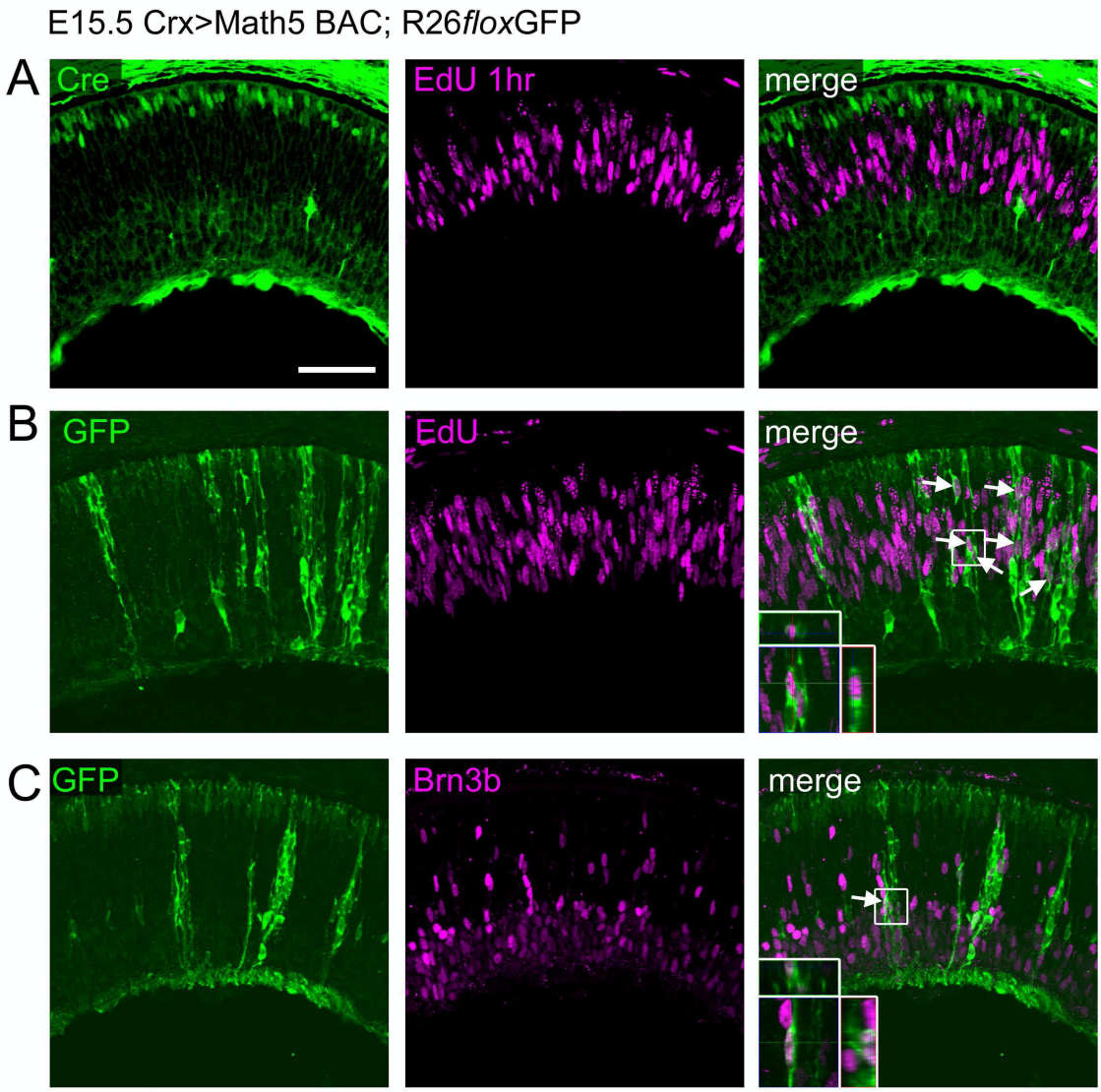

Figure V-S7. The Crx>Math5 BAC transgene is expressed at low levels in proliferative retinal progenitors. E15.5 Crx>Math5 BAC; R26*flox*GFP embryos were pulsed with EdU for 1 hr and costained for the indicated markers. (A) Projection images of 10 µm optical sections show that all Cre+ cells were EdU– indicating that Cre is not expressed at high levels during S-phase. (B) In contrast, many GFP+ stripes contain EdU+ cells (arrows, inset), consistent with stochastic Cre expression in proliferating RPCs. (C) A small number of Brn3b+ RGCs were identified among clustered GFP+ cells (arrow, inset). Scale bar, 50 µm.

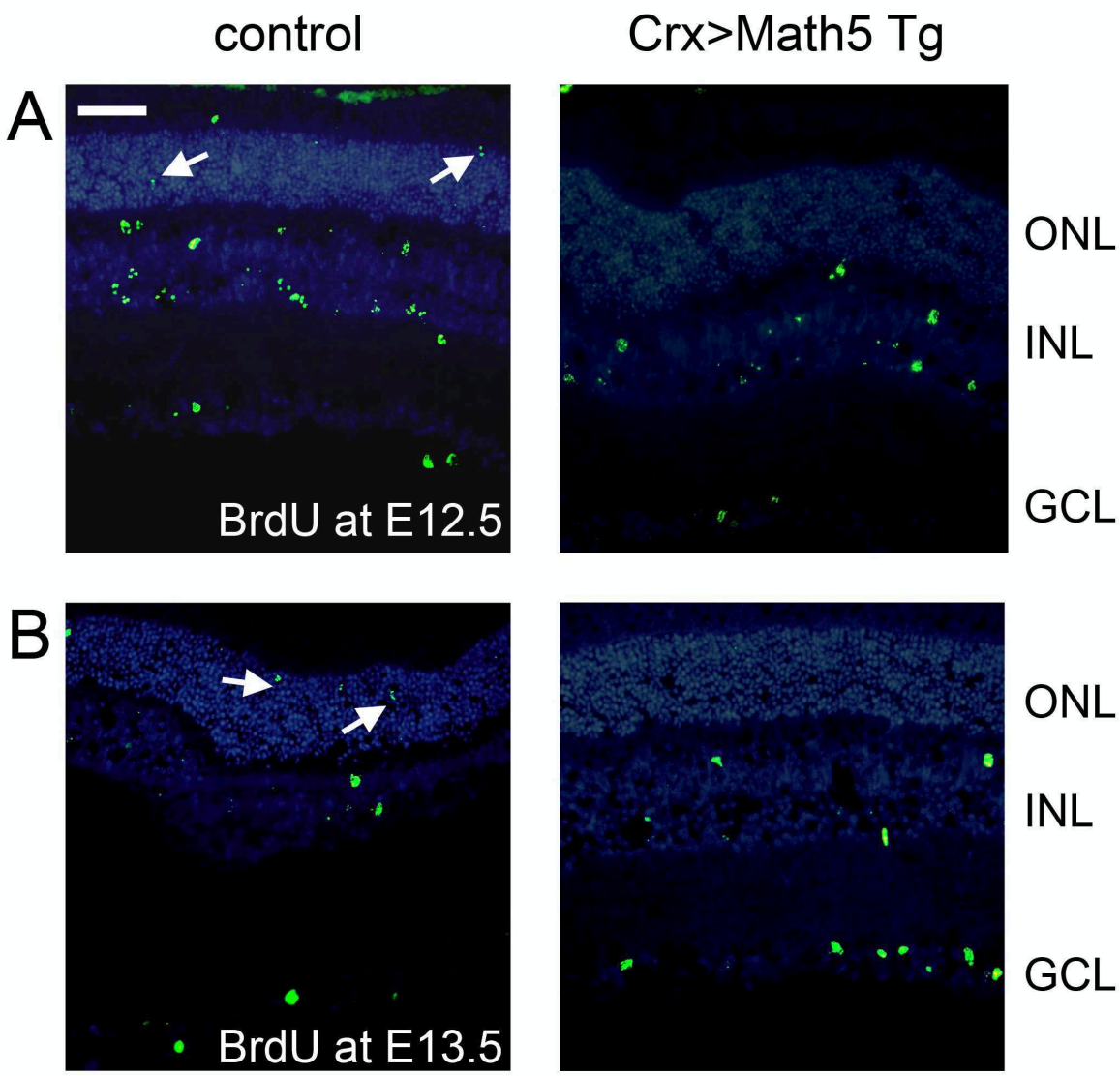

Figure V-S8. Reduced photoreceptor births at E12.5 and E13.5 in Crx>Math5 Tg mice. Retinal sections from adult Crx>Math5 Tg and control mice exposed to a single BrdU pulse at E12.5 (A) or E13.5 (B) were stained with anti-BrdU and DAPI. Few strongly BrdU+ ONL cells are evident in Crx>Math5 Tg mice, but these are apparent in control mice. Scale bar, 50 µm.

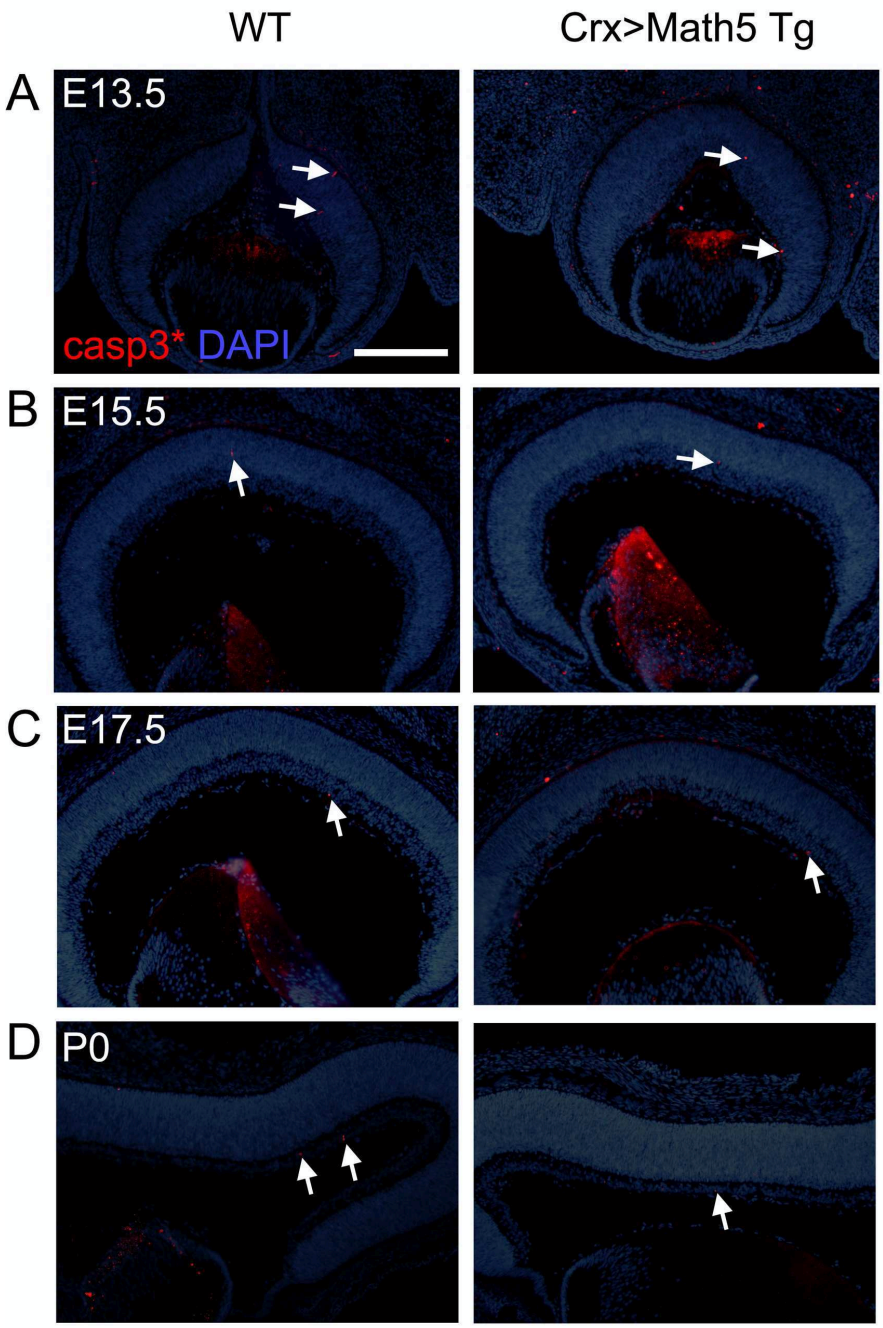

Figure V-S9. Crx>Math5 Tg mice and control mice exhibit similar levels of apoptosis throughout development. (A-D) Sections from E13.5, E15.5, E17.5 or P0 Crx>Math5 transgenic (Tg) mice or control littermates were stained with DAPI and an antibody to cleaved Caspase-3 to identify apoptotic cells (arrows). Scale bar, 200 µm.

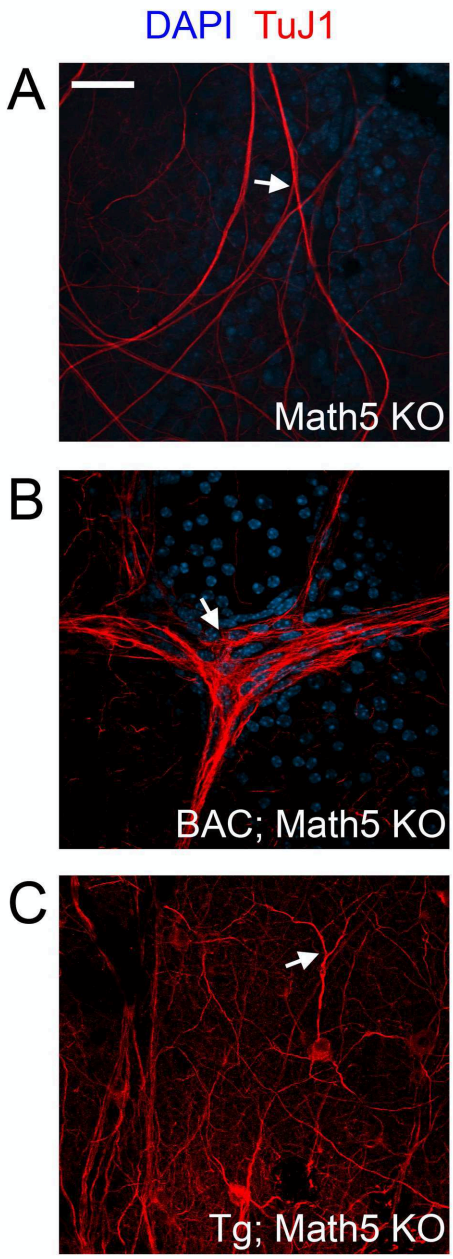

Figure V-S10. RGC axons in *Math5* KO and transgene-rescued mice exhibit severe pathfinding defects. (A-C) Confocal Z-stack projections through the ganglion cell and nerve fiber layers of retinal flatmounts from adult *Math5* KO (A), Crx>Math5 BAC; *Math5* KO (B), and Crx>Math5 Tg; *Math5* KO (C) mice. Axons marked by TuJ1 antigen exhibit severe pathfinding defects (arrows), including branched axon bundles and individual axons, tangled fibers, and nonradial trajectories. Scale bar, 50 μm.

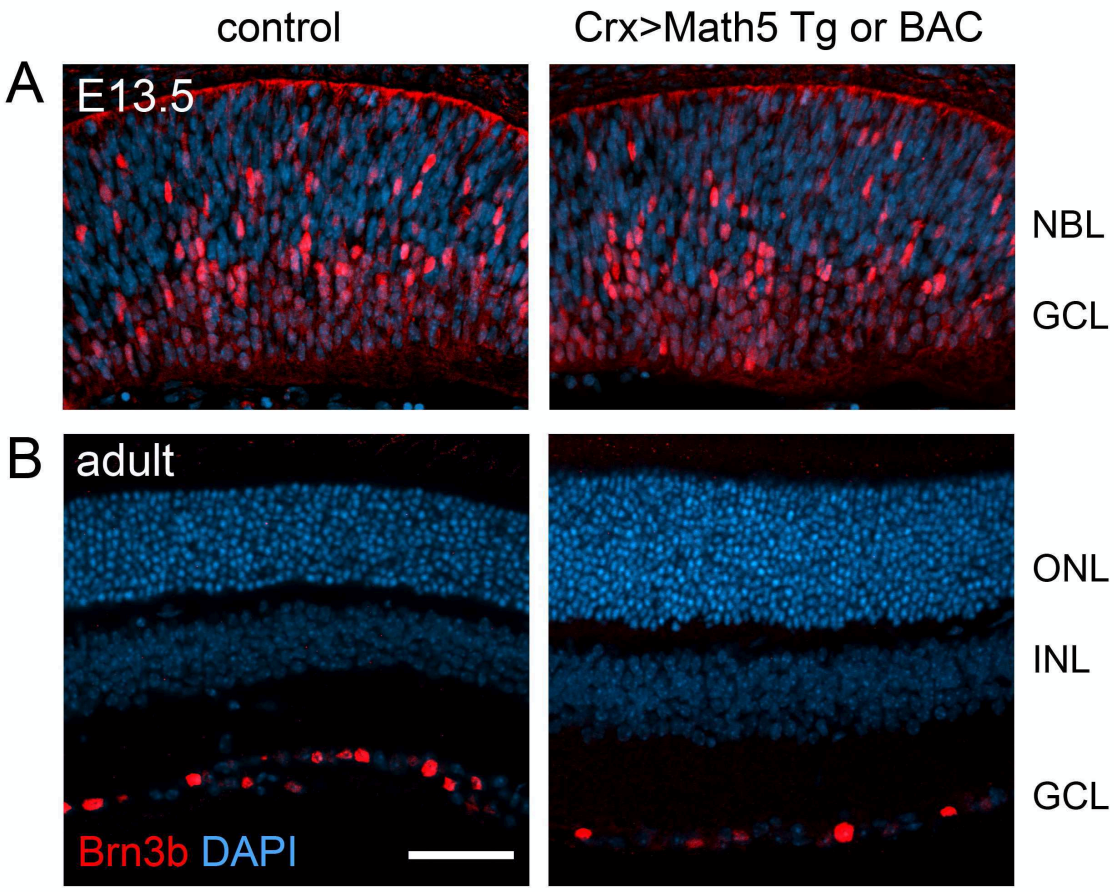

Figure V-S11. Brn3b expression in Crx>Math5 mice. (A) Tg and contol E13.5 embryonic retinas. The abundance of Brn3b+ cells is grossly similar in the two genotypes. (B) Crx>Math5 BAC and control adult retinas. There is no Brn3b immunoreactivity in the transgenic ONL and INL, where Crx>Math5 expression is abundant. Scale bar, 50 µm.

Table V-S1. Oligonucleotide primers and PCR conditions used in this study

Experiment	Forward (sense primer 5'→3')	Reverse (antisense primer)	Annealing temp[$]	Notes
ss oligo deletion for Tg[*]	TTCGAAACCTTTCTCTTCTTCTTTGGGCCCATGGTGAATTCGAAATAGGTCCCCTCACACGGGGCGACCT			
ss oligo deletion for BACs[*]	CCACAGTCTCTGAAGATCCTGTGATCTCGAAATTCACCATGGGCCCAAAGAAGAAGAGAAAGGTTTCGAA			
Crx Tg genotyping	ATACCGGAGATCATGCAAGCTGGT	CCAAACTGGAACAACACTCAACCC	55	1X Masteramp
Crx BAC genotyping	CTCTGTTCCTGCTTATTGGGG	GAGTCTGGGACATGTTCAGTT	56	
RT-PCR endogenous Math5	CGCCGCATGCAGGGGCTGAACACG	CCTCCTGAATGACGCTAGGA	60	
RT-PCR transgenic Math5	ATACCGGAGATCATGCAAGCTGGT	CCAAACTGGAACAACACTCAACCC	58	1X Masteramp
RT-PCR total Math5	CGCCGCATGCAGGGGCTGAACACG	GATTGAGTTTTCTCCCCTAAGACCC	60	
RT-PCR βactin	GCTCTTTTCCAGCCTTCCTT	GTACTTGCGCTCAGGAGGAG	58	N/A
triplex competitive RT-PCR[#]	CAGCCCAGGCTTAAAGTCG (Crx ex1)	GCCAAGGCATTGACTGAATAG (Crx ex2) GTTTGCAGGCCGACTTCATGG (Math5 Tg)	57	1X Masteramp

[*] **Single-stranded oligos were used to delete Math5 and IRES sequence by recombineering, to generate the Crx>Cre Tg, and the Crx>Cre BAC targetting construct**

[$] **All PCRs had an initial denaturation step (94°C x 3 min); followed by 40 cycles of 30-45 sec at 94°C for denaturation, 45-60 sec at the noted temperature for annealing, and 1 min at 72°C extension; with a final extension step (7 min at 72°C)**

[#] **These reactions were done using a three-primer PCR, with a common 6-FAM labeled forward primer and equal ratios of reverse primers.**

CHAPTER VI

ATOH7 MUTATIONS CAUSE AUTOSOMAL RECESSIVE PERSISTENT HYPERPLASIA OF THE PRIMARY VITREOUS

Abstract

The vertebrate basic helix-loop-helix (bHLH) transcription factor ATOH7 (Math5) is specifically expressed in the embryonic neural retina and required for genesis of retinal ganglion cells (RGC) and optic nerves. In *Atoh7* mutant mice, the absence of trophic factors secreted by RGCs prevents development of the intrinsic retinal vasculature and regression of fetal blood vessels, causing persistent hyperplasia of the primary vitreous (PHPV). We therefore screened patients with bilateral optic nerve aplasia (ONA) or hypoplasia (ONH), or hereditary PHPV, for mutations in *ATOH7*. We identified a homozygous *ATOH7* mutation (p.N46>H) in a large family with an autosomal recessive PHPV disease trait linked to 10q21, and a heterozygous variant (p.R65>G) in one of five sporadic ONA patients. High-density SNP analysis also revealed a CNTN4 duplication and an OTX2 deletion in the ONA cohort. Functional analysis of ATOH7 bHLH domain substitutions, by electrophoretic mobility shift and luciferase cotransfection assays, revealed that the N46H variant cannot bind DNA or activate transcription, consistent with structural modeling. The N46H variant also failed to rescue RGC development in mouse *Atoh7* -/- retinal

explants. The R65G variant retains all of these activities, similar to wild-type human ATOH7. Our results strongly suggest that arPHPV is caused by N46H and is etiologically related to congenital retinal nonattachment (NCRNA). The R65G allele, however, cannot explain the ONA phenotype. Our study firmly establishes *ATOH7* as a retinal disease gene and provides a functional basis to analyze new coding mutations.

Introduction

The vertebrate neural retina is a highly ordered laminar structure, which contains rod and cone photoreceptors, interneurons, specialized glia, and projection neurons (Rodieck, 1998). During development, these diverse cell types are generated in a fixed, but overlapping, temporal order from a pool of multipotent neuroepithelial progenitors (Livesey and Cepko, 2001). At the onset of retinal neurogenesis, on embryonic day E11 in mice and during the 5^{th} gestational week in humans, the first neurons exiting the cell cycle differentiate as retinal ganglion cells (RGCs). Their axons form the optic nerves, which relay all visual information to the brain.

The adult retina is nourished by two major vascular systems. The central retinal artery enters the eye along with the optic nerve and supplies the inner retina, while a tunic of choroidal vessels supplies the outer, photoreceptor layers (Fruttiger, 2002; Gariano and Gardner, 2005). The developing retina and lens primordia are perfused by a three-dimensional arterial plexus that branches from the central hyaloid artery as it emerges from the optic stalk. The hyaloid arcades

fill the vitreous and drain into annular vessels at the edge of the optic cup. During midgestation in humans and early neonatal life in mice, these hyaloid blood vessels and the associated pupillary membrane regress, and the central artery remodels to form a two-dimensional branching network that originates at the optic nerve head (Fruttiger, 2002; Gariano and Gardner, 2005). This vascular lattice spreads radially across the retinal surface along a scaffold of migrating astrocytes, which are activated by signals from nascent ganglion cells (Fruttiger et al., 1996). A second, concentric wave of vessels then branches from the surface plexus, penetrating to form two deep layers within the mature neural retina.

The development of retinal neurons is likewise controlled in tandem by intrinsic transcriptional programs and the microenvironment (Livesey and Cepko, 2001; Ohsawa and Kageyama, 2008; Yang, 2004). As an archetypal instrinsic factor, the basic helix-loop-helix (bHLH) nuclear protein Atoh7 (Math5) is transiently expressed in early retinal progenitors (Brown et al., 1998; Brzezinski et al., 2012) and is necessary for RGC fate specification. *Atoh7* -/- mice exhibit a profound deficiency of RGCs and lack optic nerves (Brown et al., 2001; Wang et al., 2001). In the absence of RGCs, the mature retinal vasculature fails to form. Consequently, the hyaloid (fetal) vessels persist, proliferate, and invade the inner retina (Brzezinski et al., 2003; Edwards et al., 2011). The structure, function, and spatiotemporal expression of Atoh7 have been highly conserved during metazoan evolution. *Atoh7* was initially identified by its homology to the invertebrate *atonal* (*ato*) and *lin32* genes (Brown et al., 1998; Brzezinski et al.,

2012), which are required to specify sensory neurons in *Drosophila* and *C. elegans*, respectively (Jarman et al., 1994; Zhao and Emmons, 1995). In zebrafish, a recessive missense mutation (*lakritz*) in the Atoh7 ortholog *ath5* causes agenesis of RGCs (Kay et al., 2001).

Congenital diseases of the optic nerve and retinal vasculature are important causes of blindness worldwide, and have some overlapping pathogenetic features. Optic nerve hypoplasia (ONH) is a common basis for visual impairment in children, in which the abundance of RGCs is significantly reduced. Few genetic causes have been identified (McCabe et al., 2011). ONH is recognized fundoscopically by small-sized optic discs, and may be associated with neurological or hypothalamic-pituitary dysfunction (Borchert and Garcia-Filion, 2008; McCabe et al., 2011). Optic nerve aplasia (ONA) is a much more severe and rare disorder, in which the optic nerves are essentially absent. Most ONA patients also have retinal vascular dysgenesis or posterior proliferation, and some have other ocular or neuroanatomical defects (Blanco et al., 1992; Brodsky et al., 2004; Lee et al., 1996; Scott et al., 1997). Retinovascular diseases such as familial exudative vitreoretinopathy (FEVR), retinopathy of prematurity (ROP), and persistent hyperplasia of the primary vitreous (PHPV), are likewise important causes of childhood blindness (Gariano and Gardner, 2005). In PHPV, the fetal hyaloid vessels fail to regress and continue to proliferate (Goldberg, 1997; Haddad et al., 1978; Reese, 1955; Shastry, 2009). This malformation is typically sporadic and unilateral, and increases the risk of retinal detachment (Pruett, 1975). PHPV can coexist with FEVR in some eyes. In FEVR, focal avascular or

dysplastic regions in the peripheral retina result from incomplete angiogenesis (Robitaille et al., 2009). Apart from FEVR mutations identified in Wnt pathway genes (Berger et al., 1992b; Warden et al., 2007), the majority of congenital retinovascular disease remains unexplained (Gariano and Gardner, 2005).

Given its unique expression pattern and direct role in RGC neurogenesis, and the importance of RGCs for blood vessel development, *ATOH7* mutations may contribute to the clinical spectrum of congenital optic nerve and retinovascular disease. Indeed, single-nucleotide polymorphisms (SNPs) in the *ATOH7* locus have been associated with quantitative variation in optic disc area among healthy individuals with no visual impairment (Khor et al., 2011; Macgregor et al., 2010; Ramdas et al., 2010), and a similar association has been reported for glaucoma disease susceptibility (Chen et al., 2012; Fan et al., 2011; Ramdas et al., 2011). We recently discovered a deletion spanning an upstream *ATOH7* transcriptional enhancer, which causes nonsyndromic congenital retinal nonattachment (NCRNA) in an Iranian Kurdish population (Ghiasvand et al., 2011). NCRNA patients lack optic nerves, similar to *Atoh7* -/- mice, and have clinical features that resemble PHPV. In two further studies, *ATOH7* point mutations were described in patients with ONH or vitreoretinal dysplasia, and may contribute to disease pathogenesis (Khan et al., 2011; Macgregor et al., 2010).

We have examined the role of *ATOH7* in optic nerve aplasia and hypoplasia, and hereditary PHPV by direct DNA sequencing, and we screened ONA cases for other genetic defects by whole-genome copy-number variation

(CNV) analysis. We identified a basic domain mutation (p.N46>H) that segregates with autosomal recessive PHPV (MIM 611311) in a previously characterized pedigree (Khaliq et al., 2001) and a heterozygous mutation (p.R65>G) in a child with optic nerve aplasia. We critically evaluated the biochemical and biological properties of these variants, and a second heterozygous variant (p.A47>T) noted in an optic nerve hypoplasia patient (Macgregor et al., 2010) using DNA binding, transcriptional activation and RGC rescue assays. We show that the p.N46>H and *lakritz* mutations cause a complete loss of function and are thus likely to be pathogenic, whereas the p.R65>G substitution has no detectable effect on activity. These studies further establish *ATOH7* mutations as a cause of congenital retinovascular and optic nerve disease, and contribute to our understanding of bHLH factor function.

Patients and Methods

Ethics statement

All human studies were approved by the University of Michigan Institutional Review Board and conform to the Declaration of Helsinki (Khaliq et al., 2001). Mouse studies were approved by the University of Michigan Committee on the Use and Care of Animals.

Human subjects

PHPV pedigree. The six-generation Pakistani family with persistent hyperplastic primary vitreous was described in the original linkage study,

including clinical phenotypes of five blind individuals (Khaliq et al., 2001). None of these patients had documented light perception, and all exhibited gross nystagmus. In the youngest patient (VI-2), retinal folds were noted in one eye, but no optic discs were seen during an exam under anesthesia, due to the presence of a dense white-gray fibrous mass in both vitreae, which obscured the central fundus. Unfortunately, the optic nerve status of affected individuals could not be assessed, and they were not available for orbital MRI examination or other clinical follow-up.

ONA cases. Patient 1 was blind at birth and has no light perception. Fundus and MRI exams revealed complete absence of optic nerves, chiasm, and optic tracts. She developed normally until 8 months, but after 12 months, was at the 5th percentile for height and weight. She exhibited severe developmental delays in spoken language and other milestones, and at 8 years of age had persistent difficulties initiating social interactions, an inability to sustain conversations, poor motor planning and processing, and deficits in sensory integration and auditory processing. Both parents have normal vision and cognition. Relevant clinical features of four unrelated ONA patients are listed in Table VI-S1, including cases 2-4, which were previously reported (Brodsky et al., 2004; Lee et al., 1996; Scott et al., 1997). Each patient has bilateral aplasia of the optic nerves, chiasm and tracts, with variable retinovascular fndings. There was no consanguinity or family history of ocular disease.

ONH cases. Thirty patients with isolated bilateral optic nerve hypoplasia and significant visual impairment or nystagmus were selected for screening. In these cases, the ratio of the horizontal disc diameter to the disc-macula distance was less than 0.3 (Borchert et al., 1995). There was no clinical hypothalamic or pituitary involvement, or brain abnormality based on imaging and endocrine functional studies.

Mutation screening and SNP genotyping

ATOH7 coding and regulatory elements were amplified from genomic DNA extracted from whole blood or saliva (Oragene collection kit, Genotek, Ontario, Canada) samples, using previously described PCR primers and conditions (Ghiasvand et al., 2011). Products were gel-purified using the Wizard SV gel system (Promega, Madison, WI) and sequenced on an ABI3730 DNA Analyzer (Applied Biosystems, Carlsbad, CA) in the University of Michigan DNA core. For genotyping arPHPV family members, products from *ATOH7* coding amplimer A (Ghiasvand et al., 2011) were digested with *Eae*I and electrophoresed through 2.5% agarose gels. For genotyping ONA Patient 1 and her family members, products from coding amplimer B (Ghiasvand et al., 2011) were generated using a ^{32}P end-labeled forward primer, digested with *Bst*UI, electrophoresed through 6% polyacrylamide gels, and exposed to X-ray film. All variants were compared to high-quality sequence reads in the NHLBI Exome Variant Database (Project).

Blood DNA from three arPHPV relatives (blind individual, known carrier, and wild-type sibling), and five sporadic ONA patients and available parents,

were analyzed using Illumina Omni1-Quad Infinium BeadChips in the University of Michigan DNA core. This platform scores 1.1 million informative SNPs, including 5400 from the arPHPV nonrecombinant interval delimited by D10S1221 and GATA121A08. Copy number variants were annotated using CNV-partition detection software in GenomeStudio (Ilumina, San Diego, CA), confirmed manually, and compared against the NCBI Database of Genomic Structural Variation. All coordinates in this report are based on NCBI reference genome build 36.1 (hg18).

Sequence alignment and structural modeling

Basic helix-loop-helix domains were aligned as previously described (Brown et al., 2002). The ATOH7 bHLH domain was modeled based on the known crystal structure of NeuroD1-E47 complexed with DNA (2QL2) (Longo et al., 2008) using the SWISS-MODEL server (Schwede et al., 2003). Wild-type and variant structures were viewed using PyMOL (Schrödinger, LLC).

Plasmid vectors

Full-length human *ATOH7* and E47 cDNAs were subcloned in pCS2 or pCS2-MT vectors (Turner and Weintraub, 1994) with the simian cytomegalovirus IE94 enhancer/promoter driving expression. For electroporation experiments, the *ATOH7* coding sequence was subcloned in the pUS2-MT-IRES-GFP vector (Zhang et al., 2012) with an N-terminal 6X-myc epitope tag (MT) and the human ubiquitin C promoter (UbC) driving expression of a bicistronic transcript that encodes MT-ATOH7 and GFP.

Expression plasmids carrying *ATOH7* variants were constructed by site-directed mutagenesis using the overhanging primer method (Liu and Naismith, 2008) with reagents and conditions noted in Table VI-S2. Reactions were performed in 1X *Pfu Ultra* reaction buffer (Stratagene, Santa Clara, CA) with 0.4 µM primers, 0.2 mM dNTPs, and 2.5 U of *Pfu Ultra* HF polymerase. Masteramp™ (Epicentre, Madison, WI) was added at 20% (v/v) to melt secondary structure in the GC-rich *ATOH7* cDNA template (Prasov et al., 2010). Products were digested with *Dpn*I and transformed into *E. coli* DH5α. The resulting clones were verified by restriction analysis and DNA sequencing.

Electrophoretic mobility shift assays (EMSA)

Nuclear extracts were prepared and electrophoretic mobility shift assays were performed using established methods (Hellman and Fried, 2007; Wadman et al., 1997). Briefly, HEK293T cells were transfected in 6 cm plates using FuGene6 reagent (Roche, Indianapolis, IN) with 1 µg plasmid DNA, consisting of an equal-ratio mixture (1:1) of wild-type or variant pCS2-ATOH7 and pCS2-E47 expression plasmids, or pCS2 empty vector. After 48 hrs, nuclear extracts were prepared following lysis in cold 10 mM HEPES, 1.5 mM $MgCl_2$, 10 mM KCl, 0.5 mM DTT, 0.5% (w/v) NP40, pH 8.0, and centrifugation at 4000 $\times$ *g* for 0.5 min. The nuclear pellets were resuspended in cold 20 mM HEPES, 1.5 mM $MgCl_2$, 420 mM NaCl, 0.2 mM EDTA, 25% (v/v) glycerol, pH 8.0 and agitated vigorously for 30 min. The protein content of soluble nuclear lysates was estimated by Bradford assay (Bradford, 1976). Ten micrograms of each extract was mixed with 3 U poly[dI-dC] (Sigma, St. Louis, MO) in binding buffer (20 mM HEPES, 50

mM KCl, 1 mM EDTA, 25% v/v glycerol, 1 mM DTT, pH 7.6). Double-stranded oligonucleotide probes were end-labeled with ^{32}P-α-dCTP using Klenow DNA polymerase, and added last to the binding reaction. For antibody blocking, 1 µg of mouse anti-ATOH7 immunoglobulin (1A5, Abnova, Taiwan, ROC) was added immediately to the binding reaction; for cold probe competition, excess unlabeled oligonucleotide (200 pmol) was introduced. After 20 min incubation at room temperature, reaction samples were electrophoresed under native conditions through 4% polyacrylamide gels. The dried gels were exposed overnight to phosphor screens, which were scanned using the Molecular Imager™ system (BioRad, Hercules, CA).

Dual luciferase cotransfection assays

HEK293T cells were transfected with 10-200 ng pCS2-ATOH7 expression plasmid (wild-type or variant), 600 ng firefly luciferase reporter with 7 tandem E-box binding sites preceding the promoter (Akazawa et al., 1995; Flora et al., 2007), and 10 ng DmPol2-*Renilla* control vector in 12-well plates, using FuGene6 reagent. After 48 hrs, the cells were disrupted with Passive Lysis Buffer (Promega) and luciferase activity was measured using a Victor-3 model 1420 luminescence plate reader (Perkin-Elmer, Waltham, MA) with Dual-Luciferase Assay reagents (Promega). *Photinus* firefly luciferase was normalized to *Renilla* luminescence, and the activities of lysates expressing ATOH7 are reported relative to lysates from cells transfected with empty pCS2 vector. At least two independent experiments were conducted for each ATOH7 variant, with parallel transfections in triplicate. Results were compared using Student's *t*-test.

Western blot analysis

Soluble proteins from whole cell or nuclear lysates were denatured in 2% SDS sample buffer, electrophoresed through NuPAGE Novex Bis-Tris 4-12% polyacrylamide gels, transferred to nitrocellulose membranes, and stained with Ponceau S. Membranes were blocked in a 1:1 mixture of Tris-buffered saline (TBS) with 0.2% Tween-20 and Odyssey buffer (LICOR Biosciences, Lincoln, NE) for 2 hrs, probed with primary antibodies overnight at 4ºC, washed in TBS with 0.1% Tween-20, incubated with IRDYE™ 800CW- or 680LT-conjugated secondary antibodies (LICOR), and scanned using the Odyssey Imaging System (LICOR). Primary antibodies were rabbit anti-E47 (1:1000, sc763, Santa Cruz Biotechnology, Santa Cruz, CA); rabbit anti-ATOH7 (1:500, D01P, Abnova) (Prasov et al., 2010); mouse anti-α-tubulin (1:1000, DM1A, Abcam, Cambridge, MA).

Protein stability assays

HEK293T cells were transfected in 6 cm plates with 2 µg of pCS2-ATOH7 expression plasmid and 0.2 µg of pUS2-GFP transfection control using FuGene6 reagent. After 24 hrs, cells were treated with cycloheximide (100 µg/mL) to block new protein synthesis (Schneider-Poetsch et al., 2010). Cell pellets were harvested after 0, 1, 2 or 5 hrs exposure and lysed in RIPA buffer. Stability was assessed by comparing the ATOH7 signal intensity over time, relative to endogenous α-tubulin, in Western blots of cleared lysates.

Retinal explants and electroporation

Retinal explants were prepared as described (Brzezinski et al., 2012), and manipulated using established DNA electroporation and culture methods (Donovan and Dyer, 2006; Wang et al., 2002b). Briefly, E13.5 *Atoh7* -/- eye cups (*Atoh7*^{tm1Gla} allele, (Brown et al., 2001)) were dissected from the sclera and retinal pigmented epithelium, and bathed with plasmid DNA (1.5 µg/µl) in Hank's balanced salt solution (HBSS). Five pulses of 20 V and 50 ms duration, separated by 950 ms recovery periods, were applied across the retina using a BTX ECM-830 electroporator and gold-plated tweezer electrodes. Eye cups were allowed to recover for 5.5 hrs in neurobasal media (Invitrogen, Grand Island, NY) containing 1X B27 and N2 supplements, glutamine (0.4 mM), BDNF (50 ng/mL, Peprotech, Rocky Hill, NJ), CNTF (10 ng/mL, Peprotech), penicillin (50 U/mL), streptomycin (50 µg/mL), and gentamicin (0.5 µg/mL). After lens removal, the retinas were flattened onto polycarbonate membranes (0.4 µm pore size, GE Healthcare, Piscataway, NJ) and cultured on Transwell inserts for three days at 37ºC at the gas-media interface in a humidified atmosphere containing 5% CO_2. After two days of culture, half the media was replaced. On the third day, explants were fixed in 4% paraformaldehyde for 30 min at room temperature, washed in PBS, and blocked for 4 hrs in 10% normal donkey serum (NDS), 1% bovine serum albumin (BSA), 90 µg/mL donkey anti-mouse IgG Fab fragment in PBTx (0.1 M $NaPO_4$ pH 7.3, 0.5% Triton X-100). Whole explants were then incubated with mouse anti-Brn3a (1:50, 14A6, sc-8429, Santa Cruz), chicken anti-GFP (1:2000, Abcam), and rabbit anti-β3-tubulin/TuJ1

antigen (1:500, MRB-435P, Covance, Princeton, NJ) primary antibodies in 3% NDS, 1% BSA, PBTx overnight at 4ºC. Explants were washed in PBS, incubated with Dylight-conjugated secondary antibodies (Jackson Immunoresearch, West Grove, PA), mounted in Prolong Gold Antifade™ (Invitrogen), and imaged as confocal Z-stacks using the Zeiss LSM 510 Meta system.

For each explant, the number of Brn3a+ RGCs was counted within the transfected population (GFP+) in two high-magnification confocal Z-stacks extending through the full thickness of GFP+ cells. The RGC fraction (Brn3a+ GFP+ / GFP+) for each *ATOH7* construct was averaged from 3-6 explants, in two series of experiments, and plotted using Prism software (Graphpad). Statistical comparisons were made using Student's *t*-test.

Competitive genomic PCR and 3' RACE analysis

Endpoints of the CNTN4 tandem duplication were defined by PCR, using primers with an inverted orientation in the reference genome (Table VI- 2, Fig. VI-S4). To co-amplify products from the wild-type (wt) and duplicated (dup) alleles, competitive genotyping PCRs were performed with a common forward primer in CNTN4 exon 12 and two allele-specific reverse primers, in introns 12 and 1. The reactions included 10% (v/v) Masteramp™ as described (Prasov et al., 2010), and followed conditions outlined in Table VI-S2.

For 3' RACE (rapid amplification of cDNA ends) analysis, total RNA was prepared from Epstein-Barr virus-transformed lymphoblastoid cell lines using the phenol-guanadinium method with Trizol reagent (Invitrogen). cDNA was generated by reverse transcription (RT) as described (Prasov et al., 2010) with

Transcriptor™ high-fidelity polymerase (Roche). 3' RACE experiments (Frohman et al., 1988) were performed in two steps, using nested primers and cycling conditions listed in Table VI-S2.

Results

ATOH7 mutation segregates with PHPV disease

A locus for autosomal recessive persistent hyperplastic primary vitreous (arPHPV) was mapped in a large consanguineous pedigree to a 13 cM region in 10q21 (Khaliq et al., 2001). This segment contains *ATOH7* and the critical region for nonsyndromic congenital retinal nonattachment (NCRNA), a clinically related recessive disorder (Ghiasvand et al., 2000) (Fig. VI-1A). In a recent study, we showed that NCRNA is most likely caused by a 6.5 kb deletion, located 21 kb upstream from the *ATOH7* start site, which removes a transcriptional enhancer with three evolutionarily conserved noncoding elements. The NCRNA patients are blind from birth, with no light perception, and have bilateral profusions of retrolental fibrovascular tissue, similar to arPHPV patients (Khaliq et al., 2001). They also have optic nerve aplasia, documented by magnetic resonance imaging (MRI), and early bilateral detachments of the retina, with an apparent tractional basis. In both diseases, the anterior chambers are shallow and there is progressive corneal opacification, most likely due to chronic endothelial blood staining (Brodrick, 1972).

Given the similarity between disease phenotypes, overlap of the linkage intervals including *ATOH7*, and potential for shared ancestry between ethnic

Kurdish and Pakistani (Baloch) populations, we first tested whether arPHPV family members carried the chromosome 10q21 NCRNA disease haplotype or *ATOH7* regulatory deletion, by high-density SNP and diagnostic PCR analysis (Ghiasvand et al., 2011). This excluded haploidentity and revealed no evidence of a deletion or duplication in the arPHPV disease interval. We then focused our analysis on the *ATOH7* coding region in three first-degree relatives. We identified a c.136A>C mutation that is homozygous in a blind individual, heterozygous in his obligate carrier mother, and absent in his unaffected brother (Fig. VI-1B). This mutation predicts a p.Asn46>His (N46H) amino acid change in the bHLH domain, and creates a novel *Eae*I restriction site, which can be used for DNA genotyping (Fig. VI-1C). We then screened blood DNA of all available family members by PCR and restriction analysis, and found that this mutation segregates with the disease as expected (Fig. VI-1D). The N46H variant was not present in the NHLBI Exome Variant Database among 2462 exomes (Project), in dbSNP, or in 72 (144 chromosomes) controls with normal vision.

ATOH7 mutation screening in ONA cases

We screened DNA from five unrelated optic nerve aplasia (ONA) cases for coding or regulatory mutations in the *ATOH7* gene, and for deletions or duplications by Ilumina Omni1-quad SNP genotyping. Two of these patients (cases 1-2) have additional neurocognitive deficits or anatomical defects, and three (cases 2-4) have been reported in the literature (Table VI-S1). In Patient 1, we identified a heterozygous c.193A>G mutation in *ATOH7*, which predicts a

p.Arg65>Lys (R65G) amino acid change (Fig. VI-2). This was confirmed by restriction analysis of PCR products, and was paternally inherited. A similar R65G variant was previously reported in a heterozygous Australian child among 12 cases of isolated optic nerve hypoplasia (Macgregor et al., 2010).

Given the potential association between *ATOH7* and optic nerve hypoplasia, we also screened 30 patients with severe isolated ONH for *ATOH7* coding mutations. No additional variants were found. Taken together, the frequency of the *ATOH7* R65G among optic nerve aplasia or hypoplasia patients is estimated to be 2 out of 94 chromosomes. This variant was identified in 7 of 6592 chromosomes from individuals with normal vision, including 0/144 in control chromosomes, 6/4924 in the exome variant database (Project), and 1/1524 reported by Macgregor *et al.* (Macgregor et al., 2010). Thus, R65G is statistically overrepresented among ONA and ONH patients (Fisher's exact test, $P = 0.007$).

Copy number variant (CNV) analysis

In addition to sequencing of *ATOH7* coding and regulatory regions, we performed high-density SNP analysis to evaluate CNVs among the ONA patients. In Patient 1, this revealed an 828 kb duplication that is predicted to disrupt the *CNTN4* (contactin) gene (Suppl. Fig 1). We mapped this duplication by junctional PCR and determined that it was a precise tandem duplication encompassing exons 2-12 (Fig. VI-S2A-C). Furthermore, in a lymphoblastoid cell line from Patient 1, this allele can generate a truncated *CNTN4* mRNA transcript by premature polyadenylation, with termination after exon 12 (Fig. VI-

S2). The CNTN4 protein (BIG-2) contains an extracellular immunoglobulin domain, is expressed throughout the brain, and mediates neural cell adhesion and axon outgrowth (Osterfield et al., 2008; Shimoda and Watanabe, 2009; Yoshihara et al., 1995). Variants in *CNTN4* (MIM 607280) and *CNTNAP2* (contactin-associated protein) (MIM 604569) genes, including CNVs, are highly associated with autism spectrum disorder (Alarcon et al., 2008; Glessner et al., 2009; Pinto et al., 2010; Roohi et al., 2009). The duplication in Patient 1 is a novel *CNTN4* disruption (Fig. VI-S1B) and relevant to her optic nerve and neurocognitive phenotypes. The duplicated allele may generate a truncated protein that could potentially interfere with normal CNTN4 function. Although CNTN4 is expressed by developing RGC axons in the retinotectal system (Osterfield et al., 2008; Yoshihara et al., 1995), complete disruption of the orthologous *Cntn4* gene in mice has no gross effect on RGC abundance or optic nerve development (T. Kaneko-Goto and Y. Yoshihara, personal communication, and data not shown). Thus, it remains unclear what direct role, if any, the rearrangement plays in the optic nerve pathology of this patient. However, in the setting of a *CNTN4* rearrangment, blindness is likely to have increased her risk of neurocognitive dysfunction (Ek et al., 2005; Mukaddes et al., 2007).

In Patient 2, CNV analysis revealed a heterozygous 1.2 Mb deletion spanning the *OTX2* gene (MIM 600037) on chromosome 14q23 (Fig. VI-S3). In addition to ONA, this patient had anatomical and functional pituitary defects (Brodsky et al., 2004), consistent with the role of the Otx2 homeodomain protein in development of the ventral brain, eye and pituitary (Matsuo et al., 1995).

Heterozygous *OTX2* loss-of-function mutations, including three whole-gene deletions, have been identified in patients with a variety of severe eye malformations, including optic nerve aplasia or hypoplasia (Bakrania et al., 2008; Dateki et al., 2010; Ragge et al., 2005; Schilter et al., 2011; Wyatt et al., 2008), suggesting a haploinsufficiency mechanism (Chatelain et al., 2006). The optic nerve phenotype may be attributed to a disruption of optic stalk development (Martinez-Morales et al., 2001).

In vitro functional analysis of *ATOH7* variants

To test the causal link between the *ATOH7* variants and disease phenotypes, we characterized their biochemical effects *in vitro* using a variety of structural and functional assays. In addition to N46H and R65G, we included the p.A47>T variant (A47T) reported by Macgregor *et al.* (Macgregor et al., 2010) in our analysis. This allele was identified in a sporadic ONH case, but was not found in normal control chromosomes (0/5248), including 4924 in the NHLBI exome variant database (Project). We first evaluated conservation of the affected residues between species and paralogs by aligning bHLH domains and comparing mutations in humans, zebrafish, *Drosophila* and *C. elegans* (Fig. VI-3A). The N46 and A47 residues are contained within the basic (DNA binding) region, which is the most highly conserved part of the bHLH domain. The R65 residue is less conserved, although it remains a basic amino acid in vertebrates (Arg or Lys).

We next modeled the ATOH7 bHLH domain (Fig. VI-3B) using the known crystal structure of the NeuroD1-E47 heterodimer bound to DNA (Longo et al., 2008). In this homology model, the Asn46 side group makes direct contact with a thymine base in the core E-box recognition site (position 5 of CANN**T**G). Introduction of a histidine residue at this position is predicted to significantly impair DNA binding (Fig. VI-3C, bottom). In contrast, the neighboring Ala47 side chain does not directly contact DNA, but the threonine substitution may alter DNA binding properties through conformational effects. The positively charged Arg65 residue, located at the end of Helix 1, is predicted to interact with the negatively charged Asp61 side group via an electrostatic bridge, which may serve to stabilize the helix or limit the flexibility of tertiary interactions (Kumar and Nussinov, 2002) (Fig. VI-3C, top).

Given the proximity of N46 and A47 residues, and direct contact between N46 and DNA (Fig. VI-2C), we tested the ability of these variants to bind an E-box DNA recognition site (Fig. VI-4A). Mammalian plasmid expression vectors for wild-type or variant ATOH7 proteins were transfected into HEK293T cells, and the resulting nuclear extracts were compared in an electrophoretic mobility shift assay (Fig. VI-4B). We also tested a humanized version of the zebrafish *lakritz* mutation (p.L56>P), which is believed to cause a complete loss-of-function (Kay et al., 2001). Because neurogenic bHLH transcription factors bind DNA as heterodimers with ubiquitous class A bHLH proteins (Murre et al., 1989), we included an expression plasmid for the binding partner E47 in some transfections, to augment the low endogenous level of E47 in the HEK293T cell

line. Heterodimeric complexes between specific class A bHLH proteins and E47 assemble on DNA and do not form in solution (Wendt et al., 1998). Although this binding of heterodimers is strongly favored, the E47 protein can also bind DNA as a homodimer, with a characteristic gel shift pattern corresponding to different phosphorylated isoforms (Sloan et al., 1996).

The radiolabeled synthetic double-stranded oligonucleotide probe contained an E-box binding site (CAGGTG) that is optimal for ATOH7 and its orthologs (Del Bene et al., 2007; Powell et al., 2004) (Fig. VI-4A). In the absence of added E47, each ATOH7 variant, including wild-type, failed to bind DNA (Fig. VI-4B). In the presence of wild-type ATOH7, faster migrating ATOH7-E47 complexes are the dominant species bound to DNA. The R65G and A47T variants formed ATOH7-E47 heterodimers on DNA that were indistinguishable from wild-type (R65G) or slightly reduced (A47T). These alleles therefore retain DNA-binding and dimerization activity *in vitro.* In contrast, extracts containing N46H or L56P variants formed only E47 homodimeric complexes, indicating that these mutants are unable to bind DNA. Because the E47 homodimeric complexes were not disrupted, N46H and L56P do not act as dominant-negative proteins, like the Id class of bHLH factors (Benezra et al., 1990).

Western analysis confirmed that equivalent levels of ATOH7 and E47 were present in nuclear extracts, suggesting that the ATOH7 variant proteins have similar stability (Fig. VI-4C). To explore this point further, we performed a cycloheximide pulse-chase experiment (Zhou, 2004) (Fig. VI-S4). Because each

protein variant decayed at approximately the same rate, the observed DNA-binding impairment cannot be attributed to decreased protein stability.

We next tested the transcriptional activity of ATOH7 variants in a luciferase cotransfection assay using HEK293T cells and an optimized synthetic reporter, which contains a multimerized E-box sequence (CAGGTG) and minimal β-actin promoter (Akazawa et al., 1995; Flora et al., 2007) (Fig 4D). Wild-type ATOH7 increased luciferase activity 25-35 fold compared to empty pCS2 vector, in a dose-dependent manner (Fig. VI-4E). The A47T variant had an intermediate level of activity compared to wild-type, 60% at the high dose (100 ng) and 20% at the low dose (20 ng). R65G was indistinguishable from wild-type at the high dose, but had 60% activity at the low dose. In contrast, N46H and L56P variants had no detectable activity. Taken together, these results suggest that ATOH7 N46H and L56P are null alleles, whereas A47T and R65G retain significant function.

Biological rescue of RGC development by *ATOH7* variants

To assess function in a biologically relevant system, we compared the potency of *ATOH7* variants in *Atoh7* -/- retinal explants. *Atoh7* mutant mice have a >95% reduction in RGCs due to defective fate specification (Brown et al., 2001; Wang et al., 2001), which is apparent as early as E11 (Brzezinski et al., 2012). To assay biological rescue of this phenotype, we removed E13.5 eye cups from *Atoh7* -/- embryos and introduced bicistronic expression vectors for ATOH7 and GFP by *ex vivo* electroporation (Fig. VI-5A). We then explanted and cultured the

retinas for 3 days *in vitro* (DIV) to allow for RGC differentiation. To assess the degree of rescue, we immunostained whole explants for GFP, the RGC nuclear marker Brn3a (Nadal-Nicolas et al., 2009; Xiang et al., 1995), and the pan-neuronal marker β3-tubulin (TuJ1) (Fig. VI-5B). We then counted the fraction of transfected (GFP+) cells that developed as ganglion cells (Brn3a+) (Fig. VI-5C). In explants electroporated with the control vector (GFP only), very few Brn3a+ cells were detected among the GFP+ cohort (7 ± 3%) and very few GFP+ TuJ1+ axons were apparent, as expected (Fig. VI-5, Fig. VI-S5A). In contrast, the majority of cells transfected with the wild-type *ATOH7* vector adopted the RGC fate (72 ± 12% Brn3a+), demonstrating a wide dynamic range for this assay. Moreover, large bundles of GFP+ TuJ1+ processes, likely representing RGC axon fascicles, were readily observed in these explants at low magnification (Fig. VI-S5B). Explants transfected with N46H or L56P variants failed to develop RGCs ($P < 10^{-5}$ compared to wild-type, Fig. VI-5C) and could not be distinguished from the negative control (GFP only), by RGC number (Fig. VI-5B,C) or axon density (Suppl. Fig 5C,D). In contrast, R65G and A47T variants did restore RGC development (Fig. VI-5B,C, Suppl. Fig 5E,F). These results support our conclusion that N46H and L56P variants are functional null alleles, while R65G and A47T retain complete or partial biological activity.

Discussion

ATOH7 has an established role RGC development (Brown et al., 2001; Wang et al., 2001) and a secondary role in retinal vascular development

(Brzezinski et al., 2003). *ATOH7* mutations are predicted to cause human blindness (Brown et al., 2002), but the clinical spectrum and molecular mechanisms remain to be defined (Ghiasvand et al., 2011; Khan et al., 2011; Macgregor et al., 2010). Given the similarity between mouse *Atoh7* phenotypes and human congenital defects involving the optic nerve or retinal vasculature, and converging genetic data (Khaliq et al., 2001), we systematically screened a family with recessive PHPV disease, and a cohort of sporadic patients with major optic nerve malformations (Table VI-S1), for intragenic or regulatory mutations in *ATOH7*. Here, we identified novel coding variants, measured their biochemical and biological effects, and proved that one variant causes arPHPV.

The N46H mutation causes arPHPV

Our data strongly support a causative role for the p.N46>H mutation in the arPHPV pedigree (Fig. VI-1) for seven reasons. First, the N46H mutation segregates with PHPV disease in an autosomal recessive pattern, and the *ATOH7* gene is contained inside the nonrecombinant interval. Second, no other DNA rearrangement was identified within the disease interval by CNV analysis. Third, the N46H mutaion removes a highly conserved amino acid residue in the bHLH domain that directly contacts DNA (Fig. VI-3). Fourth, an orthologous mutation in *Drosphila atonal* (*ato1*) eliminates activity and prevents R8 photoreceptor development in flies (Jarman et al., 1993). Fifth, the mutant ATOH7 protein had no detectable activity in three independent assays. The N46H polypeptide is stable, but does not bind DNA or activate transcription via its

cognate E-box recognition site (Fig. VI-4), and has no biological function in restoring RGC development (Fig. VI-5).

Sixth, *Atoh7* -/- mice have eye phenotypes that are similar to human PHPV. In mice, Atoh7 is exclusively expressed by cells in the neural retina (Brzezinski et al., 2012) and the primary pathology in *Atoh7* mutant mice is loss of RGCs (Brown et al., 2001). However, major vascular defects occur as a secondary consequence of the ganglion cell deficiency, because RGCs are vital for proper migration and development of retinal astrocytes (Fruttiger et al., 1996), which form a scaffold for the growth of intrinsic retinal blood vessels (Fruttiger, 2002). In *Atoh7* -/- mice, the intrinsic vasculature fails to develop, and hyaloid (fetal) vessels persist in the vitreous and proliferate to supply the retina (Brzezinski et al., 2003; Edwards et al., 2011). These abnormal vessels are prone to hemorrhage, in the subretinal and intravitreal space, and some extravasated blood communicates with the anterior chamber (hyphema). Similarly, in the arPHPV family, all affected family members were blind from birth and had bilateral retrolental masses (Khaliq et al., 2001). Persistent hyaloid vessels were clearly observed in the youngest patient. In addition, the adult patients had anterior chamber pathology, including cataracts, corneal opacity and anterior synechiae, which may be related to chronic intraocular hemorrhage (Brodrick, 1972).

Seventh, allelic *ATOH7* variants have been identified in three families with similar retinovascular pathology (Ghiasvand et al., 2011; Khan et al., 2011). In NCRNA disease, linkage, genomic, and transgenic analysis suggest that a 6.5 kb

deletion spanning a remote 5' enhancer impairs *ATOH7* transcription, causing bilateral optic nerve agenesis, abnormal vascularization, and early tractional detachment of the retina (Ghiasvand et al., 2011). Similarly, in a recent study of familial vitreoretinal dysplasia, with anterior segment involvement, Khan *et al.* identified two *ATOH7* mutations (Khan et al., 2011). One of these (E49V) is close to the N46H variant we discovered, within the basic region (Fig. VI-3A). They disrupt the core DNA-binding motif (NARER) that is highly conserved among proneural bHLH factors (Chien et al., 1996; Jarman et al., 1993). The second mutation causes a frameshift in the ATOH7 polypeptide. Although both are likely to be deleterious, the effects on protein function have not been characterized empirically. Together, these *ATOH7* mutations suggest a common pathogenic mechanism, with a primary neuronal basis, for hereditary PHPV, NCRNA, vitreoretinopathy, and related disorders (Cogan, 1971; Lahav et al., 1973). Clinical assessment of optic nerve status by orbital magnetic resonance imaging is thus important for patients with severe retinovascular disease.

ATOH7 in optic nerve aplasia and hypoplasia

The role of *ATOH7* in optic nerve aplasia and hypoplasia remains less clear. We identified an R65G mutation in one ONA case (Patient #1). This allele is unlikely to cause disease for three reasons. First, functional analysis suggests that the R65G protein has nearly full activity. The protein is stable, binds DNA, activates transcription, and promotes RGC development in *Atoh7* -/- retinal explants. The *ex vivo* rescue analysis (Fig. VI-5) is particularly important, because this biological assay is a comprehensive test of *ATOH7* function.

Second, no allelic *ATOH7* variant was identified in this patient, in coding or regulatory sequences. Heterozygous carriers of the N46H null allele or NCRNA deletion, and *Atoh7* +/- mice, have normal optic nerves and no obvious defect in retinal or vascular development (Brown et al., 2001; Brzezinski et al., 2003; Ghiasvand et al., 2011). Therefore, a single deleterious allele is not sufficient to cause disease. Third, although overrepresented in ONH and ONA cases, the R65G variant was also observed in controls with normal vision, including the heterozygous father of Patient 1.

Our analysis of the A47T variant previously reported in an ONH patient (Macgregor et al., 2010) suggests that it is a hypomorphic allele. Activity of A47T was reduced in all three assays (DNA binding, transactivation, RGC rescue). In addition, this variant was not found in a large number of normal controls. A47T may have pathogenetic effects, but is unlikely to be the sole cause of disease given that only one allele was identified. In principle, these two *ATOH7* variants (A47T and R65G) may lack protein function in a way that was not evaluated by our *in vitro* tests. For example, the affected residues may be vital for interactions between ATOH7 and transcriptional coactivators. Indeed, the A47T mutation alters one of three residues that confer bHLH specificity to Atonal (ATO) and Neurogenin (NGN) clades in the Atonal-related bHLH protein family (Quan et al., 2004).

Implications for Ato class bHLH factor function

Our analysis of the *ATOH7* variants provides unique insights into bHLH domain function. Among proneural bHLH proteins, the NARER motif is highly

conserved and important for DNA binding (Atchley and Fitch, 1997; Chien et al., 1996; Jarman et al., 1993). Our results, however, suggest that an Ala47 $\rightarrow$ Thr substitution can be tolerated. In contrast, Asn46 makes direct contact with a DNA base, and is critical for binding and function. In *Drosophila*, the orthologous residue is one of three that are altered in the *ato1* mutation (Jarman et al., 1994). Our findings suggest that the Asn $\rightarrow$ Ile substitution at this position is the primary defect in the *ato1* allele.

The *ATOH7* R65G variant is predicted to destabilize Helix 1 based on molecular modeling (Fig. VI-3) and is classified as a potentially damaging variant based on bioinformatic criteria (Macgregor et al., 2010). However, the R65G variant had a surprisingly small effect on protein function and stability *in vitro*, and on biological function *ex vivo*. Likewise, the L56P substitution in the zebrafish *lakritz* variant behaved unexpectedly. Introduction of a proline at this position is predicted to disrupt Helix 1 and decrease the overall stability of the protein. Instead, the humanized *lakritz* polypeptide was stable (Fig. VI-S1), but failed to complex with the E-box recognition site (Fig. VI-4), due to impaired dimerization with E47 or DNA binding.

In principle, variants that fail to bind DNA, such as L56P and N46H, could act as dominant-negative proteins, similar to the Id class of bHLH factors (Benezra et al., 1990). Id proteins lack DNA-binding activity, but sequester and inhibit the function of other bHLH factors (Norton, 2000; Ross et al., 2003). In contrast, our EMSA results, and the unaffected status of *lakritz* and arPHPV heterozygotes, suggest that L56P and N46H mutations are simple null alleles.

Together, our genetic, molecular, evolutionary and functional analyses of *ATOH7* mutations connect a variety of clinical and basic observations regarding hereditary blindness, neurovascular development of the eye, and proneural bHLH proteins. Our results prove that a bHLH mutation in *ATOH7* causes recessive PHPV, highlight the interdependence of neural and vascular development, and establish a set of functional tests for analysis of subsequent *ATOH7* variants.

Acknowledgements

The authors are grateful to the patients and families for participating in the study; to Nathan Vale, Dellaney Rudolph and Susan Tarlé for technical support; to Ingrid Scott, Roberto Warman and Bronwyn Bateman for providing blood samples from optic nerve aplasia patients; to Bob Lyons, Susan Dagenais and the University of Michigan DNA core for assistance with the Illumina Omni1Quad SNP analysis; to Chris Edwards and the UM microscopy and image analysis laboratory staff for technical advice; to David Turner and Huanqing Zhang for advice on retinal explants electroporation and for providing the pUS2-MT-IRES-GFP vector; to Adriano Flora and Huda Zoghbi for the (E-box)x7 luciferase reporter plasmid; to Tomomi Kaneko-Goto and Yoshihiro Yoshihara for sharing Cntn4/BIG-2 mutant mouse tissues; to the Autism Genetic Resource Exchange (AGRE) consortium for comparative genotyping data; to Donna Martin, Anthony Antonellis, Chris Chou and David Turner for valuable discussions and critical reading of the manuscript. The research was funded by grants from The

Glaucoma Foundation and the National Institutes of Health (EY14259 and EY19497) to TG. LP was supported by NIH T32 grants EY13934 and GM07863; DK and JCS were funded by the Ulverscroft Foundation.

WEB RESOURCES

NHLBI Exome Variant Database	http://evs.gs.washington.edu/EVS/
NCBI Database of Genomic Structural Variation	www.ncbi.nlm.nih.gov/dbvar/
NCBI Human Reference Genome Build 36.1	http://www.ncbi.nlm.nih.gov/genome/assembly/2928/
SWISS-MODEL server	http://swissmodel.expasy.org/

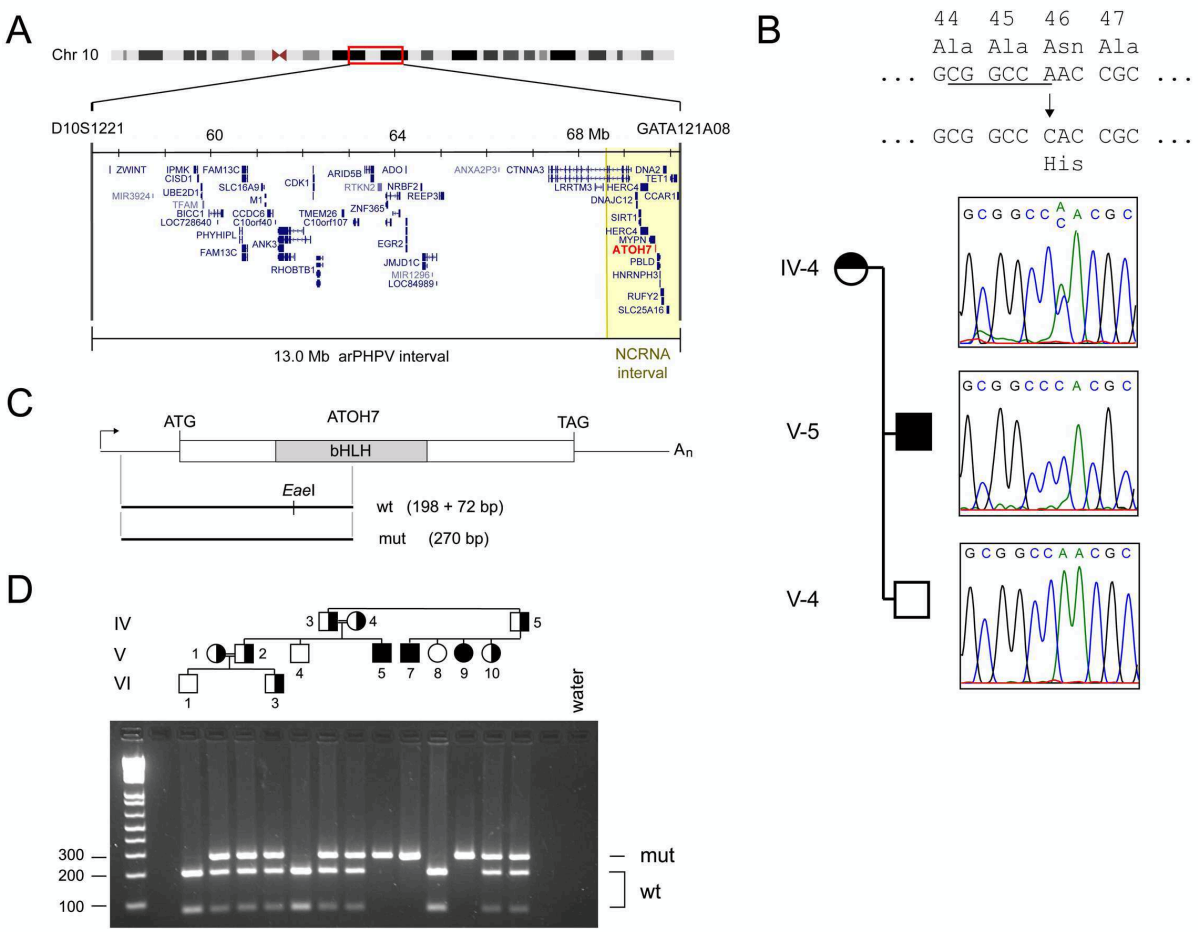

Figure VI-1. The *ATOH7* p.Asn46>His allele segregates with autosomal recessive persistent hyperplastic primary vitreous (arPHPV) disease. (A) Minimal region of shared homozygosity for arPHPV on chromosome 10q21, between D10S1221 and GATA121A08 (Khaliq et al., 2001). The *ATOH7* gene (red) and NCRNA critical region (Ghiasvand et al., 2000) (yellow) are indicated. The same distal flanking marker (GATA121A08 or D10S1418) delimits both intervals. (B) *ATOH7* sequence chromatograms from arPHPV family members. The AAC to CAC mutation causes an Asn46His amino acid substitution (N46H) in the bHLH domain and loss of an *Eae*I restriction site (underlined). This variant is heterozygous in the obligate carrier (IV−5) and homozygous in the affected individual (V−5). (C) Map of the *ATOH7* cDNA, showing the informative PCR product and *Eae*I restriction fragments. (D) Agarose gel of *Eae*I-digested PCR products amplified from arPHPV family members, numbered as previously reported (Khaliq et al., 2001). Filled and half-filled symbols show affected indivduals, and carriers assigned by haplotype (Khaliq et al., 2001), respectively. Carriers have both mutant (270 bp) and wildtype (198 and 72 bp) alleles, whereas blind individuals have only the mutant allele. NCRNA, nonsyndromic congenital retinal nonattachment; bHLH, basic helix-loop-helix domain; wt, wildtype; mut, mutant.

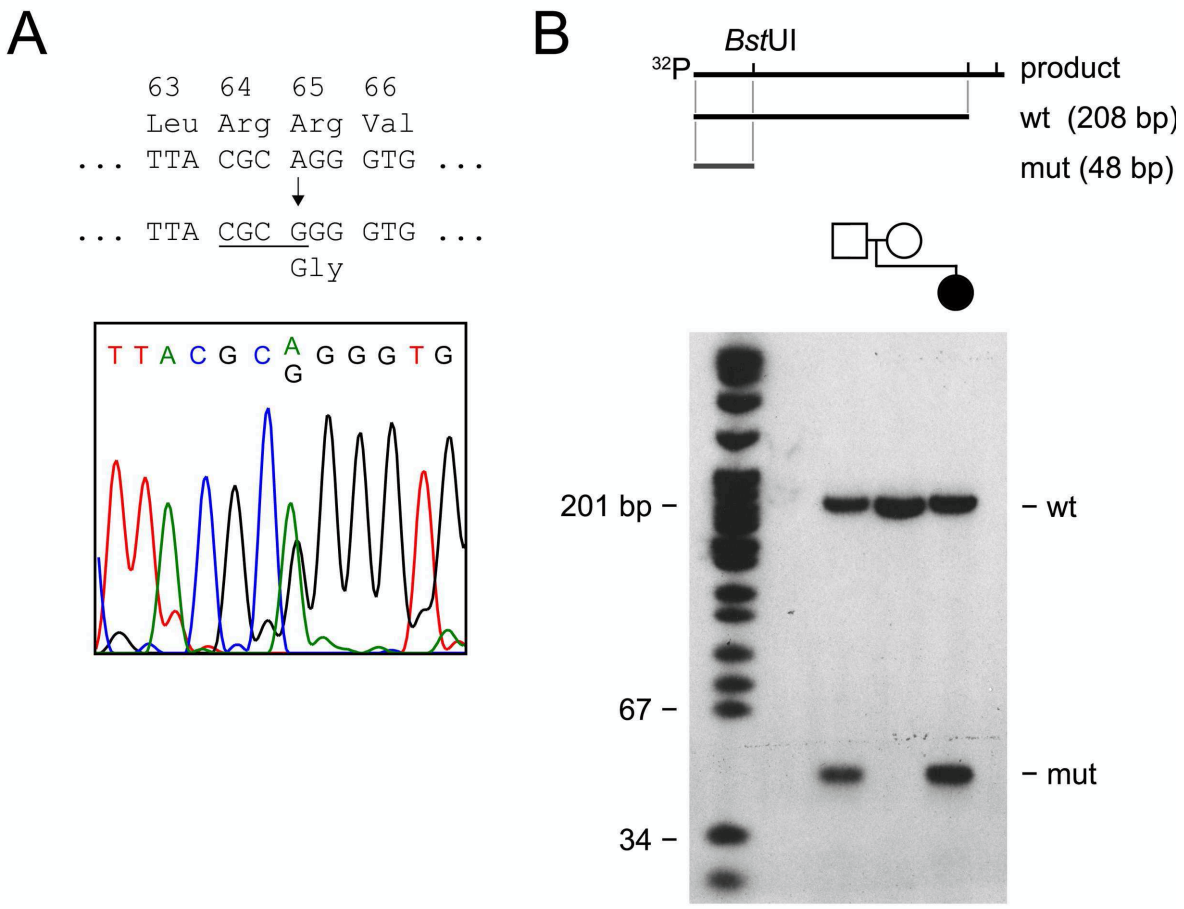

Figure VI-2. The *ATOH7* p.Arg65>Gly allele in a child with optic nerve aplasia and developmental delay. (A) Sequence chromatogram showing the heterozygous AGG to GGG variant in this case (Patient 1). The variant causes an Arg65Gly (R65G) amino acid substitution, and creates a *Bst*UI restriction site (underlined) in the PCR product. (B) Map and acrylamide gel autoradiograph showing wild-type and mutant *Bst*UI-digested PCR products. The forward PCR primer was end-labeled with ^{32}P, giving wildtype (wt, 208 bp) and mutant (mut, 48 bp) radioactive fragments, respectively. The R65G allele was paternally inherited.

Figure VI-3. Sequence alignment and structural modeling of *ATOH7* mutations. (A) Multispecies amino acid alignment of the ATOH7 bHLH domain and closely related transcription factors ATOH1 and NEUROD1. Mutations in human, zebrafish (*Danio rerio*), *Drosophila melanogaster* and *Caenorhabditis elegans* orthologs, and human NEUROD1, are highlighted (yellow). Two human alleles, N46H and E49V (Khan et al., 2011) in the basic region, affect invariant Asn46 and Glu49 residues, which are mutated in *Drosophila* and *C. elegans*, respectively. Ala47 is conserved to *Drosophila*, while the Arg65 is conserved as a basic amino acid (Arg or Lys) in vertebrates. The zebrafish *lakritz* mutation affects an invariant Leu residue, corresponding to L56 in human ATOH7. The R111L mutation in human NEUROD1 affects an invariant Arg residue and abolishes DNA binding, causing diabetes (Malecki et al., 1999). (B-C) PyMOL views of ATOH7 bHLH domains, modeled using the known X-ray crystal structure of NeuroD1-E47 heterodimers bound to DNA. (B) Low power view showing locations of the ATOH7 helix, loop and basic domains, bHLH partner E47, and the E-box DNA binding site. (C) *top*. High power view of Helix 1 showing the position of the Arg65 residue. Arg65 is predicted to make a charge-charge contact with Asp61, which may stabilize the α-helix. *bottom*. High power view of the basic region. Asn46 is predicted to directly contact a base (thymine) within the core E-box recognition site, while Ala47 faces away from the DNA. arPHPV, autosomal recessive persistent hyperplastic primary vitreous; ONA, optic nerve aplasia; ONH, optic nerve hypoplasia; VRD, vitreoretinal dysplasia; T2DM, type II diabetes mellitis.

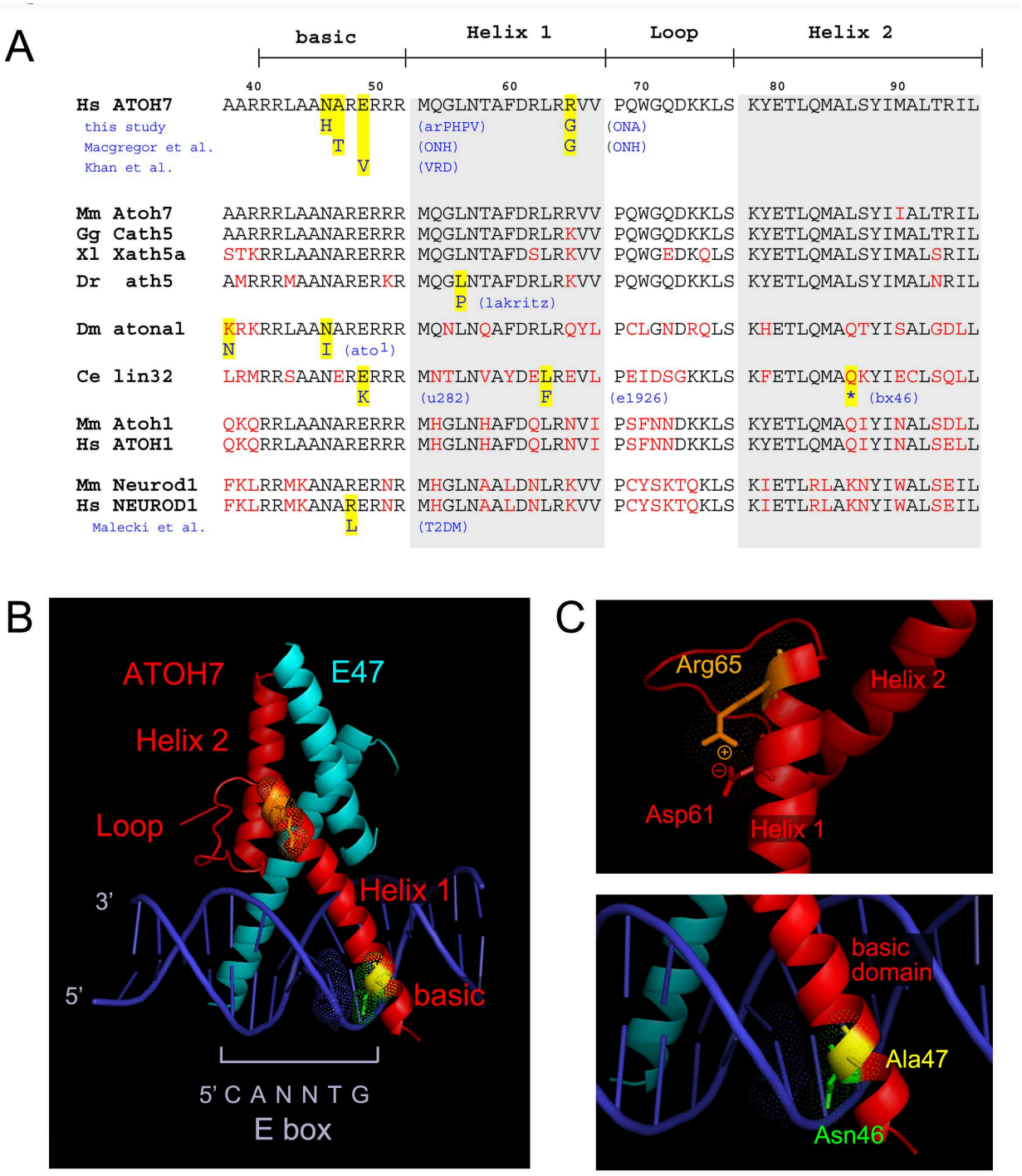
A
basic
Helix 1
Loop
Helix 2
40
50
60
70
80
90
Hs ATOH7 AARRRLAANARERRR MQGLNTAFDRLRRVV PQWGQDKKLS KYETLQMALSYIMALTRIL
this study H (arPHPV) G (ONA)
Macgregor et al. T (ONH) G (ONH)
Khan et al. V (VRD)
Mm Atoh7 AARRRLAANARERRR MQGLNTAFDRLRRVV PQWGQDKKLS KYETLQMALSYIIALTRIL
Gg Cath5 AARRRLAANARERRR MQGLNTAFDRLRKVV PQWGQDKKLS KYETLQMALSYIMALTRIL
Xl Xath5a STKRRLAANARERRR MQGLNTAFDSLRKVV PQWGEDKQLS KYETLQMALSYIMALSRIL
Dr ath5 AMRRRMAANARERKR MQGLNTAFDRLRKVV PQWGQDKKLS KYETLQMALSYIMALNRIL
P (lakritz)
Dm atonal KRKRRLAANARERRR MQNLNQAFDRLRQYL PCLGNDRQLS KHETLQMAQTYISALGDLL
N I (ato1)
Ce lin32 LRMRRSAANERERRR MNTLNVAYDELREVL PEIDSGKKLS KFETLQMAQKYIECLSQLL
K (u282) F (e1926) * (bx46)
Mm Atoh1 QKQRRLAANARERRR MHGLNHAFDQLRNVI PSFNNDKKLS KYETLQMAQIYINALSDLL
Hs ATOH1 QKQRRLAANARERRR MHGLNHAFDQLRNVI PSFNNDKKLS KYETLQMAQIYINALSELL
Mm Neurod1 FKLRRMKANARERNR MHGLNAALDNLRKVV PCYSKTQKLS KIETLRLAKNYIWALSEIL
Hs NEUROD1 FKLRRMKANARERNR MHGLNAALDNLRKVV PCYSKTQKLS KIETLRLAKNYIWALSEIL
Malecki et al. L (T2DM)
B
ATOH7
E47
Helix 2
Loop
Helix 1
3'
5'
basic
5' C A N N T G
E box
C
Arg65
Helix 2
Asp61
Helix 1
basic domain
Ala47
Asn46

Figure VI-4. The arPHPV mutant ATOH7 polypeptide (N46H) does not bind DNA or activate transcription, while A47T and R65G variants retain these functions. (A-C) Electrophoretic mobility shift assay (EMSA). (A) Sequence of EMSA probe radiolabeled with ^{32}P-α-dCTP (red). The core bHLH recognition site (E-box) is highlighted. (B) EMSA autoradiogram comparing DNA-binding activity. HEK293T cells were cotransfected with plasmids encoding wildtype (WT) or variant ATOH7 proteins, or empty vector (pCS2), with or without heterodimeric bHLH partner E47. Nuclear extracts were incubated with dsDNA probe and electrophoresed through a 6% acrylamide gel. In the absence of ATOH7, native and phosphorylated E47 isoforms (67 kDa) bind DNA as a homodimer, giving a pattern with two major complexes (E47-E47). In the presence of wildtype ATOH7 (17 kDa), faster-migrating E47-ATOH7 complexes predominate. ATOH7 variants N46H (arPHPV) and L56P (corresponding to *lakritz*) fail to bind DNA, such that only E47 homodimers are observed in these lanes. In contrast, R65G and A47T variants form ATOH7-E47 heterodimers. Addition of ATOH7 blocking antibody (Ab) or cold competitor oligo (cc) decreases the amount of probe bound by the wildtype ATOH7-E47 complex. (C) Western blots of EMSA nuclear extracts probed with ATOH7 or E47 antibodies show similar levels of these proteins. (D-E) Luciferase cotransfection assays. (D) The reporter contains 7 tandem E-box sites and a minimal β-actin promoter driving expression of firefly luciferase. (D) Comparison of ATOH7 transcriptional activity. HEK293T cells were cotransfected with *Renilla* control and firefly luciferase reporters and varying doses of *ATOH7* expression vectors. Firefly luminescence counts, normalized to *Renilla*, are reported as fold activity relative to pCS2 vector. The N46H and L56P variants have no detectable transcriptional activity, and were significantly different from wild-type (*t*-test $P < 0.03$ for 100 ng and $P < 3 \times 10^{-6}$ for 20 ng). The A47T and R65G variants are not significantly different from wild-type at the high plasmid dose (100 ng, 60% and $P = 0.09$ for A47T, 100% and $P = 0.77$ for R65G*)*, but have reduced activity at the low dose (20 ng, 20% and $P < 10^{-5}$ for A47T, 60% and $P < 0.001$ for R65G). Error bars show the standard deviation of three replicates from a representative experiment. prom, promoter.

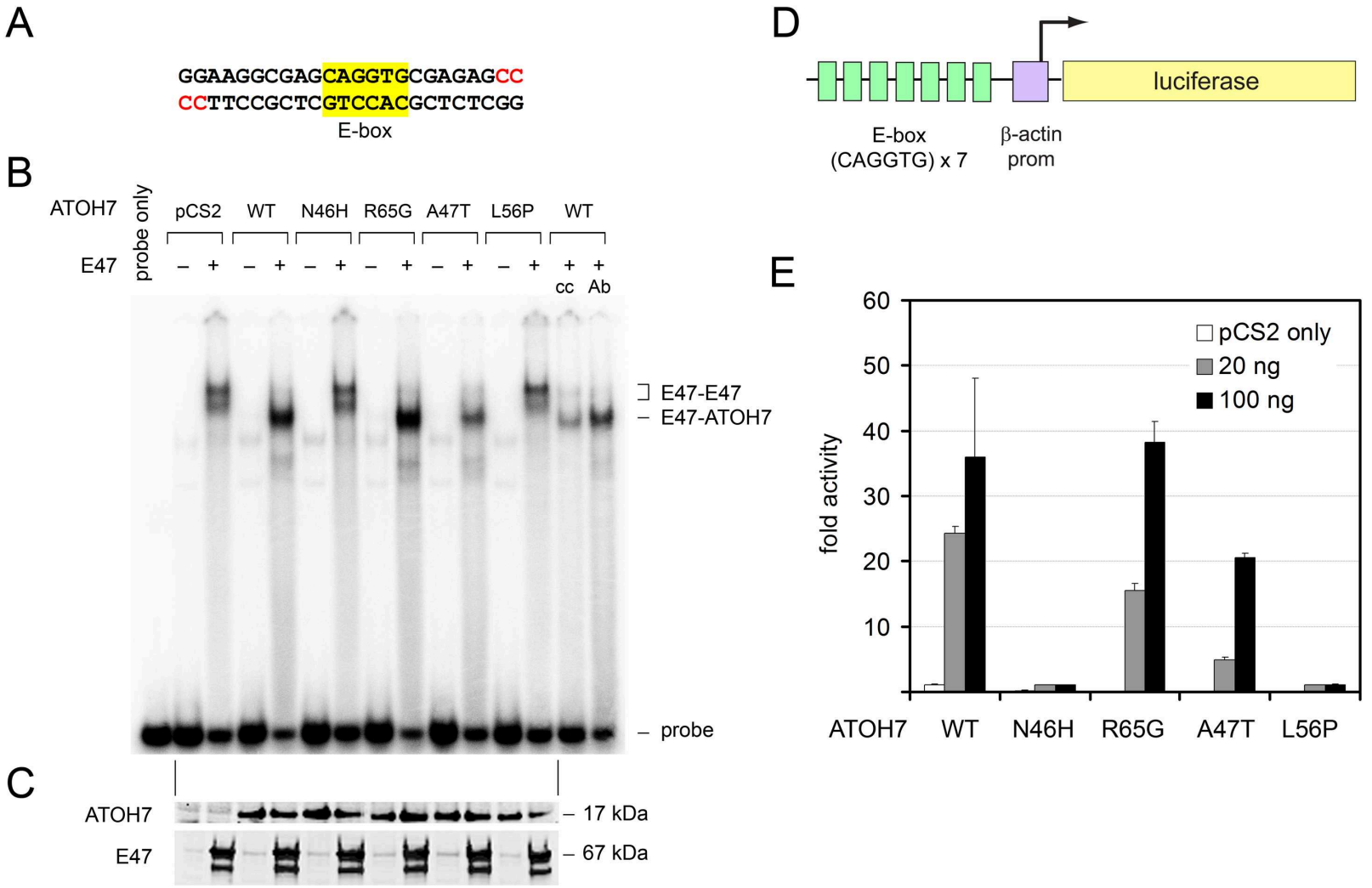
A
GGAAGGCGAGCAGGTGCGAGAGCC
CCTTCCGCTCGTCCACGCTCTCGG
E-box
B
ATOH7
probe only
pCS2
WT
N46H
R65G
A47T
L56P
WT
E47
cc
Ab
E47-E47
E47-ATOH7
probe
C
ATOH7
E47
17 kDa
67 kDa
D
luciferase
E-box
(CAGGTG) x 7
β-actin
prom
E
fold activity
pCS2 only
20 ng
100 ng
ATOH7
WT
N46H
R65G
A47T
L56P

Figure VI-5. Human *ATOH7* R65G and A47T variants rescue ganglion cell specification in *Atoh7* -/- retinal explants, but N46H and L56P mutants do not. (A) Experimental design. Eye cups from E13.5 *A*toh7 -/- embryos were electroporated *ex vivo* with a DNA solution containing bicistronic expression plasmids pUS2-myc-ATOH7-IRES-GFP (encoding wild-type or variant ATOH7 proteins) or pUS2-myc-IRES-GFP (negative control). After a 6-hour recovery period, retinas were explanted onto polycarbonate membranes, cultured for 3 days *in vitro* (DIV), fixed and immunostained as wholemount preparations. (B) Confocal images of *ATOH7*-transfected retinal explants stained with GFP and Brn3a antibodies to mark RGCs. In the absence of Atoh7 function, few RGCs are formed (GFP only). Wild-type (WT), R65G and A47T variants rescue RGC development in the transfected cell cohort, while N46H and L56P variants do not. (C) Quantitative analysis of the RGC fraction among transfected cells (GFP+). Data from two experiments (open and closed circles) are plotted together, with each point representing a different explant. The mean and SD are indicated. Each variant was compared to GFP-only or wild-type *ATOH7* controls by Student's *t*-test, with *P*-values listed below the graph. N46H and L56P mutants induce significantly fewer RGCs than wild-type *ATOH7*, and are indistinguishable from the GFP-only control. IRES, internal ribosome entry site; myc, 6X myc epitope tag; RGC, retinal ganglion cell. Scale bar, 50 μm.

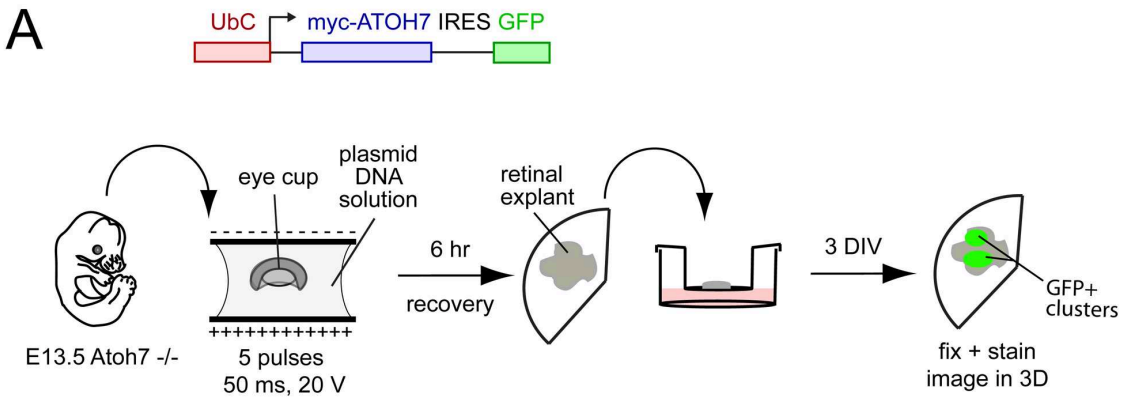

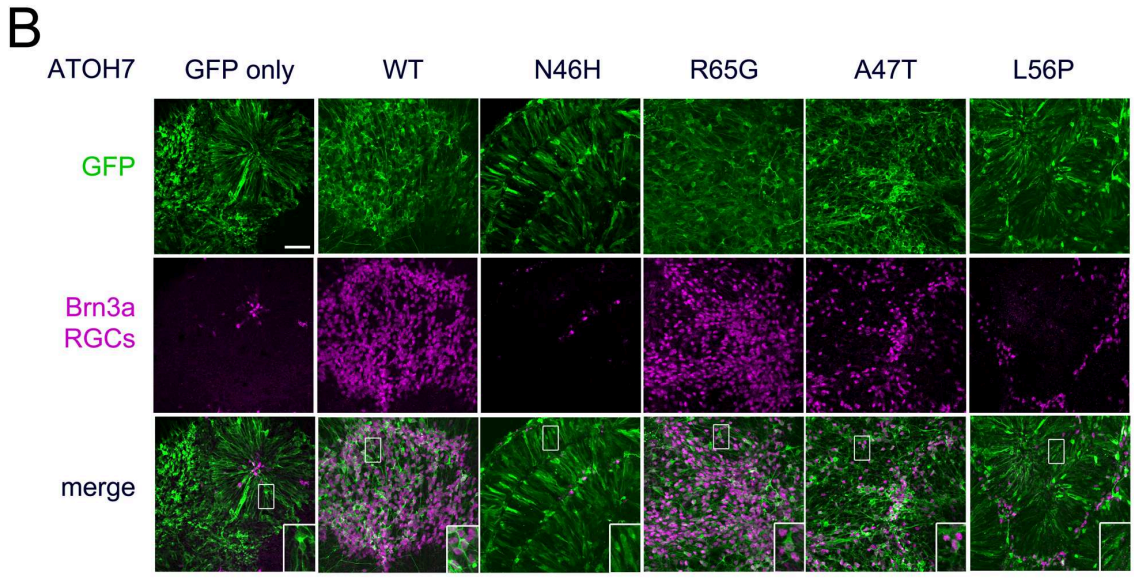

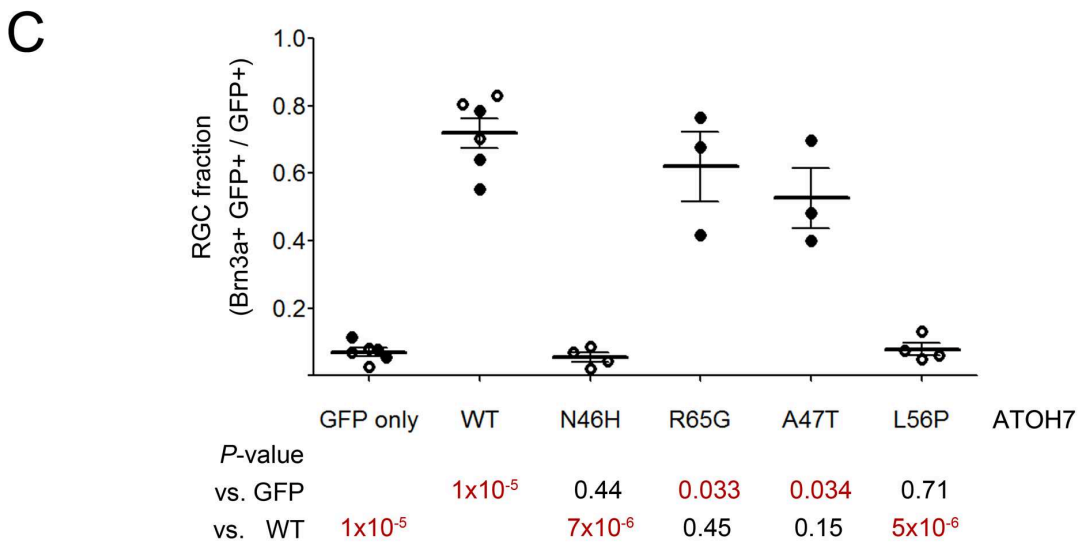

	GFP only	WT	N46H	R65G	A47T	L56P
P-value						
vs. GFP		$1x10^{-5}$	0.44	0.033	0.034	0.71
vs. WT	$1x10^{-5}$		$7x10^{-6}$	0.45	0.15	$5x10^{-6}$

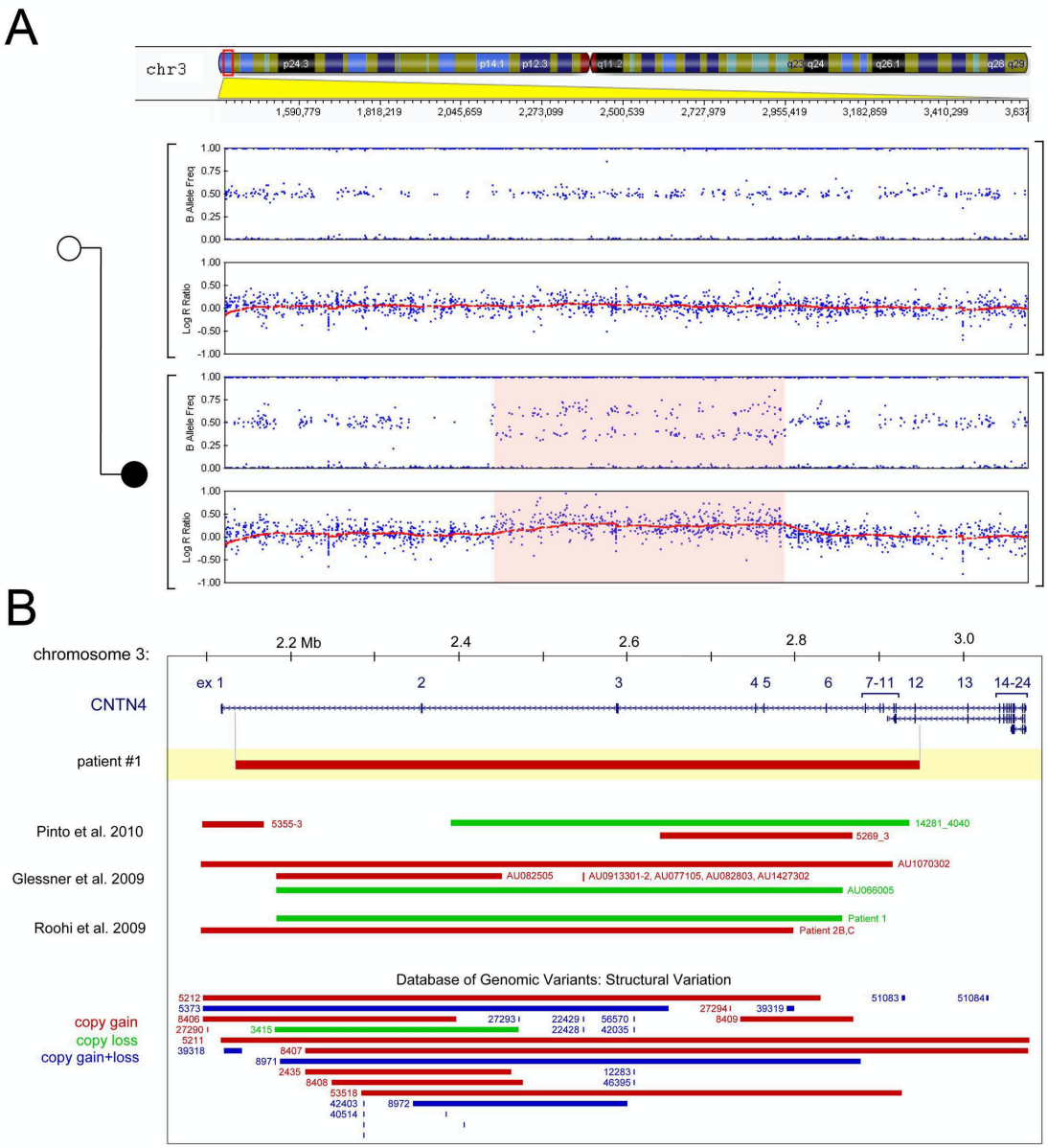

Figure VI-S1. ONA Patient 1 carries a duplication that disrupts *CNTN4*. (A) LogR ratio and B allele frequency plots show Illumina Omni1-Quad SNP genotyping for the patient and her unaffected mother. The 0.83 Mb duplication on chromosome 3p26 is shaded in red. The B-allele frequency splitting and logR ratio increase are characteristic of a 3-to-2 copy gain, which was not maternally inherited. (B) *CNTN4* (contactin-4) genomic region. The duplication in patient 1 (thick red line) spans exons 2-12 and is not present in the database of normal genomic structural variants. However, other duplications (red) and deletions (green) overlap *CNTN4* in patients with autism spectrum disorder, as reported in the indicated publications. Human genome coordinates are based on NCBI build 36 (hg18). Mb, megabase.

Figure VI-S2. The chromosome 3p26 duplication in Patient 1 is capable of producing a truncated *CNTN4* mRNA. (A) Diagram of the *CNTN4* rearrangement, which tandemly duplicates a 832 kb segment encompassing exons 2-12. Arrows mark the PCR primers used to define the molecular breakpoint between 5' (blue) and 3' (green) copies and to test the mRNA terminal structure by 3' RACE (red). (B) Standard duplex (dup) and 3-primer competitive (compet) PCRs amplify a 579 bp product (dup) that spans the novel junction between *CNTN4* intron 12 and intron 1. Only the wildtype (wt) allele was amplified in the mother (465 bp). (C) Sequence chromatogram of PCR products in (B) containing the breakpoint junction. (D,E) 3' RACE analysis of *CNTN4* mRNA in lymphoblastoid cell lines, using nested primers in exon 24 (full length) or exon 12 (truncated). (D) 3' RACE products corresponding to full-length *CNTN4* isoforms were amplified from the patient and her mother. These differ in size due to variable cDNA priming from the polyA tail and the low abundance of *CNTN4* transcripts in lymphoblastoid RNA. (E) The truncated *CNTN4* isoform, which prematurely terminates in intron 12, was only detected in the patient. (F,G) Sequence chromatograms of the wild-type (F) and truncated (G) 3' RACE products. The polyA signal is underlined. In, intron. Ex, exon.

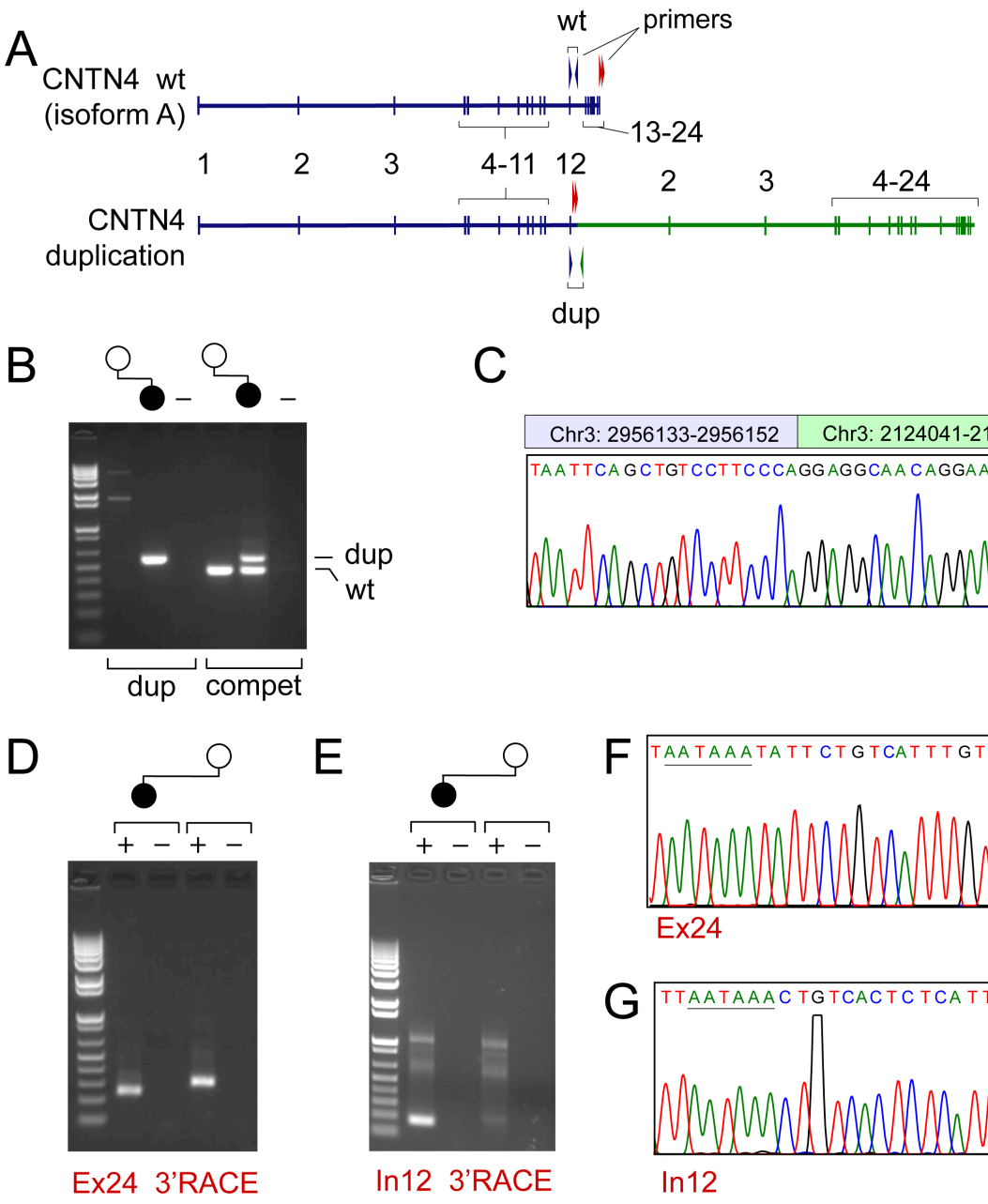
A
CNTN4 wt
(isoform A)
wt
primers
13-24
1
2
3
4-11
12
CNTN4
duplication
2
3
4-24
dup
B
dup
wt
dup
compet
C
Chr3: 2956133-2956152
Chr3: 2124041-2124060
TAATTCAGCTGTCCTTCCCAGGAGGCAACAGGAAACTTAA
D
+ − + −
Ex24 3'RACE
E
+ − + −
In12 3'RACE
F
TAATAAATATTCTGTCATTTGTAAAAA
Ex24
G
TTAATAAACTGTCACTCTCATTAAAAA
In12

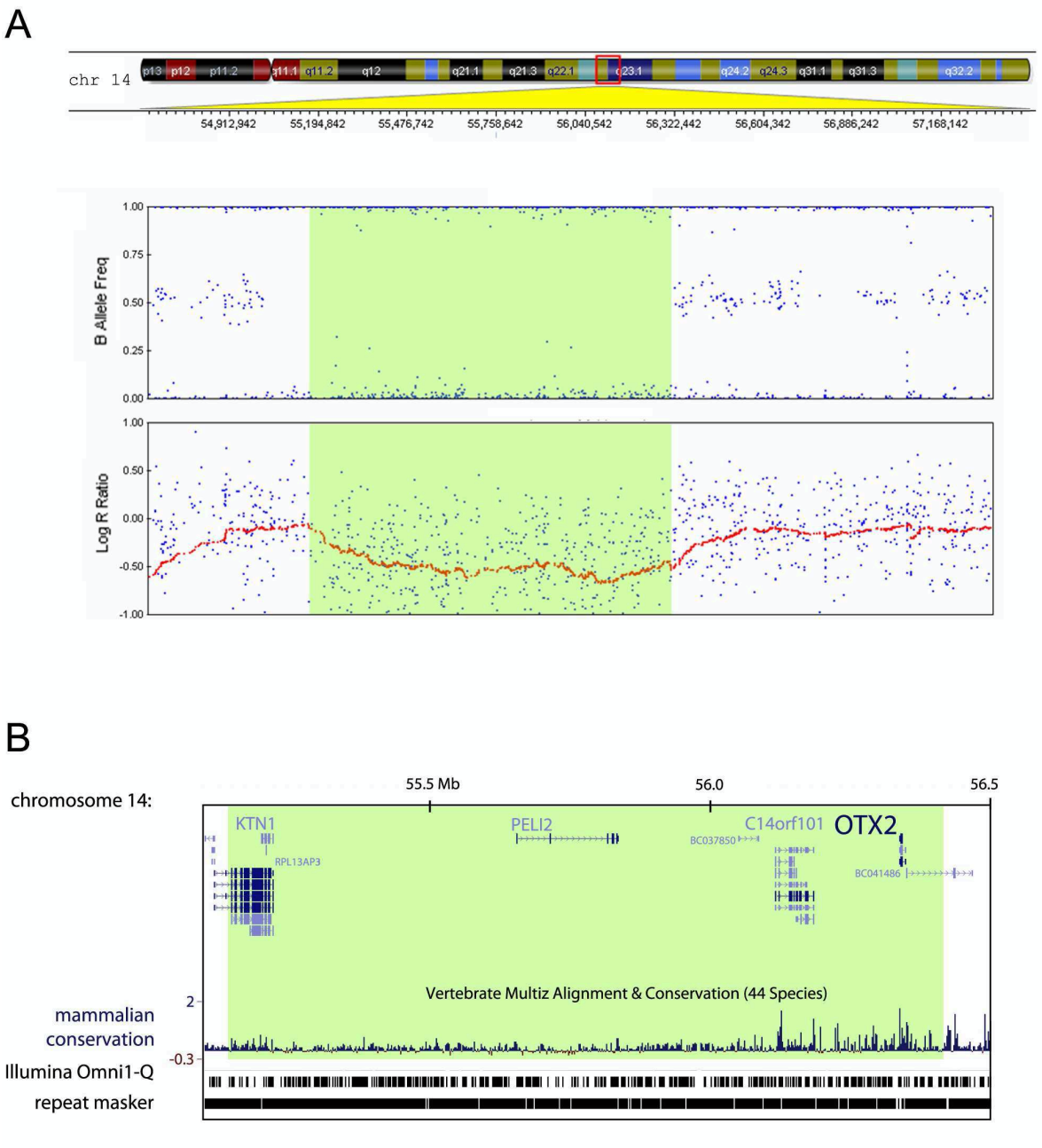

Figure VI-S3. Chromosome 14q23 deletion in optic nerve aplasia Patient 2 encompasses the *OTX2* gene. (A) LogR ratio and B allele frequency plots show Illumina Omni1-Quad SNP genotyping data. The 1.2 Mb deletion is shaded in green. The hemizygous region was identified by the pattern of homozygosity in the B-allele frequency plot and decreased intensity in logR ratio plot. (B) Expanded view of the critical region. The deletion spans four genes, including *OTX2*. The endpoints are located in repetitive DNA, so the exact coordinates and junctional sequence could not be determined. Parental DNA was not available for analysis.

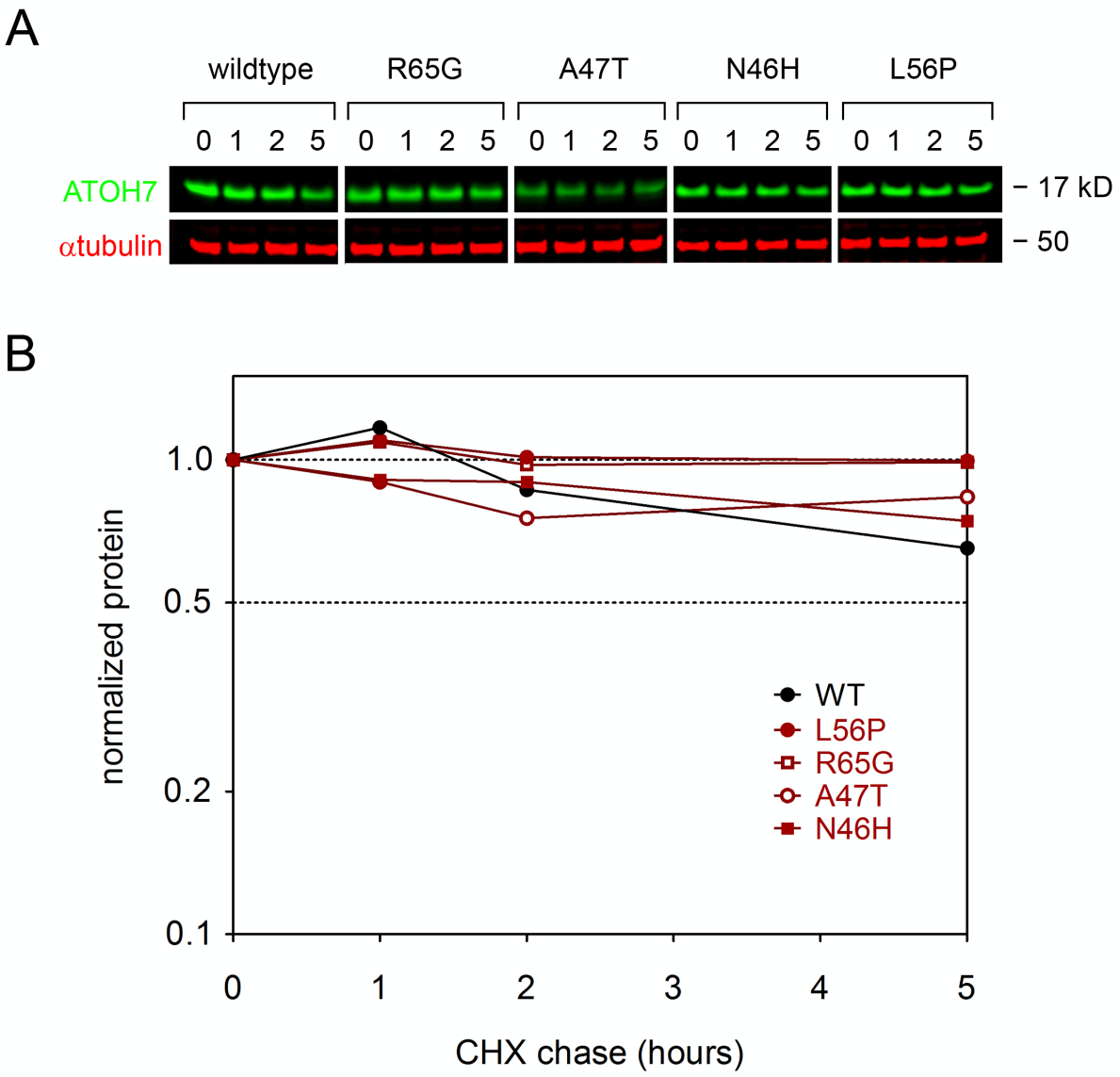

Figure VI-S4. ATOH7 variants have similar protein stability. (A) LICOR dual fluorescence Western blots of HEK293T cells transfected with wildtype or variant *ATOH7* expression plasmids. Lysates were harvested after 0-5 hours treatment with cycloheximide (CHX), which blocks synthesis of new proteins. The level of ATOH7 polypeptide was normalized to endogenous_tubulin, which has a long half-life. (B) Quantitative analysis of ATOH7 levels in (A) based on LICOR antibody fluorescence (semilog plot). The variant (red) and wildtype (black) ATOH7 proteins have equivalent decay kinetics.

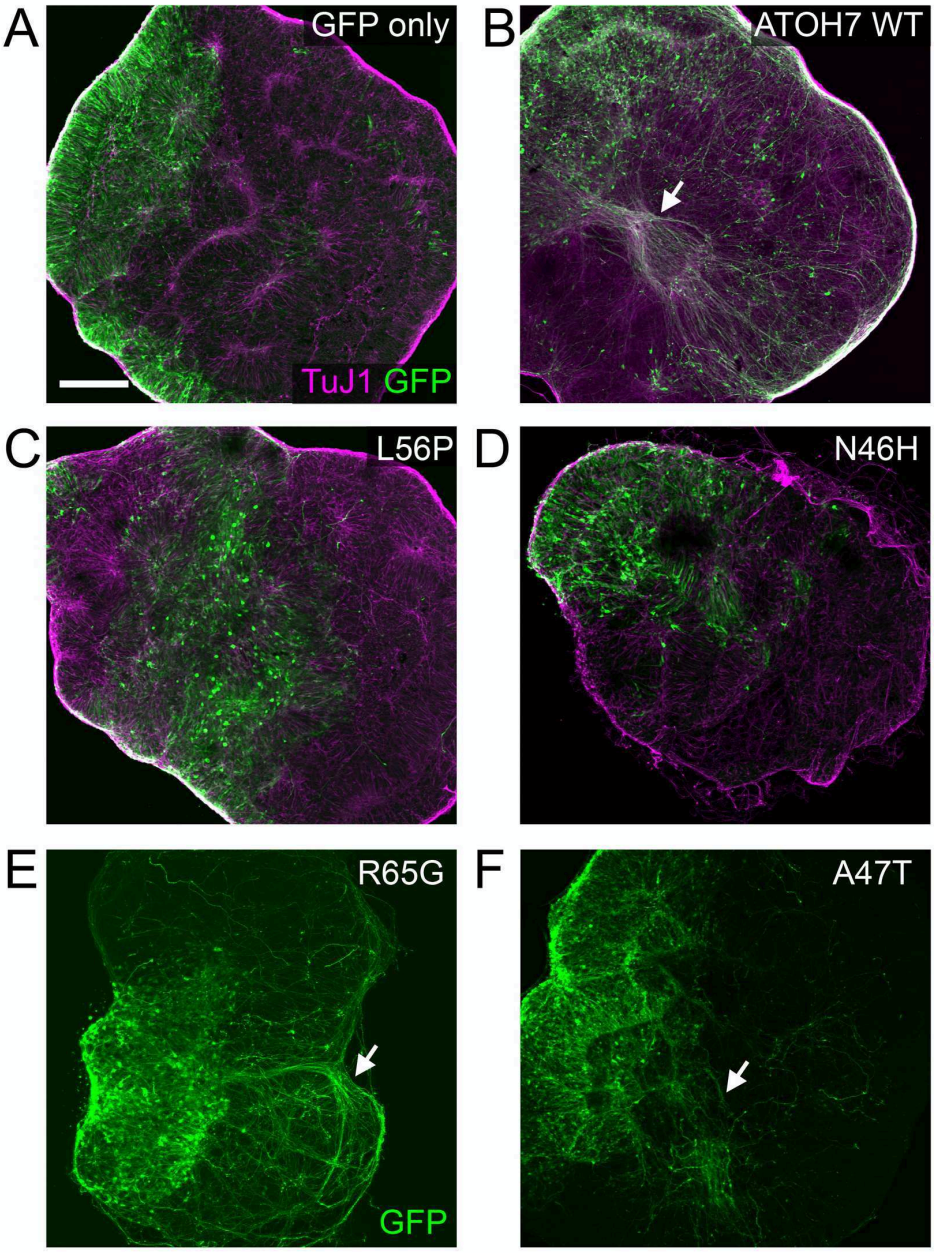

Figure VI-S5. Low power views of retinal explant rescue experiments. (A-F) Retinal explants (Fig. VI-5) coimmunostained for GFP and/or TuJ1 to mark axons. In explants transfected with wild-type *ATOH7* (B), or R65G (E) or A47T (F) variants, ganglion cell axon bundles (arrows) are abundant. However, in explants expressing GFP only (A), or *ATOH7* L56P (C) or N46H (D) variants, very few axon bundles are evident. Scale bar, 200 μm.

Table VI-S1. Clinical Features of optic nerve aplasia cases

Patient Number	Sex	Other ocular abnormalities	Septo-optic dysplasia	Endocrine or pituitary defects	Neurological or brain defects	Genetic findings	Reference
1	F	none	no	failure to thrive	developmental delay; delayed vocalization; auditory processing defects	ATOH7 p.R65>G (het); 828kb tandem dup CNTN4 ex2-12	this study
2	M	bilateral microphthalmia; retinochoroid depigmentation, absence of retinal vasculature, abnormal vessels at area of optic disc	yes	posterior pituitary ectopia; absence of pituitary infundibulum; hypothyroid, pituitary insufficiency	hypoplastic corpus callosum	1.2 MB hemizygous deletion at 14q23 (includes OTX2)	Brodsky et al. 2004
3	F	bilateral microphthalmia, bilateral iris coloboma	no	none	none		Scott et al. 1997
4	M	bilateral micropthalmia, iris coloboma (OD), pigmented epithelium mottling, choroidal neovascularization	yes	none	none		Lee et al. 1996
5	F	unilateral microopthalmia and microcornea(OS); chorioretinal atrophy; bilateral iris colobomas	no	none	none		this study

Table VI-S2. Oligonucleotide primers and PCR conditions used in this study

Experiment	Forward (sense primer 5'→3')	Reverse (antisense primer)	Cycling conditions	Notes
ATOH7 p.N46>H mut **ATOH7 p.A47>T mut** **ATOH7 p.L56>P mut**	CCTGGCGGCCCACGCGCGCGAGCGCCGCCGCATGCAG GCCTGGCGGCCAACACGCGCGAGCGCCGCCGCATGC CGCATGCAGGGGCCCAACACTGCCTTCGACCGCTTAC	GCGGCGGCGCTCGCGCGCGTGGGCCGCCAGGCGCCTG ATGCGGCGGCGCTCGCGCGTGTTGGCCGCCAGGCGCCT GCGGTCGAAGGCAGTGTTGGGCCCCTGCATGCGGCGG	94°C for 5 min; 20 cycles of [94°C for 1 min, 57°C for 1 min, 68°C 6 min]; 68°C 10 min	0.2 v/v Masteramp
ATOH7 p.R65>G mut	CTTCGACCGCTTACGCGGGGTGGTTCCCCAGTGG	CCACTGGGGAACCACCCCGCGTAAGCGGTCGAAG	95°C for 1 min; 30 cycles of [95°C for 1 min, 55°C for 1 min, 65°C 14 min]; 68°C for 10 min	0.2 v/v Masteramp
CNTN4 duplication **CNTN4 WT**	TCCAGGTGGTGGGTAAAAGA	CCAGTGTCACAGGAATGTGG ACCAACACTGAACTCTTCACCT	94°C for 3 min; 40 cycles of [94°C for 30 sec, 57°C for 1 min, 72°C 1 min]; 72°C 7 min	0.1 v/v Masteramp
3'RACE RT	N/A	GGCCACGCGTCGACTAGTACTTTTTTTTTTTTTTTT	50°C for 1 hr	
3'RACE CNTN4 ex24 upstream	TTTGCTATAGTTTGTCATTTTTGCTT	GGCCACGCGTCGACTAGTAC	94°C for 3 min; 26 cycles of [94°C for 30 sec, 57°C for 1 min, 72°C 1 min]; 72°C 7 min	
nested	TGTGTTCCTTTCTTAGTTTGATATGGT		same as above, except 33 cycles	
3'RACE CNTN4 in12 upstream	AGACAGCGTTGTTTGGCATC	GGCCACGCGTCGACTAGTAC	94°C for 3 min; 25 cycles of [94°C for 30 sec, 58°C for 1 min, 72°C 1 min]; 72°C 7 min	
nested	AGACCACTCCCTGCCAATGT		same as above, except 33 cycles and 60°C annealing	

CHAPTER VII

DISCUSSION AND FUTURE DIRECTIONS

The results in this thesis provide novel and important insights into the structure and function of *Math5* (*Atoh7*), the mechanism of RGC fate of specification, and the role of *ATOH7* in human disease. My work has opened up many new exciting avenues for future directions. My work highlights the importance of careful experimentation, proper interpretation of findings, and consideration of alternative hypotheses. In testing new ideas and hypotheses, I have often uncovered flaws in previous studies, such as the discovery of splicing of *Math5* mRNA (Kanadia and Cepko, 2010) discussed in Chapter II. In each case, I identify logical explanations for the discrepancies between our findings and the interpretations of other research groups. Lasting conclusions in science depend on reproducible results, which come from multiple lines of converging evidence. As such, there are many future directions that could expand and strengthen the conclusions presented in this dissertation.

The structure of *Math5* (*Atoh7*)

In Chapters II and VI, we examined the gene, mRNA, and protein structure of *Math5*. One observation in these studies was the high G+C content and secondary structure in the 3' terminus of the *Math5* RNA transcript, which was the likely explanation for the PCR and Northern blotting artifacts observed by

Kanadia and Cepko (2010). While this secondary structure is unlikely to disrupt transcription or RNA processing, *Math5* mRNA may be difficult to translate, and this may provide an additional level of regulation. Indeed, we observed that full-length Math5 protein could not be produced in *E. coli* (data not shown). In eukaryotes, secondary structure and high G+C content may impair translation (Baim et al., 1985; Kenneson et al., 2001). Further work is necessary to establish whether translation of *Math5* mRNA is a regulated step in retinal progenitors, and if this step is hypersensitive to ribosome functional status. In principle, impaired translation of *Math5* mRNA could contribute to the severe optic nerve hypoplasia observed in the setting of *Rpl24* riboprotein mutation in *Bst*/+ mice (Oliver et al., 2004). This could be tested directly using a Math5-HA knock-in allele (Fu et al., 2009) in *Bst* heterozygous mice, or with transfection assays in *Bst*/+ or wild-type fibroblasts *in vitro*.

The fate plasticity of *Math5* (*Atoh7*) cells

In this thesis, I have explored the plasticity of the *Math5*-expressing cells (Chapter III and V) and the timing of onset of *Math5* and RGC factor expression relative to the cell cycle (Chapters III and IV). These studies suggest that the Math5 population is heterogeneous in many aspects, including fate choice and onset of expression. Indeed, we observed that the Math5>Cre expressing population can generate all 7 major cell types on the same day during development. However, it remains unclear whether *single* Math5+ cells are multipotent at a given time during development or are heavily biased (restricted) in their fate selection. Furthermore, it remains to be determined whether the

heterogeneity in onset of Math5 expression relative to cell cycle exit has an impact on the fates chosen by Math5+ cells.

To address these questions, I propose a simple and elegant experiment: Mosaic Analysis with Double Markers (MADM) of the Math5>Cre lineage (Fig. VII-1). This technique relies on Cre-mediated interchromosomal recombination, which leads to reporter expression and sparse marking of clones (Luo, 2007; Zong et al., 2005) (Fig. VI-1A). In this system, two reciprocally chimeric reporter genes are knocked into the ubiquitously expressed ROSA26 locus (Zambrowicz et al., 1997). The two genes are chimeras of GFP and dsRed2, with two halves separated by an intron containing a loxP site, such that no functional protein is made until somatic Cre-mediated recombination occurs between these ROSA26 alleles *in trans*. If recombination occurs during G1, resulting cells are exclusively yellow, because they contain functional GFP and dsRed2 reporters (Fig. VII-1A). However, in rare mitotic recombination events during G2 or M phases, two outcomes are possible. First, one daughter may express both reporters, while the other daughter is unmarked. Second, each daughter may express a single functional reporter, such that one daughter is permanently marked by GFP, while the other is marked with dsRed2. Because these mitotic recombination events are rare, isolated clones composed of red and green cells can be readily identified (Fig. VII-1B). This is particularly evident with transiently expressed Cre-drivers, such as Ngn3>Cre (Desgraz and Herrera, 2009).

I observed that Math5>Cre transgene is expressed only in terminally mitotic progenitors or in post-mitotic precursors (Chapter III). Thus, we would

expect *only* two clone sizes from MADM analysis using Math5>Cre. Precursors in which Cre is expressed in post-mitotic (G0) cells would result in a single-cell clones that are yellow (G1 recombination pattern). In contrast, progenitors in which Cre is expressed during late S or G2 of the last cell division would generate two-cell clones with one red and one green cell (X segregation), or single-cell clones with one yellow and one unmarked cell (Z segregation). If larger clone sizes are observed, this would necessarily mean that *Math5*-expressing cells continued to cycle. Clone size could also be assessed in *Math5* -/- mice, in order to determine whether lineage cells re-enter the cell cycle.

In principle, the fates of daughters in informative two-cell clones could be concordant or discordant, and may include RGCs or other cell types. Based on our clonal analysis of explants, many progenitors that give rise to RGCs generate pairs of this cell type (Chapter IV). These data are seemingly discordant with previous clonal analysis of frog and rodent retinas (Holt et al., 1988; Turner et al., 1990), as no definitive two-RGC clones were detected in these studies. Four major differences between our study and these prior analyses could account for this discrepancy, and these could largely be reconciled by the *in vivo* MADM analysis. First, analyses were carried out in mature adult retinas, after the period of post-natal RGC culling (Farah and Easter, 2005). Thus, some RGCs among paired clones likely died during development. Second, due to technical reasons, progenitors could only be infected at E13.5 or later in the mouse, a time at which many RGCs have already exited the cell cycle. Thus, RGCs were underrepresented in clones compared to their contribution to the retina (Jeon et

al., 1998; Turner et al., 1990). Third, due to tangential dispersion (Reese and Galli-Resta, 2002) or cell migration, some RGC clones could not be definitively assigned. Fourth, species specific differences may result in different clonal properties between frogs and rodents (Holt et al., 1988).

MADM analysis with Math5>Cre would circumvent each of the limitations. As Math5>Cre is active at the onset of neurogenesis, *in vivo* clonal analysis would follow the earliest cells as they exit mitosis. Coupled with EdU birthdating, clones could be stratified based on time of cell cycle exit to precisely determine the fate spectrum *Math5*+ cells during development. Because clones are sparse and daughters in two cell clones are marked with different colors, clones could be unambiguously assigned even in the presence of cell migration. Furthermore, RGC fate could be scored in flatmounts at P0, prior to the period of post-natal culling. In the adult, the localization of reporter expression coupled with the characteristic morphologies and laminar positions of each of the major cell type would allow for unambiguous scoring of 2-cell clones. MADM analysis could also be done in *Math5* -/- mice, in order to thoroughly evaluate the secondary fate choices of cells in the *Math5* lineage. Taken together, this single experiment could confirm or challenge our previous findings, and would provide definitive and novel insights into the fate choices of Math5-expressing cells, the cell cycle timing of Math5 expression, and the frequency of symmetric RGCs clones.

The non-autonomous role of Math5-expressing cells

Though RGC development requires the function of *Math5* (Brown et al., 2001; Wang et al., 2001), we found that only 55% of RGCs are contained in the

Math5 lineage (Chapter III). Furthermore, an even smaller percentage (only 20-30%) of the earliest born cohort of RGCs expresses *Math5*, yet nearly all of these cells are lost in *Math5* -/- mice. Together, these results suggest a non-autonomous role of *Math5* in the specification of RGCs. It is likely that a secreted or cell surface factor is made by *Math5* cells, but not by neighboring neurogenic cells in the early retina.

Two sets of experiments could be used to confirm this role of *Math5* and also to identify the precise factors involved. First, analysis of chimeric mice carrying a mix of *Math5* -/- and reporter-marked wild-type cells could provide confirmation that *Math5* cells have a non-autonomous role in RGC development. Specifically, in chimeras composed predominantly of wild-type cells, we could determine whether *Math5* -/- cells are more likely to adopt the RGC fate. In reciprocal chimeras, we would expect the opposite results, i.e. wild-type cells in a *Math5* -/- environment, cannot form mature RGCs. Alternatively, *Math5* could be conditionally deleted or overexpressed using a mosaic Cre, such as Chx10>Cre (Rowan and Cepko, 2004). Second, microarray analysis could be conducted to determine the gene expression profiles of flow-sorted early *Math5*-expressing progenitors, using Math5>GFP (Hufnagel et al., 2007) or ATOH7-3034>mCherry (Ghiasvand et al., 2011) transgenic mice. These profiles could be compared in *Math5* -/- and +/+ backgrounds, to determine what specific factors are lost in *Math5* -/-. This analysis would provide candidate genes and factors that non-autonomously regulate RGC development in the early E11.5-E12.5 retina.

The RGC fate decision and the role of *Brn3b*

In recent years, clear pathways have been established to direct human embryonic stem cells towards the retinal cell fates (Lamba et al., 2006; Reh et al., 2010). Furthermore, three-dimensional culture has been used successfully to make a primordial optic cup (Eiraku et al., 2011). In addition, photoreceptor precursors derived from transgenic mice or human embryonic stem cells have been shown to integrate into the retina and restore visual function in animal models with photoreceptor degeneration (Lamba et al., 2009; MacLaren et al., 2006).

Generating retinal ganglion cells at high density and purity from embryonic stem cells has proven to be much more difficult. One missing element is a master regulatory gene for RGC development. *Math5* was a logical candidate for this role, as it occupies a central node atop the RGC differentiation cascade (Mu et al., 2005). However, the work presented in this dissertation suggests that *Math5* acts purely as a competence factor (Chapters III and V), and thus does not serve as a master regulator. The factors that bias competent progenitors towards the RGC fate remain to be determined. One potential regulator may be *Brn3b* (*Pou4f2*). I have shown that this factor is expressed in RGCs and not developing amacrine and horizontal cells (Chapter IV), and previous work has demonstrated that it is critical for terminal differentiation of RGCs and inhibition of amacrine fate (Erkman et al., 1996; Gan et al., 1996; Qiu et al., 2008; Xiang, 1998). In principle, Brn3b may substantially bias RGC fate in competent mouse progenitors, similar to that observed in chick retroviral over-expression studies

(Liu et al., 2000). However, definitive *Brn3b* lineage and over-expression studies in the mouse are lacking. To prove that Brn3b is a marker of committed RGCs, the descendents of Brn3b cells could be traced using a Brn3b>Cre BAC transgenic mouse, similar to the tracing experiments presented in Chapter III. It is expected that lineage-marked cells only contain ganglion cells. To establish the role of Brn3b in biasing RGC fate, Brn3b could be expressed in the *Math5* pattern, using a Math5>Brn3b-IRES-Cre BAC transgene. In this way, lineal descendents of *Brn3b* over-expressing cells could be followed by crossing to *floxed* reporters. It is expected that *Brn3b* would bias Math5 lineage cells towards RGCs and suppress amacrine fates. Together, these studies would determine if *Brn3b* is sufficient for stimulating ganglion cell production in competent progenitors and if it is a master regulator of RGC development.

Testing the pioneering model of RGC fate

In Chapter V, I thoroughly characterized the birthdates of ganglion cells in Crx>Math5 Tg; Math5 -/- mice. I found that high-level expression of Math5 did not extend the profile of RGC births, and that early born ganglion cells were largely lost in these mice. This event was correlated with pathfinding defects, RGC death, and incomplete rescue. These results support a pioneering model of RGC fate in the mouse, as is evident in zebrafish (Pittman et al., 2008). However, causation could not be definitely established due to confounding variables in the experiment. Thus, a cleaner experiment could directly test the pioneering model of RGC development in mice, and determine the critical embryonic times for this pioneering. In principle, the critical window of pioneering

RGC axons may be related to the closure of the optic fissure, which occurs during early development (Barishak, 1992; Gregory-Evans et al., 2004). This critical time period could be determined using an inducible *Math5* expression system in the context of a *Math5* -/- genotype, i.e. with a dual transgenic Tet-On system (reviewed in (Corbel and Rossi, 2002)). While this may be cumbersome, *Math5* expression, and thus the window of RGC births, could be precisely controlled and delayed. It is expected that induction at E11.5 would result in complete rescue, while induction at later developmental time points (e.g. E14.5) would rescue initial specification, but not terminal differentiation of RGCs.

The role of *ATOH7* (*Math5*) in human disease

Data presented in Chapter VI, together with recent studies (Ghiasvand et al., 2011; Khan et al., 2011), have established a role for *ATOH7* in congenital neurovascular diseases of the retina. Causative mutations in *ATOH7* were identified in a group of related developmental disorders, including non-syndromic congenital retinal non-attachment (NCRNA, Ghiasvand et al., 2011), vitreoretinal dysplasia (VRD, Khan et al., 2011), and persistent hyperplastic primary vitreous (PHPV, Chapter VI). These diseases all share common pathogenetic features and an overlapping clinical spectrum of symptoms. The common genetic feature among patients is a homozygous loss-of-function mutation in *ATOH7*. Thus, the underlying cause of disease is likely the agenesis of the optic nerve. This was not appreciated in many of these patients, because retinovascular disease prevented visualization of the fundus (Ghiasvand et al., 1998; Khaliq et al., 2001). Given the wide spectrum of symptoms in among NCRNA, VRD, and

PHPV, visualization of optic nerves by magnetic resonance imaging should be implemented in patients with congenital retinovascular disease. The prevalence of *ATOH7* mutations in PHPV, NCRNA, and VR has not been thoroughly established. However, *ATOH7* is a good genetic candidate for these diseases, as well as related disorders such as familial exudative vitreoretinopathy (FEVR) where no mutations have been found in Wnt signaling pathway genes (Warden et al., 2007). Thus, patients presenting with retinal vascular disease and optic nerve hypoplasia or hypoplasia, in the absence of other CNS or pituitary defects, should be screened for *ATOH7* mutations.

Concluding remarks

In summary, I have presented seminal findings about the role of mouse *Math5* in retinal development, and the role of its human ortholog *ATOH7* in disease. My thesis has clearly elucidated the structure and expression profile of the *Math5* gene. I have precisely timed the RGC fate commitment step, which revealed a striking heterogeneity among retinal progenitors. Furthermore, my work has definitively established that *Math5* is not sufficient for RGC fate specification. I have shown that *Math5*-expressing cells have a non-autonomous role in RGC development, and suggested that pioneering ganglion cells are important for the survival and pathfinding of late born RGCs. Additionally, I have identified causative mutations in *ATOH7* in PHPV, and have shown that mutations in *ATOH7* are not a common cause of isolated optic nerve hypoplasia or aplasia. Together, these findings extend our understanding of RGC development and provide novel insights that may be important for diagnostic

testing and the development of ganglion cell replacement therapies in diseases of the optic nerve.

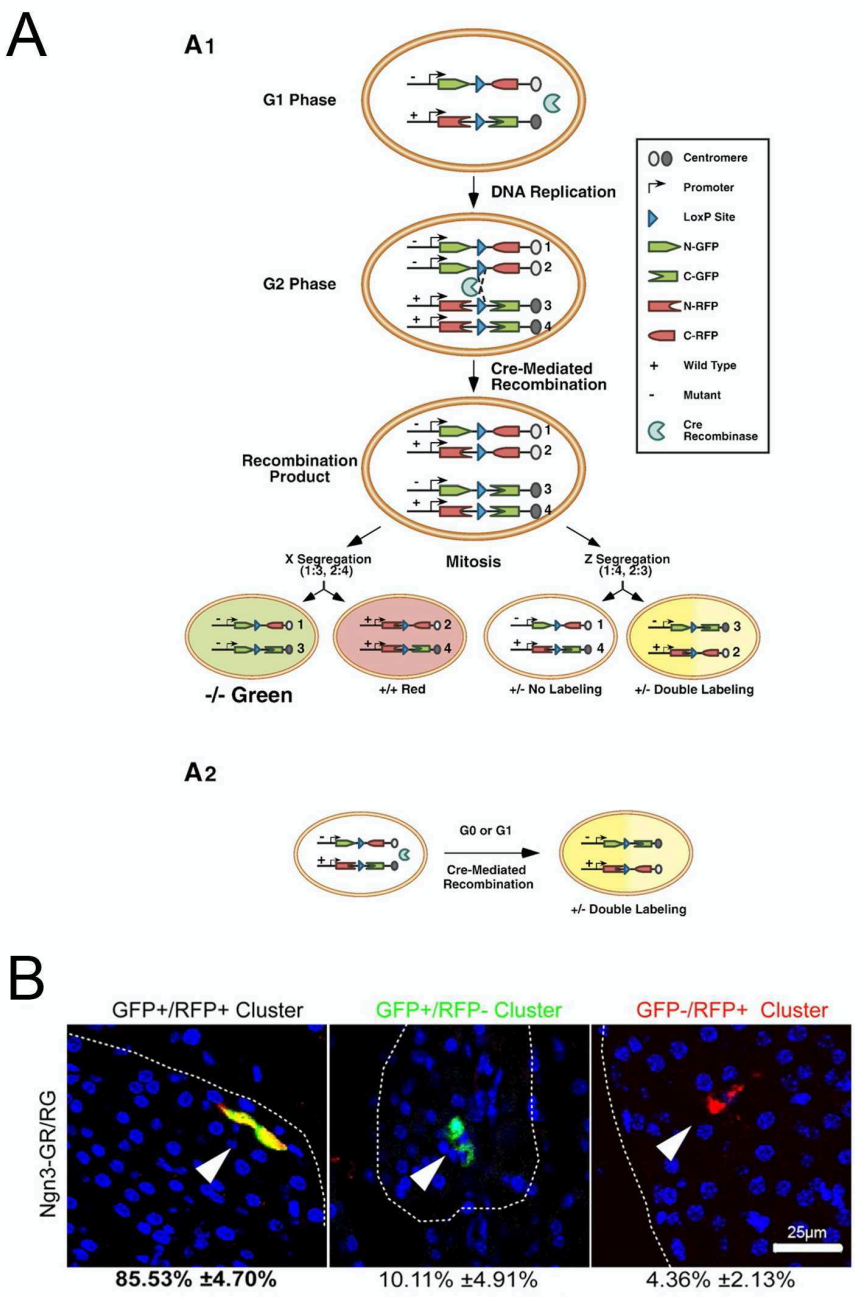

Figure VII-1. Outline of the Mosaic Analysis of Double Markers (MADM) strategy. (A) The MADM technique consists of two reciprocally chimeric reporters. Recombination can occur in G2, and be resolved by X or Z segregation. In X segregation, a single cell is double-colored. In Z segregation, both daughter cells are labeled, with one functional reporter active in each (one green and one red cells). Recombination can also occur in G1 or post-mitotic cells, which generates double-colored cells. (B) Example of sparse-labeling in pancreatic islet cells using MADM strategy with Ngn3>Cre driver. Images adapted from Zong et al., 2005 and Desgraz and Herrera, 2009.

REFERENCES

Abu-Amero, K. K. (2011). Leber's Hereditary Optic Neuropathy: The Mitochondrial Connection Revisited. *Middle East Afr J Ophthalmol* **18**, 17-23.

Adler, R. and Hatlee, M. (1989). Plasticity and differentiation of embryonic retinal cells after terminal mitosis. *Science* **243**, 391-3.

Ahmad, I., Dooley, C. M. and Polk, D. L. (1997). Delta-1 is a regulator of neurogenesis in the vertebrate retina. *Dev Biol* **185**, 92-103.

Akazawa, C., Ishibashi, M., Shimizu, C., Nakanishi, S. and Kageyama, R. (1995). A mammalian helix-loop-helix factor structurally related to the product of Drosophila proneural gene atonal is a positive transcriptional regulator expressed in the developing nervous system. *J Biol Chem* **270**, 8730-8.

Akimoto, M., Cheng, H., Zhu, D., Brzezinski, J. A., Khanna, R., Filippova, E., Oh, E. C., Jing, Y., Linares, J. L., Brooks, M. et al. (2006). Targeting of GFP to newborn rods by Nrl promoter and temporal expression profiling of flow-sorted photoreceptors. *Proc Natl Acad Sci U S A* **103**, 3890-5.

Alarcon, M., Abrahams, B. S., Stone, J. L., Duvall, J. A., Perederiy, J. V., Bomar, J. M., Sebat, J., Wigler, M., Martin, C. L., Ledbetter, D. H. et al. (2008). Linkage, association, and gene-expression analyses identify CNTNAP2 as an autism-susceptibility gene. *Am J Hum Genet* **82**, 150-9.

Alexiades, M. R. and Cepko, C. (1996). Quantitative analysis of proliferation and cell cycle length during development of the rat retina. *Dev Dyn* **205**, 293-307.

Allingham, R. R., Liu, Y. and Rhee, D. J. (2009). The genetics of primary open-angle glaucoma: a review. *Exp Eye Res* **88**, 837-44.

Alonso, S., Minty, A., Bourlet, Y. and Buckingham, M. (1986). Comparison of three actin-coding sequences in the mouse; evolutionary relationships between the actin genes of warm-blooded vertebrates. *J Mol Evol* **23**, 11-22.

Altschuler, D. M., Turner, D. L. and Cepko, C. L. (1991). Specification of cell type in the vertebrate retina. In *Cell Lineage and Cell Fate in Visual System Development*, (ed. D. M. K. Lam and C. J. Shatz), pp. 37-58. Cambridge, MA: MIT Press.

Altshuler, D. M., Turner, D. L. and Cepko, C. L. (1991). Specification of cell type in the vertebrate retina. In *Cell Lineage and Cell Fate in Visual System Development.*, (ed. D. M. K. Lam and C. J. Shatz), pp. 37-58. Cambridge, MA: MIT Press.

Andrews, B. J., Proteau, G. A., Beatty, L. G. and Sadowski, P. D. (1985). The FLP recombinase of the 2 micron circle DNA of yeast: interaction with its target sequences. *Cell* **40**, 795-803.

Applebury, M. L., Antoch, M. P., Baxter, L. C., Chun, L. L., Falk, J. D., Farhangfar, F., Kage, K., Krzystolik, M. G., Lyass, L. A. and Robbins, J. T. (2000). The murine cone photoreceptor: a single cone type expresses both S and M opsins with retinal spatial patterning. *Neuron* **27**, 513-23.

Ashery-Padan, R. and Gruss, P. (2001). Pax6 lights-up the way for eye development. *Curr Opin Cell Biol* **13**, 706-14.

Atchley, W. R. and Fitch, W. M. (1997). A natural classification of the basic helix-loop-helix class of transcription factors. *Proc Natl Acad Sci USA* **94**, 5172-6.

Austin, C. P., Feldman, D. E., Ida, J. A., Jr. and Cepko, C. L. (1995). Vertebrate retinal ganglion cells are selected from competent progenitors by the action of Notch. *Development* **121**, 3637-50.

Azuma, N., Yamaguchi, Y., Handa, H., Tadokoro, K., Asaka, A., Kawase, E. and Yamada, M. (2003). Mutations of the PAX6 gene detected in patients with a variety of optic-nerve malformations. *Am J Hum Genet* **72**, 1565-70.

Badea, T. C., Cahill, H., Ecker, J., Hattar, S. and Nathans, J. (2009). Distinct roles of transcription factors brn3a and brn3b in controlling the development, morphology, and function of retinal ganglion cells. *Neuron* **61**, 852-64.

Baim, S. B., Pietras, D. F., Eustice, D. C. and Sherman, F. (1985). A mutation allowing an mRNA secondary structure diminishes translation of Saccharomyces cerevisiae iso-1-cytochrome c. *Mol Cell Biol* **5**, 1839-46.

Baker, K. E. and Parker, R. (2004). Nonsense-mediated mRNA decay: terminating erroneous gene expression. *Curr Opin Cell Biol* **16**, 293-9.

Bakrania, P., Efthymiou, M., Klein, J. C., Salt, A., Bunyan, D. J., Wyatt, A., Ponting, C. P., Martin, A., Williams, S., Lindley, V. et al. (2008). Mutations in BMP4 cause eye, brain, and digit developmental anomalies: overlap between the BMP4 and hedgehog signaling pathways. *Am J Hum Genet* **82**, 304-19.

Barishak, Y. R. (1992). Embryology of the eye and its adnexae. *Dev Ophthalmol* **24**, 1-142.

Barnstable, C. J., Hofstein, R. and Akagawa, K. (1985). A marker of early amacrine cell development in rat retina. *Brain Res* **352**, 286-90.

Barton, K. M. and Levine, E. M. (2008). Expression patterns and cell cycle profiles of PCNA, MCM6, cyclin D1, cyclin A2, cyclin B1, and phosphorylated histone H3 in the developing mouse retina. *Dev Dyn* **237**, 672-82.

Bassett, E. A., Pontoriero, G. F., Feng, W., Marquardt, T., Fini, M. E., Williams, T. and West-Mays, J. A. (2007). Conditional deletion of activating protein 2alpha (AP-2alpha) in the developing retina demonstrates non-cell-autonomous roles for AP-2alpha in optic cup development. *Mol Cell Biol* **27**, 7497-510.

Baye, L. M. and Link, B. A. (2008). Nuclear migration during retinal development. *Brain Res* **1192**, 29-36.

Belliveau, M. J. and Cepko, C. L. (1999). Extrinsic and intrinsic factors control the genesis of amacrine and cone cells in the rat retina. *Development* **126**, 555-66.

Benezra, R., Davis, R. L., Lockshon, D., Turner, D. L. and Weintraub, H. (1990). The protein Id: a negative regulator of helix-loop-helix DNA binding proteins. *Cell* **61**, 49-59.

Berger, W., Meindl, A., van de Pol, T. J., Cremers, F. P., Ropers, H. H., Doerner, C., Monaco, A., Bergen, A. A., Lebo, R., Warburgh, M. et al. (1992a). Isolation of a candidate gene for Norrie disease by positional cloning. *Nat Genet* **2**, 84.

Berger, W., van de Pol, D., Warburg, M., Gal, A., Bleeker-Wagemakers, L., de Silva, H., Meindl, A., Meitinger, T., Cremers, F. and Ropers, H. H. (1992b). Mutations in the candidate gene for Norrie disease. *Hum Mol Genet* **1**, 461-5.

Berget, S. M. (1995). Exon recognition in vertebrate splicing. *J Biol Chem* **270**, 2411-4.

Berget, S. M., Berk, A. J., Harrison, T. and Sharp, P. A. (1978). Spliced segments at the 5' termini of adenovirus-2 late mRNA: a role for heterogeneous nuclear RNA in mammalian cells. *Cold Spring Harb Symp Quant Biol* **42 Pt 1**, 523-9.

Berk, A. J. and Sharp, P. A. (1977). Sizing and mapping of early adenovirus mRNAs by gel electrophoresis of S1 endonuclease-digested hybrids. *Cell* **12**, 721-32.

Bertrand, N., Castro, D. S. and Guillemot, F. (2002). Proneural genes and the specification of neural cell types. *Nat Rev Neurosci* **3**, 517-30.

Biagini, G., Baldelli, E., Longo, D., Contri, M. B., Guerrini, U., Sironi, L., Gelosa, P., Zini, I., Ragsdale, D. S. and Avoli, M. (2008). Proepileptic influence of a focal vascular lesion affecting entorhinal cortex-CA3 connections after status epilepticus. *J Neuropathol Exp Neurol* **67**, 687-701.

Blackburn, D. C., Conley, K. W., Plachetzki, D. C., Kempler, K., Battelle, B. A. and Brown, N. L. (2008). Isolation and expression of Pax6 and atonal homologues in the American horseshoe crab, Limulus polyphemus. *Dev Dyn* **237**, 2209-19.

Blackshaw, S., Harpavat, S., Trimarchi, J., Cai, L., Huang, H., Kuo, W. P., Weber, G., Lee, K., Fraioli, R. E., Cho, S. H. et al. (2004). Genomic analysis of mouse retinal development. *PLoS Biol* **2**, E247.

Blanco, R., Salvador, F., Galan, A. and Gil-Gibernau, J. J. (1992). Aplasia of the optic nerve: report of three cases. *J Pediatr Ophthalmol Strabismus* **29**, 228-31.

Blanks, J. C. and Johnson, L. V. (1983). Selective lectin binding of the developing mouse retina. *J Comp Neurol* **221**, 31-41.

Boije, H., Edqvist, P. H. and Hallbook, F. (2009). Horizontal cell progenitors arrest in G2-phase and undergo terminal mitosis on the vitreal side of the chick retina. *Dev Biol* **330**, 105-13.

Borchert, M. and Garcia-Filion, P. (2008). The syndrome of optic nerve hypoplasia. *Curr Neurol Neurosci Rep* **8**, 395-403.

Borchert, M., McCulloch, D., Rother, C. and Stout, A. U. (1995). Clinical assessment, optic disk measurements, and visual-evoked potential in optic nerve hypoplasia. *Am J Ophthalmol* **120**, 605-12.

Bovolenta, P., Mallamaci, A., Briata, P., Corte, G. and Boncinelli, E. (1997). Implication of OTX2 in pigment epithelium determination and neural retina differentiation. *J Neurosci* **17**, 4243-52.

Bradbury, E. M. (1992). Reversible histone modifications and the chromosome cell cycle. *Bioessays* **14**, 9-16.

Bradford, M. M. (1976). A rapid and sensitive method for the quantitation of microgram quantities of protein utilizing the principle of protein-dye binding. *Anal Biochem* **72**, 248-54.

Brett, D., Pospisil, H., Valcarcel, J., Reich, J. and Bork, P. (2002). Alternative splicing and genome complexity. *Nat Genet* **30**, 29-30.

Brincat, J. L., Pfeiffer, J. K. and Telesnitsky, A. (2002). RNase H activity is required for high-frequency repeat deletion during Moloney murine leukemia virus replication. *J Virol* **76**, 88-95.

Bringmann, A., Pannicke, T., Grosche, J., Francke, M., Wiedemann, P., Skatchkov, S. N., Osborne, N. N. and Reichenbach, A. (2006). Muller cells in the healthy and diseased retina. *Prog Retin Eye Res* **25**, 397-424.

Brodrick, J. D. (1972). Corneal blood staining after hyphaema. *Br J Ophthalmol* **56**, 589-93.

Brodsky, M. C., Atreides, S. P., Fowlkes, J. L. and Sundin, O. H. (2004). Optic nerve aplasia in an infant with congenital hypopituitarism and posterior pituitary ectopia. *Arch Ophthalmol* **122**, 125-6.

Brodsky, M. C. and Glasier, C. M. (1993). Optic nerve hypoplasia. Clinical significance of associated central nervous system abnormalities on magnetic resonance imaging. *Arch Ophthalmol* **111**, 66-74.

Brown, N. L., Dagenais, S. L., Chen, C. M. and Glaser, T. (2002). Molecular characterization and mapping of ATOH7, a human atonal homolog with a predicted role in retinal ganglion cell development. *Mamm Genome* **13**, 95-101.

Brown, N. L., Kanekar, S., Vetter, M. L., Tucker, P. K., Gemza, D. L. and Glaser, T. (1998). Math5 encodes a murine basic helix-loop-helix transcription factor expressed during early stages of retinal neurogenesis. *Development* **125**, 4821-33.

Brown, N. L., Patel, S., Brzezinski, J. and Glaser, T. (2001). Math5 is required for retinal ganglion cell and optic nerve formation. *Development* **128**, 2497-508.

Brzezinski, J. (2005). The role of Math5 in retinal development. In *Human Genetics*, vol. Ph. D. (ed., pp. 236. Ann Arbor: University of Michigan.

Brzezinski, J. A., Brown, N. L., Tanikawa, A., Bush, R. A., Sieving, P. A., Vitaterna, M. H., Takahashi, J. S. and Glaser, T. (2005). Loss of circadian photoentrainment and abnormal retinal electrophysiology in Math5 mutant mice. *Invest Ophthalmol Vis Sci* **46**, 2540-51.

Brzezinski, J. A. and Glaser, T. (2004). Math5 establishes retinal ganglion cell competence in postmitotic progenitor cells. *Invest Ophthalmol Vis Sci* **45**, 3422 E-abstract.

Brzezinski, J. A., Kim, E. J., Johnson, J. E. and Reh, T. A. (2011). Ascl1 expression defines a subpopulation of lineage-restricted progenitors in the mammalian retina. *Development* **138**, 3519-31.

Brzezinski, J. A., Lamba, D. A. and Reh, T. A. (2010). Blimp1 controls photoreceptor versus bipolar cell fate choice during retinal development. *Development* **137**, 619-29.

Brzezinski, J. A., Prasov, L. and Glaser, T. (2012). Math5 defines the ganglion cell competence state in a subpopulation of retinal progenitor cells exiting the cell cycle. *Dev Biol* **In press.**

Brzezinski, J. A., Schulz, S. M., Crawford, S., Wroblewski, E., Brown, N. L. and Glaser, T. (2003). Math5 null mice have abnormal retinal and persistent hyaloid vasculatures. *Dev Biol* **259**, 394.

Buck, S. B., Bradford, J., Gee, K. R., Agnew, B. J., Clarke, S. T. and Salic, A. (2008). Detection of S-phase cell cycle progression using 5-ethynyl-2'-deoxyuridine incorporation with click chemistry, an alternative to using 5-bromo-2'-deoxyuridine antibodies. *Biotechniques* **44**, 927-9.

Buono, L. M., Foroozan, R., Sergott, R. C. and Savino, P. J. (2002). Is normal tension glaucoma actually an unrecognized hereditary optic neuropathy? New evidence from genetic analysis. *Curr Opin Ophthalmol* **13**, 362-70.

Carelli, V., Ross-Cisneros, F. N. and Sadun, A. A. (2002). Optic nerve degeneration and mitochondrial dysfunction: genetic and acquired optic neuropathies. *Neurochem Int* **40**, 573-84.

Carter-Dawson, L. D. and LaVail, M. M. (1979). Rods and cones in the mouse retina. II. Autoradiographic analysis of cell generation using tritiated thymidine. *J Comp Neurol* **188**, 263-72.

Cayouette, M., Barres, B. A. and Raff, M. (2003). Importance of intrinsic mechanisms in cell fate decisions in the developing rat retina. *Neuron* **40**, 897-904.

Cech, T. R. (1986). The generality of self-splicing RNA: relationship to nuclear mRNA splicing. *Cell* **44**, 207-10.

Cepko, C. L. (1999). The roles of intrinsic and extrinsic cues and bHLH genes in the determination of retinal cell fates. *Curr Opin Neurobiol* **9**, 37-46.

Cepko, C. L., Austin, C. P., Yang, X., Alexiades, M. and Ezzeddine, D. (1996). Cell fate determination in the vertebrate retina. *Proc Natl Acad Sci U S A* **93**, 589-95.

Challa, P. (2004). Glaucoma genetics: advancing new understandings of glaucoma pathogenesis. *Int Ophthalmol Clin* **44**, 167-85.

Chatelain, G., Fossat, N., Brun, G. and Lamonerie, T. (2006). Molecular dissection reveals decreased activity and not dominant negative effect in human OTX2 mutants. *J Mol Med (Berl)* **84**, 604-15.

Chen, J. and Smith, L. E. (2007). Retinopathy of prematurity. *Angiogenesis* **10**, 133-40.

Chen, J. H., Wang, D., Huang, C., Zheng, Y., Chen, H., Pang, C. P. and Zhang, M. (2012). Interactive effects of ATOH7 and RFTN1 in association with adult-onset primary open angle glaucoma. *Invest Ophthalmol Vis Sci*.

Chen, P., Johnson, J. E., Zoghbi, H. Y. and Segil, N. (2002). The role of Math1 in inner ear development: Uncoupling the establishment of the sensory primordium from hair cell fate determination. *Development* **129**, 2495-505.

Chen, S., Wang, Q. L., Nie, Z., Sun, H., Lennon, G., Copeland, N. G., Gilbert, D. J., Jenkins, N. A. and Zack, D. J. (1997). Crx, a novel Otx-like paired-homeodomain protein, binds to and transactivates photoreceptor cell-specific genes. *Neuron* **19**, 1017-30.

Cheng, H., Aleman, T. S., Cideciyan, A. V., Khanna, R., Jacobson, S. G. and Swaroop, A. (2006). In vivo function of the orphan nuclear receptor NR2E3 in establishing photoreceptor identity during mammalian retinal development. *Hum Mol Genet* **15**, 2588-602.

Chien, C. T., Hsiao, C. D., Jan, L. Y. and Jan, Y. N. (1996). Neuronal type information encoded in the basic-helix-loop-helix domain of proneural genes. *Proc Natl Acad Sci USA* **93**, 13239-44.

Cho, E. A. and Dressler, G. R. (1998). TCF-4 binds beta-catenin and is expressed in distinct regions of the embryonic brain and limbs. *Mech Dev* **77**, 9-18.

Chooniedass-Kothari, S., Emberley, E., Hamedani, M. K., Troup, S., Wang, X., Czosnek, A., Hube, F., Mutawe, M., Watson, P. H. and Leygue, E. (2004). The steroid receptor RNA activator is the first functional RNA encoding a protein. *FEBS Lett* **566**, 43-7.

Chow, R. L. and Lang, R. A. (2001). Early eye development in vertebrates. *Annu Rev Cell Dev Biol* **17**, 255-96.

Cocquet, J., Chong, A., Zhang, G. and Veitia, R. A. (2006). Reverse transcriptase template switching and false alternative transcripts. *Genomics* **88**, 127-31.

Cogan, D. G. (1971). Congenital anomalies of the retina. *Birth Defects Orig Artic Ser* **7**, 41-51.

Cohen, J. (1960). A coefficient of agreement for nominal scales. *Educ Psychol Meas* **20** 37–46.

Copt, R. P., Thomas, R. and Mermoud, A. (1999). Corneal thickness in ocular hypertension, primary open-angle glaucoma, and normal tension glaucoma. *Arch Ophthalmol* **117**, 14-6.

Corbel, S. Y. and Rossi, F. M. (2002). Latest developments and in vivo use of the Tet system: ex vivo and in vivo delivery of tetracycline-regulated genes. *Curr Opin Biotechnol* **13**, 448-52.

Crespo, D., O'Leary, D. D. and Cowan, W. M. (1985). Changes in the numbers of optic nerve fibers during late prenatal and postnatal development in the albino rat. *Brain Res* **351**, 129-34.

Cui, S., Otten, C., Rohr, S., Abdelilah-Seyfried, S. and Link, B. A. (2007). Analysis of aPKClambda and aPKCzeta reveals multiple and redundant functions during vertebrate retinogenesis. *Mol Cell Neurosci* **34**, 431-44.

Cushman, L. J., Burrows, H. L., Seasholtz, A. F., Lewandoski, M., Muzyczka, N. and Camper, S. A. (2000). Cre-mediated recombination in the pituitary gland. *Genesis* **28**, 167-74.

Dakubo, G. D. and Wallace, V. A. (2004). Hedgehogs and retinal ganglion cells: organizers of the mammalian retina. *Neuroreport* **15**, 479-82.

Dakubo, G. D., Wang, Y. P., Mazerolle, C., Campsall, K., McMahon, A. P. and Wallace, V. A. (2003). Retinal ganglion cell-derived sonic hedgehog signaling is required for optic disc and stalk neuroepithelial cell development. *Development* **130**, 2967-80.

Das, G., Choi, Y., Sicinski, P. and Levine, E. M. (2009). Cyclin D1 fine-tunes the neurogenic output of embryonic retinal progenitor cells. *Neural Dev* **4**, 15.

Das, T., Payer, B., Cayouette, M. and Harris, W. A. (2003). In vivo time-lapse imaging of cell divisions during neurogenesis in the developing zebrafish retina. *Neuron* **37**, 597-609.

Dateki, S., Kosaka, K., Hasegawa, K., Tanaka, H., Azuma, N., Yokoya, S., Muroya, K., Adachi, M., Tajima, T., Motomura, K. et al. (2010). Heterozygous orthodenticle homeobox 2 mutations are associated with variable pituitary phenotype. *J Clin Endocrinol Metab* **95**, 756-64.

Dattani, M. T., Martinez-Barbera, J. P., Thomas, P. Q., Brickman, J. M., Gupta, R., Martensson, I. L., Toresson, H., Fox, M., Wales, J. K., Hindmarsh, P. C. et al. (1998). Mutations in the homeobox gene HESX1/Hesx1 associated with septo-optic dysplasia in human and mouse. *Nat Genet* **19**, 125-33.

De Morsier, G. (1962). Median craioencephalic dysraphias and olfactogenital dysplasia. *World Neurol* **3**, 485-506.

Del Bene, F., Ettwiller, L., Skowronska-Krawczyk, D., Baier, H., Matter, J. M., Birney, E. and Wittbrodt, J. (2007). In vivo validation of a computationally predicted conserved Ath5 target gene set. *PLoS Genet* **3**, 1661-71.

Derjaguin, B. V. and Churaev, N. V. (1973). Nature of 'anomalous' water. *Nature* **244**, 430-431.

Desai, A. R. and McConnell, S. K. (2000). Progressive restriction in fate potential by neural progenitors during cerebral cortical development. *Development* **127**, 2863-72.

Desgraz, R. and Herrera, P. L. (2009). Pancreatic neurogenin 3-expressing cells are unipotent islet precursors. *Development* **136**, 3567-74.

Dogan, R. I., Getoor, L., Wilbur, W. J. and Mount, S. M. (2007). SplicePort--an interactive splice-site analysis tool. *Nucleic Acids Res* **35**, W285-91.

Dokucu, M. E., Zipursky, S. L. and Cagan, R. L. (1996). Atonal, rough and the resolution of proneural clusters in the developing Drosophila retina. *Development* **122**, 4139-47.

Donovan, S. L. and Dyer, M. A. (2006). Preparation and square wave electroporation of retinal explant cultures. *Nat Protoc* **1**, 2710-8.

Dorrell, M. I., Aguilar, E. and Friedlander, M. (2002). Retinal vascular development is mediated by endothelial filopodia, a preexisting astrocytic template and specific R-cadherin adhesion. *Invest Ophthalmol Vis Sci* **43**, 3500-10.

Drager, U. C. (1985). Birth dates of retinal ganglion cells giving rise to the crossed and uncrossed optic projections in the mouse. *Proc R Soc Lond B Biol Sci* **224**, 57-77.

Dyer, M. A. and Cepko, C. L. (2000). p57(Kip2) regulates progenitor cell proliferation and amacrine interneuron development in the mouse retina. *Development* **127**, 3593-605.

Dyer, M. A. and Cepko, C. L. (2001a). p27Kip1 and p57Kip2 regulate proliferation in distinct retinal progenitor cell populations. *J Neurosci* **21**, 4259-71.

Dyer, M. A. and Cepko, C. L. (2001b). Regulating proliferation during retinal development. *Nat Rev Neurosci* **2**, 333-42.

Dyer, M. A., Livesey, F. J., Cepko, C. L. and Oliver, G. (2003). Prox1 function controls progenitor cell proliferation and horizontal cell genesis in the mammalian retina. *Nat Genet* **34**, 53-8.

Dymecki, S. M., Rodriguez, C. I. and Awatramani, R. B. (2002). Switching on lineage tracers using site-specific recombination. In *Embryonic Stem Cells: Methods and Protocols*, vol. 185 (ed. K. Turksen), pp. 309-34: Humana Press.

Echelard, Y., Vassileva, G. and McMahon, A. P. (1994). Cis-acting regulatory sequences governing Wnt-1 expression in the developing mouse CNS. *Development* **120**, 2213-24.

Edwards, M. M., McLeod, D. S., Li, R., Grebe, R., Bhutto, I., Mu, X. and Lutty, G. A. (2011). The deletion of Math5 disrupts retinal blood vessel and glial development in mice. *Exp Eye Res*.

Eiraku, M., Takata, N., Ishibashi, H., Kawada, M., Sakakura, E., Okuda, S., Sekiguchi, K., Adachi, T. and Sasai, Y. (2011). Self-organizing optic-cup morphogenesis in three-dimensional culture. *Nature* **472**, 51-6.

Eisenstein, M. (2005). A look back: making mapping easy to digest. *Nat Methods* **2**, 396.

Ek, U., Fernell, E. and Jacobson, L. (2005). Cognitive and behavioural characteristics in blind children with bilateral optic nerve hypoplasia. *Acta Paediatr* **94**, 1421-6.

Elliott, J., Jolicoeur, C., Ramamurthy, V. and Cayouette, M. (2008). Ikaros confers early temporal competence to mouse retinal progenitor cells. *Neuron* **60**, 26-39.

Elshatory, Y., Deng, M., Xie, X. and Gan, L. (2007a). Expression of the LIM-homeodomain protein Isl1 in the developing and mature mouse retina. *J Comp Neurol* **503**, 182-97.

Elshatory, Y., Everhart, D., Deng, M., Xie, X., Barlow, R. B. and Gan, L. (2007b). Islet-1 controls the differentiation of retinal bipolar and cholinergic amacrine cells. *J Neurosci* **27**, 12707-20.

Enge, M., Bjarnegard, M., Gerhardt, H., Gustafsson, E., Kalen, M., Asker, N., Hammes, H. P., Shani, M., Fassler, R. and Betsholtz, C. (2002). Endothelium-specific platelet-derived growth factor-B ablation mimics diabetic retinopathy. *Embo J* **21**, 4307-16.

Engelbrecht, J., Knudsen, S. and Brunak, S. (1992). G+C-rich tract in 5' end of human introns. *J Mol Biol* **227**, 108-13.

Erkman, L., McEvilly, R. J., Luo, L., Ryan, A. K., Hooshmand, F., O'Connell, S. M., Keithley, E. M., Rapaport, D. H., Ryan, A. F. and Rosenfeld, M. G. (1996). Role of transcription factors Brn-3.1 and Brn-3.2 in auditory and visual system development. *Nature* **381**, 603-6.

Erkman, L., Yates, P. A., McLaughlin, T., McEvilly, R. J., Whisenhunt, T., O'Connell, S. M., Krones, A. I., Kirby, M. A., Rapaport, D. H., Bermingham, J. R. et al. (2000). A POU domain transcription factor-dependent program regulates axon pathfinding in the vertebrate visual system. *Neuron* **28**, 779-92.

Erskine, L. and Herrera, E. (2007). The retinal ganglion cell axon's journey: insights into molecular mechanisms of axon guidance. *Dev Biol* **308**, 1-14.

Esumi, N., Kachi, S., Hackler, L., Jr., Masuda, T., Yang, Z., Campochiaro, P. A. and Zack, D. J. (2009). BEST1 expression in the retinal pigment epithelium is modulated by OTX family members. *Hum Mol Genet* **18**, 128-41.

Ezzeddine, Z. D., Yang, X., DeChiara, T., Yancopoulos, G. and Cepko, C. L. (1997). Postmitotic cells fated to become rod photoreceptors can be respecified by CNTF treatment of the retina. *Development* **124**, 1055-67.

Fan, B. J., Wang, D. Y., Pasquale, L. R., Haines, J. L. and Wiggs, J. L. (2011). Genetic variants associated with optic nerve vertical cup-to-disc ratio are risk factors for primary open angle glaucoma in a US Caucasian population. *Invest Ophthalmol Vis Sci* **52**, 1788-92.

Fantl, V., Stamp, G., Andrews, A., Rosewell, I. and Dickson, C. (1995). Mice lacking cyclin D1 are small and show defects in eye and mammary gland development. *Genes Dev* **9**, 2364-72.

Farah, M., Olson, J., Sucic, H., Hume, R., Tapscott, S. and Turner, D. (2000). Generation of neurons by transient expression of neural bHLH proteins in mammalian cells. *Development* **127**, 693-702.

Farah, M. H. and Easter, S. S., Jr. (2005). Cell birth and death in the mouse retinal ganglion cell layer. *J Comp Neurol* **489**, 120-34.

Fawcett, J. W., O'Leary, D. D. and Cowan, W. M. (1984). Activity and the control of ganglion cell death in the rat retina. *Proc Natl Acad Sci U S A* **81**, 5589-93.

Fedorov, A., Saxonov, S., Fedorova, L. and Daizadeh, I. (2001). Comparison of intron-containing and intron-lacking human genes elucidates putative exonic splicing enhancers. *Nucleic Acids Res* **29**, 1464-9.

Feinberg, A. P. and Vogelstein, B. (1983). A technique for radiolabeling DNA restriction endonuclease fragments to high specific activity. *Anal Biochem* **132**, 6-13.

Feng, L., Eisenstat, D. D., Chiba, S., Ishizaki, Y., Gan, L. and Shibasaki, K. (2011). Brn-3b inhibits generation of amacrine cells by binding to and negatively regulating DLX1/2 in developing retina. *Neuroscience* **195**, 9-20.

Feng, L., Xie, Z. H., Ding, Q., Xie, X., Libby, R. T. and Gan, L. (2010). MATH5 controls the acquisition of multiple retinal cell fates. *Mol Brain* **3**, 36.

Fisher, R. A. (1925). Statistical Methods for Research Workers: Oliver & Boyd.

Flora, A., Garcia, J. J., Thaller, C. and Zoghbi, H. Y. (2007). The E-protein Tcf4 interacts with Math1 to regulate differentiation of a specific subset of neuronal progenitors. *Proc Natl Acad Sci U S A* **104**, 15382-7.

Fox-Walsh, K. L., Dou, Y., Lam, B. J., Hung, S. P., Baldi, P. F. and Hertel, K. J. (2005). The architecture of pre-mRNAs affects mechanisms of splice-site pairing. *Proc Natl Acad Sci U S A* **102**, 16176-81.

Frankfort, B. J. and Mardon, G. (2002). R8 development in the Drosophila eye: a paradigm for neural selection and differentiation. *Development* **129**, 1295-306.

Frohman, M. A. (1993). Rapid amplification of complementary DNA ends for generation of full-length complementary DNAs: thermal RACE. *Methods Enzymol* **218**, 340-56.

Frohman, M. A., Dush, M. K. and Martin, G. R. (1988). Rapid production of full-length cDNAs from rare transcripts: amplification using a single gene-specific oligonucleotide primer. *Proc Natl Acad Sci U S A* **85**, 8998-9002.

Fruttiger, M. (2002). Development of the mouse retinal vasculature: angiogenesis versus vasculogenesis. *Invest Ophthalmol Vis Sci* **43**, 522-7.

Fruttiger, M. (2007). Development of the retinal vasculature. *Angiogenesis* **10**, 77-88.

Fruttiger, M., Calver, A. R., Kruger, W. H., Mudhar, H. S., Michalovich, D., Takakura, N., Nishikawa, S. and Richardson, W. D. (1996). PDGF mediates a neuron-astrocyte interaction in the developing retina. *Neuron* **17**, 1117-31.

Fruttiger, M., Calver, A. R. and Richardson, W. D. (2000). Platelet-derived growth factor is constitutively secreted from neuronal cell bodies but not from axons. *Curr Biol* **10**, 1283-6.

Fu, X., Kiyama, T., Li, R., Russell, M., Klein, W. H. and Mu, X. (2009). Epitope-tagging Math5 and Pou4f2: new tools to study retinal ganglion cell development in the mouse. *Dev Dyn* **238**, 2309-17.

Fuhrmann, S., Kirsch, M. and Hofmann, H. D. (1995). Ciliary neurotrophic factor promotes chick photoreceptor development in vitro. *Development* **121**, 2695-706.

Fujita, S. (1962). Kinetics of cellular proliferation. *Exp Cell Res* **28**, 52-60.

Fujitani, Y., Fujitani, S., Luo, H., Qiu, F., Burlison, J., Long, Q., Kawaguchi, Y., Edlund, H., MacDonald, R. J., Furukawa, T. et al. (2006). Ptf1a determines horizontal and amacrine cell fates during mouse retinal development. *Development* **133**, 4439-50.

Furukawa, A., Koike, C., Lippincott, P., Cepko, C. L. and Furukawa, T. (2002). The mouse Crx 5'-upstream transgene sequence directs cell-specific and developmentally regulated expression in retinal photoreceptor cells. *J Neurosci* **22**, 1640-7.

Furukawa, T., Morrow, E. M. and Cepko, C. L. (1997). Crx, a novel otx-like homeobox gene, shows photoreceptor-specific expression and regulates photoreceptor differentiation. *Cell* **91**, 531-41.

Furukawa, T., Morrow, E. M., Li, T., Davis, F. C. and Cepko, C. L. (1999). Retinopathy and attenuated circadian entrainment in Crx-deficient mice. *Nat Genet* **23**, 466-70.

Furukawa, T., Mukherjee, S., Bao, Z. Z., Morrow, E. M. and Cepko, C. L. (2000). rax, Hes1, and notch1 promote the formation of Muller glia by postnatal retinal progenitor cells. *Neuron* **26**, 383-94.

Galli-Resta, L. and Ensini, M. (1996). An intrinsic time limit between genesis and death of individual neurons in the developing retinal ganglion cell layer. *J Neurosci* **16**, 2318-24.

Gan, L., Wang, S. W., Huang, Z. and Klein, W. H. (1999). POU domain factor Brn-3b is essential for retinal ganglion cell differentiation and survival but not for initial cell fate specification. *Dev Biol* **210**, 469-80.

Gan, L., Xiang, M., Zhou, L., Wagner, D. S., Klein, W. H. and Nathans, J. (1996). POU domain factor Brn-3b is required for the development of a large set of retinal ganglion cells. *Proc Natl Acad Sci U S A* **93**, 3920-5.

Gariano, R. F. and Gardner, T. W. (2005). Retinal angiogenesis in development and disease. *Nature* **438**, 960-6.

Garrick, D., Fiering, S., Martin, D. I. and Whitelaw, E. (1998). Repeat-induced gene silencing in mammals. *Nat Genet* **18**, 56-9.

Gentles, A. J. and Karlin, S. (1999). Why are human G-protein-coupled receptors predominantly intronless? *Trends Genet* **15**, 47-9.

Georgi, S. A. and Reh, T. A. (2010). Dicer is required for the transition from early to late progenitor state in the developing mouse retina. *J Neurosci* **30**, 4048-61.

Gerfen, C. R., Holmes, A., Sibley, D., Skolnick, P., Wray, S. and (Eds.). (2001). Common Stock Solutions, Buffers, and Media. In *Current Protocols in Neuroscience*: John Wiley & Sons, Inc.

Ghelli, A., Zanna, C., Porcelli, A. M., Schapira, A. H., Martinuzzi, A., Carelli, V. and Rugolo, M. (2003). Leber's hereditary optic neuropathy (LHON) pathogenic mutations induce mitochondrial-dependent apoptotic death in transmitochondrial cells incubated with galactose medium. *J Biol Chem* **278**, 4145-50.

Ghiasvand, N. M., Fleming, T. P., Helms, C., Avisa, A. and Donis-Keller, H. (2000). Genetic fine mapping of the gene for nonsyndromic congenital retinal nonattachment. *Am J Med Genet* **92**, 220-3.

Ghiasvand, N. M., Rudolph, D. D., Mashayekhi, M., Brzezinski, J. A., Goldman, D. and Glaser, T. (2011). Deletion of a remote enhancer near ATOH7 disrupts retinal neurogenesis, causing NCRNA disease. *Nat Neurosci* **14**, 578-86.

Ghiasvand, N. M., Shirzad, E., Naghavi, M. and Vaez Mahdavi, M. R. (1998). High incidence of autosomal recessive nonsyndromal congenital retinal nonattachment (NCRNA) in an Iranian founding population. *Am J Med Genet* **78**, 226-32.

Ghosh, K. K., Bujan, S., Haverkamp, S., Feigenspan, A. and Wassle, H. (2004). Types of bipolar cells in the mouse retina. *J Comp Neurol* **469**, 70-82.

Glessner, J. T., Wang, K., Cai, G., Korvatska, O., Kim, C. E., Wood, S., Zhang, H., Estes, A., Brune, C. W., Bradfield, J. P. et al. (2009). Autism genome-wide copy number variation reveals ubiquitin and neuronal genes. *Nature* **459**, 569-73.

Goldberg, M. F. (1997). Persistent fetal vasculature (PFV): an integrated interpretation of signs and symptoms associated with persistent hyperplastic primary vitreous (PHPV). LIV Edward Jackson Memorial Lecture. *Am J Ophthalmol* **124**, 587-626.

Goldowitz, D., Rice, D. S. and Williams, R. W. (1996). Clonal architecture of the mouse retina. *Prog Brain Res* **108**, 3-15.

Gomes, F. L., Zhang, G., Carbonell, F., Correa, J. A., Harris, W. A., Simons, B. D. and Cayouette, M. (2011). Reconstruction of rat retinal progenitor cell lineages in vitro reveals a surprising degree of stochasticity in cell fate decisions. *Development* **138**, 227-35.

Gong, S., Yang, X. W., Li, C. and Heintz, N. (2002). Highly efficient modification of bacterial artificial chromosomes (BACs) using novel shuttle vectors containing the R6Kgamma origin of replication. *Genome Res* **12**, 1992-8.

Gooley, J. J., Lu, J., Chou, T. C., Scammell, T. E. and Saper, C. B. (2001). Melanopsin in cells of origin of the retinohypothalamic tract. *Nat Neurosci* **4**, 1165.

Gotz, M. and Huttner, W. B. (2005). The cell biology of neurogenesis. *Nat Rev Mol Cell Biol* **6**, 777-88.

Gown, A. M. and Willingham, M. C. (2002). Improved detection of apoptotic cells in archival paraffin sections: immunohistochemistry using antibodies to cleaved caspase 3. *J Histochem Cytochem* **50**, 449-54.

Gray, N. K. and Hentze, M. W. (1994). Regulation of protein synthesis by mRNA structure. *Mol Biol Rep* **19**, 195-200.

Gregory-Evans, C. Y., Williams, M. J., Halford, S. and Gregory-Evans, K. (2004). Ocular coloboma: a reassessment in the age of molecular neuroscience. *J Med Genet* **41**, 881-91.

Gutierrez, C., McNally, M. and Canto-Soler, M. V. (2011). Cytoskeleton proteins previously considered exclusive to ganglion cells are transiently expressed by all retinal neuronal precursors. *BMC Dev Biol* **11**, 46.

Haddad, N. G. and Eugster, E. A. (2005). Hypopituitarism and neurodevelopmental abnormalities in relation to central nervous system structural defects in children with optic nerve hypoplasia. *J Pediatr Endocrinol Metab* **18**, 853-8.

Haddad, R., Font, R. L. and Reeser, F. (1978). Persistent hyperplastic primary vitreous. A clinicopathologic study of 62 cases and review of the literature. *Surv Ophthalmol* **23**, 123-34.

Harlow, E. and Lane, D. (1988). Antibodies. A laboratory manual. Cold Spring Harbor, NY: CSH Press.

Harrington, E. D., Boue, S., Valcarcel, J., Reich, J. G. and Bork, P. (2004). Estimating rates of alternative splicing in mammals and invertebrates: authors reply. *Nat Genet* **36**, 916-7.

Harris, W. A. and Hartenstein, V. (1991). Neuronal determination without cell division in Xenopus embryos. *Neuron* **6**, 499-515.

Hatakeyama, J. and Kageyama, R. (2002). Retrovirus-mediated gene transfer to retinal explants. *Methods* **28**, 387-95.

Hattar, S., Liao, H. W., Takao, M., Berson, D. M. and Yau, K. W. (2002). Melanopsin-containing retinal ganglion cells: architecture, projections, and intrinsic photosensitivity. *Science* **295**, 1065-70.

Hawley, R. G. (1994). High-titer retroviral vectors for efficient transduction of functional genes into murine hematopoietic stem cells. *Ann N Y Acad Sci* **716**, 327-30.

Hayden, S. A., Mills, J. W. and Masland, R. M. (1980). Acetylcholine synthesis by displaced amacrine cells. *Science* **210**, 435-7.

Heintz, N. (2001). BAC to the future: the use of bac transgenic mice for neuroscience research. *Nat Rev Neurosci* **2**, 861-70.

Hellman, L. M. and Fried, M. G. (2007). Electrophoretic mobility shift assay (EMSA) for detecting protein-nucleic acid interactions. *Nat Protoc* **2**, 1849-61.

Helms, A. W., Abney, A. L., Ben-Arie, N., Zoghbi, H. Y. and Johnson, J. E. (2000). Autoregulation and multiple enhancers control Math1 expression in the developing nervous system. *Development* **127**, 1185-96.

Henke, W., Herdel, K., Jung, K., Schnorr, D. and Loening, S. A. (1997). Betaine improves the PCR amplification of GC-rich DNA sequences. *Nucleic Acids Res* **25**, 3957-8.

Hennig, A. K., Peng, G. H. and Chen, S. (2008). Regulation of photoreceptor gene expression by Crx-associated transcription factor network. *Brain Res* **1192**, 114-33.

Hertel, K. J. (2008). Combinatorial control of exon recognition. *J Biol Chem* **283**, 1211-5.

Holt, C. E., Bertsch, T. W., Ellis, H. M. and Harris, W. A. (1988). Cellular determination in the Xenopus retina is independent of lineage and birth date. *Neuron* **1**, 15-26.

Howell, N. (1998). Leber hereditary optic neuropathy: respiratory chain dysfunction and degeneration of the optic nerve. *Vision Res* **38**, 1495-504.

Hsiung, F. and Moses, K. (2002). Retinal development in Drosophila: specifying the first neuron. *Hum Mol Genet* **11**, 1207-14.

Hu, M., Krause, D., Greaves, M., Sharkis, S., Dexter, M., Heyworth, C. and Enver, T. (1997). Multilineage gene expression precedes commitment in the hemopoietic system. *Genes Dev* **11**, 774-85.

Hufnagel, R. B., Le, T. T., Riesenberg, A. L. and Brown, N. L. (2010). Neurog2 controls the leading edge of neurogenesis in the mammalian retina. *Dev Biol* **340**, 490-503.

Hufnagel, R. B., Riesenberg, A. N., Saul, S. M. and Brown, N. L. (2007). Conserved regulation of Math5 and Math1 revealed by Math5-GFP transgenes. *Mol Cell Neurosci* **36**, 435-48.

Hutcheson, D. A., Hanson, M. I., Moore, K. B., Le, T. T., Brown, N. L. and Vetter, M. L. (2005). bHLH-dependent and -independent modes of Ath5 gene regulation during retinal development. *Development* **132**, 829-39.

Hutcheson, D. A. and Vetter, M. L. (2001). The bHLH factors Xath5 and XNeuroD can upregulate the expression of XBrn3d, a POU-homeodomain transcription factor. *Dev Biol* **232**, 327-38.

Huttner, W. B. and Kosodo, Y. (2005). Symmetric versus asymmetric cell division during neurogenesis in the developing vertebrate central nervous system. *Curr Opin Cell Biol* **17**, 648-57.

Irimia, M. and Roy, S. W. (2008). Spliceosomal introns as tools for genomic and evolutionary analysis. *Nucleic Acids Res* **36**, 1703-12.

Jadhav, A. P., Cho, S. H. and Cepko, C. L. (2006). Notch activity permits retinal cells to progress through multiple progenitor states and acquire a stem cell property. *Proc Natl Acad Sci U S A* **103**, 18998-9003.

Jaillon, O., Bouhouche, K., Gout, J. F., Aury, J. M., Noel, B., Saudemont, B., Nowacki, M., Serrano, V., Porcel, B. M., Segurens, B. et al. (2008). Translational control of intron splicing in eukaryotes. *Nature* **451**, 359-62.

James, J., Das, A. V., Bhattacharya, S., Chacko, D. M., Zhao, X. and Ahmad, I. (2003). In vitro generation of early-born neurons from late retinal progenitors. *J Neurosci* **23**, 8193-203.

Jameson, B. A. and Wolf, H. (1988). The antigenic index: a novel algorithm for predicting antigenic determinants. *Comput Appl Biosci* **4**, 181-6.

Jarman, A. P. (2000). Developmental genetics: vertebrates and insects see eye to eye. *Curr Biol* **10**, R857-9.

Jarman, A. P., Grau, Y., Jan, L. Y. and Jan, Y. N. (1993). *atonal* is a proneural gene that directs chordotonal organ formation in the *Drosophila* peripheral nervous system. *Cell* **73**, 1307-1321.

Jarman, A. P., Grell, E. H., Ackerman, L., Jan, L. Y. and Jan, Y. N. (1994). *atonal* is the proneural gene for *Drosophila* photoreceptors. *Nature* **369**, 398-400.

Jeffares, D. C., Penkett, C. J. and Bahler, J. (2008). Rapidly regulated genes are intron poor. *Trends Genet* **24**, 375-8.

Jensen, A. M. and Wallace, V. A. (1997). Expression of Sonic hedgehog and its putative role as a precursor cell mitogen in the developing mouse retina. *Development* **124**, 363-71.

Jeon, C. J., Strettoi, E. and Masland, R. H. (1998). The major cell populations of the mouse retina. *J Neurosci* **18**, 8936-46.

Kageyama, R. and Nakanishi, S. (1997). Helix-loop-helix factors in growth and differentiation of the vertebrate nervous system. *Curr Opin Genet Dev* **7**, 659-65.

Kanadia, R. N. and Cepko, C. L. (2010). Alternative splicing produces high levels of noncoding isoforms of bHLH transcription factors during development. *Genes Dev* **24**, 229-34.

Kanekar, S., Perron, M., Dorsky, R., Harris, W. A., Jan, L. Y., Jan, Y. N. and Vetter, M. L. (1997). Xath5 participates in a network of bHLH genes in the developing Xenopus retina. *Neuron* **19**, 981-94.

Kay, J. N., Finger-Baier, K. C., Roeser, T., Staub, W. and Baier, H. (2001). Retinal ganglion cell genesis requires lakritz, a Zebrafish atonal Homolog. *Neuron* **30**, 725-36.

Kelberman, D. and Dattani, M. T. (2007). Genetics of septo-optic dysplasia. *Pituitary* **10**, 393-407.

Kenneson, A., Zhang, F., Hagedorn, C. H. and Warren, S. T. (2001). Reduced FMRP and increased FMR1 transcription is proportionally associated with CGG repeat number in intermediate-length and premutation carriers. *Hum Mol Genet* **10**, 1449-54.

Key, G., Becker, M. H., Baron, B., Duchrow, M., Schluter, C., Flad, H. D. and Gerdes, J. (1993). New Ki-67-equivalent murine monoclonal antibodies (MIB 1-3) generated against bacterially expressed parts of the Ki-67 cDNA containing three 62 base pair repetitive elements encoding for the Ki-67 epitope. *Lab Invest* **68**, 629-36.

Khaliq, S., Hameed, A., Ismail, M., Anwar, K., Leroy, B., Payne, A. M., Bhattacharya, S. S. and Mehdi, S. Q. (2001). Locus for autosomal recessive nonsyndromic persistent hyperplastic primary vitreous. *Invest Ophthalmol Vis Sci* **42**, 2225-8.

Khan, K., Logan, C. V., McKibbin, M., Sheridan, E., Elcioglu, N. H., Yenice, O., Parry, D. A., Fernandez-Fuentes, N., Abdelhamed, Z. I., Al-Maskari, A. et al. (2011). Next generation sequencing identifies mutations in Atonal homolog 7 (ATOH7) in families with global eye developmental defects. *Hum Mol Genet*.

Khor, C. C., Ramdas, W. D., Vithana, E. N., Cornes, B. K., Sim, X., Tay, W. T., Saw, S. M., Zheng, Y., Lavanya, R., Wu, R. et al. (2011). Genome-wide association studies in Asians confirm the involvement of ATOH7 and TGFBR3, and further identify CARD10 as a novel locus influencing optic disc area. *Hum Mol Genet* **20**, 1864-72.

Kim, D. S., Ross, S. E., Trimarchi, J. M., Aach, J., Greenberg, M. E. and Cepko, C. L. (2008). Identification of molecular markers of bipolar cells in the murine retina. *J Comp Neurol* **507**, 1795-810.

Kim, J., Wu, H. H., Lander, A. D., Lyons, K. M., Matzuk, M. M. and Calof, A. L. (2005). GDF11 controls the timing of progenitor cell competence in developing retina. *Science* **308**, 1927-30.

Kitabayashi, M. and Esaka, M. (2003). Improvement of reverse transcription PCR by RNase H. *Biosci Biotechnol Biochem* **67**, 2474-6.

Kiyama, T., Mao, C. A., Cho, J. H., Fu, X., Pan, P., Mu, X. and Klein, W. H. (2011). Overlapping spatiotemporal patterns of regulatory gene expression are required for neuronal progenitors to specify retinal ganglion cell fate. *Vision Res* **51**, 251-9.

Koike, C., Nishida, A., Akimoto, K., Nakaya, M. A., Noda, T., Ohno, S. and Furukawa, T. (2005). Function of atypical protein kinase C lambda in differentiating photoreceptors is required for proper lamination of mouse retina. *J Neurosci* **25**, 10290-8.

Kolpak, A., Zhang, J. and Bao, Z. Z. (2005). Sonic hedgehog has a dual effect on the growth of retinal ganglion axons depending on its concentration. *J Neurosci* **25**, 3432-41.

Kriss, J. P. and Revesz, L. (1962). The distribution and fate of bromodeoxyuridine and bromodeoxycytidine in the mouse and rat. *Cancer Res* **22**, 254-65.

Kumar, S. and Nussinov, R. (2002). Close-range electrostatic interactions in proteins. *Chembiochem* **3**, 604-17.

Lahav, M., Albert, D. M. and Wyand, S. (1973). Clinical and histopathologic classification of retinal dysplasia. *Am J Ophthalmol* **75**, 648-67.

Lamba, D. A., Gust, J. and Reh, T. A. (2009). Transplantation of human embryonic stem cell-derived photoreceptors restores some visual function in Crx-deficient mice. *Cell Stem Cell* **4**, 73-9.

Lamba, D. A., Karl, M. O., Ware, C. B. and Reh, T. A. (2006). Efficient generation of retinal progenitor cells from human embryonic stem cells. *Proc Natl Acad Sci U S A* **103**, 12769-74.

Lambert, S. R., Hoyt, C. S. and Narahara, M. H. (1987). Optic nerve hypoplasia. *Surv Ophthalmol* **32**, 1-9.

Lang, R., Lustig, M., Francois, F., Sellinger, M. and Plesken, H. (1994). Apoptosis during macrophage-dependent ocular tissue remodelling. *Development* **120**, 3395-403.

Laterra, J., Guerin, C. and Goldstein, G. W. (1990). Astrocytes induce neural microvascular endothelial cells to form capillary-like structures in vitro. *J Cell Physiol* **144**, 204-15.

LaVail, M. M., Faktorovich, E. G., Hepler, J. M., Pearson, K. L., Yasumura, D., Matthes, M. T. and Steinberg, R. H. (1991). Basic fibroblast growth factor protects photoreceptors from light-induced degeneration in albino rats. *Ann N Y Acad Sci* **638**, 341-7.

Le, T. T., Wroblewski, E., Patel, S., Riesenberg, A. N. and Brown, N. L. (2006). Math5 is required for both early retinal neuron differentiation and cell cycle progression. *Dev Biol* **295**, 764-78.

Lee, B. L., Bateman, J. B. and Schwartz, S. D. (1996). Posterior segment neovascularization associated with optic nerve aplasia. *Am J Ophthalmol* **122**, 131-3.

Lee, D. A. and Higginbotham, E. J. (2005). Glaucoma and its treatment: a review. *Am J Health Syst Pharm* **62**, 691-9.

Lee, E. C., Yu, D., Martinez de Velasco, J., Tessarollo, L., Swing, D. A., Court, D. L., Jenkins, N. A. and Copeland, N. G. (2001). A highly efficient Escherichia coli-based chromosome engineering system adapted for recombinogenic targeting and subcloning of BAC DNA. *Genomics* **73**, 56-65.

Lehner, B. (2011). Molecular mechanisms of epistasis within and between genes. *Trends Genet* **27**, 323-31.

Levine, E. M., Roelink, H., Turner, J. and Reh, T. A. (1997). Sonic hedgehog promotes rod photoreceptor differentiation in mammalian retinal cells in vitro. *J Neurosci* **17**, 6277-88.

Leygue, E., Murphy, L., Kuttenn, F. and Watson, P. (1996). Triple primer polymerase chain reaction. A new way to quantify truncated mRNA expression. *Am J Pathol* **148**, 1097-103.

Li, Q., Lee, J. A. and Black, D. L. (2007). Neuronal regulation of alternative pre-mRNA splicing. *Nat Rev Neurosci* **8**, 819-31.

Li, S., Mo, Z., Yang, X., Price, S. M., Shen, M. M. and Xiang, M. (2004). Foxn4 controls the genesis of amacrine and horizontal cells by retinal progenitors. *Neuron* **43**, 795-807.

Li, Z., Hu, M., Ochocinska, M. J., Joseph, N. M. and Easter, S. S., Jr. (2000). Modulation of cell proliferation in the embryonic retina of zebrafish (Danio rerio). *Dev Dyn* **219**, 391-401.

Lin, B., Wang, S. W. and Masland, R. H. (2004). Retinal ganglion cell type, size, and spacing can be specified independent of homotypic dendritic contacts. *Neuron* **43**, 475-85.

Little, L. E., Whitmore, P. V. and Wells, T. W., Jr. (1976). Aplasia of the optic nerve. *J Pediatr Ophthalmol* **13**, 84-8.

Liu, H. and Naismith, J. H. (2008). An efficient one-step site-directed deletion, insertion, single and multiple-site plasmid mutagenesis protocol. *BMC Biotechnol* **8**, 91.

Liu, W., Khare, S. L., Liang, X., Peters, M. A., Liu, X., Cepko, C. L. and Xiang, M. (2000). All Brn3 genes can promote retinal ganglion cell differentiation in the chick. *Development* **127**, 3237-47.

Liu, W., Mo, Z. and Xiang, M. (2001). The Ath5 proneural genes function upstream of Brn3 POU domain transcription factor genes to promote retinal ganglion cell development. *Proc Natl Acad Sci U S A* **98**, 1649-54.

Livak, K. J. and Schmittgen, T. D. (2001). Analysis of relative gene expression data using real-time quantitative PCR and the 2(-Delta Delta C(T)) Method. *Methods* **25**, 402-8.

Livesey, F. J. and Cepko, C. L. (2001). Vertebrate neural cell-fate determination: lessons from the retina. *Nat Rev Neurosci* **2**, 109-18.

Lobe, C. G., Koop, K. E., Kreppner, W., Lomeli, H., Gertsenstein, M. and Nagy, A. (1999). Z/AP, a double reporter for cre-mediated recombination. *Dev Biol* **208**, 281-92.

Longo, A., Guanga, G. P. and Rose, R. B. (2008). Crystal structure of E47-NeuroD1/beta2 bHLH domain-DNA complex: heterodimer selectivity and DNA recognition. *Biochemistry* **47**, 218-29.

Lu, B., Jan, L. and Jan, Y. N. (2000). Control of cell divisions in the nervous system: symmetry and asymmetry. *Annu Rev Neurosci* **23**, 531-56.

Luo, L. (2007). Fly MARCM and mouse MADM: genetic methods of labeling and manipulating single neurons. *Brain Res Rev* **55**, 220-7.

MacDonald, R. J., Swift, G. H., Przybyla, A. E. and Chirgwin, J. M. (1987). Isolation of RNA using guanidinium salts. *Methods Enzymol* **152**, 219-27.

Macgregor, S., Hewitt, A. W., Hysi, P. G., Ruddle, J. B., Medland, S. E., Henders, A. K., Gordon, S. D., Andrew, T., McEvoy, B., Sanfilippo, P. G. et al. (2010). Genome-wide association identifies ATOH7 as a major gene determining human optic disc size. *Hum Mol Genet* **19**, 2716-24.

MacLaren, R. E., Pearson, R. A., MacNeil, A., Douglas, R. H., Salt, T. E., Akimoto, M., Swaroop, A., Sowden, J. C. and Ali, R. R. (2006). Retinal repair by transplantation of photoreceptor precursors. *Nature* **444**, 203-7.

MacNeil, M. A. and Masland, R. H. (1998). Extreme diversity among amacrine cells: implications for function. *Neuron* **20**, 971-82.

Mader, R. M., Schmidt, W. M., Sedivy, R., Rizovski, B., Braun, J., Kalipciyan, M., Exner, M., Steger, G. G. and Mueller, M. W. (2001). Reverse transcriptase template switching during reverse transcriptase-polymerase chain reaction: artificial generation of deletions in ribonucleotide reductase mRNA. *J Lab Clin Med* **137**, 422-8.

Maillard, I., Weng, A. P., Carpenter, A. C., Rodriguez, C. G., Sai, H., Xu, L., Allman, D., Aster, J. C. and Pear, W. S. (2004). Mastermind critically regulates Notch-mediated lymphoid cell fate decisions. *Blood* **104**, 1696-702.

Malecki, M. T., Jhala, U. S., Antonellis, A., Fields, L., Doria, A., Orban, T., Saad, M., Warram, J. H., Montminy, M. and Krolewski, A. S. (1999). Mutations in NEUROD1 are associated with the development of type 2 diabetes mellitus. *Nat Genet* **23**, 323-8.

Mao, C. A., Kiyama, T., Pan, P., Furuta, Y., Hadjantonakis, A. K. and Klein, W. H. (2008a). Eomesodermin, a target gene of Pou4f2, is required for retinal ganglion cell and optic nerve development in the mouse. *Development* **135**, 271-80.

Mao, C. A., Wang, S. W., Pan, P. and Klein, W. H. (2008b). Rewiring the retinal ganglion cell gene regulatory network: Neurod1 promotes retinal ganglion cell fate in the absence of Math5. *Development* **135**, 3379-88.

Mao, X., Fujiwara, Y., Chapdelaine, A., Yang, H. and Orkin, S. H. (2001). Activation of EGFP expression by Cre-mediated excision in a new ROSA26 reporter mouse strain. *Blood* **97**, 324-6.

Maquat, L. E. and Li, X. (2001). Mammalian heat shock p70 and histone H4 transcripts, which derive from naturally intronless genes, are immune to nonsense-mediated decay. *RNA* **7**, 445-56.

Margulies, E. H., Kardia, S. L. and Innis, J. W. (2001). Identification and prevention of a GC content bias in SAGE libraries. *Nucleic Acids Res* **29**, E60-0.

Marquardt, T. (2003). Transcriptional control of neuronal diversification in the retina. *Prog Retin Eye Res* **22**, 567-77.

Marquardt, T. and Gruss, P. (2002). Generating neuronal diversity in the retina: one for nearly all. *Trends Neurosci* **25**, 32-8.

Martinez-Morales, J. R., Signore, M., Acampora, D., Simeone, A. and Bovolenta, P. (2001). Otx genes are required for tissue specification in the developing eye. *Development* **128**, 2019-30.

Martinou, J. C., Dubois-Dauphin, M., Staple, J. K., Rodriguez, I., Frankowski, H., Missotten, M., Albertini, P., Talabot, D., Catsicas, S., Pietra, C. et al. (1994). Overexpression of Bcl-2 in transgenic mice protects neurons from naturally occurring cell death and experimental ischemia. *Neuron* **13**, 1017-1030.

Masai, I. (2000). [Mechanisms underlying induction and progression of a neurogenic wave in the zebrafish developing retina]. *Tanpakushitsu Kakusan Koso* **45**, 2782-90.

Masland, R. H. (1988). Amacrine cells. *Trends Neurosci* **11**, 405-10.

Masland, R. H. (2001). Neuronal diversity in the retina. *Curr Opin Neurobiol* **11**, 431-6.

Mastick, G. S. and Andrews, G. L. (2001). Pax6 Regulates the Identity of Embryonic Diencephalic Neurons. *Mol Cell Neurosci* **17**, 190-207.

Mathews, D. H., Sabina, J., Zuker, M. and Turner, D. H. (1999). Expanded sequence dependence of thermodynamic parameters improves prediction of RNA secondary structure. *J Mol Biol* **288**, 911-40.

Matsuo, I., Kuratani, S., Kimura, C., Takeda, N. and Aizawa, S. (1995). Mouse Otx2 functions in the formation and patterning of rostral head. *Genes Dev* **9**, 2646-58.

Matter-Sadzinski, L., Matter, J. M., Ong, M. T., Hernandez, J. and Ballivet, M. (2001). Specification of neurotransmitter receptor identity in developing retina: the chick ATH5 promoter integrates the positive and negative effects of several bHLH proteins. *Development* **128**, 217-31.

Mayer, W., Smith, A., Fundele, R. and Haaf, T. (2000). Spatial separation of parental genomes in preimplantation mouse embryos. *J Cell Biol* **148**, 629-34.

McCabe, M. J., Alatzoglou, K. S. and Dattani, M. T. (2011). Septo-optic dysplasia and other midline defects: the role of transcription factors: HESX1 and beyond. *Best Pract Res Clin Endocrinol Metab* **25**, 115-24.

McConnell, S. K. and Kaznowski, C. E. (1991). Cell cycle dependence of laminar determination in developing neocortex. *Science* **254**, 282-5.

McCullough, A. J. and Berget, S. M. (2000). An intronic splicing enhancer binds U1 snRNPs to enhance splicing and select 5' splice sites. *Mol Cell Biol* **20**, 9225-35.

McLoon, S. C. and Barnes, R. B. (1989). Early differentiation of retinal ganglion cells: an axonal protein expressed by premigratory and migrating retinal ganglion cells. *J Neurosci* **9**, 1424-32.

Melchior, W. B., Jr. and Von Hippel, P. H. (1973). Alteration of the relative stability of dA-dT and dG-dC base pairs in DNA. *Proc Natl Acad Sci U S A* **70**, 298-302.

Melton, D. A., Krieg, P. A., Rebagliati, M. R., Maniatis, T., Zinn, K. and Green, M. R. (1984). Efficient in vitro synthesis of biologically active RNA and RNA hybridization probes from plasmids containing a bacteriophage SP6 promoter. *Nucleic Acids Res* **12**, 7035-56.

Mercer, T. R., Dinger, M. E. and Mattick, J. S. (2009). Long non-coding RNAs: insights into functions. *Nat Rev Genet* **10**, 155-9.

Miller, M. W. and Nowakowski, R. S. (1988). Use of bromodeoxyuridine-immunohistochemistry to examine the proliferation, migration and time of origin of cells in the central nervous system. *Brain Res* **457**, 44-52.

Mitrovich, Q. M. and Anderson, P. (2000). Unproductively spliced ribosomal protein mRNAs are natural targets of mRNA surveillance in C. elegans. *Genes Dev* **14**, 2173-84.

Moore, K. B., Schneider, M. L. and Vetter, M. L. (2002). Posttranslational mechanisms control the timing of bHLH function and regulate retinal cell fate. *Neuron* **34**, 183-95.

Moshiri, A., Gonzalez, E., Tagawa, K., Maeda, H., Wang, M., Frishman, L. J. and Wang, S. W. (2008). Near complete loss of retinal ganglion cells in the math5/brn3b double knockout elicits severe reductions of other cell types during retinal development. *Dev Biol* **316**, 214-27.

Mu, X., Beremand, P. D., Zhao, S., Pershad, R., Sun, H., Scarpa, A., Liang, S., Thomas, T. L. and Klein, W. H. (2004). Discrete gene sets depend on POU domain transcription factor Brn3b/Brn-3.2/POU4f2 for their expression in the mouse embryonic retina. *Development* **131**, 1197-1210.

Mu, X., Fu, X., Beremand, P. D., Thomas, T. L. and Klein, W. H. (2008). Gene regulation logic in retinal ganglion cell development: Isl1 defines a critical branch distinct from but overlapping with Pou4f2. *Proc Natl Acad Sci U S A* **105**, 6942-7.

Mu, X., Fu, X., Sun, H., Beremand, P. D., Thomas, T. L. and Klein, W. H. (2005). A gene network downstream of transcription factor Math5 regulates retinal progenitor cell competence and ganglion cell fate. *Dev Biol* **280**, 467-81.

Mu, X. and Klein, W. H. (2004). A gene regulatory hierarchy for retinal ganglion cell specification and differentiation. *Semin Cell Dev Biol* **15**, 115-23.

Mukaddes, N. M., Kilincaslan, A., Kucukyazici, G., Sevketoglu, T. and Tuncer, S. (2007). Autism in visually impaired individuals. *Psychiatry Clin Neurosci* **61**, 39-44.

Muranishi, Y., Sato, S., Inoue, T., Ueno, S., Koyasu, T., Kondo, M. and Furukawa, T. (2010). Gene expression analysis of embryonic photoreceptor precursor cells using BAC-Crx-EGFP transgenic mouse. *Biochem Biophys Res Commun* **392**, 317-22.

Muranishi, Y., Terada, K., Inoue, T., Katoh, K., Tsujii, T., Sanuki, R., Kurokawa, D., Aizawa, S., Tamaki, Y. and Furukawa, T. (2011). An essential role for RAX homeoprotein and NOTCH-HES signaling in Otx2 expression in embryonic retinal photoreceptor cell fate determination. *J Neurosci* **31**, 16792-807.

Murre, C., McCaw, P. S., Vaessin, H., Caudy, M., Jan, L. Y., Jan, Y. N., Cabrera, C. V., Buskin, J. N., Hauschka, S. D. and Lassar, A. B. (1989). Interactions between heterologous helix-loop-helix proteins generate complexes that bind specifically to a common DNA sequence. *Cell* **58**, 537-44.

Mytelka, D. S. and Chamberlin, M. J. (1996). Analysis and suppression of DNA polymerase pauses associated with a trinucleotide consensus. *Nucleic Acids Res* **24**, 2774-81.

Nadal-Nicolas, F. M., Jimenez-Lopez, M., Sobrado-Calvo, P., Nieto-Lopez, L., Canovas-Martinez, I., Salinas-Navarro, M., Vidal-Sanz, M. and Agudo, M. (2009). Brn3a as a marker of retinal ganglion cells: qualitative and quantitative time course studies in naive and optic nerve-injured retinas. *Invest Ophthalmol Vis Sci* **50**, 3860-8.

Nagy, A. (2000). Cre recombinase: the universal reagent for genome tailoring. *Genesis* **26**, 99-109.

Nelson, B. R., Hartman, B. H., Georgi, S. A., Lan, M. S. and Reh, T. A. (2007). Transient inactivation of Notch signaling synchronizes differentiation of neural progenitor cells. *Dev Biol* **304**, 479-98.

Ng, L., Lu, A., Swaroop, A., Sharlin, D. S. and Forrest, D. (2011). Two transcription factors can direct three photoreceptor outcomes from rod precursor cells in mouse retinal development. *J Neurosci* **31**, 11118-25.

Nishida, A., Furukawa, A., Koike, C., Tano, Y., Aizawa, S., Matsuo, I. and Furukawa, T. (2003). Otx2 homeobox gene controls retinal photoreceptor cell fate and pineal gland development. *Nat Neurosci* **6**, 1255-63.

Norton, J. D. (2000). ID helix-loop-helix proteins in cell growth, differentiation and tumorigenesis. *J Cell Sci* **113 (Pt 22)**, 3897-905.

Nurse, P. (2000). A long twentieth century of the cell cycle and beyond. *Cell* **100**, 71-8.

O'Leary, D. D., Fawcett, J. W. and Cowan, W. M. (1986). Topographic targeting errors in the retinocollicular projection and their elimination by selective ganglion cell death. *J Neurosci* **6**, 3692-705.

Oh, E. C., Khan, N., Novelli, E., Khanna, H., Strettoi, E. and Swaroop, A. (2007). Transformation of cone precursors to functional rod photoreceptors by bZIP transcription factor NRL. *Proc Natl Acad Sci U S A* **104**, 1679-84.

Ohnuma, S. and Harris, W. A. (2003). Neurogenesis and the cell cycle. *Neuron* **40**, 199-208.

Ohnuma, S., Hopper, S., Wang, K. C., Philpott, A. and Harris, W. A. (2002). Co-ordinating retinal histogenesis: early cell cycle exit enhances early cell fate determination in the Xenopus retina. *Development* **129**, 2435-46.

Ohnuma, S., Philpott, A., Wang, K., Holt, C. E. and Harris, W. A. (1999). p27Xic1, a Cdk inhibitor, promotes the determination of glial cells in Xenopus retina. *Cell* **99**, 499-510.

Ohsawa, R. and Kageyama, R. (2008). Regulation of retinal cell fate specification by multiple transcription factors. *Brain Res* **1192**, 90-8.

Olichon, A., Guillou, E., Delettre, C., Landes, T., Arnaune-Pelloquin, L., Emorine, L. J., Mils, V., Daloyau, M., Hamel, C., Amati-Bonneau, P. et al. (2006). Mitochondrial dynamics and disease, OPA1. *Biochim Biophys Acta* **1763**, 500-9.

Oliver, E. R., Saunders, T. L., Tarle, S. A. and Glaser, T. (2004). Ribosomal protein L24 defect in belly spot and tail (Bst), a mouse Minute. *Development* **131**, 3907-20.

Oster, S. F., Deiner, M., Birgbauer, E. and Sretavan, D. W. (2004). Ganglion cell axon pathfinding in the retina and optic nerve. *Semin Cell Dev Biol* **15**, 125-36.

Osterfield, M., Egelund, R., Young, L. M. and Flanagan, J. G. (2008). Interaction of amyloid precursor protein with contactins and NgCAM in the retinotectal system. *Development* **135**, 1189-99.

Pan, L., Deng, M., Xie, X. and Gan, L. (2008). ISL1 and BRN3B co-regulate the differentiation of murine retinal ganglion cells. *Development* **135**, 1981-90.

Pan, L., Yang, Z., Feng, L. and Gan, L. (2005). Functional equivalence of Brn3 POU-domain transcription factors in mouse retinal neurogenesis. *Development* **132**, 703-12.

Pear, W. (2001). Transient transfection methods for preparation of high-titer retroviral supernatants. *Curr Protoc Mol Biol* **Chapter 9**, Unit9 11.

Pearson, B. J. and Doe, C. Q. (2003). Regulation of neuroblast competence in Drosophila. *Nature* **425**, 624-8.

Peichl, L. and Gonzalez-Soriano, J. (1993). Unexpected presence of neurofilaments in axon-bearing horizontal cells of the mammalian retina. *J Neurosci* **13**, 4091-100.

Peichl, L. and Gonzalez-Soriano, J. (1994). Morphological types of horizontal cell in rodent retinae: a comparison of rat, mouse, gerbil, and guinea pig. *Vis Neurosci* **11**, 501-17.

Pequignot, M. O., Provost, A. C., Salle, S., Taupin, P., Sainton, K. M., Marchant, D., Martinou, J. C., Ameisen, J. C., Jais, J. P. and Abitbol, M. (2003). Major role of BAX in apoptosis during retinal development and in establishment of a functional postnatal retina. *Dev Dyn* **228**, 231-8.

Perron, M., Kanekar, S., Vetter, M. L. and Harris, W. A. (1998). The genetic sequence of retinal development in the ciliary margin of the Xenopus eye. *Dev Biol* **199**, 185-200.

Perry, V. H. and Walker, M. (1980). Amacrine cells, displaced amacrine cells and interplexiform cells in the retina of the rat. *Proc R Soc Lond B Biol Sci* **208**, 415-31.

Pfeiffer, J. K. and Telesnitsky, A. (2001). Effects of limiting homology at the site of intermolecular recombinogenic template switching during Moloney murine leukemia virus replication. *J Virol* **75**, 11263-74.

Pinto, D. Pagnamenta, A. T. Klei, L. Anney, R. Merico, D. Regan, R. Conroy, J. Magalhaes, T. R. Correia, C. Abrahams, B. S. et al. (2010). Functional impact of global rare copy number variation in autism spectrum disorders. *Nature* **466**, 368-72.

Pittman, A. J., Law, M. Y. and Chien, C. B. (2008). Pathfinding in a large vertebrate axon tract: isotypic interactions guide retinotectal axons at multiple choice points. *Development* **135**, 2865-71.

Plouhinec, J. L., Sauka-Spengler, T., Germot, A., Le Mentec, C., Cabana, T., Harrison, G., Pieau, C., Sire, J. Y., Veron, G. and Mazan, S. (2003). The mammalian Crx genes are highly divergent representatives of the Otx5 gene family, a gnathostome orthology class of orthodenticle-related homeogenes involved in the differentiation of retinal photoreceptors and circadian entrainment. *Mol Biol Evol* **20**, 513-21.

Poggi, L., Vitorino, M., Masai, I. and Harris, W. A. (2005). Influences on neural lineage and mode of division in the zebrafish retina in vivo. *J Cell Biol* **171**, 991-9.

Powell, L. M., Zur Lage, P. I., Prentice, D. R., Senthinathan, B. and Jarman, A. P. (2004). The proneural proteins Atonal and Scute regulate neural target genes through different E-box binding sites. *Mol Cell Biol* **24**, 9517-26.

Prasov, L., Brown, N. L. and Glaser, T. (2010). A critical analysis of Atoh7 (Math5) mRNA splicing in the developing mouse retina. *PLoS One* **5**, e12315.

Prasov, L. and Glaser, T. (2012). Dynamic expression of ganglion cell markers in retinal progenitors during the terminal cell cycle. *J Cell Biol* **(under review)**.

Prasov, L., Masud, T., Khaliq, S., Mehdi, S. Q., Abid, A., Oliver, E. R., Silva, E. D., Lewanda, A., Brodsky, M. C., Borchert, M. et al. (2012). *ATOH7* mutations cause autosomal recessive persistent hyperplasia of the primary vitreous. *Am J Hum Genet*.

Project, N. E. S. Exome Variant Server vol. 2011 (ed. Seattle, WA.

Provencio, I., Jiang, G., De Grip, W. J., Hayes, W. P. and Rollag, M. D. (1998). Melanopsin: An opsin in melanophores, brain, and eye. *Proc Natl Acad Sci U S A* **95**, 340-5.

Provis, J. M. (2001). Development of the primate retinal vasculature. *Prog Retin Eye Res* **20**, 799-821.

Pruett, R. C. (1975). The pleomorphism and complications of posterior hyperplastic primary vitreous. *Am J Ophthalmol* **80**, 625-9.

Qiu, F., Jiang, H. and Xiang, M. (2008). A comprehensive negative regulatory program controlled by Brn3b to ensure ganglion cell specification from multipotential retinal precursors. *J Neurosci* **28**, 3392-403.

Quan, X. J., Denayer, T., Yan, J., Jafar-Nejad, H., Philippi, A., Lichtarge, O., Vleminckx, K. and Hassan, B. A. (2004). Evolution of neural precursor

selection: functional divergence of proneural proteins. *Development* **131**, 1679-89.

Quigley, H. A. (1996). Number of people with glaucoma worldwide. *Br J Ophthalmol* **80**, 389-93.

Rachel, R. A., Dolen, G., Hayes, N. L., Lu, A., Erskine, L., Nowakowski, R. S. and Mason, C. A. (2002). Spatiotemporal features of early neuronogenesis differ in wild-type and albino mouse retina. *J Neurosci* **22**, 4249-63.

Ragge, N. K., Brown, A. G., Poloschek, C. M., Lorenz, B., Henderson, R. A., Clarke, M. P., Russell-Eggitt, I., Fielder, A., Gerrelli, D., Martinez-Barbera, J. P. et al. (2005). Heterozygous mutations of OTX2 cause severe ocular malformations. *Am J Hum Genet* **76**, 1008-22.

Ramdas, W. D., van Koolwijk, L. M., Ikram, M. K., Jansonius, N. M., de Jong, P. T., Bergen, A. A., Isaacs, A., Amin, N., Aulchenko, Y. S., Wolfs, R. C. et al. (2010). A genome-wide association study of optic disc parameters. *PLoS Genet* **6**, e1000978.

Ramdas, W. D., van Koolwijk, L. M., Lemij, H. G., Pasutto, F., Cree, A. J., Thorleifsson, G., Janssen, S. F., Jacoline, T. B., Amin, N., Rivadeneira, F. et al. (2011). Common genetic variants associated with open-angle glaucoma. *Hum Mol Genet* **20**, 2464-71.

Rapaport, D. H., Patheal, S. L. and Harris, W. A. (2001). Cellular competence plays a role in photoreceptor differentiation in the developing Xenopus retina. *J Neurobiol* **49**, 129-41.

Rapaport, D. H., Wong, L. L., Wood, E. D., Yasumura, D. and LaVail, M. M. (2004). Timing and topography of cell genesis in the rat retina. *J Comp Neurol* **474**, 304-24.

Raper, J. and Mason, C. (2010). Cellular strategies of axonal pathfinding. *Cold Spring Harb Perspect Biol* **2**, a001933.

Rees, W. A., Yager, T. D., Korte, J. and von Hippel, P. H. (1993). Betaine can eliminate the base pair composition dependence of DNA melting. *Biochemistry* **32**, 137-44.

Reese, A. B. (1955). Persistent hyperplastic primary vitreous. *Am J Ophthalmol* **40**, 317-31.

Reese, B. E. and Colello, R. J. (1992). Neurogenesis in the retinal ganglion cell layer of the rat. *Neuroscience* **46**, 419-29.

Reese, B. E. and Galli-Resta, L. (2002). The role of tangential dispersion in retinal mosaic formation. *Prog Retin Eye Res* **21**, 153-68.

Reese, B. E., Necessary, B. D., Tam, P. P., Faulkner-Jones, B. and Tan, S. S. (1999). Clonal expansion and cell dispersion in the developing mouse retina. *Eur J Neurosci* **11**, 2965-78.

Reh, T. A. (1992). Cellular interactions determine neuronal phenotypes in rodent retinal cultures. *J Neurobiol* **23**, 1067-83.

Reh, T. A. and Cagan, R. L. (1994). Intrinsic and extrinsic signals in the developing vertebrate and fly eyes: viewing vertebrate and invertebrate eyes in the same light. *Perspect Dev Neurobiol* **2**, 183-90.

Reh, T. A. and Kljavin, I. J. (1989). Age of differentiation determines rat retinal germinal cell phenotype: induction of differentiation by dissociation. *J Neurosci* **9**, 4179-89.

Reh, T. A., Lamba, D. and Gust, J. (2010). Directing human embryonic stem cells to a retinal fate. *Methods Mol Biol* **636**, 139-53.

Repka, A. M. and Adler, R. (1992). Accurate determination of the time of cell birth using a sequential labeling technique with [3H]-thymidine and bromodeoxyuridine ("window labeling"). *J Histochem Cytochem* **40**, 947-53.

Rhodes, K. J. and Trimmer, J. S. (2006). Antibodies as valuable neuroscience research tools versus reagents of mass distraction. *J Neurosci* **26**, 8017-20.

Riesenberg, A. N., Liu, Z., Kopan, R. and Brown, N. L. (2009). Rbpj cell autonomous regulation of retinal ganglion cell and cone photoreceptor fates in the mouse retina. *J Neurosci* **29**, 12865-77.

Robitaille, J. M., Wallace, K., Zheng, B., Beis, M. J., Samuels, M., Hoskin-Mott, A. and Guernsey, D. L. (2009). Phenotypic overlap of familial exudative vitreoretinopathy (FEVR) with persistent fetal vasculature (PFV) caused by FZD4 mutations in two distinct pedigrees. *Ophthalmic Genet* **30**, 23-30.

Rockhill, R. L., Daly, F. J., MacNeil, M. A., Brown, S. P. and Masland, R. H. (2002). The diversity of ganglion cells in a mammalian retina. *J Neurosci* **22**, 3831-43.

Rodieck, R. W. (1998). The First Steps in Seeing. Sunderland, MA: Sinauer.

Roe, T., Reynolds, T. C., Yu, G. and Brown, P. O. (1993). Integration of murine leukemia virus DNA depends on mitosis. *Embo J* **12**, 2099-108.

Rompani, S. B. and Cepko, C. L. (2008). Retinal progenitor cells can produce restricted subsets of horizontal cells. *Proc Natl Acad Sci U S A* **105**, 192-7.

Roohi, J., Montagna, C., Tegay, D. H., Palmer, L. E., DeVincent, C., Pomeroy, J. C., Christian, S. L., Nowak, N. and Hatchwell, E. (2009).

Disruption of contactin 4 in three subjects with autism spectrum disorder. *J Med Genet* **46**, 176-82.

Ross, S. E., Greenberg, M. E. and Stiles, C. D. (2003). Basic helix-loop-helix factors in cortical development. *Neuron* **39**, 13-25.

Rowan, S. and Cepko, C. L. (2004). Genetic analysis of the homeodomain transcription factor Chx10 in the retina using a novel multifunctional BAC transgenic mouse reporter. *Dev Biol* **271**, 388-402.

Roy, S. W. and Irimia, M. (2008). When good transcripts go bad: artifactual RT-PCR 'splicing' and genome analysis. *Bioessays* **30**, 601-5.

Rupp, R. A., Snider, L. and Weintraub, H. (1994). Xenopus embryos regulate the nuclear localization of XMyoD. *Genes Dev* **8**, 1311-23.

Ruvkun, G. (1997). Patterning the Nervous System.

Sadun, A. A. and Carelli, V. (2003). Mitochondrial function and dysfunction within the optic nerve. *Arch Ophthalmol* **121**, 1342-3.

Sakharkar, M. K., Chow, V. T., Chaturvedi, I., Mathura, V. S., Shapshak, P. and Kangueane, P. (2004). A report on single exon genes (SEG) in eukaryotes. *Front Biosci* **9**, 3262-7.

Samson, M., Emerson, M. M. and Cepko, C. L. (2009). Robust marking of photoreceptor cells and pinealocytes with several reporters under control of the Crx gene. *Dev Dyn* **238**, 3218-25.

Sanchez-Camacho, C. and Bovolenta, P. (2008). Autonomous and non-autonomous Shh signalling mediate the in vivo growth and guidance of mouse retinal ganglion cell axons. *Development* **135**, 3531-41.

Saper, C. B. and Sawchenko, P. E. (2003). Magic peptides, magic antibodies: guidelines for appropriate controls for immunohistochemistry. *J Comp Neurol* **465**, 161-3.

Sato, S., Inoue, T., Terada, K., Matsuo, I., Aizawa, S., Tano, Y., Fujikado, T. and Furukawa, T. (2007). Dkk3-Cre BAC transgenic mouse line: a tool for highly efficient gene deletion in retinal progenitor cells. *Genesis* **45**, 502-7.

Saul, S. M., Brzezinski, J. A., Altschuler, R. A., Shore, S. E., Rudolph, D. D., Kabara, L. L., Halsey, K. E., Hufnagel, R. B., Zhou, J., Dolan, D. F. et al. (2008). Math5 expression and function in the central auditory system. *Mol Cell Neurosci* **37**, 153-69.

Scheetz, A. J., Williams, R. W. and Dubin, M. W. (1995). Severity of ganglion cell death during early postnatal development is modulated by both neuronal activity and binocular competition. *Vis Neurosci* **12**, 605-10.

Schiller, P. H. and Malpeli, J. G. (1977). Properties and tectal projections of monkey retinal ganglion cells. *J Neurophysiol* **40**, 428-45.

Schilter, K. F., Schneider, A., Bardakjian, T., Soucy, J. F., Tyler, R. C., Reis, L. M. and Semina, E. V. (2011). OTX2 microphthalmia syndrome: four novel mutations and delineation of a phenotype. *Clin Genet* **79**, 158-68.

Schneider-Poetsch, T., Ju, J., Eyler, D. E., Dang, Y., Bhat, S., Merrick, W. C., Green, R., Shen, B. and Liu, J. O. (2010). Inhibition of eukaryotic translation elongation by cycloheximide and lactimidomycin. *Nat Chem Biol* **6**, 209-217.

Schneider, M. L., Turner, D. L. and Vetter, M. L. (2001). Notch signaling can inhibit Xath5 function in the neural plate and developing retina. *Mol Cell Neurosci* **18**, 458-72.

Schonbrunner, N. J., Fiss, E. H., Budker, O., Stoffel, S., Sigua, C. L., Gelfand, D. H. and Myers, T. W. (2006). Chimeric thermostable DNA polymerases with reverse transcriptase and attenuated 3'-5' exonuclease activity. *Biochemistry* **45**, 12786-95.

Schwede, T., Kopp, J., Guex, N. and Peitsch, M. C. (2003). SWISS-MODEL: An automated protein homology-modeling server. *Nucleic Acids Res* **31**, 3381-5.

Scott, I. U., Warman, R. and Altman, N. (1997). Bilateral aplasia of the optic nerves, chiasm, and tracts in an otherwise healthy infant. *Am J Ophthalmol* **124**, 409-10.

Shastry, B. S. (2009). Persistent hyperplastic primary vitreous: congenital malformation of the eye. *Clin Experiment Ophthalmol* **37**, 884-90.

Shen, Q., Wang, Y., Dimos, J. T., Fasano, C. A., Phoenix, T. N., Lemischka, I. R., Ivanova, N. B., Stifani, S., Morrisey, E. E. and Temple, S. (2006). The timing of cortical neurogenesis is encoded within lineages of individual progenitor cells. *Nat Neurosci* **9**, 743-51.

Shen, Y. C. and Raymond, P. A. (2004). Zebrafish cone-rod (crx) homeobox gene promotes retinogenesis. *Dev Biol* **269**, 237-51.

Shimoda, Y. and Watanabe, K. (2009). Contactins: emerging key roles in the development and function of the nervous system. *Cell Adh Migr* **3**, 64-70.

Shkumatava, A., Fischer, S., Muller, F., Strahle, U. and Neumann, C. J. (2004). Sonic hedgehog, secreted by amacrine cells, acts as a short-range signal

to direct differentiation and lamination in the zebrafish retina. *Development* **131**, 3849-58.

Sidman, R. L. (1961). Histogenesis of mouse retina studied with thymidine-H3. In *Structure of the Eye*, (ed. G. K. Smelser), pp. 487-506. New York: Academic Press.

Silva, A. O., Ercole, C. E. and McLoon, S. C. (2003). Regulation of ganglion cell production by Notch signaling during retinal development. *J Neurobiol* **54**, 511-24.

Simeone, A., Acampora, D., Mallamaci, A., Stornaiuolo, A., D'Apice, M. R., Nigro, V. and Boncinelli, E. (1993). A vertebrate gene related to orthodenticle contains a homeodomain of the bicoid class and demarcates anterior neuroectoderm in the gastrulating mouse embryo. *Embo J* **12**, 2735-47.

Simpson, J. I. (1984). The accessory optic system. *Annu Rev Neurosci* **7**, 13-41.

Sinitsina, V. F. (1971). [DNA synthesis and cell population kinetics in embryonal histogenesis of the retina in mice]. *Arkh Anat Gistol Embriol* **61**, 58-67.

Sloan, S. R., Shen, C. P., McCarrick-Walmsley, R. and Kadesch, T. (1996). Phosphorylation of E47 as a potential determinant of B-cell-specific activity. *Mol Cell Biol* **16**, 6900-8.

Snow, R. L. and Robson, J. A. (1994). Ganglion cell neurogenesis, migration and early differentiation in the chick retina. *Neuroscience* **58**, 399-409.

Spemann, H. (1901). Ueber korrelationen in der entwicklung des auges. *Verh. Anat. Ges.* **15**, 61–79.

Stacey, D. W. (2003). Cyclin D1 serves as a cell cycle regulatory switch in actively proliferating cells. *Curr Opin Cell Biol* **15**, 158-63.

Stolting, K. N., Gort, G., Wust, C. and Wilson, A. B. (2009). Eukaryotic transcriptomics in silico: optimizing cDNA-AFLP efficiency. *BMC Genomics* **10**, 565.

Strom, R. C. and Williams, R. W. (1998). Cell production and cell death in the generation of variation in neuron number. *J Neurosci* **18**, 9948-53.

Sun, Y., Kanekar, S. L., Vetter, M. L., Gorski, S., Jan, Y. N., Glaser, T. and Brown, N. L. (2003). Conserved and divergent functions of Drosophila atonal, amphibian, and mammalian Ath5 genes. *Evol Dev* **5**, 532-41.

Swaroop, A., Kim, D. and Forrest, D. (2010). Transcriptional regulation of photoreceptor development and homeostasis in the mammalian retina. *Nat Rev Neurosci* **11**, 563-76.

Swift, S., Lorens, J., Achacoso, P. and Nolan, G. P. (2001). Rapid production of retroviruses for efficient gene delivery to mammalian cells using 293T cell-based systems. *Curr Protoc Immunol* **Chapter 10**, Unit 10 17C.

Tabaska, J. E. and Zhang, M. Q. (1999). Detection of polyadenylation signals in human DNA sequences. *Gene* **231**, 77-86.

Takatsuka, K., Hatakeyama, J., Bessho, Y. and Kageyama, R. (2004). Roles of the bHLH gene Hes1 in retinal morphogenesis. *Brain Res* **1004**, 148-55.

Taylor, D. (2007). Developmental abnormalities of the optic nerve and chiasm. *Eye (Lond)* **21**, 1271-84.

Telesnitsky, A. and Goff, S. (1997). Reverse transcription and the generation of retroviral DNA. In *Retroviruses*, (ed. J. M. Coffin S. H. Hughes and H. E. Varmus), pp. 121-160. Cold Spring Harbor, NY: CSH Press.

Thomason, L. C., Costantino, N., Shaw, D. V. and Court, D. L. (2007). Multicopy plasmid modification with phage lambda Red recombineering. *Plasmid* **58**, 148-58.

Trimarchi, J. M., Stadler, M. B. and Cepko, C. L. (2008). Individual retinal progenitor cells display extensive heterogeneity of gene expression. *PLoS One* **3**, e1588.

Triplett, J. W., Pfeiffenberger, C., Yamada, J., Stafford, B. K., Sweeney, N. T., Litke, A. M., Sher, A., Koulakov, A. A. and Feldheim, D. A. (2011). Competition is a driving force in topographic mapping. *Proc Natl Acad Sci U S A*.

Turner, D. L. and Cepko, C. L. (1987). A common progenitor for neurons and glia persists in rat retina late in development. *Nature* **328**, 131-6.

Turner, D. L., Snyder, E. Y. and Cepko, C. L. (1990). Lineage-independent determination of cell type in the embryonic mouse retina. *Neuron* **4**, 833-45.

Turner, D. L. and Weintraub, H. (1994). Expression of achaete-scute homolog 3 in Xenopus embryos converts ectodermal cells to a neural fate. *Genes Dev* **8**, 1434-47.

Van Gelder, R. N., Wee, R., Lee, J. A. and Tu, D. C. (2003). Reduced pupillary light responses in mice lacking cryptochromes. *Science* **299**, 222.

Van Parijs, L., Refaeli, Y., Lord, J. D., Nelson, B. H., Abbas, A. K. and Baltimore, D. (1999). Uncoupling IL-2 signals that regulate T cell proliferation, survival, and Fas-mediated activation-induced cell death. *Immunity* **11**, 281-8.

Vecino, E., Hernandez, M. and Garcia, M. (2004). Cell death in the developing vertebrate retina. *Int J Dev Biol* **48**, 965-74.

Voinescu, P. E., Kay, J. N. and Sanes, J. R. (2009). Birthdays of retinal amacrine cell subtypes are systematically related to their molecular identity and soma position. *J Comp Neurol* **517**, 737-50.

von Bohlen und Halbach, O. (1999). The isolated mammalian brain: an in vivo preparation suitable for pathway tracing. *Eur J Neurosci* **11**, 1096-100.

Voyvodic, J. T., Burne, J. F. and Raff, M. C. (1995). Quantification of normal cell death in the rat retina: implications for clone composition in cell lineage analysis. *Eur J Neurosci* **7**, 2469-78.

Wadman, I. A., Osada, H., Grutz, G. G., Agulnick, A. D., Westphal, H., Forster, A. and Rabbitts, T. H. (1997). The LIM-only protein Lmo2 is a bridging molecule assembling an erythroid, DNA-binding complex which includes the TAL1, E47, GATA-1 and Ldb1/NLI proteins. *Embo J* **16**, 3145-57.

Wahle, E. (1995). Poly(A) tail length control is caused by termination of processive synthesis. *J Biol Chem* **270**, 2800-8.

Waid, D. K. and McLoon, S. C. (1995). Immediate differentiation of ganglion cells following mitosis in the developing retina. *Neuron* **14**, 117-24.

Waid, D. K. and McLoon, S. C. (1998). Ganglion cells influence the fate of dividing retinal cells in culture. *Development* **125**, 1059-66.

Wallace, V. A. and Raff, M. C. (1999). A role for Sonic hedgehog in axon-to-astrocyte signalling in the rodent optic nerve. *Development* **126**, 2901-9.

Wang, S. W., Kim, B. S., Ding, K., Wang, H., Sun, D., Johnson, R. L., Klein, W. H. and Gan, L. (2001). Requirement for math5 in the development of retinal ganglion cells. *Genes Dev* **15**, 24-9.

Wang, S. W., Mu, X., Bowers, W. J., Kim, D. S., Plas, D. J., Crair, M. C., Federoff, H. J., Gan, L. and Klein, W. H. (2002a). Brn3b/Brn3c double knockout mice reveal an unsuspected role for Brn3c in retinal ganglion cell axon outgrowth. *Development* **129**, 467-77.

Wang, S. W., Mu, X., Bowers, W. J. and Klein, W. H. (2002b). Retinal ganglion cell differentiation in cultured mouse retinal explants. *Methods* **28**, 448-56.

Wang, Y., Dakubo, G. D., Thurig, S., Mazerolle, C. J. and Wallace, V. A. (2005). Retinal ganglion cell-derived sonic hedgehog locally controls proliferation and the timing of RGC development in the embryonic mouse retina. *Development* **132**, 5103-13.

Wang, Y., Smallwood, P. M., Cowan, M., Blesh, D., Lawler, A. and Nathans, J. (1999). Mutually exclusive expression of human red and green visual pigment-

reporter transgenes occurs at high frequency in murine cone photoreceptors. *Proc Natl Acad Sci U S A* **96**, 5251-6.

Wang, Z. and Burge, C. B. (2008). Splicing regulation: from a parts list of regulatory elements to an integrated splicing code. *RNA* **14**, 802-13.

Warden, S. M., Andreoli, C. M. and Mukai, S. (2007). The Wnt signaling pathway in familial exudative vitreoretinopathy and Norrie disease. *Semin Ophthalmol* **22**, 211-7.

Warming, S., Costantino, N., Court, D. L., Jenkins, N. A. and Copeland, N. G. (2005). Simple and highly efficient BAC recombineering using galK selection. *Nucleic Acids Res* **33**, e36.

Watanabe, M., Rutishauser, U. and Silver, J. (1991). Formation of the retinal ganglion cell and optic fiber layers. *J Neurobiol* **22**, 85-96.

Watanabe, T. and Raff, M. C. (1988). Retinal astrocytes are immigrants from the optic nerve. *Nature* **332**, 834-7.

Watanabe, T. and Raff, M. C. (1990). Rod photoreceptor development in vitro: intrinsic properties of proliferating neuroepithelial cells change as development proceeds in the rat retina. *Neuron* **4**, 461-7.

Wee, R., Castrucci, A. M., Provencio, I., Gan, L. and Van Gelder, R. N. (2002). Loss of photic entrainment and altered free-running circadian rhythms in math5-/- mice. *J Neurosci* **22**, 10427-33.

Weissensteiner, T. and Lanchbury, J. S. (1996). Strategy for controlling preferential amplification and avoiding false negatives in PCR typing. *Biotechniques* **21**, 1102-8.

Wendt, H., Thomas, R. M. and Ellenberger, T. (1998). DNA-mediated folding and assembly of MyoD-E47 heterodimers. *J Biol Chem* **273**, 5735-43.

Wessells, N. K. (1977). Tissue Interactions and Development. Menlo Park, CA: W.A. Benjamin.

Wetts, R. and Fraser, S. E. (1988). Multipotent precursors can give rise to all major cell types of the frog retina. *Science* **239**, 1142-5.

Willbold, E., Rothermel, A., Tomlinson, S. and Layer, P. G. (2000). Muller glia cells reorganize reaggregating chicken retinal cells into correctly laminated in vitro retinae. *Glia* **29**, 45-57.

Wodarz, A., Ramrath, A., Grimm, A. and Knust, E. (2000). Drosophila atypical protein kinase C associates with Bazooka and controls polarity of epithelia and neuroblasts. *J Cell Biol* **150**, 1361-74.

Wong, L. L. and Rapaport, D. H. (2009). Defining retinal progenitor cell competence in Xenopus laevis by clonal analysis. *Development* **136**, 1707-15.

Wu, F., Sapkota, D., Li, R. and Mu, X. (2012). Onecut 1 and onecut 2 are potential regulators of mouse retinal development. *J Comp Neurol* **520**, 952-69.

Wu, W., Blumberg, B. M., Fay, P. J. and Bambara, R. A. (1995). Strand transfer mediated by human immunodeficiency virus reverse transcriptase in vitro is promoted by pausing and results in misincorporation. *J Biol Chem* **270**, 325-32.

Wyatt, A., Bakrania, P., Bunyan, D. J., Osborne, R. J., Crolla, J. A., Salt, A., Ayuso, C., Newbury-Ecob, R., Abou-Rayyah, Y., Collin, J. R. et al. (2008). Novel heterozygous OTX2 mutations and whole gene deletions in anophthalmia, microphthalmia and coloboma. *Hum Mutat* **29**, E278-83.

Xiang, M. (1998). Requirement for Brn-3b in early differentiation of postmitotic retinal ganglion cell precursors. *Dev Biol* **197**, 155-69.

Xiang, M., Zhou, L., Macke, J. P., Yoshioka, T., Hendry, S. H., Eddy, R. L., Shows, T. B. and Nathans, J. (1995). The Brn-3 family of POU-domain factors: primary structure, binding specificity, and expression in subsets of retinal ganglion cells and somatosensory neurons. *J Neurosci* **15**, 4762-85.

Xiang, M., Zhou, L., Peng, Y. W., Eddy, R. L., Shows, T. B. and Nathans, J. (1993). Brn-3b: a POU domain gene expressed in a subset of retinal ganglion cells. *Neuron* **11**, 689-701.

Yamada, E. (1969). Some structural features of the fovea centralis in the human retina. *Arch Ophthalmol* **82**, 151-9.

Yang, K., Hitomi, M. and Stacey, D. W. (2006). Variations in cyclin D1 levels through the cell cycle determine the proliferative fate of a cell. *Cell Div* **1**, 32.

Yang, X. J. (2004). Roles of cell-extrinsic growth factors in vertebrate eye pattern formation and retinogenesis. *Semin Cell Dev Biol* **15**, 91-103.

Yang, Z., Ding, K., Pan, L., Deng, M. and Gan, L. (2003). Math5 determines the competence state of retinal ganglion cell progenitors. *Dev Biol* **264**, 240-54.

Yao, J., Sun, X., Wang, Y., Xu, G. and Qian, J. (2007). Math5 promotes retinal ganglion cell expression patterns in retinal progenitor cells. *Mol Vis* **13**, 1066-72.

Yaron, O., Farhy, C., Marquardt, T., Applebury, M. and Ashery-Padan, R. (2006). Notch1 functions to suppress cone-photoreceptor fate specification in the developing mouse retina. *Development* **133**, 1367-78.

Yau, K. W. and Baylor, D. A. (1989). Cyclic GMP-activated conductance of retinal photoreceptor cells. *Annu Rev Neurosci* **12**, 289-327.

Yoshihara, Y., Kawasaki, M., Tamada, A., Nagata, S., Kagamiyama, H. and Mori, K. (1995). Overlapping and differential expression of BIG-2, BIG-1, TAG-1, and F3: four members of an axon-associated cell adhesion molecule subgroup of the immunoglobulin superfamily. *J Neurobiol* **28**, 51-69.

Young, R. W. (1984). Cell death during differentiation of the retina in the mouse. *J Comp Neurol* **229**, 362-73.

Young, R. W. (1985a). Cell differentiation in the retina of the mouse. *Anat Rec* **212**, 199-205.

Young, R. W. (1985b). Cell proliferation during postnatal development of the retina in the mouse. *Brain Res* **353**, 229-39.

Young, T. L. and Cepko, C. L. (2004). A role for ligand-gated ion channels in rod photoreceptor development. *Neuron* **41**, 867-79.

Yu, C., Mazerolle, C. J., Thurig, S., Wang, Y., Pacal, M., Bremner, R. and Wallace, V. A. (2006). Direct and indirect effects of hedgehog pathway activation in the mammalian retina. *Mol Cell Neurosci* **32**, 274-82.

Yuodelis, C. and Hendrickson, A. (1986). A qualitative and quantitative analysis of the human fovea during development. *Vision Res* **26**, 847-55.

Zambrowicz, B. P., Imamoto, A., Fiering, S., Herzenberg, L. A., Kerr, W. G. and Soriano, P. (1997). Disruption of overlapping transcripts in the ROSA beta geo 26 gene trap strain leads to widespread expression of beta-galactosidase in mouse embryos and hematopoietic cells. *Proc Natl Acad Sci U S A* **94**, 3789-94.

Zaphiropoulos, P. G. (2002). Template switching generated during reverse transcription? *FEBS Lett* **527**, 326.

Zhang, H., Deo, M., Thompson, R. C., Uhler, M. D. and Turner, D. L. (2012). Negative regulation of Yap during neuronal differentiation. *Dev Biol* **361**, 103-15.

Zhang, J., Gray, J., Wu, L., Leone, G., Rowan, S., Cepko, C. L., Zhu, X., Craft, C. M. and Dyer, M. A. (2004). Rb regulates proliferation and rod photoreceptor development in the mouse retina. *Nat Genet* **36**, 351-60.

Zhang, X. M. and Yang, X. J. (2001). Regulation of retinal ganglion cell production by Sonic hedgehog. *Development* **128**, 943-57.

Zhao, C. and Emmons, S. W. (1995). A transcription factor controlling development of peripheral sense organs in C. elegans. *Nature* **373**, 74-8.

Zhou, P. (2004). Determining protein half-lives. *Methods Mol Biol* **284**, 67-77.

Zhu, M., Provis, J. M. and Penfold, P. L. (1999). The human hyaloid system: cellular phenotypes and inter-relationships. *Exp Eye Res* **68**, 553-63.

Zhu, X. and Craft, C. M. (2000). Modulation of CRX transactivation activity by phosducin isoforms. *Mol Cell Biol* **20**, 5216-26.

Zong, H., Espinosa, J. S., Su, H. H., Muzumdar, M. D. and Luo, L. (2005). Mosaic analysis with double markers in mice. *Cell* **121**, 479-92.

Zuker, M. (2003). Mfold web server for nucleic acid folding and hybridization prediction. *Nucleic Acids Res* **31**, 3406-15.